

https://dspace.org/

Quantitative aspects of mining induced seismicity in a part of the Welkom Goldfield /cRicardo Isidro Loureiro Ferreira.

Ferreira, Ricardo Isidro Loureiro.

1997
https://hdl.handle.net/10539/24376

Downloaded from a DSpace repository. https://dspace.org/

QUANTITATIVE ASPECTS OF MINING-INDUCED SEISMICITY IN A PART OF THE WELKOM GOLDFIELD

Ricardo Isidro Loureiro Ferreira

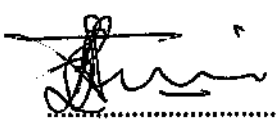
A dissertation submitted to the Faculty of Science, University of the Witwatersrand, Johannesburg, in fulfilment of the requirements for the degree of Master of Science in Geophysics.

Johannesburg, 1997

VOLUME 1

DECLARATION

I declare that this dissertation is my own, unaided work. It is being submitted for the Degree of Master of Science in Geophysics in the University of the Witwatersrand, Johannesburg. It has not been submitted before for any degree or examination in any other university.



R.I.L. Ferreira

22nd day of DECEMBER 1997.

ABSTRACT

Rockbursts continue to be one of the more high profile and problematic worker hazards in the South African gold mining industry. Recent advances in the technology of seismic monitoring systems and seismic data analysis and interpretation methods hold considerable promise towards improving the success rate of rockburst control measures. This study tests different methods for the evaluation of the response of geological structures to mining induced stress changes.

A small part of Western Holdings Gold Mine in the Welkom goldfield -- the Postma Area -- offers a challenge because of its geological complexity, accessibility and high incidence of seismicity. The sensitivity of the local network to ground motions in this area of interest and the expected spatial location accuracy is established and deemed adequate for a detailed investigation of seismic activity. The local mining geometry, geology and methods of mining are discussed. The fractured state of the rock mass observed *in situ*, close to the stope faces, is in agreement with the results of numerical elastic modelling and the high stresses inferred seismically. Almost immediately after the incidence of a large event (M_L 3.7) which occurred close to one end of a dyke, an increased rate of seismic activity became apparent at another part of the same dyke, some 250 m to the east. A change in the state of seismic stress, before and after the large event, points to a transfer of stress along this geological discontinuity.

A quantitative analysis of recorded seismicity indicates spatial and temporal variations in the state of stress and strain throughout the rock mass surrounding mining excavations. The elastic stress modelling performed routinely by rock mechanics engineers in the deep gold mines is, by itself, incapable of catering for the rheological nature of the rock mass, but taken together with independent seismic evaluations of a fault orthogonal to a highly stressed dyke it is shown that both methods are mutually complementary and can enhance the assessment of the seismic instability of the structures. A back-analysis is conducted on ten large seismic events ($M_L > 2.5$) to identify precursors. These show that the timely recognition of high gradients in physical seismic parameters pertaining to strain rate and stress in time and space immediately prior to major seismic events is a real and practical possibility, as such constituting an early warning mechanism. The fore-warning of a large event is best served by an analysis of seismicity over the short term (weeks or days) through time-history variations and/or contouring of various seismic parameters, although long-term seismic responses (months or weeks) characterise specific patterns and trends which are useful in the forecast.

DEDICATION

Foi o teu suor do trabalho, pai, que me trouxe a este ponto. Foste tu, mãe, que me deste coragem e força de vontade.

I dedicate this work to you.

ACKNOWLEDGEMENTS

I am greatly indebted to ISS International (Welkom) for the unrestricted access to their computer facilities and seismic data base, as well as the support and expertise of their highly professional staff. Special thanks to Dr G. van Aswegen for his ready interest and guidance in the progress of this dissertation, making it a worthwhile exercise, and also to Dr A. Cichowicz for his help and criticism. I am grateful to the Management and Rock Mechanics staff of Western Holdings Gold Mine for their permission to use the Postma area as the subject of this study, and to all the people on the mine who assisted me in various other ways.

I also acknowledge the time and use of the computer facilities of the Rock Mechanics and Seismic Department of East Driefontein Gold Mine (A Division of Driefontein Consolidated Limited), who afforded me the opportunity to bring this work to completion.

The greatest praise, glory and exultation I reserve for my God and personal Saviour, Jesus. You alone are worthy. What is mere man that You care for him ? Yet, Lord, you have renewed my strength, and as I look upon Your countenance and the effects of Your hand in my life I can but marvel:

how great You are.

QUANTITATIVE ASPECTS OF MINING-INDUCED SEISMICITY IN A PART OF THE WELKOM GOLDFIELD

Contents **Page no.**

VOLUME 1:

Declaration i

Abstract ii

Dedication iii

Acknowledgements iv

Contents v

List of Figures x

List of Tables xxiii

List of Symbols xxiv

[1] INTRODUCTION 1

(1.1) Organisation of the Dissertation 1

(1.2) Objectives 2

(1.3) The Welkom Goldfield 4

(1.4) The Welkom Seismological Network 8

(1.5) Regional Seismicity 9

(1.6) The Study Area 12

[2] THEORETICAL BACKGROUND 18

(2.1) Review of Earthquake Precursory Phenomena 18

(2.1.1) General 18

(2.1.2) Seismic patterns 20

(2.1.3) Seismic wave propagation 30

(2.1.4) Stochastic methodologies in hazard assessment 34

(2.2) Seismic Source Parameters 45

(2.3) Fault / Dyke Stability in the Mining Environment 50

(2.3.1) Asperities 50

(2.3.2) Undulations, depth, fault gauge, dip and K-ratio 52

(2.3.3) Stress variations and excess shear stress 54

(2.4) Recent Hypotheses in Rockmass Stability 59

(2.5) Numerical Aspects in Seismicity Analysis 66

(2.5.1) Time and space windows in the selection of seismic events for analysis 66

(2.5.2) Contouring of seismic parameters 69

(2.5.3) Time-history variations of seismic parameters 70

(2.6) Summary 71

[3] SEISMIC COVERAGE AND CORRELATION OF SEISMICITY WITH MINING IN THE POSTMA AREA 74

(3.1) Sensitivity of Local Network 74

(3.2) Location, Methods of Mining and In-situ Observations 78

(3.3) Spatial and Temporal Distribution of Seismicity 88

(3.4) State of Stress Inferred Seismically 92

(3.4.1) Stress transfer along the Postma dyke 97

(3.5) Summary and Discussion 101

[4] QUANTITATIVE ANALYSIS OF SEISMICITY IN THE POSTMA AREA 104

(4.1) Stress Levels and Implications of Mining Adjacent to the Postma Dyke and Basson Fault 104

(4.1.1) Calculation of stresses using elastic-continuum modelling 104

(4.1.2) Seismic stress and deformation rates through recorded seismicity 117

(4.1.3) Summary 131

(4.2) Back Analysis of Large Events to Identify Precursors 133

(4.2.1) Event 910825 of local magnitude 2.5 134

(4.2.2) Events 920826a and 920826b of local magnitudes 2.8 and 2.6 respectively 142

(4.2.3) Event 930314 of local magnitude 2.6 147

(4.2.4) Event 931108 of local magnitude 2.6 147

(4.2.5) Event 940424 of local magnitude 2.7 149

(4.2.6) Event 940513 of local magnitude 2.8 151

(4.2.7) Events 940627a, 940627b and 940627c of local magnitudes 3.7, 3.2 and 2.7 respectively 154

(4.3) Summary 161

[5] **CONCLUSION** 168

REFERENCES 173

VOLUME 2:

Contents xxvi

APPENDIX A: Sections through the Basal Reef, showing the extent of discontinuities and local structure (figs. 1.7 a-f; refer to fig. 1.6, Sec 1.6, Chap 1) 182

APPENDIX B: Sketches and photographic record of stoping areas visited (figs. 3.8 and 3.9; refer to fig. 3.6, Sec 3.2, Chap 2) 186

APPENDIX C: Concentrations of recorded seismic events in the Postma area during the first and second semesters of 1994, respectively (figs. 3.10b and 3.10c; Sec 3.3, Chap 3) 199

APPENDIX D: Selective analysis of seismicity around the Postma dyke (figs. 4.8 b-d) and the Basson fault (figs. 4.9 b-d) for the contouring of seismic viscosity and energy index. The contours of seismic viscosity are overlaid on contours of energy index for visual effect and ease of combined evaluation/interpretation of the source

	parameters (Sec 4.1.2, Chap 4)	201
APPENDIX E:	(a) All recorded seismicity in the Postma area from 1/1/91 to 25/8/91 in terms of energy index (figs. 4.12 and 4.15), seismic apparent stress (fig. 4.13) and apparent volume (fig. 4.14); (Sec 4.2.1, Chap 4)	209
	(b) Contours of seismic fluidity (fig. 4.17) for the delineation of the clustering of seismicity during the time period considered	211
	(c) Reduced areal extent used for time-history analysis with the new selection of events for seismic evaluation (fig. 4.18)	211
APPENDICES F1 to F7:	Time-history and contour plots used in the analysis of large events ($M_L > 2.5$) to identify precursors; (Section 4.2, Chapter 4)	212 - 308
APPENDIX G:	Sensitivity of source parameter calculations to length of time windows used (figs. 4.169-4.198) (Sec 4.2.7, Chap 4)	309
APPENDIX H:	Clustering of seismicity immediately before the occurrence of a large event (figs. 4.199-4.205) (Sec 4.3, Chap 4)	325
APPENDIX I:	Energy indicators used as 'likelihood' indicators of imminent instability (figs. 4.206-4.211) (Sec 4.3, Chap 4)	330

List of Figures

Figure		Page no.
1.1	The Witwatersrand Basin, with the various mining districts. The city of Welkom lies on the south-western corner of the Basin, within the Welkom Goldfield.	5
1.2	Stratigraphic column through the Central Rand Group in the Welkom Goldfield, showing various reefs, including the Basal Reef.	6
1.3	Structural section from west to east through the Welkom Goldfield (after Minter et al, 1986).	7
1.4	Gutenberg-Richter frequency-magnitude plot based on events located within the Welkom Goldfield, for which a minimum of five triggered and associated seismic stations were used for source parameter calculations.	11
1.5	Extent and location of Western Holdings Gold Mine within the Welkom goldfield in relation to some of the neighbouring mines. The squares represent mine shafts; the configuration of seismic stations at the time of this study in indicated by the numbered triangles. The rectangle south of Western Holdings' #3 Shaft encloses the study area.	13
1.6	Plan of the study area with the outline of mining faces along the Basal Reef (as at September 1993 -- shaded portion indicates mined reef) and positions of major geological structure (with dip directions and throw as indicated). The lines represent the location, extent and orientation of sections through the reef, shown in fig. 1.7, in Appendix A.	14

Appendix A:

1.7 a-f Sections through the Basal Reef, showing the extent of discontinuities and the local structure at depth. The location of each section is delineated in fig. 1.6. 183 - 185

1.8 Simplified geometrical '3D' models of the Postma dyke and Basson fault surfaces. 17

2.1 Displacement spectrum of a seismic tremor (after McGarr, Seismic Design of Embankments and Caverns, 1983), typical of recorded ground motions in deep gold mines. The curve is described by three independent parameters: the low-frequency spectral level, the corner frequency and the high-frequency decay. The spectrum relates to a more complex rupture model, which the Brune model approximates. 47

2.2 Schematic models of rupture using the asperity scenario (after McGarr Seismic Design of Embankments and Caverns, 1983). Model A involves an annular region where shear failure has previously taken place, surrounding a stronger asperity. The preceding failure may have taken place through fault creep or as a series of previous earthquakes. Occasionally, some of the preceding failure may occur earlier in the same seismic event (Model B), where the failure of multiple asperities leads to an enhanced loading of a major asperity that finally fails. 51

2.3 An isolated stope at depth with stress lobes (S), locality and mode of failure of possible future events. Zone C lies in front of the immediate stope face, characterised by very high concentrations of compressive stress. As mining progresses, zones C and S impinge on discontinuities,

forming the source regions of imminent seismic events. Slip on nearby discontinuities may also load the rock at the excavation interface beyond its load-carrying capacity. 55

2.4 The concept of energy index: ratio of measured energy to that which is expected (average) for a given moment for some seismic event. 61

3.1 Gutenberg-Richter frequency-magnitude plot based on events for which a minimum of four triggered and associated seismic stations were used for source parameter calculations. The magnitudes were calculated using seismic moment (e.g. Hanks and Kanamori, 1979). 75

3.2 Same frequency-magnitude relation as fig. 3.1, but using a minimum of five triggered and associated stations. 76

3.3a The study area with locations of eight nearest seismic stations. The Postma dyke and Basson fault are represented by the gridded surfaces. Arrows point to the locations of stations outside the frame of the figure. The asterisk marks the hypocentre of an event whose waveform is displayed in fig. 3.3b. 77

3.3b An example of a processed waveform (with P- and S-wave picks), recorded by one of the tri-axial geophone sets shown in fig. 3.3a, belonging to one of the larger events (M_L 3.2 on 27/06/1194) which occurred in the area. 77

3.4a Expected spatial hypocentral accuracy: extent of detectability for events of minimum local magnitude 0.1. The numbers represent the expected location errors associated with seismic events located at those points, in metres. Outside the boundary of the contour lines the seismic sensors are 'deaf' to local magnitudes less than 0.1. 79

3.4b Expected spatial hypocentral accuracy: extent of detectability for events of minimum local magnitude 0.8. As with fig. 3.4a, the numbers refer to expected errors in location of seismic events occurring at those points, in metres. 79

3.5 Section through a stope in a gold mine showing typical rockmass conditions at depth (strike-parallel joints and blast fractures not visible). (Source: An Industry Guide to Methods of Ameliorating the Hazards of Rockfalls and Rockbursts, 1988 edition, COMRO). 81

3.6 Areas of recent mining activity in the vicinity of the Postma Dyke and Basson Fault. Sites 1, 2 and 3 were documented photographically (see Appendix B). 83

3.7 Sketch of panels 10A and 10B, site 1, with the mining configuration and the locations of photographs taken. The photographs whose numbers are preceded by an asterisk are located in Appendix B. 85

Appendix B: 186

3.8 Panels of site 2, with indications of where photographs were taken. 191

3.9 Sketch of site 3, with areas of mining and locations of photographs. 195

3.10a Plot from the software package '4Di' showing the outline of the old mine faces (red lines) on plan, the Postma dyke and Basson fault (yellow mesh), and all the seismicity recorded in the area during the second half of 1993. The locations of the circular symbols (denoting V_a) correspond to event locations; symbol colour indicates time of occurrence; symbol size scales the volume of deformation. 89

Appendix C: 199

3.10b Same as fig. 3.10a, but showing all seismic events recorded in the Postma area during the first half of 1994. 200

3.10c Same as fig. 3.10a, but showing all the seismic events recorded in the Postma area during the second half of 1994. 200

3.11a Selected events with local magnitudes greater than 1.5 in the time period 1/1/91 until 31/12/94. The symbols representing the events, in this case, denote local magnitude. 90

3.11b Same as fig. 3.11a but looking sectionaly eastwards along reef horizon. For vertical scale consider the vertical extent (dip length) of the Basson fault model (280 m). 90

3.12 Selected seismic events during the 6 months encompassing the last quarter of 1993 and the first quarter of 1994 with EI > 1.0. Symbol colour portrays the energy index of the tremors; symbol size corresponds to local magnitude. 93

3.13 Contour plot of seismic stress. The time range of seismicity is the same as fig. 3.12. 93

3.14 Distribution of events selected in the time period 1/1/93 - 30/3/94 and seismic moment range 8.5 to 9.5 (in log[J]). Symbol colour portrays EI; symbol size denotes σ_a. 95

3.15a Relation between E and M_0 using events selected 100m either side of the Postma dyke during the first half of 1994. 98

3.15b Same as fig. 3.15a, but using events recorded during the second half of 1994. 98

3.16 Time-variation of EI during the period between July 1993 and December 1994. The data was averaged over a 15-day time-window

to reduce short term fluctuations. 100

4.1 The Postma area with a gridded surface superimposed on the mined-out reef. At intersection points of the grid the amount of vertical stress (TZZ in MPa) was calculated using elastic-continuum modelling. The amount of TZZ, altered by mining, is represented by the symbol size. 107

4.2a Orthographic view of the mined-out reef of the study area, looking westwards. The 'dashes' represent principal stress vectors on a vertical plane orthogonal to the line of view, the length of which indicates the strength of the stress field at that point. 108

4.2b Same as fig. 4.2a, but looking northwards. 108

4.3a The Postma area with a gridded model representing the Basson fault, using the same principle demonstrated in fig. 4.1. 110

4.3b Similar to fig. 4.3a, but showing the calculated (elastic-modelled) vertical stresses at points on the Postma dyke. 110

4.4a Extent and magnitude of the major principal stress, with orientation of stress vectors about the mined-out reef, at the same points on the grid model. 111

4.4b Similar to fig. 4.4a, but showing the principal stress acting on the Postma dyke. 111

4.5a Extent of positive ESS at points along the Basson fault. The stage of mining to which the modelling applies corresponds to that represented by the mined-out reef. 113

4.5b Similar to fig. 4.5a; ESS results at points on the Postma dyke. 113

4.6a-b Similar to figs. 4.5a and 4.5b, respectively, but ESS results now correspond to the recent (post-1992) mining only. 114

4.7 Contours of average EI during the second quarter of 1993. Note the seismic gap and absence of higher stress in the middle-to-bottom half of the rectangle. The expanded rectangle shows events located in the area between July 1990 and April 1993, indicating a release of strain energy (or shear stress) in this part of the Basson fault. 118

4.8a Contours of log(EI) overlaid by contours of log(seismic viscosity), based on source parameters of seismicity recorded during the first quarter of 1994. The seismicity was selected 100 m into the footwall and hangingwall of Postma dyke and characterizes the behaviour of the dyke in terms of stress change (energy index) and strain rate (seismic viscosity). For depth scale consider the dip extent of the dyke model (340 m). 122

Appendix D: 201

4.8b-d Same as fig. 4.8a, but the time periods of seismicity associated with the Postma dyke are the 2nd, 3rd and 4th quarters of 1994, respectively. 202 - 204

4.9a Contours of log(EI) overlaid by contours of log(seismic viscosity), based on source parameters of seismicity recorded during the first quarter of 1994. The seismicity was selected 100 m into the footwall and hangingwall of Basson fault and characterizes the behaviour of the fault in terms of stress change (energy index) and strain rate (seismic viscosity). For depth scale consider the dip extent of the fault model (280 m). 124

Appendix D: 201

4.9b-d Same as fig. 4.9a, but the time periods of seismicity associated with the Basson fault are the 2nd, 3rd and 4th quarters of 1994, respectively. 205 - 207

4.10a A sectional perspective view of the Basal Reef horizon, looking northwards along the strike of the Basson fault and onto the footwall side of the Postma dyke. Seismicity selected 100m either side of the Postma dyke two weeks preceding the M_L 3.7 event (its location is indicated by the 'hourglass' symbol) is contoured in terms of seismic strain. Contour highs indicate regions of greater rock deformation. 130

4.10b Same as fig. 4.10a but the contours now show EI, thus contour lows indicate regions where stress drop took place. 130

4.11 Selection of events of local magnitude greater than 2.5 in the vicinity of the Postma dyke and Basson fault in the time period 1/1/91 to 31/12/94. Events are represented by apparent volume (symbol size) and time of occurrence (colour scale). The centre of the symbol (in this case a circle) corresponds to the location of the respective event on plan. 135

Appendix E: 208

4.12 Distribution of events up to and including event 910825 in the vicinity of the Postma area since January 1991. The red lines outline old mine faces (on plan). The mesh represents the Basson fault (north-south) and the Postma dyke (roughly east-west). Symbol colour represents event time; symbol size denotes energy index. 209

4.13 Same as fig. 4.12 but symbol size now portrays apparent stress. 209

4.14 Same as fig. 4.12; symbol size portrays apparent volume. 210

4.15 Same as fig. 4.12 but looking perspectively on section, westwards, along the strike of the Postma dyke, onto the mesh representing the Basson fault (for depth scale consider the dip extent of the fault model (280 m)). 210

4.16 Contours of seismic Deborah number based on source parameters of seismicity recorded in the time period 1/1/91 to 25/8/91 (up to, but excluding, event 910825) to delineate the clustering of seismicity in the Postma area and enable the 'preparation zone' for event 910825 to be identified. 139

Appendix E: 208

4.17 Same as fig. 4.16 (events up to and excluding event 910825), but the contours are of log(seismic fluidity), for the identification of the 'preparation zone' for event 910825. 211

4.18 Polygon denoting the boundary of the smaller area selected for time-history analysis according to contours of seismic Deborah number and seismic fluidity (window length: 8 samples and/or 5 days). 211

4.19 Time-history of ΣV_a and moving median EI (window length: 8 samples and/or 5 days) for the seismicity associated with the 'preparation zone' of event 910825. The arrows depict the large events (denoted by log(E) > 7.0) in time -- the second arrow (latest in time) refers to event 910825. 139

Appendix F1: 212

4.20 - 4.23 Time-histories used in the analysis of event 910825 to identify precursors. 213 - 214

4.24 Contours of apparent volume using seismicity recorded in the time period 1/1/91 to 25/8/91 (up to, but excluding, event 910825 -- its position is merely indicated by the 'hourglass' symbol). 141

Appendix F1: 212

4.25 - 4.30 Contours used in the analysis of event 910825 to identify precursors. 215 - 217

4.31 Similar to fig. 4.24; time period of seismicity ranges over the three months before event 910825. 141

Appendix F1: 212

4.32 - 4.37 Contours used in the analysis of event 910825 to identify precursors. 218 - 220

4.38 Distribution of recorded events in the time period 1/1/91 to 26/8/92 in terms of energy index (symbol size) and time of occurrence (colour scale). Events 920826a and 920826b are included. The inner 'rectangle' enclosing the red lines (old mine faces) forms a polygon for the selection of events used in subsequent time-history analysis. 144

Appendix F2: 221

4.39 Same as fig. 4.38 but symbol size denotes apparent stress. 222

4.40 Same as fig. 4.38 but symbol size denotes apparent volume. 222

4.41 Section looking eastward onto the Basson fault, along the dip of the reef, showing the distribution of recorded events in depth around the Postma dyke (for depth scale consider the dip extent of the Basson fault model (280 m)) in terms of event time and apparent stress. 223

4.42 - 4.58 Time-history and contour plots used in the analysis of events 920826a and 920826b to identify precursors. 224 -234

Appendix F3: 235

4.59 - 4.75 Time-history and contour plots used in the analysis of event 930314 to identify precursors. 236 - 246

Appendix F4: 247

4.76 - 4.92 Time-history and contour plots used in the analysis of event 931108 to identify precursors. 248 - 258

Appendix F5: 259

4.93 - 4.109 Time-history and contour plots used in the analysis of event 940424 to identify precursors. 260 - 270

4.110 Time-history of ΣV_a and log(EI) for event 940513 using the same polygon for events' selection as in previous cases (with a moving median window of 8 samples and/or 5 days). Since event 940513 is spatially removed from the clustering of seismicity around the Postma dyke, the polygon used for the previous selection of events must be

modified in order to obtain better precursory trends/results. 153

4.111 The use of smaller, overlapping polygons creates a systematic means of covering an entire area of interest. As delineated, the polygons overlap by 50% from left to right and from the top down. The analysis of seismicity then entails looking at those events located within each of the individual polygons and identifying precursory trends. The distribution of recorded events in the time period 14/5/93 to 13/5/94 is also shown. 153

Appendix F6: 271

4.112a The rectangle in the top-left-hand corner of the Postma area denotes the polygon used for the selection of events to produce improved results in time-history analysis. Events, in this case, are represented in time (colour) and local magnitude (symbol size). 272

4.112b Perspective view of the selection of events within the polygon delivering clearer precursory changes in the variation of seismic source parameters with time. Events are denoted by apparent stress (symbol size) and time (colour). 272

4.113 - 4.130 Time-history and contour plots used in the analysis of event 940513 to identify precursors. 273 - 284

4.131 Distribution of seismicity recorded in the time period 28/3/94 to 27/6/94 (three months before and including events 940627a, 940627b and 940627c). Note the greater concentration of events near the fault-dyke intersection, close to the hypocentre of event 940627a. 156

Appendix F7: 285

4.132 Section looking northwards, along the plane of the Basson fault, onto the Postma dyke, with events 940627a, 940627b and 940627c represented by seismic apparent volume in relation to the broken 'planes' of the Basal reef. For vertical scale consider the dip extent of the Postma dyke model (340 m). 286

4.133 Same as fig. 4.132, but looking eastwards along the plane of the Postma dyke, onto the Basson fault, downdip along the Basal reef. For vertical scale consider the dip extent of the Basson fault model (280 m). 286

4.134 - 4.168 Time-history and contour plots used in the analysis of events 940627a, 940627b and 940627c to identify precursors. 287 - 308

Appendix G: 309

4.169 - 4.198 Sensitivity of source parameter calculations to the length of time windows used. 310 - 324

Appendix H: 325

4.199 - 4.205 Clustering of seismicity immediately before the occurrence of a large event. 326 - 329

Appendix I: 330

4.206 - 4.211 Energy indicators used as 'likelihood indicators' of imminent instability. 331 - 333

Table		Page no.
1	Major seismic events recorded in the Welkom Goldfield (after van Aswegen, 1990)	10
2	Major seismic events and attributed losses	10
3	Some source parameters attributed to the seismic events of local magnitudes greater than 2.5, located within the Postma area in the time period 1 January 1991 to 31 December 1994	135
4	Summary of results for contoured seismic parameters for event 910825	143
5	Summary of results for contoured seismic parameters for events 920826a and 920826b	146
6	Summary of results for contoured seismic parameters for event 930314	148
7	Summary of results for contoured seismic parameters for event 931108	150
8	Summary of results for contoured seismic parameters for event 940424	152
9	Summary of results for contoured seismic parameters for event 940513	155
10	Summary of results for contoured seismic parameters for events 940627a, 940627b and 940627c	158
11	Summary of the precursory performance of the seismic parameters investigated for two methods of analysis. Regarding the contours, the long term analysis refers to the period of 'months in advance'; the short term analysis refers to 'weeks in advance'	165

List of Symbols

Quantity	Symbol
angle of friction	ϕ
apparent volume	V_a
apparent stress	σ_a
area	A
attenuation intensity (scattering)	Q_s^{-1}
coefficient of friction, dynamic	μ
corner frequency	f_0
density (mass density)	ρ
displacement, distance	D
energy index	EI
excess shear stress	ESS
low-frequency asymptote to displacement spectrum	Ω_0
magnitude, seismic	M
, local	M_L
, minimum	M_{min}
seismic Deborah number	De_s
seismic diffusion	d_s
seismic diffusivity	D_s
seismic efficiency	η
seismic energy, total	E
, flux	E_c
, P-wave (compressional)	E_p
, S-wave (shear)	E_S
seismic moment	M_0
seismic relaxation time	τ_s

seismic Schmidt number.....Sc_s

seismic softening.....S_s

seismic strain.....ϵ_s

seismic strain rate.....$\dot{\epsilon}_s$

seismic stress.....σ_s

seismic viscosity.....η_s

shear modulus, modulus of rigidity.....G

static stress drop.....$\Delta\sigma$

strain, linear.....ϵ

stress, linear.....σ

, normal.....σ_n

, shear.....τ

source radius (seismic).....r_0

travel time, P-wave (compressional).....t_p

, S-wave (shear).....t_s

time.....t

velocity, P-wave(compressional).....V_p

, S-wave (shear).....V_s

volume.....V

wave, compressional.....P

, shear.....S

, radiation pattern of.....F_c

, amplitude (free-surface amplification of).....R_c

, site correction factor of.....S_c

1

INTRODUCTION

Deep level gold mining is an important industry in South Africa, contributing significantly to the wealth of the country. Rockbursting is one of the most important threats to the industry. The characterisation of the rockmass response to mining-induced stress changes and the spatial and temporal prediction of strong mine tremors causing rockbursts are subjects of ongoing research, to which this dissertation attempts to make some contribution.

(1.1) Organisation of the Dissertation

The objectives of this study are explained in Section 1.2. Sections 1.3 to 1.6 introduce the study area.

Since seismic tremors are simply small earthquakes, their study relies heavily on theory and concepts developed in crustal seismology. Section 2.1 summarises known earthquake precursory phenomena and considers their applicability to the mining environment. The estimation of seismic source parameters is described in Section 2.2. Relevant factors governing the stability of faults and/or dykes under the influence of mining-induced stress changes are discussed in Section 2.3, with reference to the two primary geological structures -- a steep fault orthogonal to a dyke -- in the study area. Some recent hypotheses pertaining to rockmass stability characterisation pertinent to this study are outlined in Section 2.4. Numerical aspects concerning elastic stress modelling and the format of presentation of seismic data are considered in Section 2.5.

Section 3.1 evaluates the sensitivity of the local network to ground motions in the area of interest and establishes the expected spatial location accuracy. *In situ* observations concerning the fractured state of the rockmass are detailed photographically in Section 3.2, along with the local geology and methods of mining. The distribution of recorded seismicity in space and time, and the state of stress inferred seismically, in relation to mining methods and/or configuration, are investigated in Sections 3.3 and 3.4. The possibility of stress transfer along a seismically active dyke after a large (local magnitude 3.7) event took place at one end of this geological structure is briefly investigated in the latter section.

The implications of mining adjacent to the same highly stressed dyke and an orthogonal fault are independently discussed in Section 4.1, using results of elastic stress modelling and the seismic responses of these structures. The two methods of analysis (elastic modelling and seismicity evaluation) are weighted against each other; the merits/strengths of one are used to supplement the results of the other. Section 4.2 performs a back analysis of events with local magnitudes greater than 2.5 in an attempt to identify those seismic parameters, or methods of evaluation, that in practicality might best be used as precursors.

The conclusions to this study follow as the last chapter of this dissertation.

(1.2) Objectives

In order to obtain confidence in further detailed seismological analysis of the stress changes and strains to which the rockmass surrounding excavated voids at depth is subjected, actual underground observations concerning rock face fracture conditions and location/configuration of mining are compared with the spatial and temporal distribution of recorded events and with the state of stress inferred seismically.

The stress gradients produced by mining excavations create states of disequilibrium within the rock, the adjustment of which should occur through a dissipation/diffusion/transferral of stresses. Such a transfer is intended to be demonstrated along a highly stressed dyke by its seismic reaction to mining, before and after a large event associated with it.

The numerical stress modelling performed routinely by rock mechanics practitioners in South African mines often uses a boundary element computer program which calculates stresses on- and off-reef, anticipated displacements and other parameters useful for the planning of mining layouts. However, these numerical methods do not take the fractured zone around underground openings or the rheological nature of the rockmass into account. This shortfall of elastic modelling is expected to be mitigated, to some extent, by incorporating an evaluation of recorded seismicity into the assessment of the rockmass around underground stopes. The seismic response of a dyke and part of an orthogonal fault to the dyke are used as examples, together with modelled stresses along these structures. It is hoped that feed-back information for the possible modification of mining strategies may be shown to be determinable and/or input parameters and results verifiable during mining. In other words, those assumptions and criteria used in the numerical modelling intended to guide the mining should reflect actual seismic observations; when and/or where the two depart, the seismic reaction of the rockmass -- characterised by a spatio-temporal behaviour in terms of induced stresses and strain rates (as indicated by the recorded seismicity) -- should help to reconcile both methods of analysis, and hence produce better mining and a safer working environment.

The occurrence of larger seismic tremors has been proposed to be preceded by observable changes in some seismological parameters developed recently. The timely recognition of high temporal and spatial gradients in seismic parameters pertaining to strain rate and stress just prior to major seismic events constitute an early warning mechanism for the safety of underground workers. A detailed back-analysis of events of local magnitude 2.5 and above, which tests this hypothesis, comprises the main

objective of this study. The performance of various seismic source parameters and practicality of evaluation techniques are highlighted.

(1.3) The Welkom Goldfield

An area of 400 square kilometres approximately 270 kilometres south-west of Johannesburg has, since the first gold bar was poured in October 1951, yielded close to 10 million kilograms of gold. This area, the Welkom Goldfield, lies at an approximate elevation of 1370 m above sea level and is of low relief (about 100m).

Fig. 1.1 shows the location of the city of Welkom on the south-western corner of the Witwatersrand Basin in which a number of goldfields have contributed towards the wealth of South Africa. Welkom itself was designed and sited in 1947 within the hub of mining activity.

Separate placers at five levels of stratigraphy in the Welkom goldfield have been exploited extensively by various mines. These include numerous reefs in the Eldorado Formation, the A Reef, the B Reef, the Leader Reef and the Basal Reef (fig. 1.2 shows a stratigraphic column of the Central Rand Group through Number 3 shaft of Western Holdings Gold Mine Ltd., the closest shaft to the study area.). The latter reef has been the most important orebody. The placers were deposited into the Central Rand Group between 1085 and 2120 m above its base. They are associated with eight fluvial-fan formations, a consequence of local folding.

The present structure of the goldfield is synformal in nature, trending north-south and split close to its axis by two major faults, the De Bron and Homestead (see fig. 1.3). The two faults form a central horst block, triangular in shape, which lies between an eastern section (Virginia) and a western section (Odendaalsrus). The stratiform ore deposits are structurally preserved in these sections, with an eastward dip. The other major faults showing large right-lateral displacements (between 1.2 and 4.7 km) are

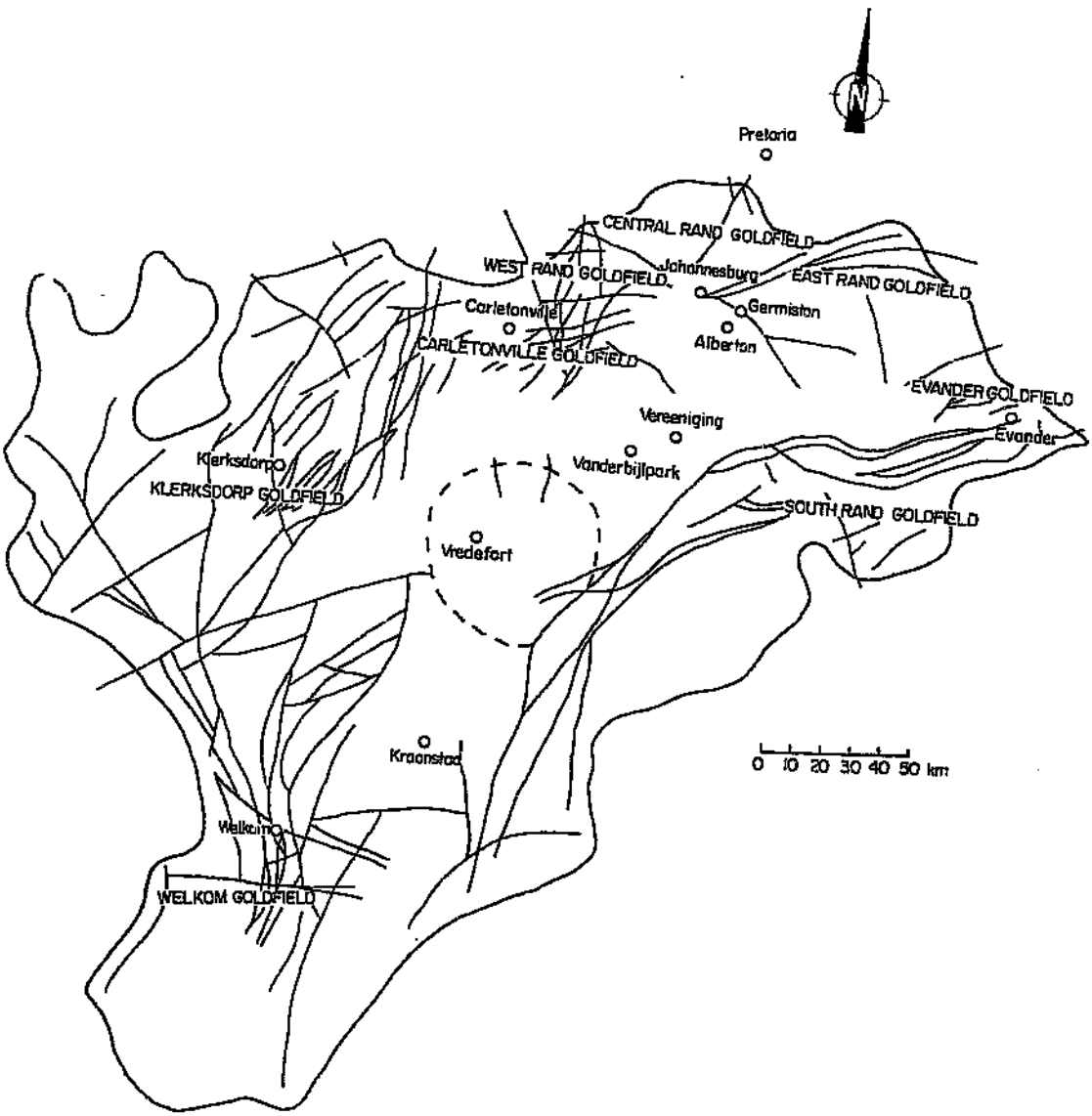


Fig. 1.1: The Witwatersrand Basin, with the various mining districts. The city of Welkom lies on the south-western corner of the Basin, within the Welkom Goldfield.

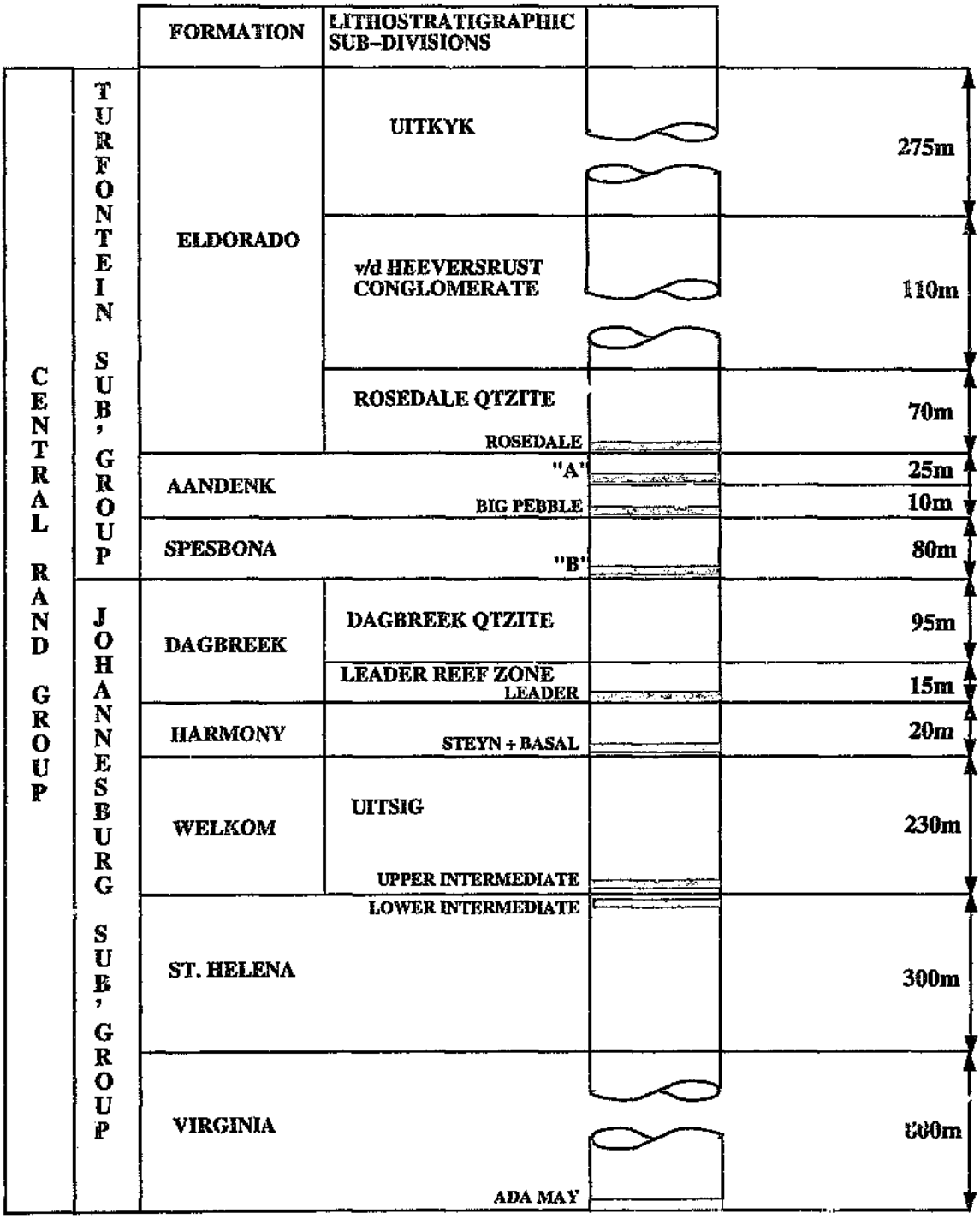
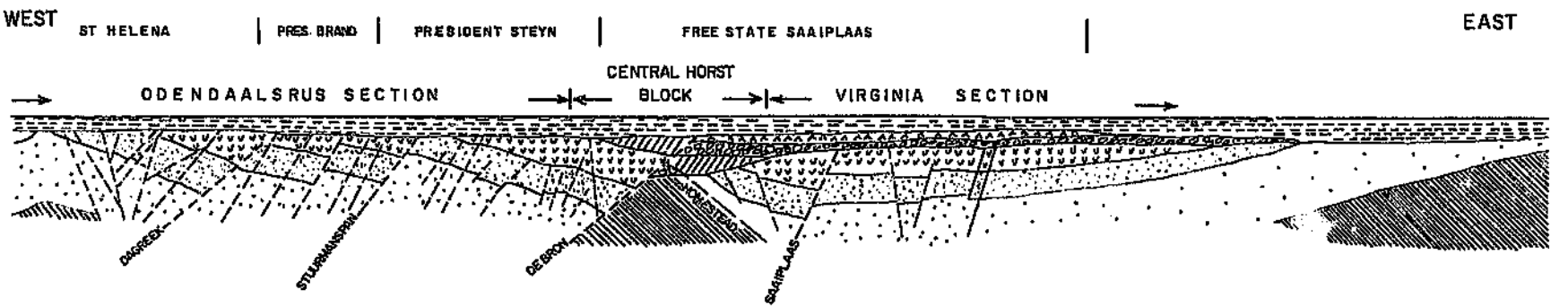


Fig. 1.2: Stratigraphic column of Central Rand Group in the Welkom Goldfield, showing various reefs, including the Basal Reef.

THE WELKOM GOLDFIELD



REFERENCE

- KAROO SEQUENCE
- ALLANRIDGE FORMATION
- BOTHAVILLE FORMATION
- KLIPPAN FORMATION
- KLIPRIVIERSBERG GROUP
- TURFFONTEIN SUBGROUP
- JOHANNESBURG SUBGROUP
- JEPPESTOWN SUBGROUP

0 5km

Fig. I.3
Structural section from west to east through the Welkom Goldfield.

the Dagbreek and the Stuirmanspan (or Arrarat further north). A swarm of vertical mafic dykes striking normal to the faults contributes to the disruption (Minter, Hill, Kidger, Kingsley and Snowden, 1986, p504-507,532). An overlying cover of carboniferous Karoo strata appears tectonically undisturbed.

In the present mining areas the Basal Reef horizon varies between some 1000 and 2500 m below surface.

(1.4) The Welkom Seismological Network

In the mid 1960's Harmony Gold Mine began to study seismic activity in the Goldfield with an analogue seismic monitoring system, since then discontinued (Mendecki, van Aswegen, Brown and Hewlett, 1990, p237). In 1980 an automatic seismic location system (COSMOS) covering several mines was installed. This was upgraded in 1988 to a fully digital mine seismological network -- the Welkom Seismological Network (WSN) -- covering an area of roughly 400 square kilometres with some 50 underground and surface stations.

Integrated Seismic Systems International (ISSI) Ltd., which develops and markets hardware and software for seismic monitoring systems for mines, assumes the daily running and maintenance of the WSN.

For each seismic event, three orthogonal components for each station which triggers (north-south, east-west, up-down) produce complete seismograms. The initial data capture is accomplished through a single board computer at each geophone site, where an analogue to digital conversion is also done. The data are sent by radio to the central computer, a UNIX-based workstation. Here, with real-time network control, the data

are collected and automatically processed (with manual checking). The hypocentre and other source parameters like seismic moment, seismic energy, corner frequency and static and dynamic stress drop are obtained for each event and stored in a database.

Dynamic control of data acquisition is possible through the central computer; system parameters and the status of a particular station may be determined and modified, communications may be started or stopped at any time. Software allows the display and manipulation of associated triggers (in full three-component seismograms). The processed events are used to update the database on a daily basis, providing immediate and high quality seismic information with ease of access.

(1.5) Regional Seismicity

Table 1 lists seven major fault slip events occurring over the past quarter century in the Welkom goldfield (van Aswegen, 1990, p718; van Aswegen, personal communication). Fig. 1.4 shows a Gutenberg-Richter frequency-magnitude plot based on events located within the goldfield, for which a minimum of five triggered and associated seismic stations were used for source parameter calculations (minimum local magnitude is approximately 1.0).

The largest event ever recorded in the Welkom goldfield, in 1976, registered a local magnitude of 5.1. The observable damage underground was in the form of a severe shakedown of rock from the side-wall and hanging-wall of tunnels as well as the closure of stopes very close to an area of the Dagbreek Fault Zone (DFZ). This structure has a finite oblique displacement exceeding 1000 m and a complex multicomponent internal structure, dipping westwards at an average of 60^0 (e.g. Berry, 1988, p1,3, 27-28; van Aswegen, 1990, p718).

Table 1: Major seismic events recorded in the Welkom Goldfield (after van Aswegen, 1990)

Date	Magnitude	Fault	Dip displacement as measure of fault size	Max. observable coseismic slip
1972	4.5	Erfdeel	300m	?
1976	5.1	Dagbreek	900m	(>>) 15cm
1982	4.8	Wesselia	360m	41cm
1986	4.9	Dagbreek	900m	(>) 20cm
1989	4.6	Brand	350m	37 cm
1990	4.6	Stuirmanspan	800m	(>>) 10cm
1993	4.6	Saaiplaas	300m	37 cm

Table 2: Major seismic events and attributed losses:

Event	Damage / Losses
Erdfeel (1972)	Steel work and concrete lining of FSG Mine no. 1 shaft; production lost for several days.
Dagbreek (1976)	Severe shakedown of rock in tunnels and closure of stopes close to the Dagbreek Fault Zone (DFZ); collapse of a multi-storey apartment building on surface, without loss of life.
Wesselia (1982)	Significant damage underground (shakedown) and surface. Both no.1 and no.4 shafts of FSG Mine inoperative for several days.
Dagbreek (1986)	Similar to that found during 1976 event, concentrated along DFZ in the vicinity of the hypocentre.
Brand (1989)	Disruption of central business area on surface; number of buildings suffered significant cracks. Underground rockburst-type damage confined to stressed pillars and dykes -- similar to 1976 event.
Stuirmanspan (1990)	Severe damage to openings close to the fault on the deep levels of President Brand no. 2 and no. 4 Shafts.
Saaiplaas (1993)	Extensive regional falls of ground; an elevation survey of the grade track after the tremor revealed 37cm normal displacement on the fault.

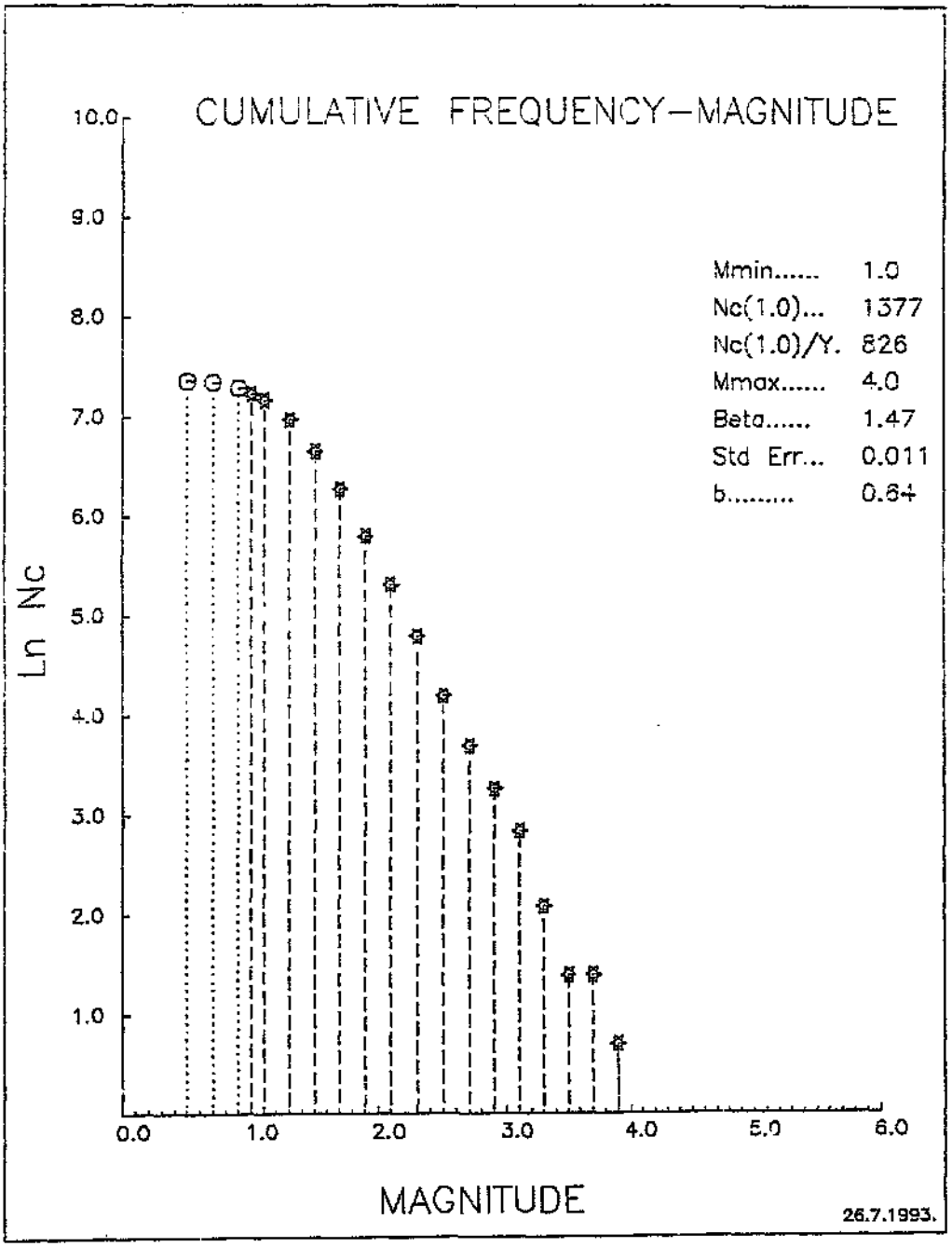


Fig. 1.4: Gutenberg-Richter frequency-magnitude plot based on events located within the Welkom Goldfield, for which a minimum of five triggered and associated seismic stations were used for source parameter calculations.

In situ investigations soon after the event revealed a maximum co-seismic single displacement of 15 cm on one particular component of the DFZ. No indication of co-seismic slip was found in the deeper exposures of the DFZ (i.e. more than 50 m below reef) (van Aswegen, 1990). Surface damage was limited to the collapse of a multi-storey apartment building some time after the main event, without loss of life. The other major seismic events and the losses caused are summarised in Table 2. The January 1989 event was the largest (thus far) recorded by the WSN since its inception. Each of 12 underground stations (at that time) recorded full waveforms, the closest site approximately 700 m from the source.

(1.6) The Study Area

The Postma dyke and environs provide a good opportunity for analysing seismicity in terms of rock mass behaviour and stability because of the structural complexity and high incidence of seismicity. Geophone coverage is good and in some instances it has been possible to correlate recorded tremors with actual underground observations of deformations (van Aswegen, personal communication). The location of Western Holdings Gold Mine within the Welkom goldfield in relation to some neighbouring mines is pictured in fig. 1.5. Mine shafts are indicated by the squares; seismic stations are indicated by the triangles. The rectangle south of Western Holdings' number three shaft encloses the study area, shown on plan in fig. 1.6, with the outline of the mining faces along the Basal Reef and the positions of the major structures. The areal extent is relatively small: approximately 800m by 800m. The major geological structures can be well represented by simple geometric models to assist with visualisation and interpretation (see fig. 1.8).

The depth of mining of the Basal Reef is around 1800m below datum (1500m below surface) but varies according to reef blocks by up to 100m. A vertical stress gradient of 0.030 MPa/m produces a vertical stress of 45 MPa; the horizontal stress is half of

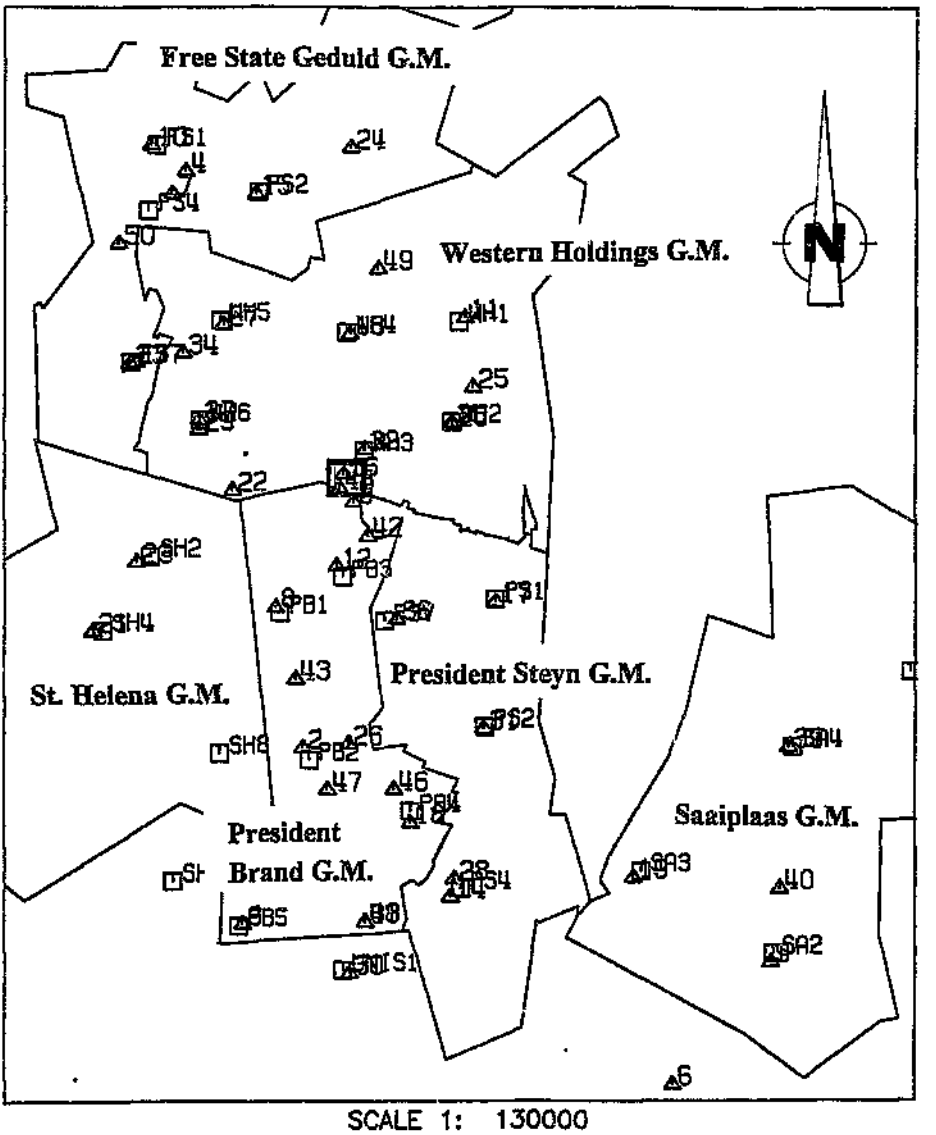


Fig. 1.5: Extent and location of Western Holdings Gold Mine within the Welkom goldfield in relation to some of the neighbouring mines. The squares represent mine shafts; the configuration of seismic stations at the time of this study is indicated by the numbered triangles. The rectangle south of Western Holdings' #3 Shaft encloses the study area.

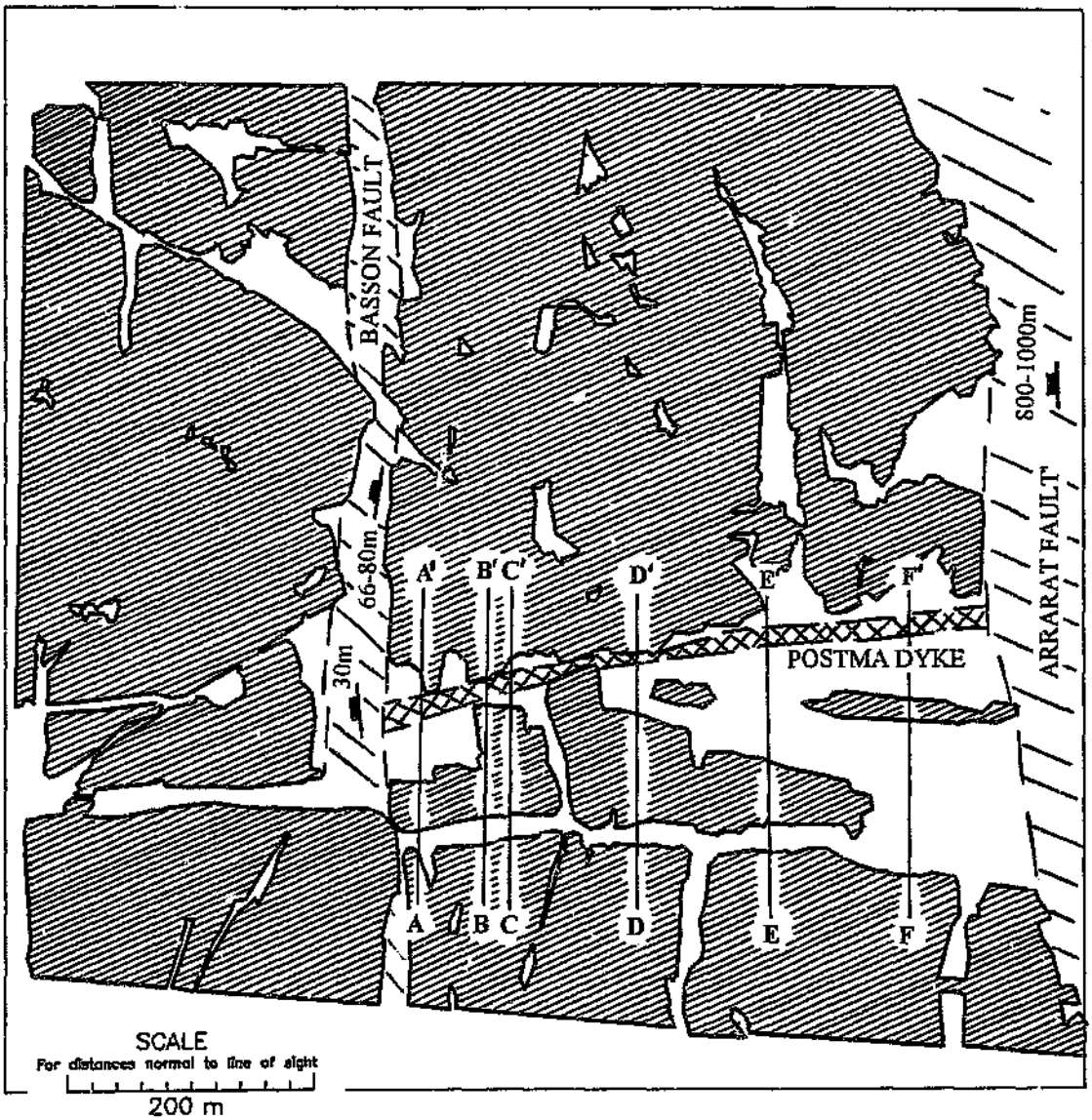


Fig. 1.6: Plan of the study area with the outline of mining faces along the Basal Reef (as at September 1993 -- shaded portion indicates mined reef) and positions of major geological structure (with dip direction and throw as indicated). The lines represent the location, extent and orientation of sections through the reef, shown in fig. 1.7, in Appendix A.

that. The reef blocks are displaced by north-south striking, westerly dipping faults in a normal sense, with minor shifts in dip and strike directions. The general dip is approximately 25^0 eastwards. Most of the reef has been mined out; remnants that were not extracted previously were the focus of all mining activity at the time of this study.

Basal Reef is over- and underlain by medium bedded quartzites. Bed thicknesses vary from 0.2m to 1.0m and thin (0.002m to 0.02m) argillaceous layers separate the individual quartzite bands in many cases. The direct hanging-wall of the ore-body consists locally of the khaki shale in a band between 0.2m and 0.8m thick, separated from the Basal Reef by about 1.0m of quartzite. It creates hangingwall instability with frequent back-breaks in stoping areas. The mining area was limited in the east by the Arrarat Fault and in the west by the Basson Fault.

The most important geological structure from mining and seismicity considerations is the Postma dyke. Several strong tremors have been directly linked to it. The dyke is approximately 10m thick, dips northerly at an average of 85^0 and has an average strike of 264^0. It is planar over the area of interest. It consists of dolerite with a uniaxial compressive strength of 160 - 190 MPa and Young's modulus of around 70 GPa – i.e. it is approximately 25% stronger than the country rock (J. Lategan, personal communication, 1994). Three joint sets characterise the dyke, one vertical and parallel to the dyke, one almost horizontal and the third nearly vertical and normal to the dyke. The joints are, however, welded and only become visible where the rock is broken through blasting or rockbursting. Diamond drill cores from beyond the stress fracture zone of mine openings are solid and broken only by the logistics of the diamond drilling process (van Aswegen, personal communication).

Geological sections are presented in figs. 1.7a-f (Appendix A); the location and orientation of these sections is shown in fig. 1.6. North of the Postma dyke, in some parts, a dolerite sill lies above the reef and interacts with the band of khaki shale, disrupting mining. The sill is another intrusive body with similar properties to the

Postma dyke. It is generally situated in the footwall south of the Postma dyke, at a greater depth in the east than in the west, and is displaced by various minor faults. Both the Arrarat and Basson faults dip westerly at about 65^0.

Simplified geometric '3D' models of the Postma dyke and Basson fault surfaces are displayed in fig. 1.8.

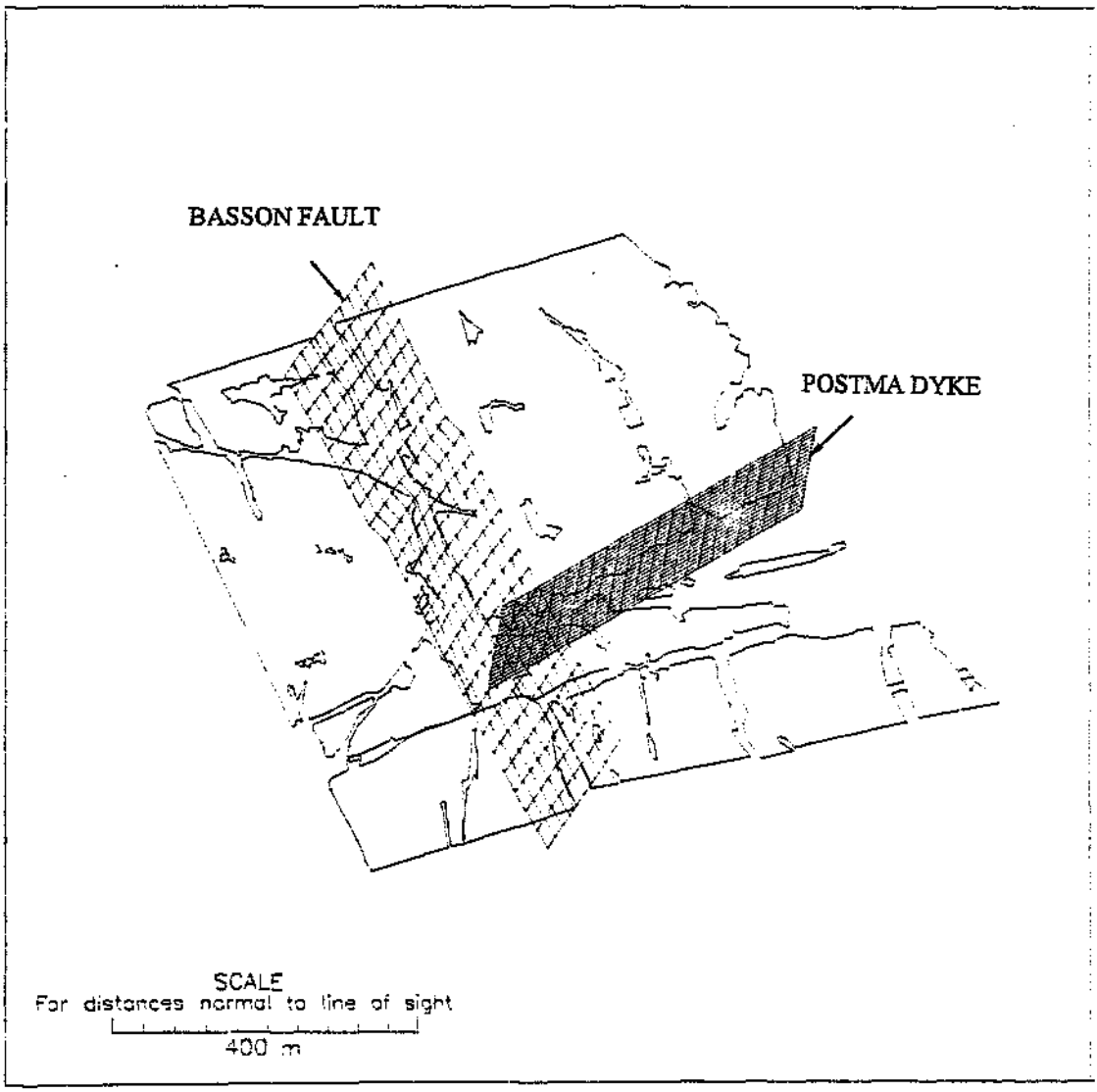


Fig. 1.8: Simplified geometrical '3D' models of the Postma dyke and Basson fault surfaces.

2

THEORETICAL BACKGROUND

(2.1) Review of Earthquake Precursory Phenomena

Seismic events in mines range from minor microtremors (rock talk) to tremors of considerable magnitude, comparable to and physically indistinguishable from natural earthquakes (e.g. McGarr, 1983, p121-124, Scholz, 1988, p331). Much of the science and thinking that applies to one also applies to the other. The following sections in this chapter review precursory phenomena and methodologies in earthquake prediction, as a background to the hypotheses tested in later chapters.

(2.1.1) General

Over the last century many precursory procedures have been proposed in an attempt to distinguish the best strategies for the difficult subject of earthquake prediction. More specifically, earthquake prediction specifies the expected size, geographical area and time within which the impending earthquake is expected to occur (Iyer, 1986, p1-2; Scholz, 1988, p335-337).

Prediction is usually based on three categories: long-term (years to decades in advance), intermediate term (a few weeks to years in advance) and short-term (hours to a few weeks in advance). In the long term, major engineering works are planned and implemented, to mitigate damage and loss of life. The recurrence time of

earthquakes on a certain fault segment are determined and the approximate time of the next earthquake is predicted using the known time (and size) of the previous one. In the intermediate term preparations can be made and emergency services established. Over the short term warnings and alarms are issued to the general population. Both intermediate and short term prediction involve the identification of precursory phenomena or any anomalous signals of various kinds observed in the vicinity of and some time prior to the occurrence of an earthquake.

The analysis of seismicity in mines, in comparison, involves much shorter time periods and sizes of tremors usually several orders of magnitude less than natural earthquakes. Studies attempting to estimate the increased likelihood of imminent instabilities are limited by the size of the available microseismic database, usually only a couple of years. Precursors thus obtained are labelled 'long-term'; over a shorter time scale (say, days to weeks before a 'major' tremor) they are denoted as 'short-term'.

Natural earthquake prediction projects normally bring together various fields, including geodetic, seismic, geomagnetic, geoelectric, hydrologic, oceanographic and geochemical studies, along with other continuous observations of crustal deformation, gravimetric surveys and seismic velocity changes (Mogi, 1980, p635; Asada, 1986, p13).

Seismic precursory methodologies for tremor prediction are mostly divided between those dealing with observations concerning the propagation of seismic waves, those concerned with time and space characteristics of seismic events, and those formulated in hazard analysis. Some approaches use a combination of the above (e.g. Scholz, 1988, p336, 348).

(2.1.2) Seismic patterns:

As an example of a direct application of 'patterns' -- in this case to delineate a structure, not to predict an event -- it has been observed that microearthquake alignments in a highly seismogenic region were able to indicate several linear active structures, which were subsequently geologically identified on the ground (Saha, 1986, p247).

More geared towards actual prediction, the seismic cycle hypothesis proposes that a principal rupture constituting some major seismic event is followed by an aftershock sequence, decaying hyperbolically in time into a postseismic period of quiescence (a significant decrease in the rate of occurrence of background earthquakes below the normal rate). About 50 - 70% of the total time before the next large event is occupied by the quiescent period, which usually extends over the entire region surrounding the rupture zone. Then follows a general increase in the 'background' seismicity, followed by a shorter (intermediate- term) length of quiescent time. Typically it extends over the whole zone surrounding the source, lasting for several years, and a 'doughnut pattern' appears (e.g. Mogi (1985), as discussed by Scholz, p340-341). The subsequent principal rupture may be preceded by immediate foreshocks, usually beginning weeks or days before the mainshock and normally concentrated close to the focus. A short-term quiescence which produces a pronounced lull in foreshock activity is often apparent, occurring just prior to the final rupture. The foreshocks and the third period of quiescence may be regarded as short-term precursors, and the pattern of foreshocks, the 'doughnut pattern' and the second period of quiescence as intermediate-term precursors (Scholz, 1988, p341).

Segments of tectonic plate boundaries which have exhibited long periods (decades to centuries) of seismic quiescence are known as seismic gaps, a concept developed by Fedotov, Mogi and others, as described by Iyer (1986, p2). This theory is generally applicable only to moderate and large earthquakes (magnitudes greater than 7) and does not provide predictions for time frames less than 10 years. Zones of seismic quiescence extend only over a few tens of kilometres. These have been called 'gaps of the second kind' by Mogi (1985)(Iyer, 1986, p4), and should not be confused with the gaps described above.

Kisslinger (1986, p23) described seismic quiescence as one of the most promising intermediate-term precursors of large events, citing a case study which generally fulfilled the forecast. The 'normal' rate of occurrence and its geographical location was determined empirically; fluctuations from the average rate of occurrence were tested for statistical significance, whereupon 'activation' or 'quiescence' was identified. Errors of the order of 0.5 units in magnitude, 50 km in distance and 6 months in time were acceptable, but a high false alarm rate was not. Kisslinger also conducted a search for rate changes in the aftershock sequences but did not find evidence that the strongest aftershocks were preceded by relative quiescence, which could have been useful for real-time prediction.

The importance of separation and recognition of actual decreased seismicity rates from artificial rate changes was discussed by Wyss (1986, p201-215; 1987, p526-528). The removal of aftershocks, foreshocks, swarms and doublets from a seismic catalogue, and the correction of the catalogue for inhomogeneities in reporting (e.g. change in the number of stations covering some area may change the rate of events located; magnitude shifts due to the difference between the various magnitude scales and

between different regions; changes in recording devices, or even personnel changes), defines the true seismicity background.

A method of detecting seismic quiescence involves an analysis of the available seismic catalogue to make certain that changes in reported seismicity rates are not artificial. Events which are not homogeneously reported may be eliminated by using a lower magnitude cut-off (M_{min}). The more the data, the better the definition of quiescence, so M_{min} should be chosen as low as possible. Since magnitude shifts also create artificial rate changes omitting small earthquakes below M_{min} does not guarantee a corrected, homogeneous catalogue (Wyss, 1987, p527).

Wyss reported two successful predictions of mainshocks based on the interpretation of locally decreased seismicity rates as precursory quiescence. A seismic gap was used to define a target volume. Next, the calibration area was defined (i.e. the tectonic area used for evaluating the rate of occurrence of quiescence similar in significance to the 'target anomaly'), ideally of uniform tectonic character and about 10 times larger than the target area (e.g. for a mainshock source length of 7 km, a segment of a fault between 60 and 100 km was used for comparison). The calibration area was searched systematically, and in randomly positioned volumes, for significant rate changes other than the 'target anomaly'. The calibration area was subdivided into segments of dimensions equal to the target volume. The intent was to search each of the subsegments for seismicity rate fluctuations. In the next step the duration of the target window was defined, and the time of change from background seismicity rate to the reduced rate before the mainshock was measured. Next, the significance of the anomaly and the false alarm rate was evaluated. After following this procedure the anomaly was 'defined' quantitatively with the following parameters: duration, amount

of change, relative significance compared to other periods of low rate and other cases of precursory quiescence, and the approximate spatial extent of the anomaly. Rastogi (1986, p79-84) studied space-time patterns of tremors in several micro-earthquake sequences in reservoir areas and reported increased foreshock activity for six days preceding about a day of relative quiescence prior to the main shock. In two instances tremors of magnitudes 2.8 and 2.2 were successfully predicted.

During seismic quiescence the activity rate may decrease from 45% by up to 90% (Wyss, 1987, p526). All quiescent anomalies seem to have abrupt beginnings, and the rate during the anomalous time is fairly constant. The duration of the precursors range from 15 to 75 months, and although mainshocks can be predicted, interpretation of the data in real time is difficult and non-unique. The failure to predict may be around 50%, even in carefully monitored areas. False alarm rates may be less than 50%, using corrected data sets. Tectonic environments with low microseismic activity render quiescence, as a precursor, unusable (Wyss, 1987, p526).

A magnitude dependence of precursory seismicity patterns was reported by Taylor, Snoke, Sacks and Takanami (1991, p1254). Significant changes in seismicity preceding a large earthquake (M = 7.1) were noticed: there was quiescence for the two years preceding the main shock, surrounding, but excluding, the immediate epicentre, and only for magnitudes 3.0 and greater. During the same time span, there was an increase in the number of small (magnitudes less than 2.4) events restricted to the general focal region of the main shock.

Conventional methods such as cumulative number of events versus time for selected magnitudes in a bounded geographical region allow seismicity anomalies to be seen,

but knowledge or assumptions about the prospective target region and magnitude range are required *a priori*.

Long sequences of foreshocks are not common, but small numbers of foreshocks occur before a large fraction of major earthquakes (M 7.0 and greater). Jones and Molnar (1979, p3596, 3607) investigated characteristics of foreshocks and their possible relationship with premonitory slip on faults. Along the idea of a seismic cycle, as discussed earlier, the authors found an increase in seismicity approximately as the inverse of the time before the main shock (except for a possible temporary decrease about six hours before). The relationship was essentially unrelated to the magnitude of the mainshock. The magnitude of the largest foreshock was also unrelated to the magnitude of the main shock. By assuming the existence of an inhomogeneous fault plane Jones et al. derived an equation for accelerating premonitory fault slip as a function of time, in agreement with the observed time dependence of foreshocks. They suggested that foreshocks alone are insufficient for earthquake prediction.

Migration of seismicity has been observed to accompany large earthquakes, usually along a seismic belt or a tectonic zone corresponding to a boundary of tectonic blocks. The velocity of migration was found to be several to 10km per year in the area investigated by Yoshida (1991, p167-169, 174). A change of seismic activity was considered a good indicator of stress state in the crust, and was often observed along zones (tectonic belts, boundary zones) passing through the focal region of large tremors. This supports the notion that a change of stress due to the occurrence of a large earthquake is likely to be transferred along tectonic block boundaries (i.e. the spatial pattern of seismicity change reflects tectonic structure in each region and may

thus be used as a precursory indicator of large events to come). Patterns were not always the same for different regions, but allowed an estimation to be made on how the focal region was interrelated mechanically with surrounding areas, and what regions were most influenced by main shocks, indicating where the next large earthquake might occur (Yoshida, 1991, p170-171, 174). Four earthquakes ranging in magnitude from 6.1 to 6.4 were predicted from the migration of seismic activity in one direction along a seismic belt (Mogi, 1980, p644).

Four earthquake sequences were studied by Latoussakis, Stavrakakis, Drokopoulos, Papanastassion and Drakatos (1991, p299, 309), in order to investigate temporal patterns in aftershock activities prior to large aftershocks (which were followed by secondary aftershocks). It was recognised that before such large aftershocks, the whole aftershock area of the main shock became quiescent, with a subsequent recovery of the aftershock activity to a normal level, or an increase beyond the normal level prior to the large aftershock. The authors concluded that if quiescence and recovery were observed in real time, then a significant aftershock could be expected, with a location in the vicinity of the aftershocks during the recovered stage. The precise magnitude and time of large aftershock occurrence remained elusive.

The usefulness of a precursor for actual predictions depends on the number of false alarms generated (Wyss, 1987, p528).

Time predictable models indicate that if the fault slip associated with a previous large earthquake (or the average fault slip of the past several earthquakes) is known, and using a known slip rate, then the time of occurrence of the next major earthquake may be estimated. This concept has led to three possible earthquake recurrence models,

originally explained by Shimazaki and Nakata (1980) (Iyer, 1986, p2-3). In the first model, the fault slip is constant for every earthquake, leading to a constant recurrence interval. In the second model, the fault slips are not constant, and it can be assumed that the time interval is proportional to the amount of slip in the previous earthquake. In the third model, the time interval is proportional to the amount of fault slip in the following earthquake.

Geodetic measurements and analysis of seismic waves in some regions of the world give the amounts of co-seismic strain or stress drop of large earthquakes. These, along with known deformation rates, may be used to calculate recurrence intervals of tremors. An investigation of repeat times of large earthquakes at plate boundaries had earlier led Sykes and Quittmeyer to the following conclusions (Iyer, 1986, p3):

Time predictable models have a predictable and a random component. The predictable component is the critical or failure stress (which remains more or less constant). The random component is the stress drop associated with the tremor itself. It could vary, depending on the arrest of rupture by asperities (described in Section 2.3.1) as well as other factors. If a pair of previous calibration events are available whose ratio of displacements are known or can be calculated, then the repeat times may be estimated to within 2% to 5% of observed times. Average displacements, stress drops and repeat times (which could vary by a factor of two or more in the same locality) are strongly related to the size of the rupture zone. When a shock smaller than expected occurs, the next shock should occur sooner, rather than being a large one to make up the deficit.

On the basis of recurrence time or regularity in seismic activity coupled with crustal deformation from geodetic surveys and observations of other non-seismic precursors (such as linear and volumetric strainmeters, tiltmeters, tide gauges, groundwater levels and temperatures, and Rn content) some regions have displayed an increased potential for large tremors in the near future (years) (Mogi, 1980, p635, 660-661, 663).

The spatio-temporal distributions of micro-earthquakes (with magnitudes of around 1.0 and 2.0) are considered important for prediction (Mogi, 1980, p640), the delineation of which have been found along a number of active faults. In other cases, along some active faults, no appreciable activity has been recorded, suggesting either a difference in the mechanical state of the active faults or a difference in stages of fault movements.

Fault planes that are flat and homogeneous may permit relative movement without any marked stress concentration. In such a fault zone, the degree of appearance of precursory phenomena may be low, as suggested by laboratory experiments (Mogi, 1980, p661-662). Faults which are highly compressed, fractured and irregular may have stress concentrations at many singular points and show appreciable precursory activities, such as foreshocks and deformations, at these points, corroborated in the laboratory, before large earthtremors (Mogi, 1980, p662; in Section 2.3, factors which influence the stability along faults and dykes are discussed).

Relevance of seismic patterns in natural earthquake studies to the analysis of mining-induced seismicity:

More than any other method used in seismic precursory methodologies for mining-induced tremors, the identification, delineation and inter-relation between seismic patterns have proved to be the most successful. It is usually a clustering of seismic events in space and time within some volume of the rockmass that first draws attention to a particular area. Experience has shown that an imminent instability may often be preceded by an increased rate of seismicity, or 'foreshocks', a few days or hours before the main event, usually in the vicinity of the main rupture focus. The clustering and increased rate of seismic occurrences may be regarded as a precursor, the timely identification of which could be viewed as prediction.

Kijko and Funk (1994, p3,4-6) described the formulation of a space-time clustering analysis algorithm to detect anomalous clusters of seismicity in mines. When applied to one seismically active gold mine in South Africa, the algorithm was shown to be able to detect several clusters of seismicity in the mine, with an interaction of seismicity amongst clusters. The degree of interaction was found to be a function of distance; as distance increased, a distinct decrease in the value of correlation coefficients (during cross-correlation analysis of the seismic activity rates and radiated energy) was noticed.

Dennison (1993), studying the behaviour of faults, describes a seismic cycle (e.g. Scholz, 1988, p222-224, 340-341), akin to that proven for crustal earthquakes, consisting of three phases: firstly, aseismic shear deformation as a function of adjacent mining; secondly, coseismic shear deformation, due to the advance of the zones of strain in the previous phase, leading to foreshocks preceding large events, which form

the third phase of the cycle. Each phase depends on the previous, in terms of magnitude and extent, and fault-related seismicity was shown to be a sequential occurrence of seismic events, in accordance with an asperity model. The asperity model applied to the spatial prediction of mine tremors along geological discontinuities is possibly the single most useful direct application of earthquake seismology theory in mines (van Aswegen, personal communication) and is discussed in more detail in Section 2.3.1. As an extension of the asperity model, seismic gaps, re-defined as volumes of restricted seismic strain surrounded by volumes of high seismic strain, are recognised as important for the spatial prediction of mine tremors (e.g. Mendecki, 1997, Chapter 11).

Experience has shown that fluctuations from the average rate of event occurrence, or activity rate, must, in the mining environment, be interpreted with caution. It is required to distinguish fluctuations directly resulting from fluctuations in mining rate to that possibly pertaining to large instabilities.

A time-analysis of seismicity may sometimes show an almost constant recurrence interval of larger magnitude tremors, leading to time predictable models. These models, along with the algorithm proposed by Kijko and Funk (1994, p4-6), fall into the realm of probabilistic methodologies (discussed in Section 2.1.4) which can be applied to generalised hazard quantification (a pre-requisite for risk assessment) but is of limited use in temporal prediction.

(2.1.3) Seismic wave propagation:

The propagation of seismic waves through a seismic source region can give an indication of a change in physical properties (Scholz, 1988, p348). The ratio of compressional and shear velocities (V_p/V_s) has been found to decrease by between 10 and 15% within a zone surrounding the rupture and then to recover to its normal value just prior to the tremor (Dieterich, 1978, p3940; Scholtz, 1988, p348).

In the course of a study of reservoir-induced seismicity, Stevenson and Talwani (1986, p117-133) monitored changes in the ratio of shear and compressional travel times (t_s/t_p). They found premonitory changes in four out of ten larger events (local magnitudes around 2.0 and 3.0), and went on to predict two earthquakes at a later stage by noting anomalous changes in the t_s/t_p ratios of events (foreshocks) that preceded them. For homogeneous conditions, the V_p/V_s ratio is equivalent to t_s/t_p, and the two terms have been used interchangeably.

By recording seismicity associated with the impounding of reservoirs, Rastogi (1986) reported t_s/t_p anomalies one to four weeks prior to tremors of magnitudes ranging from 2.1 to 2.7.

Stevenson and Talwani (1986, p118) observed that the duration of the anomaly from the moment the t_s/t_p ratio began to decrease until the time it returned to normal (or t_s/t_p 'bay') was proportional to the magnitude of the impending earthquake.
Iyer (1986, p6) declared this technique as being no worse or no better than any other of the intermediate- or short-term earthquake precursors, and has recently been less favoured as a predictive tool (Asada, 1986, p16; Scholz, 1988, p348).

Scholz (1988, p348) notes that the shear wave coda is a scattered wavetrain that samples a volume, the study of which is better suited to investigate the rupture preparation zone. According to him, V_p/V_s observations to indicate seismic wave velocity changes are inappropriate since body waves are refracted away from the rupture zone.

Vertical seismograms of small earthquakes which occurred in a small volume in an aftershock region of a magnitude 6.0 crustal earthquake were analysed by Sato (1986, p2049; 1987, p1356). A seismic source emits a shear wavelet which is scattered by heterogeneities in the earth medium, arriving at the receiver after the direct S-wavelet. A number of these waves, scattered by distributed heterogeneities, arrive at different times, and create a smoothly decaying tail or coda. The coda excitation is dependant on the attenuation and scattering characteristics of the local earth medium between the source and receiver. The shorter the coda duration, the smaller is the extent of the scattering volume traversed by the coda waves (Sato, 1987, p1357). Observations were interpreted in terms of the coda duration and the attenuation intensity (or scattering) of the S-wave (Q^{-1}_s). The average magnitude was defined as the arithmetic mean of station magnitudes which were calculated from the maximum amplitudes of direct waves. The temporal change in attenuation intensity was measured for a period of months before and after the main shock using two methods: firstly, the station magnitude, as calculated from the maximum amplitude of each station, was compared with the average of station magnitudes; secondly, the S-coda duration from the origin time was measured and was compared with the average magnitude. In the first instance, deviations of station magnitude from the average magnitude at five stations in the vicinity of the aftershock area were found to have increased after the main shock relative to the situation before. In the latter, an increase in the S-coda duration

for the same average magnitude was observed after the main shock at two stations close to the main shock epicentre.

In another case, where the temporal variations of coda durations were studied in relation to a crustal earthquake of magnitude 6.8, Sato (1987, p1356-1357) found that the coda durations for earthquakes of the same average magnitude were significantly longer during the 16-month period preceding the main shock than those before and after this period. Although the results were contradictory in terms of coda durations measured before a main shock, it appears that a change in Q^{-1}_{s} some time preceding an earthquake may be interpreted as an earthquake precursor, usually with a temporal increase.

The time variation of physical parameters obtained from waveform analysis of microevents (local magnitudes from -3.0 to -1.0) occurring before and after large mining-induced seismic events (local magnitudes greater than 0.5), originating on a stressed dyke due to mining in the vicinity, were investigated by Cichowicz (1991, p16). The degree of polarisation of P-waves was found to decrease before each large event, beginning from 0.5 to 2.0 days before the main events. The data also indicated higher stress drops associated with foreshocks than with the average corresponding microevents.

The anomalous variations of the degree of polarisation, together with other independent precursory measurements could reduce the number of false alarms, increasing reliability of hazard assessment (Cichowicz, 1991, p19).

A shear wave, upon entering an anisotropic region, necessarily splits into two fixed polarisations which travel at different velocities, becoming separated in time, originally described by Crampin (1984, 1987) (Booth, 1991, p299; Peacock, Crampin and Booth, 1987, p6). A characteristic signature is produced by the shear wavetrain. At incident angles less than about 30^0 to the crack planes of a medium (which are parallel), the component polarised normal to the crack face travels slower and is more attenuated than the component with displacement parallel to the cracks. The polarisation of the leading (faster) split S-wave is fixed by the crack geometry along the propagation path. The directional alignment imposed by local stress fields creates stress-aligned fluid-filled cracks in most rocks of the earth's crust. These cracks are seismically anisotropic and their distribution is known as extensive- dilatancy anisotropy (EDA).

Since shear waves are more sensitive than P-waves to details of the internal structure of the rockmass along the raypath, and since the build-up of stress and strain before an earthquake must involve significant changes, then it is this analysis of S-waves and S-wave splitting that offers an indication of changes in the rockmass before earthquakes (Crampin, 1991, p305). An increase of stress will modify the behaviour of the shear wave splitting (or birefringence), changes in which have been reported before and after large earthquakes (Crampin, 1991, p306; Booth, 1991, p299-302), suggesting that such variations are a precursor to earthquakes (Peacock *et al.*, 1987, p2).

Foreshocks do not have a recognisable distinction from other earthquakes, which makes their utility difficult in earthquake prediction (Scholz, 1988, p356). Fujiura (1979) had earlier found that the waveforms of some earthquakes in an earthquake

swarm were completely similar, while the waveforms in a foreshock sequence of a large earthquake were always different (as reported by Mogi, 1980, p651). Waveform similarity could therefore be a useful method of discriminating foreshocks from earthquake swarms.

Analysis of seismic wave propagation in mining-induced seismicity:

Seismic tomographic imaging of seismic wave velocities through 3D inversion of mine seismic data has been shown to be useful for the demarcation of rock strength / stress variation in mines by Prof. Paul Young and his co-workers (e.g. Maxwell and Young, 1996). In a back analysis of data from the Postma dyke area, they show how a local magnitude 3.7 event (see Section 4.2.7, Chapter 4, for a description of this tremor) was preceded by a high in seismic wave velocity, indicating local stress concentration prior to failure (see Mendecki, 1997, Chapter 6). Although their work holds obvious promise, the lack of software that can be routinely used in the mining environment severely limits the application of the technology.

(2.1.4) Stochastic methodologies in hazard assessment:

Estimating the hazard presented by earthquakes is related to long-term prediction. When employed for a specific region stochastic methods assess the seismic hazard and express it in probabilistic terms (Scholz, 1988, p377).

The combination of various precursors to increase prediction effectiveness several times has been approached, and Sobolev, Chelidze, Zavyabov, Slavina and Nikoladze (1991, p255, 260-262) describe a technique for the compilation of maps of expected

earthquakes. The conditional probability of future tremors was obtained using geotectonic data, geodetic measurements and spatio-temporal changes in a number of seismic parameters, including density of seismogenic faults, slope of the recurrence curve, seismic quiescence, seismic energy release and ratio of P- and S-wave travel times. The probabilities of false alarms and detection, mean recurrence times and areas, and efficiency of prediction were calculated from back-analysis of earthquakes with local magnitudes greater than 5.0. Main zones with a high probability of future earthquakes were delineated on the map. In retrospect it was found that earthquakes, if and when they occur, will be expected to be located within the indicated zones of increased probability, but outside the centres of anomalously active zones. This suggests that the larger earthquakes generally occur at the edges of areas of maximum seismic activity, and would be consistent with one hypothesis tested later in this dissertation, in Chapter 4, namely, that high gradients in (seismic) strain are conducive to sudden unstable deformation.

The effects of incomplete data coverage have often been mitigated by using the frequency-magnitude relation (Scholz, 1988, p378). Small earthquakes are recorded in a region, and then extrapolated to calculate the recurrence time of potentially damaging earthquakes of larger magnitude. However, if the larger magnitude events belong to a different fractal set or population group than smaller earthquakes, they cannot be predicted by such extrapolation.

The b-value of acoustic emissions in the frequency-magnitude relation (i.e. the slope of the line relating earthquake magnitude and the logarithm of the number of earthquakes in that magnitude) has been shown empirically to decrease prior to rock fracture, whether by increasing stress or time (in creep tests) (Scholz, 1988, p356). Time variations of the b-value for the world earthquake catalogue (1964 - 1980, M4.0 and greater) within days and hours before a mainshock showed a drop to half during a few hours before mainshocks (Molchan and Dmitrieva, 1990, p99). The effect is not always observed, however, and a tremor may be accompanied by an increase of

background seismicity without a change of b-value. Regional events are usually preceded by a low b-value (e.g. Rastogi, 1986, p79, 83-84; Guha, 1986, p31-37; Biswas, 1986. p217-221; Scholz, 1988, p356; Imoto, 1991, p311, 322-324), likely at or below the level of the long-term mean minus one standard deviation (Niazi, 1986, p91). Reported successes in prediction have been mixed, but seem to be more associated with reservoir-induced seismicity (Iyer, 1986, p7).

Imoto (1991, p311) described a method to estimate temporal and spatial variations in the magnitude-frequency relation, where the space-time volume under investigation was divided into a number of segments with equal volumes, for which b-values were estimated. The introduction of a prior distribution smoothed the b-values (i.e. made the b-values stable and inhibited direct effects) and enabled the spatio-temporal variations of b-values for microearthquake activity to be studied. The quantitative definition of patterns of b-decreases made it possible to determine whether the decrease in b is a precursor of -- or only coincidental with -- earthquakes. A time sequence of b-values was used for a certain region, and a segment in time was defined as a 'decrease' if it satisfied some strict conditions. The results of the analyses indicated that decreases in b-values are likely to appear a few years before earthquakes having a magnitude of 6.0 and greater.

In a departure from the approaches above, Keilis-Borok and Kossobokov (1990a, p73-74; 1990b, p12413) described an algorithm designed for diagnosis of times of increased probability (TIPs) of strong earthquakes, which the authors called 'algorithm M8'. The name refers to the world's strongest earthquakes with M 8.0 and greater, for which the algorithm was first designed. The earthquake flow was considered within a certain area, and the TIPs associated with earthquakes of magnitudes equal to or above

a certain threshold M_t were searched for, unless they were aftershocks of some stronger earthquake. The magnitude M_t of the strong earthquakes for which TIPs were diagnosed determined the size of an area (several times larger than that of an incipient earthquake). The seismic territory under consideration was scanned by overlapping areas. Several integral traits of earthquake flow (current levels of seismic activity; the deviation of seismicity from a long linear trend; the concentration of mainshocks in space, and the clustering of earthquakes as depicted by the maximal count of aftershocks) were estimated as functions of a sliding time window. If most of them became extremely large within a certain narrow time interval a TIP was diagnosed for a time period in each area independently.

In the course of a world-wide test the algorithm revealed TIPs before 34 out of 38 strong earthquakes (Keilis-Borok *et al.*, 1990b, p12422). Other results indicated that 39 out of 44 earthquakes investigated were preceded by specific activation of the earthquake flow in the lower magnitude range, as highlighted by the algorithm M8, thereby suggesting the possibility of intermediate-term prediction of the strongest earthquakes in the regions considered (Keilis-Borok *et al.*, 1990a, p73).

In a similar procedure -- algorithm CN -- TIPs were declared for a time period of one year and an area with linear dimensions of a few hundred kilometres, which could be extended in time. The algorithm was based on traits of an earthquake flow such as level of seismic activity; its temporal variation; clustering of earthquakes in space and time; their concentration in space, and their long-range interaction. The algorithm was normalised, enabling it to be applied to different regions without readaptation. TIPs were found to precede about 80% of strong earthquakes and take on average approximately 24% of the total time (Keilis-Borok and Rotwain, 1990, p57-58).

Kossobokov and Keilis-Borok (1990, pR1-R4) proposed that after a TIP had been diagnosed (by algorithm M8) for a certain territory, this area could have been narrowed down further by additional analysis of recent seismicity. The hypotheses considered a territory U diagnosed with a TIP. Earthquakes with $M > M_t - 4$ (e.g. if $M_t = 7.0$, then $M > 3.0$) were considered in the territory U during the time period, starting 6 years before the TIP. This territory was scanned by overlapping squares with sides equal to 3D/16, where D referred to a square territory U with size $D(M) = [\exp(M - 5.6) + 1]$ in degrees of meridian, or a circle of diameter D. Within the smaller squares the number of earthquakes in consecutive overlapping time intervals, of 2 months length, with 1 month step, were considered. Abnormally quiescent squares were singled out, where the number of earthquakes were in < 90% of all time windows. When at least 4 such squares formed a continuous cluster in time-space, then an area V < U was identified, where V consisted of all squares belonging to such clusters. The results of tests conducted on epicentres of strong earthquakes showed that the reduction of territorial uncertainty of forecasting (i.e. the ratio U/V) varied from 4 to 14. There was a failure to predict in only one instance. Final tests by advance forecasting remained to be done.

Molchan (1990, p80; 1991, p267-268) and Molchan and Kagan (1992, p4823-4825) presented the optimisation (minimisation) of a certain loss function (or goal function) in earthquake prediction which was dependent on two parameters: fraction of alarm time and fraction of failures to predict. By themselves, these parameters are two types of errors in earthquake prediction. However, taking into account the stochastic nature of earthquakes, long-term errors (i.e. the parameters above) become specifications of prediction strategy.

A statistical model was proposed by Lindh (1986, p189-190). It assumed that after the occurrence of an event on a given segment of a fault system the expected time of reoccurrence of another event on that segment was a random variable with a Gaussian distribution and standard deviation. The mean recurrence time was considered to scale with the ratio of the strain accumulation rate to the strain drop in the last event. The model also assumed that there was a characteristic stress threshold for each segment at which failure was likely to occur. Estimates were reported for a number of segments, which essentially constituted an assessment of the relative seismic hazard of some major active faults.

Ogata (1992, p19845, 19850-19853) discussed a statistical model for the detection of precursory relative quiescence before large earthquakes. Quiescence was defined as a decrease from the expected rate. Aftershocks were considered a useful signal for the investigation of seismicity, best left unremoved from original occurrence data. Using occurrence time and magnitude data a model was formulated. Known as Epidemic Type Aftershock Sequences (ETAS), the model identified patterns in an earthquake sequence, permitting detection of a clear, relatively quiet stage before large earthquakes in some parts of the world.

A formal definition of premonitory seismic quiescence was described by Schreider (1990, p113-115, 125-126). He suggested an algorithm which allowed the space-time distribution of zones of quiescence in a seismic region to be obtained through the non-linear transformation of the time scale into a discrete sequence of seismic events. During the transition to 'events scale' a function arose which was dependent on the number of a seismic event. It was defined as the difference of occurrence times of the

current event and the preceding one (i.e. the function defined the rate of seismic processes). Schreider suggested that abnormally large values of this function computed in a circle of some given radius should be interpreted as an indicator of seismic quiescence in this circle. The procedure of scanning a whole seismic region by mutually intersecting circles enabled the distribution of quiescent zones for the whole area under study to be obtained. Results indicated that all main shocks in a seismic region with M 7.1 and greater were preceded by seismic quiescent zones; over 50% of the total number of background seismicity events were also preceded by these zones. Similar results were obtained for a second region. The algorithm when applied to aftershock sequences also showed quiescence before the strongest aftershocks in a swarm.

A significant percentage of earthquakes have been preceded by foreshocks (Console, Murru and Alessandrini, 1991, p22). The usefulness of real-time hazard assessment with the probability that a given earthquake will be followed by a main shock, rather than preceded by a foreshock was evaluated. Console *et al.* (1991) made use of an algorithm which revealed foreshocks: having a catalogue of tremors, each with origin time, epicentral co-ordinates and magnitude, they considered as foreshocks the events exceeding a given threshold magnitude, provided these follow a period of quiescence and occur before a mainshock within a given distance range. The analysis of data indicated that the identification of foreshocks and their activity could be regarded as a useful precursor.

The time of occurrence of a future tremor depends on the size and the time of the occurrence of the last event (Anagnos and Kiremidjian, 1984, p2593-2594). The larger the earthquake the longer the time to the next earthquake. This observation led to the

development of a time-predictable stochastic model for earthquake occurrences. Essentially, stress accumulation and release on a section of a fault was investigated. It was found that stress build-up occurred at a constant rate until the accumulated stress reached a threshold. An earthquake then occurred, which released some portion of the accumulated stress. The size of the earthquake was proportional to the change in stress level on the fault. The occurrence time of the next tremor was determined by the length of time required to accumulate sufficient stress to reach the threshold and trigger another event. Since stress accumulation and release are difficult to measure, coseismic slip was used to estimate the change in stress levels; geological and historical data was used to calculate repeat times.

Time-predictable recurrence makes it possible to forecast the time of the next earthquake, given the size of the preceding event, but gives no information concerning the size of that tremor. Hazard estimates for a section of a fault, where data has suggested time-predictable behaviour, indicated a mean holding time of between 6 years for magnitudes 4.5 - 5.0 and 263 years for magnitudes above 7.5 (Anagnos *et al.*, 1984, p2593-2594).

Shaw, Carlson and Langer (1992, p479-480) made an analysis of patterns of seismic activity preceding large events in a mechanical block-and-spring model of a fault. The significance of the model (introduced in 1967 by Burridge and Knopoff) lies in the fact that, in the absence of stochasticity or spatial inhomogeneities, it generates dynamically a statistical distribution of both small and large slipping events, consistent with that observed under natural circumstances for a single fault. For the smaller events, the magnitude-frequency distribution N(m) of events of magnitude m is in

agreement with the fundamental statistical law governing the rate of earthquake occurrence (i.e. $N(m) = ae^{-bm}$, first presented by Gutenberg and Richter in 1954). The larger events were found to occur at a rate greater than the value extrapolated from the magnitude-frequency relationship, as observed along some major faults. The activity patterns of smaller events, preceding larger events, were studied statistically. With the model, the activity was found to accelerate very fast preceding a large event, reaching usually a maximum in the vicinity of the future epicentre. The results were compared with actual seismic data along a fault, where the model would forecast a large earthquake in the region. A tremor subsequently occurred some 30 km within the section of the fault where increased activity was recorded. However, the intrinsic dynamic properties of single faults are not known with precision, and many aspects of the subject remain controversial (Carlson, Langer and Shaw, 1992, p658). The catalogues of seismic events on which the Gutenberg-Richter law is based are usually associated with large regions containing many faults. The main benefits obtained from such studies are the insight gained in interpreting real data and the contribution towards the development of more realistic models, providing practical, quantitative tests for the validity of prediction schemes.

Stochastic methodologies in the analysis of mining-induced seismicity:

Statistical methods are likely to find their greatest application in seismic hazard assessment when large quantities of microseismic information need to be processed in a short period of time, requiring the automation of techniques not only in waveform processing, but also in the quantification of the rockmass response to stress changes (e.g. Sciocatti and Kijko, 1994, p4), to better identify instabilities in space and time.

Kijko, Funk and v.Z. Brink (1993, p1, 3-4) stressed the importance of a significant volume of high quality seismic data for the identification of anomalous patterns in time-dependent mine seismicity. They proposed a methodology, involving a cluster identification algorithm, operating in real time and independent of local geology or mining configuration, which detects clusterings of seismicity in space and time, possibly leading to a strong event. Temporal variations in seismic parameters inside the clusters were employed to assign a probability of occurrence of a seismic event (PSE), as a function of time, which would be above some specified value. The authors demonstrated the algorithm successfully, using seismic data from a deep-level gold mine in South Africa, and found that large events occurred during high or rapidly increasing PSE.

Stochastic models may describe the complexity of space-time distributions of seismicity generated by rupture processes (Sciocatti and Kijko, 1994, p3), explaining most of the observed statistical features of seismic event occurrence. One of the techniques used is based on the concept of fractals (originally introduced by Mandelbrot, 1989), which characterise sets exhibiting irregularity, regardless of the scale at which the set is examined. Sciocatti and Kijko (1994, p3) observed that, generally, processes close to a certain critical stage create power law distributions, such as the fractal relation. The authors pointed out that when applied to natural earthquake occurrence, and from microfracturing experiments on rock samples, it had previously been shown that this seismicity has a fractal nature with respect to space, time and size. Extending these concepts, they described the development of a fractal based stochastic model of seismicity in mines (p4-15), to determine whether a temporal variation in fractal dimension (associated with time and size distribution of tremors) may be used for prediction of strong tremors. In addition, they explained how

such a model can be used in mines for continuous evaluation of the probability of seismic event occurrence within a specified time interval (p15-17), giving an example of an application to an area surrounding a stope in a deep gold mine in South Africa (p17-18). The prediction in time of larger events (seismic energy greater than $5.5X10^6J$) appears to be subjective, but the authors, nevertheless, show that these events took pl e during periods of high, or increasing, probabilities of their occurrence.

The b-value in the frequency-magnitude relation should not be used in extrapolation procedures aimed at prediction using mining-induced small scale seismicity, mainly because larger magnitude tremors, in many cases, belong to a different population group of events or fractal set than the smaller tremors (e.g. Scholz, 1988, p378). In their cluster identification algorithm, Kijko *et al.* (1993, p2), however, account for curvature in the frequency-magnitude relation for a better evaluation of PSE.

Parts of 'algorithm M8' (Keilis-Borok and Kossobokov, 1990a, p73-74; 1990b, p12412; Keilis-Borok and Rotwain, 1990, p57-58), desig. ed for diagnosis of times of increased probability of occurrence of strong earthquakes in the tectonic scenario, are analogous to some concepts proposed by Kijko *et al.* (1993, p1-5) and Sciocatti *et al.* (1993, p1-22), applied to seismicity generated by mining. The authors (Keilis-Borok *et al.*, 1990a, 1990b, 1990c; Kijko *et al.*, 1993; Sciocatti *et al.*, 1993) describe promising methodologies, using overlapping areas to scan a seismic territory, deviation of seismicity from some previous trend, clusterings in space and time, and analyses involving time windows. But, as with analyses of the propagation of seismic waves (Section 2.1.3), the lack of software that can be used in the mining environment on a routine basis limits their application. It is possible that in the near future, where

seismic data of high quality and quantity (with enhanced computational power) are available, this type of prediction could be applied more extensively.

(2.2) Seismic Source Parameters

Seismic source parameters in South African mines are generally based on the Brune model, interpreting the seismic source as a circular dislocation on a plane (e.g. a fault plane), with two parameters describing it as the radius and the average displacement.

The far-field displacement spectrum is characterised by three independent parameters: the low-frequency spectral level (Ω_0), the corner frequency (f_0) (i.e. the intersection of the high- and low-frequency asymptotes) and the slope coefficient which governs the rate of high-frequency decay of the spectrum (fig. 2.1). This slope is assumed to be constant for the Brune model; the primary input quantities used in the calculation of source parameters are Ω_0 and f_0, obtained from the spectra of P- and S-waves at each station.

(a) The **seismic moment** (M_0), or scalar moment, is the most reliable and useful quantity measuring the strength of a seismic event (Gibowicz, 1993). Using the double-couple shear dislocation mechanism, this parameter is related to the faulting (e.g. Aki and Richards, 1980) as

$$M_0 = GAD$$
$$= G\pi r_0^2 D \quad \text{..... [1]}$$

where G = modulus of rigidity (or shear modulus)
r_0 = source radius
D = average displacement over the fault surface

A = area of rupture or slip

For mine tremors this parameter is obtainable from the displacement spectrum of seismic records (see fig. 2.1) through the equation (Gibowicz and Kijko, 1994)

$$M_0 = \frac{(4\pi V^3 \rho R \Omega_0)}{F_c R_c S_c} \quad \text{..... [2]}$$

where V = wave velocity (P or S)

ρ = density of the medium

R = hypocentral distance

Ω_0 = low-frequency asymptote to the displacement spectrum

F_c = wave radiation pattern (P or S)

R_c = free-surface amplification of wave amplitudes (P or S) (not underground)

S_c = site correction of waves (P or S)

Considering all the constraints in [2] it is clear that seismic moment depends entirely on the low frequencies of the displacement spectrum through Ω_0.

(b) Magnitude scales are often defined by amplitudes measured over some limited spectral band. However, the frequency range of radiated seismic energy changes with earthquake size (Aki, 1967), leading to limitations in recordable data. There are also discrepancies between the various magnitude scales (Hanks and Kanamori, 1979). More conveniently, the **moment magnitude** is defined as

$$M = (2/3)\log M_0 - 6.1 \quad \text{..... [3]}$$

where M_0 is in [Nm].

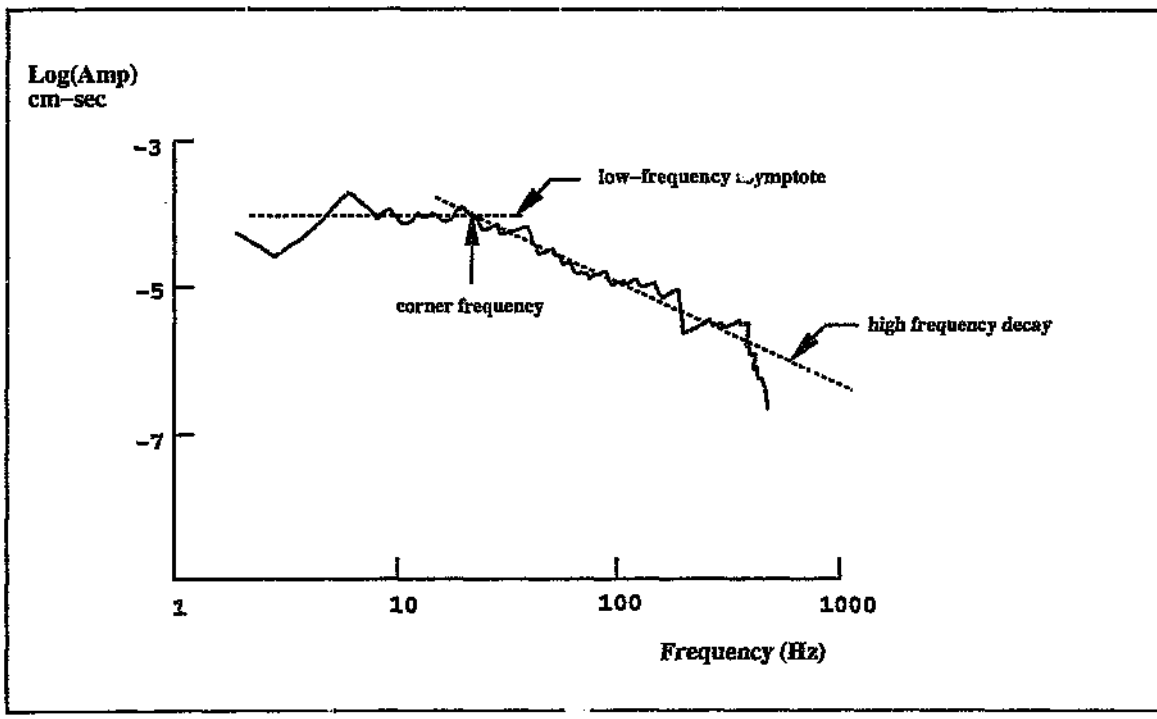


Fig. 2.1: Displacement spectrum of a seismic tremor (after McGarr, Seismic Design of Embankments and Caverns, 1983), typical of recorded ground motions in deep gold mines. The curve is described by three independent parameters: the low–frequency spectral level, the corner frequency and the high–frequency decay. The spectrum relates to a more complex rupture model, which the Brune model approximates.

The relation of **energy magnitude** was formulated by Gibowicz (1963) as

$$M = (0.526)\log E - 1.2 \quad \text{..... [4]}$$

where E is the total radiated seismic energy, in [J].

The present evaluation of **local magnitude** by the WSN follows the equation

$$M = 0.405\log(M_0) + 0.249\log(E) - 4.543 \quad \text{..... [5]}$$

which takes into account both moment and energy. The coefficients were obtained empirically.

(c) Determination of the corner frequency (f_0 -- see fig. 2.1) of either P- or S-waves allows source dimensions to be calculated. The **source radius** (m) is obtained from (Brune, 1970, 1971)

$$r_0 = \frac{KV_S}{2\pi f_0} \quad \text{..... [6]}$$

K is a constant dependent on source model and V_S is the shear wave velocity. For the simple Brune model (a circular area of displacement with immediate stress release), K=2.34, for S waves only. Gibowicz has shown on various occasions that in Polish mines this model is not applicable; whenever the size and geometry of underground damage caused by rockbursts could be estimated, the radius was considerably smaller than predicted (Cichowicz, personal communication).

(d) Various estimates of stress release during earthquakes have been used (Gibowicz, 1990); a representation of a change in stress is given by the static **stress drop**, defined as the average difference between the initial and final stress levels over a fault surface, determined from

$$\Delta\sigma = \frac{7}{16}(M_0/r_c^3) \quad \text{..... [7]}$$

It represents the decrease in shear stress promoting seismic slip over some circular fault area (Brune, 1970, 1971).

(e) Whereas seismic moment describes the general size (and deformation) of an earthquake, **seismic energy** gives a better description of the potential for earthquake damage to man-made structures (e.g. Gibowicz, 1993). It is a measure of the total elastic energy radiated by a seismic event. In relation to moment, the total energy ($E = E_s + E_p$) may vary by as much as a factor of 20 (Gibowicz, 1990; Mendecki, 1996). The radiated seismic energy of either P or S waves may be estimated directly from an integral, J (originally proposed by Snoke, 1987 (e.g. Gibowicz, 1988)), which expresses the energy flux of either P or S waves, through

$$E_c = \frac{4\pi\rho VR^2J}{F^2_c} \quad \text{..... [8]}$$

The loss of energy from attenuation is accounted for in the calculation of the energy flux (refer to, e.g., Gibowicz (1988) for a more complete description of this parameter), obtainable from seismic spectra.

(2.3) Fault / Dyke Stability in the Mining Environment

Geological structures are geometrically irregular and vary spatially in strength and, as such, there are factors which need to be considered when determining their stability under the influence of mining-induced stress changes.

(2.3.1) Asperities

Elastic rebound theory pertaining to natural earthquakes uses the earthquake cycle (e.g. Mogi (1985), as described by Scholz (1988, p340 - 341; discussed in Section 2.1.2, Chapter 2) towards prediction, proposing that faults remain locked while strain energy slowly accumulates in the surrounding rock and then sudden slip occurs, releasing this energy. The failure of the strongest and most dominant asperity completes a particular earthquake cycle.

In the mining context, the asperity model uses similar spatial heterogeneity in order to explain the characteristics of faults producing earth tremors. Asperities exhibit a stronger resistance to slip movements, being regions or patches on the fault surface with strong cohesion and/or frictional properties, thus opposing slip. Fig. 2.2 shows two schematic models of rupture which use the asperity scenario. The first model produces simple waveforms with the shearing of a single asperity. The second model, which is of comparable size of rupture and moment to the first, leads to multiple sub-events and a more complex seismic signature (McGarr, 1983, p117, 120). Stress accumulates at these points resisting movement on a creeping fault so that shear stresses or shear strength has to vary spatially.

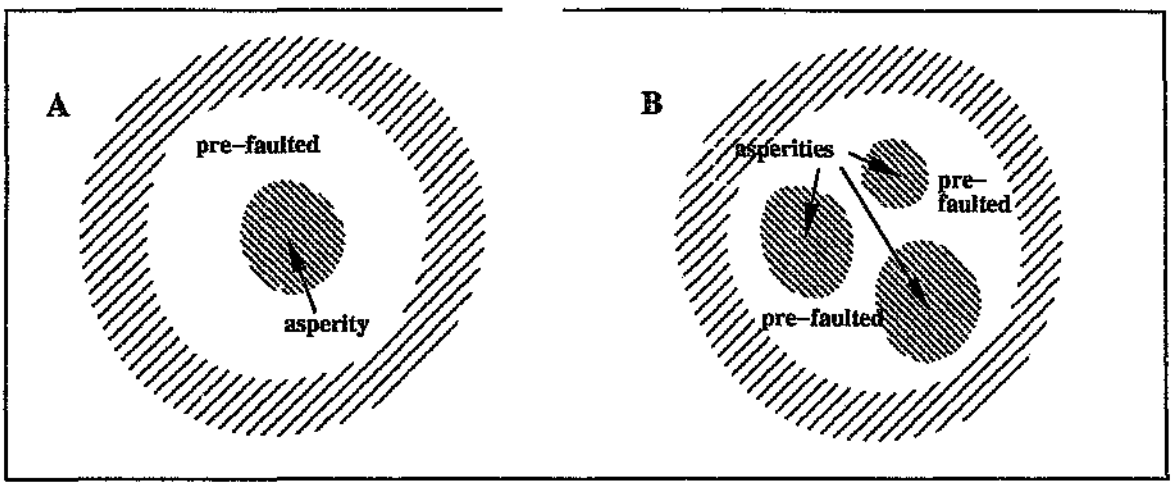


Fig. 2.2: Schematic models of rupture using the asperity scenario (after McGarr, Seismic Design of Embankments and Caverns, 1983). Model A involves an annular region where shear failure has previously taken place, surrounding a stronger asperity. The preceding failure may have taken place through fault creep or as a series of previous earthquakes. Occasionally, some of the preceding failure may occur earlier in the same seismic event (Model B), where the failure of multiple asperities leads to an enhanced loading of a major asperity that finally fails.

In his study of the stability of the Tanton fault at President Steyn no. 4 Shaft, Dennison (1993) found the asperity model ideally suited to explain the seismic behaviour of the structure in response to adjacent mining. Foreshocks cluster around the edge of the asperity and advance towards the main shock focus, decreasing the area of the asperity and causing its failure (previously proposed by Ritikate, 1982). As the asperities are broken the stress becomes uniform over the fault, analogous to a smoothing process.

Back analysis of large fault slip seismic events and simple seismological theory had earlier led van Aswegen (1990) to propose the model for fault stability evaluation in the Welkom Goldfield. He explained how the strength of an asperity along with the rate of shear deformation dictates the outcome of a tremor, so that recognition of potentially hazardous asperities could be regarded as spatial prediction.

(2.3.2) Undulations, depth, fault gauge, dip and K-ratio

The undulation of faults (or other planes of weakness), with wavelengths ranging from micrometers to kilometres, affects their roughness and friction. The undulatory character causes non-uniform deformation, where under conditions of subvertical maximum principal stress the steeper zones have a greater slip potential, and the shallower zones have less of a slip potential. A part of a fault with reduced dip has an increased shear strength through greater normal stress. Mining at deep levels is associated with large confining pressures. Small scale roughness parameters and undulations become negligible as they are crushed by the greater normal stresses. Medium and large scale undulations, with wavelengths greater

than a few meters and amplitudes less than a metre, are too large to be crushed by the confining pressures. In these areas there will be localised increases in shear strength and a resistance to shear deformation (Dennison, 1993).

Gauge reduces the stress drop associated with the release of energy by seismic events. Gauge properties and its irregular distribution over a surface contribute to the heterogeneous behaviour of the surface. The degree of undulation, the amount of strong constituent minerals of the fault rock and the magnitude of normal stresses are the biggest factors controlling stick-slip behaviour of a fault. Softer, thicker gauge allows stable, relative sliding between two surfaces, mainly because the thickness of the gauge keeps asperity surfaces apart. The density of asperities' areal contact increases in relation to the magnitude of normal stresses.

Dennison (1993) showed that increased surface roughness of a fault surface led to an increase in the angle of friction, and areas with a soft, thick argillaceous gauge decreased the angle of friction. The shear strength of a fault is dependant on mineralogical and geometrical properties of the surface and fault gauge.

A steep fault, at the depth of mining encountered in the Welkom goldfield, under the influence of a modified maximum principal stress due to mining in the environs, may experience a large amount of shear stress (discussed in the next section). The ratio of horizontal stress to vertical stress (K-ratio) is about one half. The magnitude of shear stress and the ratio of shear stress to normal stress thus depends largely on the dip of the structure.

If the K-ratio and the orientation of a potential slip surface remain constant, the ratio of shear and normal stress does not change with increasing depth. Thus, depth does not influence the stability of a fault. When mining starts, however, the ratio of these stresses changes, according to excavation configurations. The higher the stress levels, the greater the rate of closure and deformation of openings, and more potential energy is stored by the rockmass in the form of elastic strain.

(2.3.3) Stress variations and excess shear stress

Stress changes acting on planes of weakness, induced by some approaching mining sequence, may be considerable, and are affected, to different degrees, by mining depth, state of prevailing stress, presence of asperities and gauge on a fault plane, and geometry. The extent of mining of reef close to a fault governs the amount of stress change that will take place. Induced shear stresses, exceeding shear strength, cause relative displacement along the fault.

Consider an isolated stope at depth, as depicted in fig. 2.3, showing stress lobes and possible focii of future seismic events: in front of the immediate face is a zone, C, characterised by very high concentrations of compressive stress. C_1 and, when the stoping reaches it, C_2 are possible focii of crush-type (as observed from a nearby opening) seismic events when zone C progresses with mining and impinges on these discontinuities. Note the presence of lobes, S, of moderately high concentrations of shear stress. As the face advances, these lobes sweep through volumes of 'intact' rock, normally, in the relatively shallow mining depths of the Welkom Goldfield, leaving no

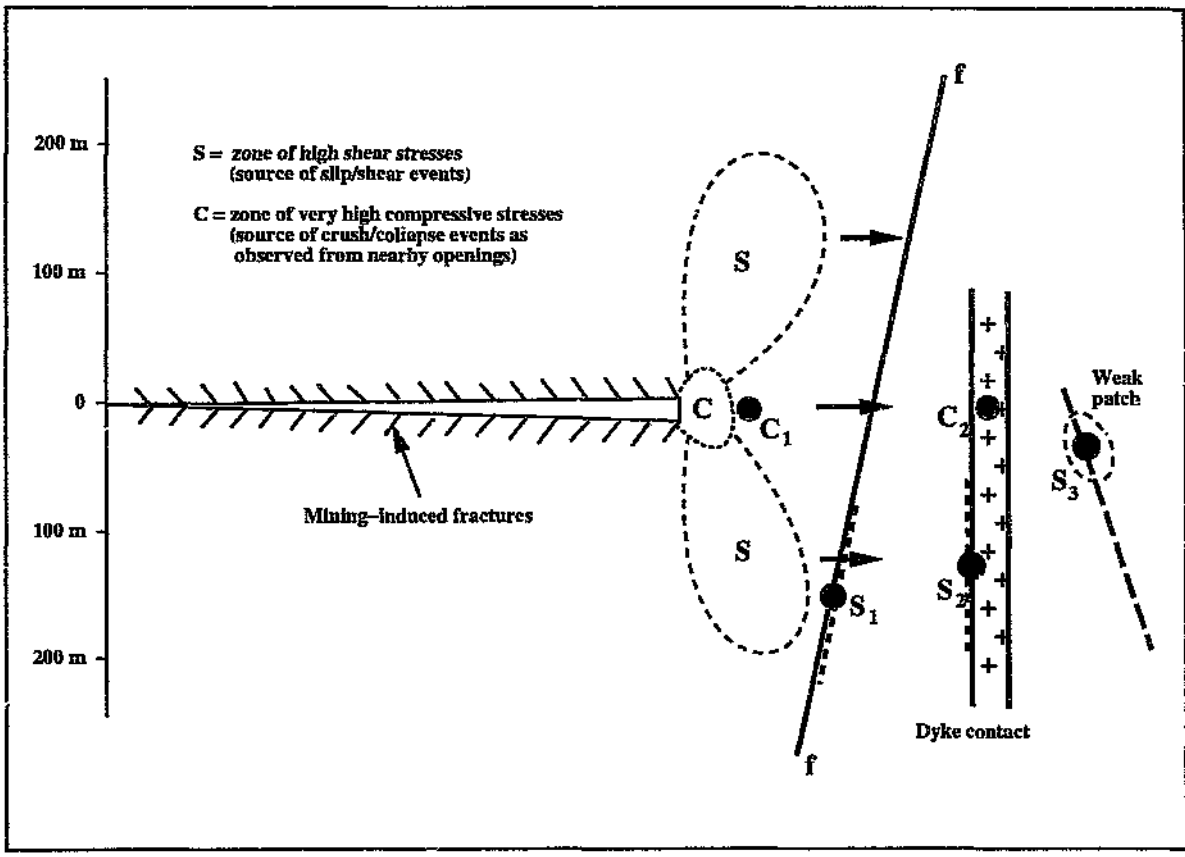


Fig. 2.3: An isolated stope at depth with stress lobes (S), locality and mode of failure of possible future events. Zone C lies in front of the immediate stope face, characterised by very high concentrations of compressive stress. As mining progresses, zones C and S impinge on discontinuities, forming the source regions of imminent seismic events. Slip on nearby discontinuities may also load the rock at the excavation interface beyond its load–carrying capacity.

evidence of their passage behind them. Occasionally, a lobe may impinge on a pre-existing plane of weakness, such as a fault, joint, or dyke contact, creating the possibility for a slip/shear type seismic event (e.g. S_1, S_2 and S_3).

The excess shear stress (ESS) concept (Ryder, 1988, p27-30, 37) quantifies the effects of mining on geological structures. ESS may be described as the difference of prevailing (modelled) shear stress (τ) acting on a plane prior to slip and the dynamic strength of the plane (the product of dynamic friction (μ) and the normal stress (σ_n) acting on that plane at some point):

$$ESS = \tau - \mu\sigma_n \quad \text{..... [9]}$$

It measures the shearing effect of mining induced stresses on geological structures directly. The amount of ESS may indicate zones with greater potential for deformation and/or slip, usually greatest on a plane of weakness at the zones of positive ESS (Ryder, 1988, p29-30; van Aswegen and Butler, 1993, p4). An increase in ESS should precede a large seismic event, and the focus of the event would likely be in the area of highest ESS.

The key parameters needed for ESS analysis are the angle of dynamic friction, and the likely stress drop, for which representative values for planes of weakness may be 30^0 and 10 MPa (Ryder, 1988, p37). In the Welkom region a lower angle of friction (e.g. 25^0) is, from experience, deemed more appropriate.

For the situation where a planar orebody is mined on both sides of a normal fault, Dennison (1993) evaluated those parameters influencing the extent and magnitude of ESS zones through numerical modelling and observed the following:

-- The magnitudes of induced shear stress and ESS are at a maximum adjacent to abutments.

-- Extent of mining (or mining span) affected the convergence of an excavated slot, an increase of which resulted in an increase in both size and maximum shear stress magnitude within the shear stress lobe. Pillars and/or adjacent faulting break the effective mining span, reducing the closure and magnitude and extent of an induced shear stress lobe. Consequently, the extent of positive ESS on an adjacent fault is also reduced.

-- Generally, the maximum shear stress and the size of the shear stress lobes increased with greater mining depth. However, the shear strength of a fault which also increased with depth (due to a corresponding increase in the magnitude of the clamping normal stress) limited the amount of ESS: the size of the zone of positive ESS increased marginally with increased depth; the maximum magnitude of ESS contained within the zone increased significantly with depth

-- A more inclined mining slot experienced a greater influence of horizontal stresses. The higher the K-ratio, the more significant the convergence, and the more intense the shear stress and extent of shear stress lobes.

-- The steeper the fault, the less the normal stress acting on it, and the greater the effect of K-ratio upon the extent of ESS. Increased normal stress limited the extent of positive ESS; reduced normal stress was found to contribute to the formation of positive ESS zones. For K-ratio < 0.5, the extent of positive ESS and ESS_{max} values increased very significantly with decreasing K-ratio; for K-ratio > 0.5 the extent of positive ESS was influenced very little, regardless of fault dip or mine layout, while ESS_{max} values decreased very significantly (the influence of higher clamping stress acting on the steep fault overcame the influence of relatively larger induced shear stress).

-- From geometric considerations, steeper dipping faults were observed to intersect high shear stress lobes more readily and more extensively, over a greater length of their surface. Shear stresses increased with steeper faults, and the length of the fault surface itself was noted to be increasingly exposed to higher shear stresses.
-- The normal stress acting on a fault was found to decrease with an increase in dip, where, generally, the horizontal stress was less than the vertical stress. ESS values and the extent of zones of positive ESS on the fault thus increased in proportion to the dip of the fault.
-- Where the reef is mined out on both sides of a normal fault, shear stress concentrations from both sides are imposed on the area on the fault between the upthrown and downthrown reef blocks, ie. two shear stress lobes exist. For a given depth and dip of the fault, the superposition of shear stress in the fault loss area resulting from the mining on both sides of the fault will be maximum for a given displacement. As displacement increases, the total area of high shear stress will increase in the fault loss area, but the maximum value will decrease until the two shear stress lobes cease to intersect.

An unmined dyke intersecting a fault is analogous to a stabilising pillar (Meijer, 1993, p21). At the region of intersection it could reduce shear stresses acting on the fault due to stope closure. The dyke material is usually harder and more brittle than the surrounding rock, acting as a stress concentrator. The encroachment of mining towards a dyke enhances the stress concentration.

The stability of a fault is further affected by the relative angle between the mined-out reef and the fault. Stoping influences a fault considerably in over- and understoped areas. The Basson fault, for example, displaces the reef by up to 80m on dip. The angle between the reef and the faults is approx. 90^0. The stress field is rearranged in such a way that there exists an elevated shear stress component in the overstoped and understoped parts of the Basson fault, and an increased normal stress component in the fault loss portion.

(2.4) Recent Hypotheses in Rockmass Stability

By 1992 ISS International Ltd. began to demonstrate the application of particular parameters from seismic data to rockburst prediction. The author was part of the ISSI research team responsible for testing some of the new concepts. This section summarises part of chapter 10 of the book 'Seismic Monitoring in Mines' (Mendecki, 1997).

Quality seismic information (with each seismic event being recorded by at least five three-component geophone stations, having a signal-to-noise ratio of the recorded waveforms $\geq$ 10 for all stations, and all waveforms undergoing processing with inbuilt quality control), allows the time of occurrence, hypocentre location, radiated seismic energy (E) and seismic moment (M_0) to be obtained. From this, it is claimed, the rockmass behaviour may be quantified, in terms of parameters pertaining to stress (apparent stress, energy index and seismic stress) and strain (cumulative apparent volume, seismic strain rate and seismic viscosity):

(a) The total radiated seismic energy (E) and the seismic moment (M_0) of an event, obtainable from digital waveform records, are two independent measures of seismic deformation. The ratio of E over M_0 is known as **apparent stress:**

$$\sigma_a = (GE)/M_0$$
$$= \eta\sigma \quad \text{..... [10]}$$

where η = seismic efficiency
$\sigma = (\sigma_1 + \sigma_2)/2$ is the average shear stress on a fault; σ_1 is the stress before a seismic event and σ_2 is the stress after.

Mendecki (1997) describes apparent stress as an expression of the amount of the radiated seismic energy per unit volume of inelastic coseismic deformation (i.e. a measure of stress release at the source).

Fig. 2.4 shows the relationship between E and M_0. Variations in the energies of events with similar moments differentiates seismic source regions of different stress regimes and rockmass properties. Consider the source of a seismic event associated with a geological discontinuity that is relatively weaker (i.e. 'softer') than the surrounding rock. This source is expected to yield in a slower manner, subject to lower differential stress, giving rise to an event characterised by larger seismic moment with less seismic energy radiated than the norm. The event will appear as a 'slow' or low apparent stress event, and vice-versa.

(b) One of the parameters that is looked at more frequently in order to distinguish areas of higher than average rockburst potential is the **energy index** (EI) (van Aswegen and Butler, 1993, p2), defined by

EI = (measured energy) / (average energy for a given moment) ..... [11]

The denominator above is determined empirically (see fig. 2.4). For a given M_0 the large variation in E is considered physically meaningful and not erroneous -- radiated seismic energy and seismic moment are essentially independent variables. van Aswegen and Butler (1993) suggested that EI > 1 (i.e. measured seismic energy greater than the average seismic energy for a given moment) can indicate higher than average shear stress at the source location, and vice-versa. This parameter has been noted to correlate with observable damage underground from postseismic investigations (van Aswegen, personal communication).

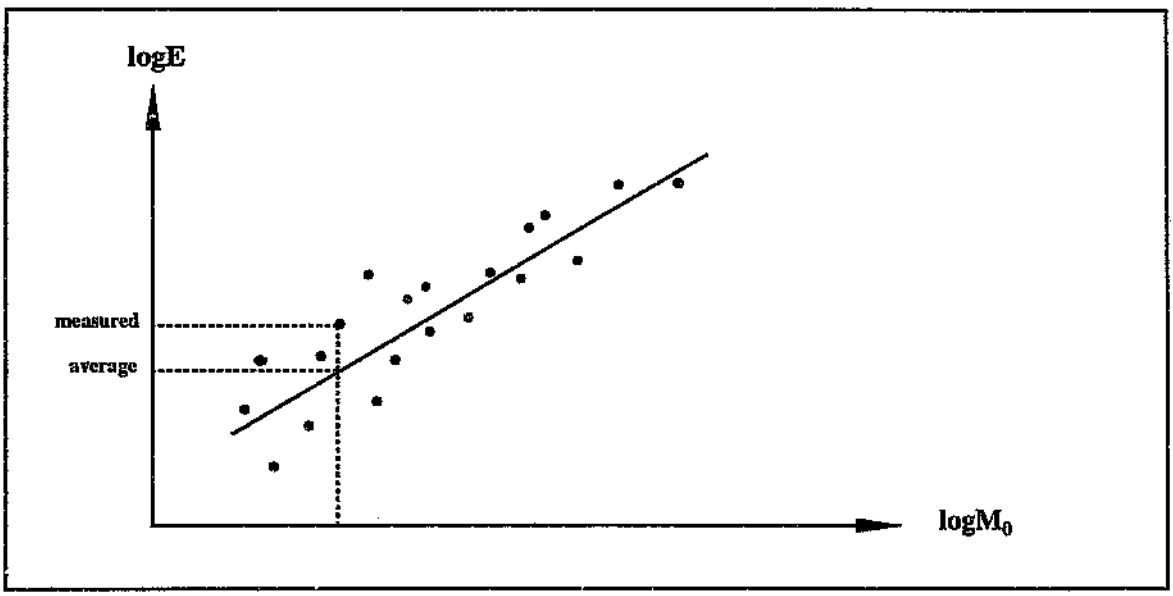


Fig. 2.4: The concept of energy index: ratio of measured energy to that which is expected (average) for a given moment for some seismic event.

(c) **Apparent volume** (m^3) is defined as (Mendecki, 1997):

$$V_a = M_0 / (2\sigma_a)$$
$$= M_0^2 / (2GE) \quad \text{..... [12]}$$

where σ_a = apparent stress
E = energy released

As with apparent stress, apparent volume depends on energy and moment, but is a scalar with units of m^3. As such, it is a cumulative quantity and may be totalled for a specified area during a specified time range.

(d) An average **seismic strain** within a volume ΔV over the time period $\Delta t = t_1 - t_2$, is related to the sum of the seismic moments of all events occurring within ΔV during Δt (Kostrov, 1974) as

$$\epsilon_s (\Delta V, \Delta t) = (\Sigma M_0) / (2G\Delta V) \quad \text{..... [13]}$$

where the summation is from t_1 to t_2, and the average **seismic strain rate** (s^{-1}) is then

$$\dot{\epsilon}_s (\Delta V, \Delta t) = (\Sigma M_0) / (2G\Delta V \Delta t) \quad \text{..... [14]}$$

It describes the rate of rock mass deformation due to seismicity.

(e) The average **seismic stress** (Pa) may be defined (e.g. Kostrov and Das, 1988, as quoted by Mendecki (1997), 'Seismic Monitoring in Mines', chapter 10) as

$$\sigma_s(\Delta V, \Delta t) = (\Sigma E) / (\epsilon_s \Delta V \Delta t) = (2G\Sigma E) / (\Sigma M_0) \quad \text{..... [15]}$$

where ΣE is the radiated seismic energy of all events in ΔV during Δt.

Seismic stress quantifies stress changes which take place within a volume ΔV of rock due to seismicity; it is not a direct measurement of stress to which the rock volume is subjected.

(f) The ratio of seismic stress to seismic strain rate is a measure of **seismic viscosity** (expressed in Pa.s). It indicates rockmass resistance to the flow of coseismic inelastic deformation (originally defined by Kostrov 1974, quoted by Mendecki (1997) in 'Seismic Monitoring in Mines'), expressed as follows:

$$\eta_s(\Delta V, \Delta t) = \sigma_s / \dot{e}_s = (4G^2 \Delta V \Delta t \Sigma E) / (\Sigma M_0)^2 \quad \text{..... . [16a]}$$

where the summations are from t_1 to t_2.

The inverse of viscosity is termed **fluidity** (η_s^{-1} -- [16b]). Low values of seismic viscosity (high fluidity) imply that the seismicity promotes an easier transfer of stresses within the rockmass, and a rockmass response to mining where, for comparable seismic moments, less energy is, generally, radiated; an 'easier flow' of seismic inelastic deformation takes place.

(g) The seismic **relaxation time** (s) establishes the rate of decay of seismic stress with time and defines the usefulness of past data in the predictability of the 'seismic flow' of rock (quoted by Mendecki, 1997):

$$\tau_s(\Delta V, \Delta t) = \eta_s / G \quad \text{..... [17]}$$

It quantifies the rate of change of seismic stress during the 'seismic flow' of rock. A low relaxation time indicates that the time span of useful past data is short.

(h) The seismic **Deborah number** (De_s) may be defined as the ratio of τ_s to the time of observation (or flow time) Δt (as defined by Reiner, 1969):

$$De_s(\Delta V, \Delta t) = \tau_s / \Delta t \quad \text{..... [18]}$$

It measures the ratio of inelastic viscous forces in the 'seismic flow' of rock and delineates volumes of rock 'softened' by seismic activity. For small De_s the rock material behaves like a fluid; for large De_s it behaves like a solid.

(i) For a seismically active cube (side length = l) of volume $\Delta V = l.l.l$ the average

seismic diffusivity (D_s) within ΔV over $\Delta t = t_2 - t_1$ is expressed as

$$D_s(\Delta V, \Delta t) = l^2 / \tau_s = l^2 G / \eta_s = l^2 (\Sigma M_0)^2 / (4G \Delta V \Delta t \Sigma E) = (\Sigma M_0)^2 / (4Gl \Delta t \Sigma E)$$
$$\text{..... [19]}$$

where τ_s is the seismic relaxation time and η_s is the seismic viscosity. The summations range over t_1 and t_2.

D_s has dimensions m^2/s, and is higher for seismicity quantified by lower apparent stress. It decreases with an increase in seismic viscosity.

Alternatively, define the **seismic diffusion** d_s for a cluster of seismic events as

$$d_s = (\langle X \rangle)^2 / \langle t \rangle \quad \text{..... [20]}$$

where $\langle t \rangle$ = average time between events

$\langle X \rangle$ = average distance between consecutive sources (including source sizes) of interacting seismic events.

It quantifies the localisation of the migration of seismic activity and associated transfer of stress in space and time (Mendecki, 1997).

(j) The ratio of viscosity over diffusion is termed the seismic **Schmidt number**:

$$Sc_s = \eta_s / (\rho d_s) \quad \text{..... [21]}$$

An increase/decrease in seismic viscosity is accompanied by a decrease/increase in seismic diffusion, and Schmidt number takes both parameters into account, rising/falling accordingly. It measures the degree of turbulence in the 'seismic flow' of rock (McComb, 1990, quoted by Mendecki, 1997).

(k) Finite increments in stress (σ) and strain ($\in$) from the one state at $t_1[\sigma(t_1), \in (t_1)]$ to the next state at $t_2[\sigma(t_2), \in (t_2)]$ within a volume of rock ΔV, translates into **seismic softening** as

$$S_s(\Delta V, \Delta t_1, \Delta t_2) = [(\Sigma_{t_1}^{t_2} E \Sigma_{t_0}^{t_1} M_0 - \Sigma_{t_0}^{t_1} E \Sigma_{t_1}^{t_2} M_0)\Sigma_{t_0}^{t_2} M_0] / (\Delta V \Sigma_{t_1}^{t_2} M_0 \Sigma_{t_0}^{t_1} M_0)$$
$$< 0 \quad \text{..... [22]}$$

where $\Delta t_1 = t_1 - t_0$ and $\Delta t_2 = t_2 - t_1$, for $t_0 < t_1 < t_2$ (see Mendecki, 1997, chapter 10, for a description of the development of eqn. [22], with references).

Seismic 'hardening' occurs if S_s is greater than zero.

(2.5) Numerical Aspects in Seismicity Analysis

The analysis and interpretation of seismic data to describe the rock mass response to mining in terms of the spatial and temporal variations in stress and strain rate requires that due prior consideration be given to event location accuracy (consistent coverage and adequate sensitivity is needed, as discussed in Section 3.1, Chapter 3) and to the length and size of the window used for the selection of events from the database (described below).

Note: Apart from data quality considerations, effects to the way in which seismic parameters are portrayed are of particular reference to '4Di', an interactive seismic visualisation and interpretation software package. This software has analytical tools, the output of which is used extensively -- in the display and evaluation of seismic source parameters in space / time, as contour plots and time-history graphs -- in Chapters 3 and 4 of this dissertation. The 4Di suite of programmes allows three dimensional display of seismic events in relation to physical phenomena (e.g. excavated / mined-out portions of reef at depth, tunnels and haulages, geological discontinuities such as faults and dykes, or some other appropriate features) and a user-specified co-ordinate system.

(2.5.1) Time and space windows in the selection of seismic events for analysis

Before any characterisation of the seismic reaction of some volume of rock to stress changes can be attempted it is fundamentally important that

consideration be given to the quality (see Section 3.1, Chapter 3) and amount of data (a function of window length and/or local sensitivity to ground motions) and its location in time and space for evaluation.

To illustrate the proper location of a space window consider a back-analysis of some large event: experience has shown that a volume with a diameter approximately 10 times that of its source volume, centred at the event focus and expressed in terms of apparent volume or Brune source radius, should be taken into account. This should encompass all relevant seismic activity, and provide information leading to, or concerning, the event. van Aswegen (ISSI internal report, 1994) describes three zones of interest:

(a) a *nucleation zone* with a volume smaller than the source volume (where rupture may continue beyond its limits) - characterised by an elevated seismic fluidity (eqn. [16b]) with easier transfer of stress due to seismicity (or 'strain softening' (eqns. [16a] or [16b]), as explained in Section 2.4, Chapter 2) prior to instability and the focus of seismic energy release.

(b) a *preparation zone* as the volume where the event was created (i.e. the volume containing the greatest stress and strain changes in preparation for the coming large event); it cannot be smaller than the source volume and is expected to have a radius two to five times that of the source;

(c) an *outer zone*, which is at least twice the size of the preparation zone, as the required volume to distinguish the activities in the preparation zone from that outside.

The 'preparation zone' may be spatially identified through the contouring (see later, in Section 2.5.2) of seismic parameters -- such as seismic fluidity (eqn. [16b]) and/or seismic Deborah number (eqn. [18]; refer to Section 2.4) -- scaling the volumetric deformation of the rockmass. The limits of this zone are defined by the high gradients in these parameters. The preparation zone usually appears as a clustering of seismic events forming a distinguishable pattern spatially removed from other seismic patterns.

The length of time window depends on the method of evaluation (e.g. variation of seismic parameters over time (time-histories), contouring of seismic parameters, or patterns of seismicity (see Section 2.1.2)) and/or the type of information required (e.g. short-term, delineating recent stress/strain changes, or longer-term analysis revealing the historical character of some area of interest).

The inherent nature of the rock lends itself to the analysis of events, according to the seismic parameter, in some instances better over the long term, and in other cases better over the short term. Too small a time span misses some important action and too large a span may include seismicity overshadowing the recent more pertinent events, which may be smaller in magnitude. The optimal window length is often established empirically.

Once deformed, it will take years (depending on the deformation and rate of closure) for the rockmass to heal itself. Those seismic parameters related to strain (or cumulative deformation), when viewed over a long time period, should expose 'intact' patches of rock with a tendency to accumulate energy, thereby loading asperities and other inhomogeneities which could fail suddenly as a result of the stressed conditions or be triggered by ground motions from a distant tremor. Seismic stress (and related

parameters) and strain rates, looked at over the short term, will reveal the recent conditions of the rockmass in terms of potential instabilities -- directly by maxima and minima, or indirectly by 'seismic gaps'. In addition, the activity rate for an area must be studied to decide on the usefulness of some time span, so that the number of events considered in the type of interpretation to be done will describe deformation processes, and allow meaningful quantification and interpretation of these processes.

(2.5.2) Contouring of seismic parameters

One way of representing seismic information is through contouring, which has visual impact and is particularly useful in defining regions showing high gradients of individual parameters (Chapter 11, 'Seismic Monitoring in Mines'). This may then be attributed to local rockmass conditions.

The initiation of instability of some portion of the rockmass and its detection in time depends on information originating in a specific volume -- i.e. the 'preparation zone' (or the volume containing the greatest stress and strain changes in preparation for the future large event). Once this volume is demarcated the time span of seismicity that should be investigated comes into consideration (see previous section).

The contouring procedure employed by part of the software used in this study ('4Di') uses a two-dimensional rectangular grid covering the area of interest. A rectangular space window of size equal to- or a multiple of- the grid spacing selects seismic events around each grid point (as described in chapter 11, 'Seismic Monitoring in Mines').

The depth co-ordinate of the reef at each grid point is calculated to ensure a constant volume per grid point, where a fixed vertical span for event selection is used, centred symmetrically around the elevation of the reef at the grid point. Cumulative and average values of seismic source parameters corresponding to those selected events can then be calculated and attributed to the sequence of grid points. In the final stage, during the contouring process, some smoothing may (or may not) be applied to the contour lines.

(2.5.3) Time-history variations of seismic parameters

In this type of analysis a number of events are averaged over a previously defined time window. The averaging of the seismic parameters is performed over a moving window for a smoothing of the seismic data. The aim is to identify a rate of change in some parameter or to establish particular trends in seismicity over time, at some location of interest, that may be considered significant as an indicator for a larger magnitude event to come (i.e. for temporal detection of instabilities). The sensitivity of some parameters to the length of moving time window will be investigated later.

In the study area, unless otherwise specified, time-histories (used frequently in Chapter 4) conform to a 5 days / 8 events (samples) averaging format, which from experience, has been found to be adequate to characterise stress/strain changes in the area.

(2.6) Summary

Tectonic seismological theory can, to some extent, be projected down in scale to describe the seismicity recorded in mines (e.g. Mendecki, 1997). The scope to which seismic precursory methodologies have been investigated and their possible application to the mining environment was determined by a review of recent pertinent literature. Percursory studies for natural earthquake prediction have mostly been divided between those incorporating time and space characteristics of seismic events, those involving observations concerning the propagation of seismic waves, and those formulated in hazard analysis. Few of these approaches have been successfully imported into the routine evaluation of mine seismic data. The asperity model, applied to the spatial prediction of mine tremors along geological discontinuities, is likely the single most useful direct application of crustal seismology theory in mines.

Applying the Brune model for seismic source parameter calculations in South African mines, the seismic source is regarded as a circular dislocation on a plane of weakness. With this assumption, the source can be described by its radius and average coseismic displacement, from which the seismic moment, seismic energy, stress drop and local magnitude may be calculated.

In the study area, factors affecting the stability of the major structures of interest (i.e. the Postma dyke and the Basson fault) which need to be considered include asperities along the planes of weakness (resisting relative movement), undulations (resulting in localised increases in shear strength and a resistance to shear deformation), gauge properties (the presence of which can reduce the angle of friction used in the

calculation of shear stresses), constituent material of the inhomogeneity (i.e. the Postma dyke, being stronger than the surrounding rock, acts as a stress concentrator as mining continues in its vicinity), dip of the structures (where a steeper dip is more conducive to the creation of positive ESS), reef displacement (resulting in an increased normal stress component in the fault loss portion) and extent of mining (an increase of which should increase both size and maximum shear stress magnitude within shear stress lobes, and consequently, positive ESS). Such factors are expected to be reflected in the character and/or extent of the seismic activity.

It has been proposed that seismic data of good quality enables the behaviour of the rockmass to be quantified. It is also postulated that the physical mechanisms of rock instability require ***strain softening*** (i.e. easier stress transfer with seismicity, and a response of the rockmass to mining characterised by events with lower seismic energies (for similar seismic moments) than the norm; seismic indicators are energy index (eqn. [11]), seismic viscosity (eqn. [16]), seismic diffusion (eqn. [20]), seismic Schmidt number (eqn. [21]), seismic softening (eqn. [22])), ***stress drop*** (indicated by apparent stress (eqn. [10]), energy index (eqn. [11]), seismic stress (eqn. [15])), and an ***increase in strain rate*** (indicated by cumulative apparent volume (eqn. [12]), seismic strain (eqn. [13]), seismic strain rate (eqn. [14]), seismic viscosity (eqn. [16]), seismic Deborah number (eqn [18]), seismic diffusion (eqn. [20]), seismic Schmidt number (eqn. [21]), seismic softening (eqn. [22])) prior to failure. Incremental rock deformation should tend to diffuse at a rate proportional to the source size of the imminent instability. These and other concepts are tested in later chapters, in the seismic response of the rockmass to mining induced stress changes.

The presentation of recorded seismic data within some volume of the rockmass may take several forms. The locations of events in space/time could simply be represented around an active stope or geological feature at depth. A more sophisticated approach, where techniques of analysis of seismicity may be employed, might involve the variation of some seismic source parameter over time, or through contouring, with modification of user-defined filtering/scaling options to enhance the possible identification of instabilities. These analytical tools are offered through the '4Di' suite of programmes, and form the basis of seismic evaluations in this study.

3

SEISMIC COVERAGE AND CORRELATION OF SEISMICITY WITH MINING IN THE POSTMA AREA

The layout of a seismic network has a large influence on the degree of event detection and location accuracy. Better accuracy of hypocentre locations lends a greater confidence to analysis and interpre.ations. In the study area, as in other areas of the Welkom goldfield, seismic activity is closely monitored on a daily basis. For all recorded seismic events three orthogonal components for each station (north-south, east-west, up-down) produce complete seismograms.

(3.1) Sensitivity of Local Network

The location and spread of the recorded seismicity within the Postma area will be shown in Section 3.3 to correlate well with active stoping areas and geological structure. The geophone coverage of the study area allowed recording of seismicity of moment magnitude greater than approximately -0.6 for a minimum of four triggered and associated stations, during the second half of 1993 and most of 1994 (see fig. 3.1). For a minimum of five associated stations the sensitivity decreases and the minimum moment magnitude increases to 1.0, as shown in fig. 3.2.

The locations of the eight closest stations are indicated in fig. 3.3a. An example of a

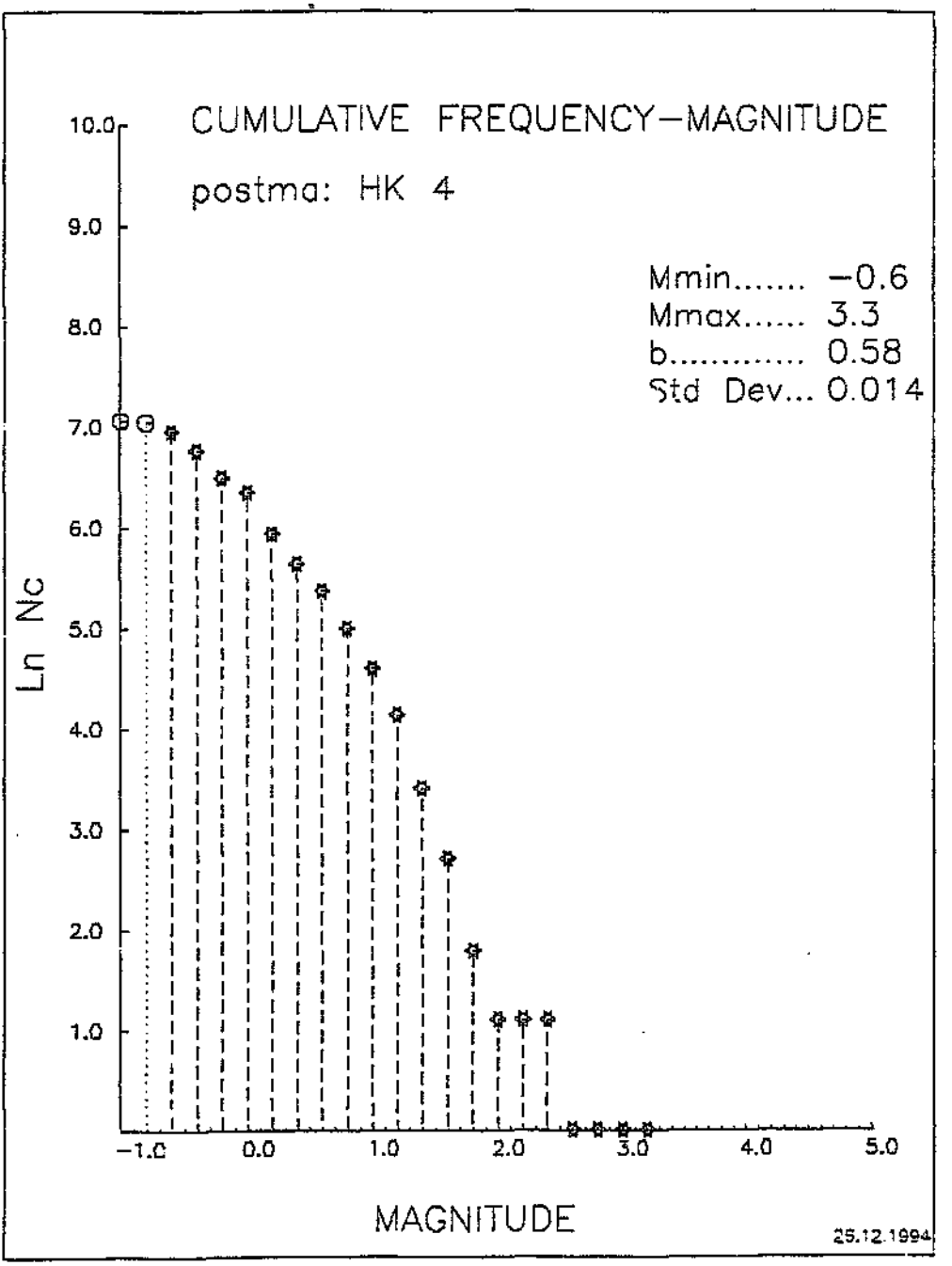


Fig. 3.1: Gutenberg-Richter frequency-magnitude plot based on events for which a minimum of four triggered and associated seismic stations were used for source parameter calculations. The magnitudes were calculated using seismic moment (e.g. Hanks and Kanamori, 1979).

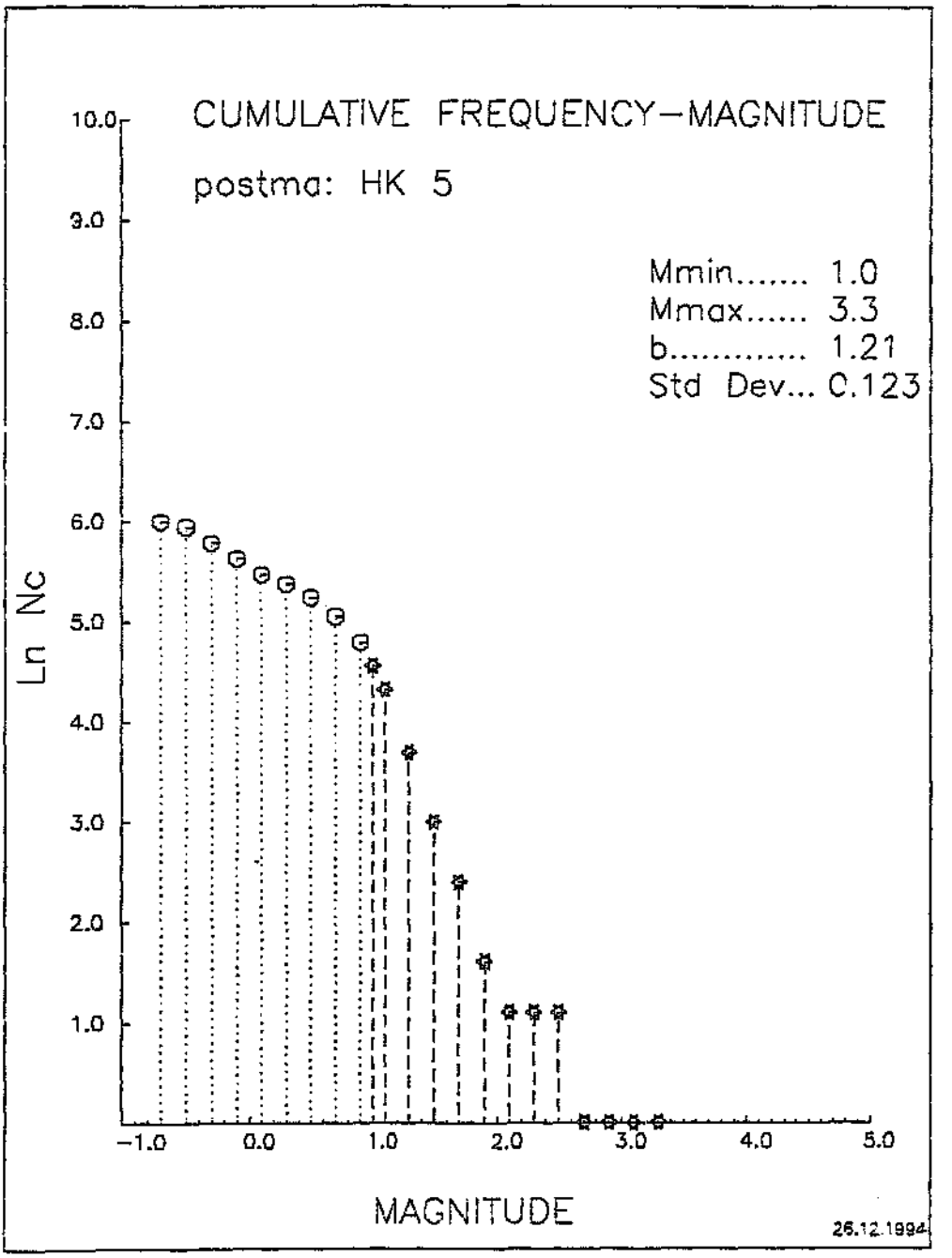


Fig. 3.2: Same frequency-magnitude relation as fig. 3.1, but using a minimum of five triggered and associated stations.

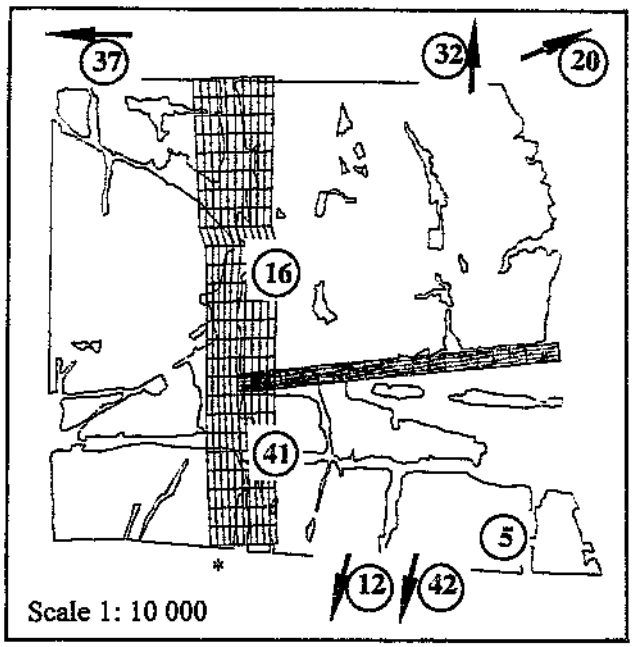
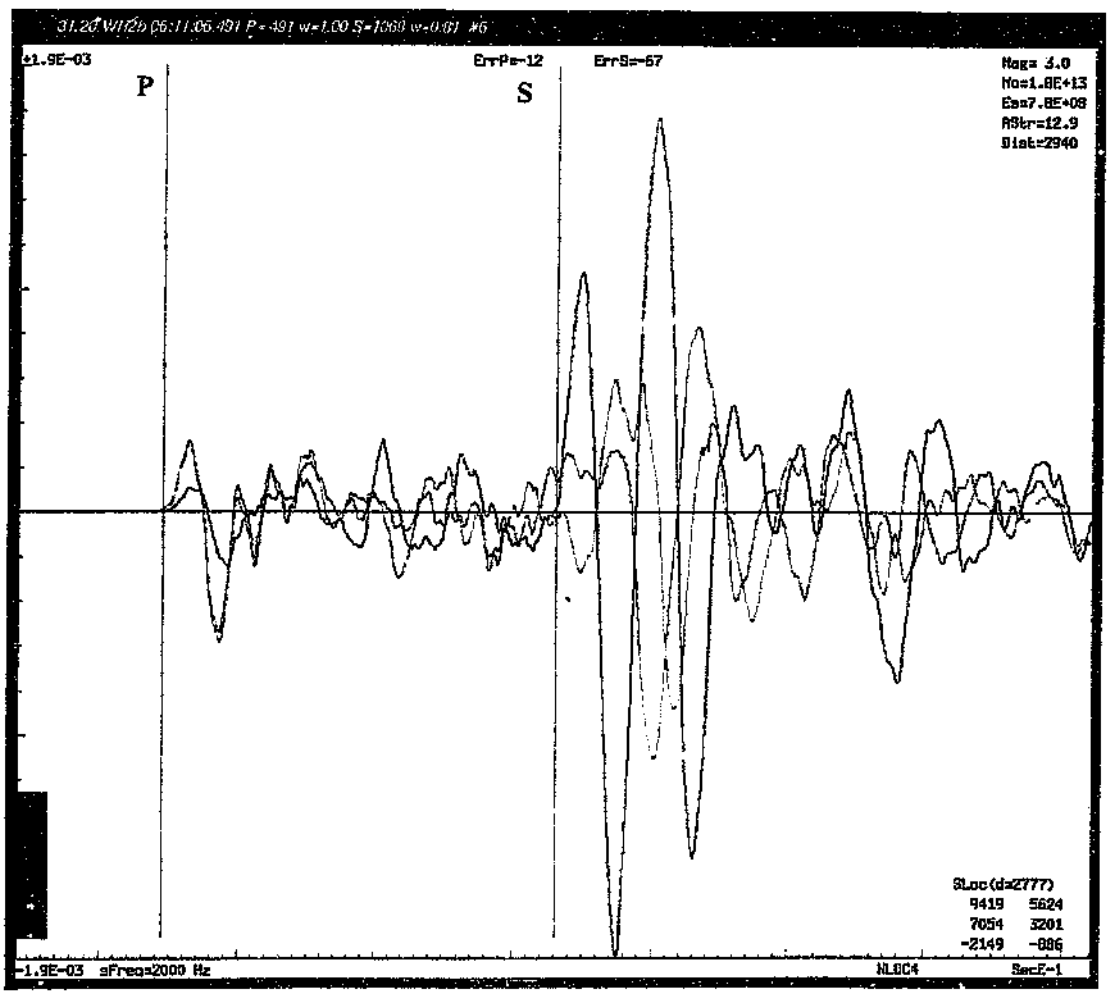


Fig. 3.3a (left):
The study area with locations of eight nearest seismic stations. ThePostma dyke and Basson fault are represented by the gridded surfaces. Arrows point to the locations of stations outside the frame of the figure. The asterisk marks the hypo-centre of an event whose waveform is displayed in fig. 3.3b.

Fig. 3.3b (below):
An example of a processed waveform (with P- and S-wave picks), recorded by one of the tri-axial geophone sets shown in fig. 3.3a, belonging to one of the larger events (M_L 3.2 on 27/06/1994) which occurred in the area.



processed waveform, corresponding to one of the large events recorded by one of the tri-axial sensors shown in fig. 3.3a, is displayed in fig. 3.3b.

Figs. 3.4a and 3.4b show the expected spatial (XYZ) hypocentral accuracy in terms of magnitude in the area of interest, for five stations. The extent of detectability for events of local magnitude 0.1 is displayed in fig. 3.4a (outside the boundary of the contour lines the seismic sensors don't associate and the system is relatively 'deaf'); in fig. 3.4b (local magnitudes greater than 0.8) the best areas of coverage at a depth of 1750m below datum have expected minimum location errors under 20m. The diagram remains unchanged for higher local event magnitudes. (This analysis was carried out using the software package 'Errmap' [Sciocatti, M.J.; Optimal Spatial Distribution of Seismic Stations to Minimise Expected Location Error (Optinet and Errmap), ISSI internal report, June 1994]).

(3.2) Location, Methods of Mining and In-situ Observations:

The final stages of extraction of a mining area usually creates blocks of ground isolated and surrounded by extensive mining. These remnants are difficult to mine because a reduction in their size is often accompanied by a sharp increase in stress levels, stress induced fracturing and seismicity, depending on local geology and existing rockmass conditions and stress levels.

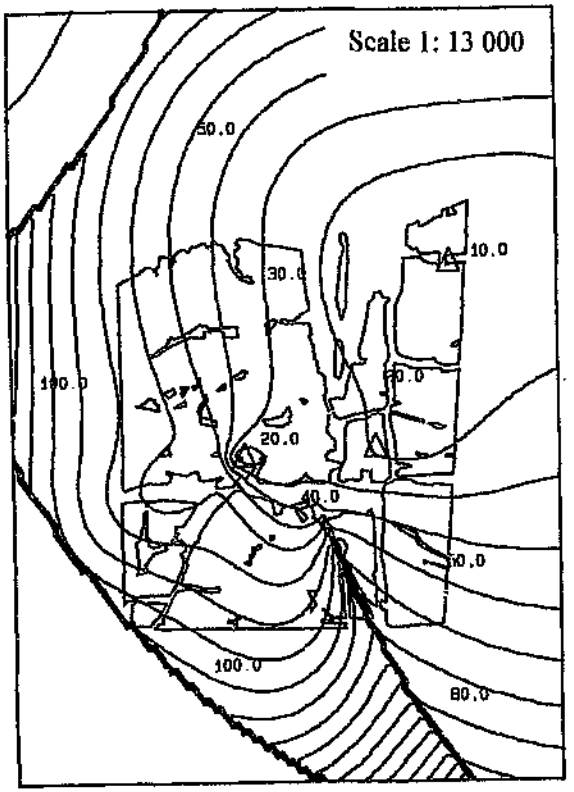


Fig. 3.4a: Expected spatial hypocentral accuracy: extent of detectability for events of minimum local magnitude 0.1. The numbers represent the expected location errors associated with seismic events located at those points, in metres. Outside the boundary of the contour lines the seismic sensors are 'deaf' to local magnitudes less than 0.1.

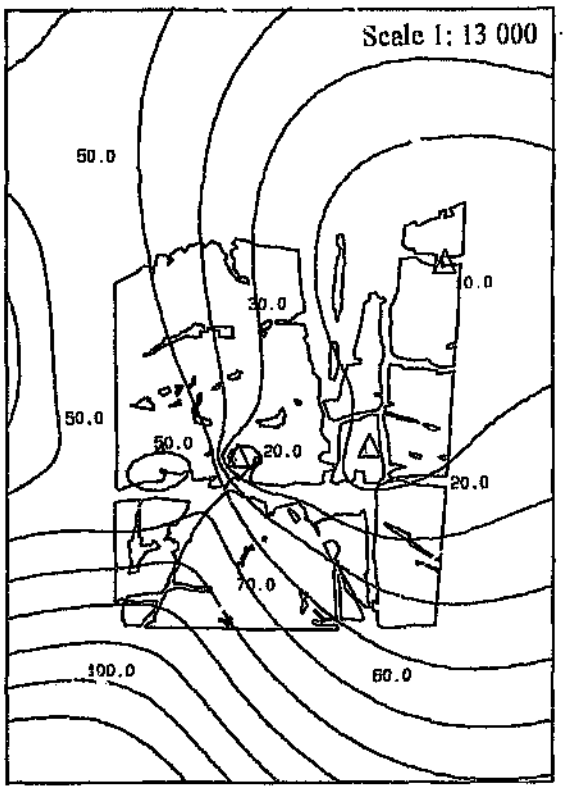


Fig. 3.4b: Expected spatial hypocentral accuracy: extent of detectability for events of minimum local magnitude 0.8. As with fig. 3.4a, the numbers refer to expected errors in location of seismic events occurring at those points, in metres.

The mining activity in the Postma area was centred on the extraction of payable reef locked up in remnants. The mining method was, of necessity, of a scattered nature, with negotiation of geologically disturbed ground.

The removing of remnants from within extensively mined-out areas may result in the transfer of stress onto peripheral solid areas or geological weaknesses. The latter is of particular significance here, where the Basal reef is being mined adjacent to the Postma dyke and to a lesser extent along the Bacson and Arrarat faults.

The general orientation of fractures around underground excavations is normally curved back, away from the direction of mining, but the fracture envelope is complex, and may include, amongst others, shear and extension fractures, bedding plane fractures and fractures caused by blasting (see fig. 3.5). The extent and intensity of the fracture zone increases with increasing depth (stress). Development advanced ahead of a face or close enough to modify the stress field, affects the intensity, orientation and dip of these fractures. The remnants in the Postma area, by virtue of being isolated and considerably stressed are also highly fractured, as will be shown later.

Mining of the Basal Reef horizon is complicated by the presence of a band of khaki shale (between 0.2m and 0.8m thick in places), parallel to the strata, located approximately one metre above the reef, overlying the basal quartzite. The weak waxy brown leader quartzite overlies the khaki shale.

The intermediate depth of this mining (approximately 1500m below surface) induces compressive horizontal stresses of sufficient magnitude (around 23 MPa -- refer to

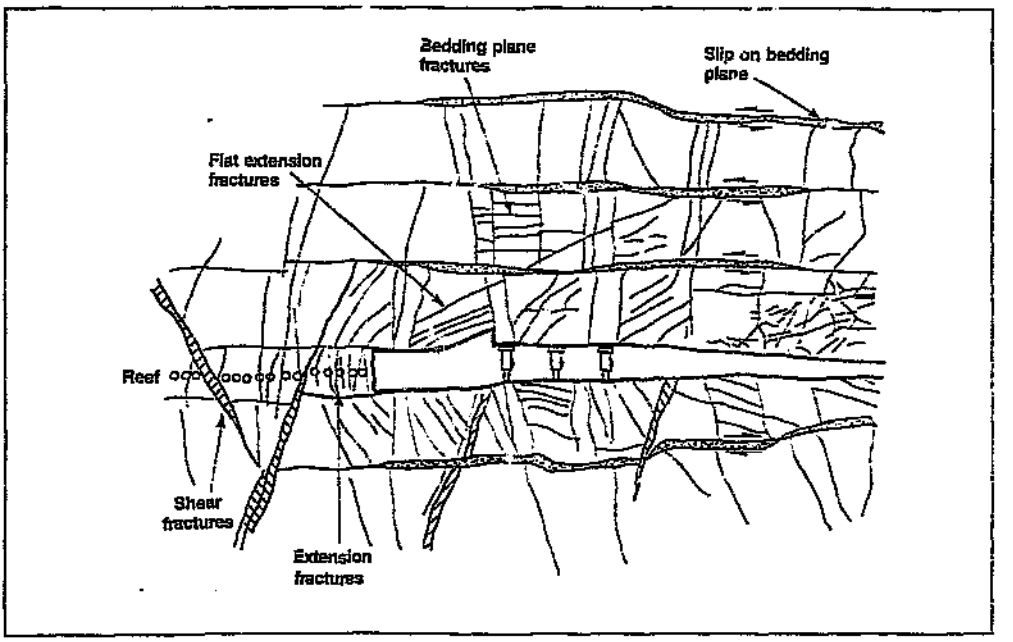


Fig. 3.5: Section through a stope in a gold mine showing typical rockmass conditions at depth (strike-parallel joints and blast fractures not visible). (Source: An Industry Guide to Methods of Ameliorating the Hazards of Rockfalls and Rockbursts, 1988 edition, COMRO)

Section 1.6, Chapter 1) to clamp the mining-induced fractures and other near-vertical planes of weakness in the hangingwall and footwall, enhancing the stability of the strata. However, large unsupported spans of shale hangingwall were observed to collapse easily (even with normal stoping -- due to vibrations, closure and bed separation (gravity and buckling effects as a result of horizontal compressive stresses)), and capable of heavy disruption of production with seismicity. With undercutting the problem was alleviated. The stoping width was also reduced, with less wastage.

Three main areas of mining were in progress during the first quarter of 1994, as indicated in fig. 3.6. The scattered mining in the Postma area, with its other adverse conditions, required the development of updip and downdip panels, not necessarily in an ideal fashion, but rather according to site conditions and recommended approaches by rock mechanics engineers. The directions of mining advances were also site dependant.

Observations:

Stope support generally included solid timber packs 2m apart and a double row of rapid yielding hydraulic props 1.5m apart and 1.0m from the face, according to the set standard for the mine. When and where necessary, mine poles and mechanical props with headboards were used.

Stoping width varied from less than 0.8m, in some instances (where the Khaki shale band was undercut), to over 1.0m, depending on strata conditions.

Various sites were visited regularly during the first three months of 1994, as indicated

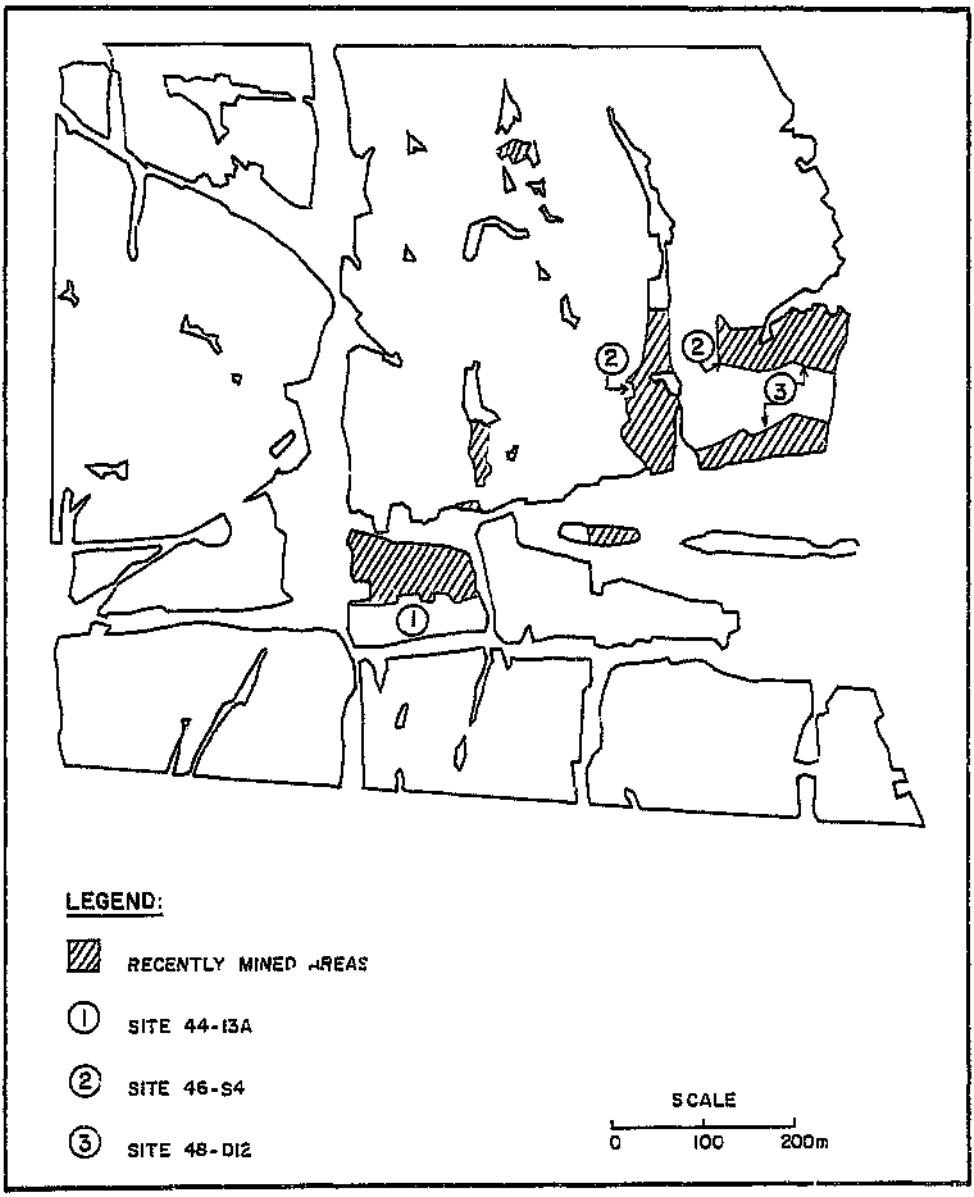


Fig. 3.6: Areas of recent mining activity in the vicinity of the Postma Dyke and Basson Fault. Sites 1, 2 and 3 were documented photographically (see Appendix B).

also in fig. 3.6. Documented observations are summarised below. A photographic record is intended to portray the extent of fractured condition of the rockmass encountered underground, to give an indication of the amount of stress to which the rock surrounding the active stoping sites was subjected. Fracturing on sidewalls, hangingwalls and footwalls is mostly face-parallel.

Note: *As used locally, the term 'undercut' means the leaving intact of the Basal quartzite immediately above the Basal Reef, thus not exposing the overlying Khaki shale. Where the whole sequence (Basal Reef, Basal quartzite and Khaki shale) is removed, the mining method is referred to as 'open stoping'.*

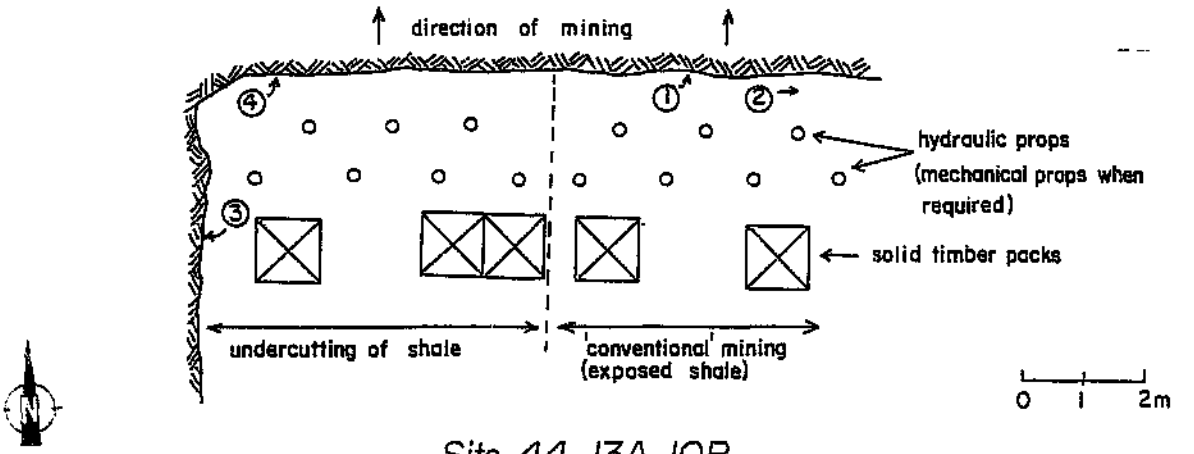
Site 1: 44-13A

In this area of operations 'conventional' (scattered) mining, with undercutting of the shale band in places, was performed. The undercutting was done in an attempt to increase the integrity of the hangingwall, reducing the amount of rockfalls that were likely to occur. Fig. 3.7 shows a sketch of panels 10A and 10B, with the mining configuration and the locations of photographs taken (see also Appendix B).

Site 2: 46-S4

At this site, on level 46 (1402m below surface), two mining faces were visited: 46-S4-S1 and 46-S4-W8. In both cases no undercutting was performed and the shale band was clearly visible.

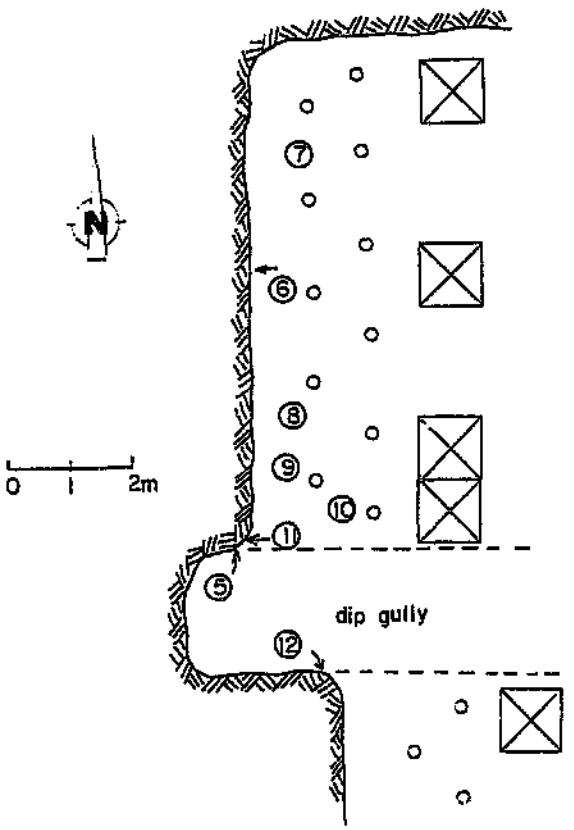
Fig. 3.8 (Appendix B) shows the panels, indicating where the photographs were taken.



Site 44-13A-10B

Photographs:

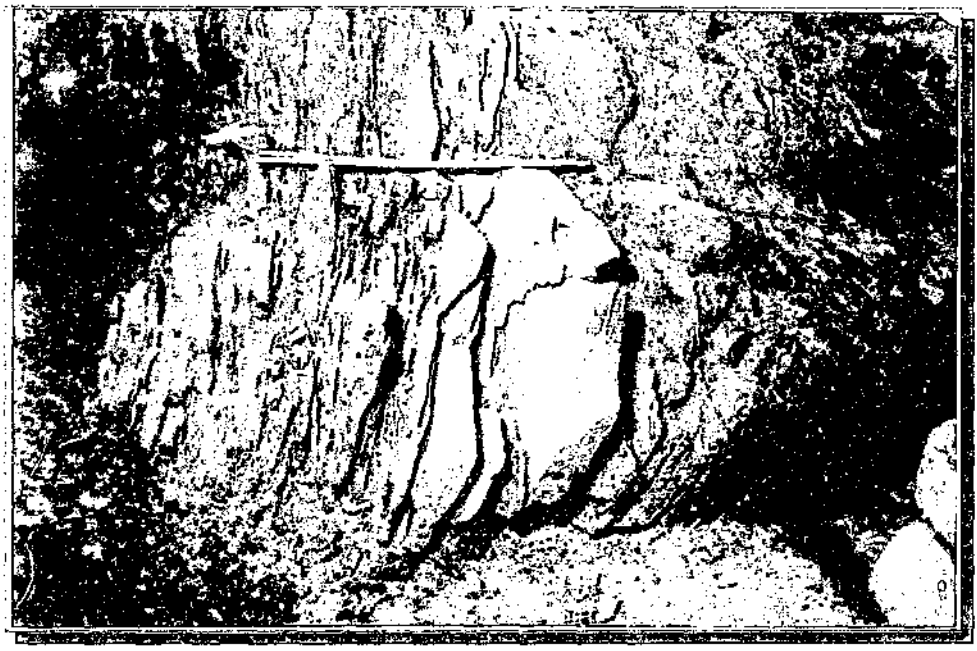
* [1] stope face with shale band exposed (stoping width ~ 0.8m)
* [2] stope face (downdip; eastwards)
[3] slabbing of west sidewall
[4] undercut face



Site 44-13A-10A

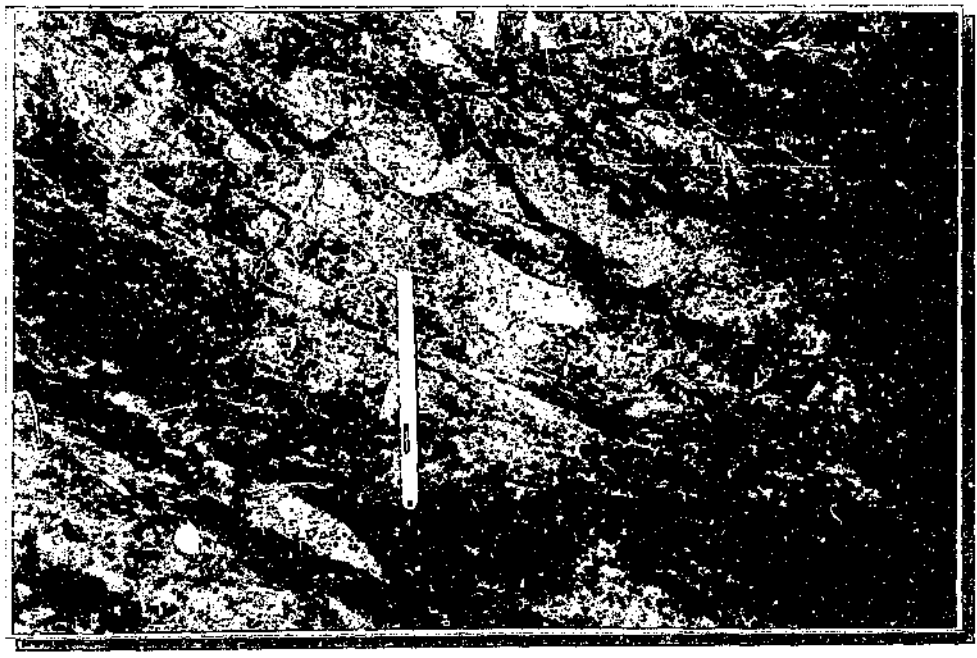
* [5] updip panel; fractures ahead of the face as seen from dip gully
* [6] stope face (shale is undercut)
[7] footwall (~ 1.2m from face)
[8] footwall (~ 1.0m from face)
* [9] hangingwall (~ 1.0m from face)
* [10] stope face corner with gully
* [11] hangingwall at stope face corner with gully
* [12] dip gully sidewall

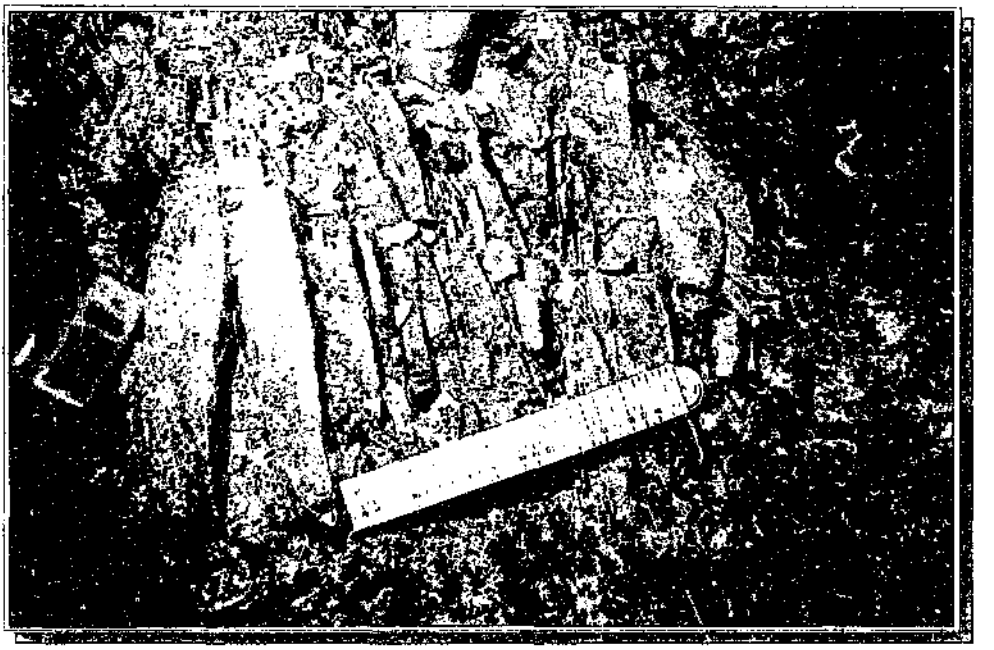
Fig. 3.7:
Sketch of panels 10A and 10B, site 1, with the mining configuration and the locations of photographs taken. The photographs whose numbers are preceded by an asterisk are located in Appendix B.



Above: Site 44-13A-10B, Photo No 3

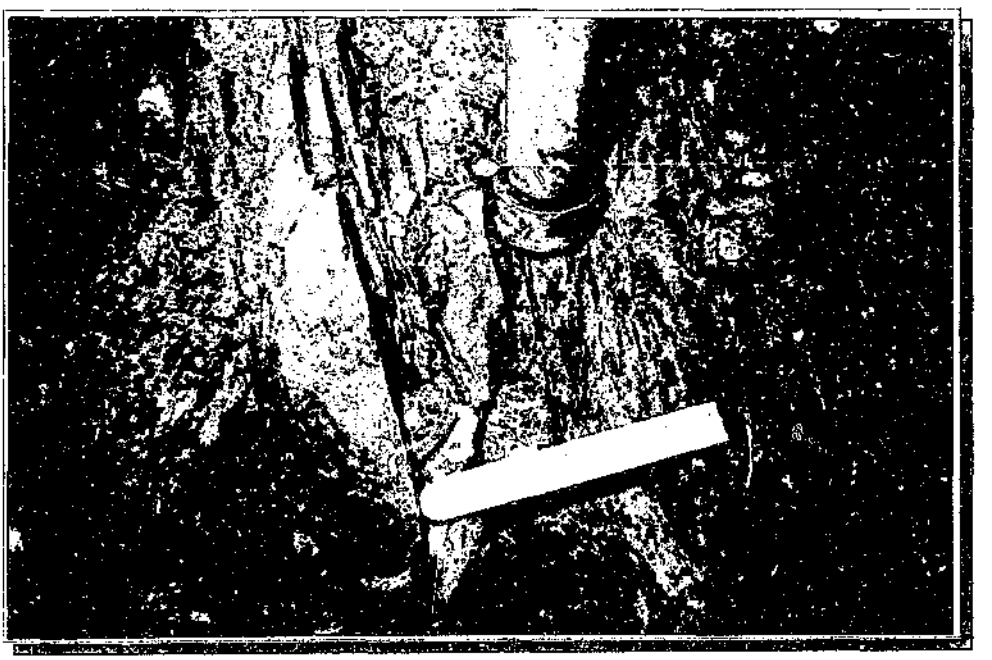
Below: Site 44-13A-10B, Photo No 4





Above: Site 44-13A-10A. Photo No 7

Below: Site 44-13A-10A. Photo No 8



Site 3: 48-D12

On level 48 (1463m below surface), two areas of mining were again visited. In the first instance, at 48-D12-N2, the mining was breast undercut, northwards, at a stoping width of 1.0m, abutting against a 100m[illegible] pillar which locks the Arrarat fault in the east.

The panels on 48-D12-N6, in the second instance, were also undercut and advancing in a direction dictated by the best possible negotiation of this remnant.

Fig. 3.9 (Appendix B) sketches the area[illegible]ning and locations of photographs.

(3.3) Spatial and Temporal Distribution of Seismicity

A total of almost 3000 events were recorded in the Postma area from the beginning of January 1991 to the end of December 1994. Figs. 3.10a-c (the latter two are located in Appendix C) and 3.11a-b show plots obtained from the seismic visualisation and interpretation software package '4Di' (refer to Section 2.5, Chapter 2 for a description of the capabilities of the software; the plots (in either plan or sectional view, as indicated) show the faces of the mined-out reef, the Postma dyke and Basson fault, and the locations of recorded events in relation to these. The 'colour scale' indicates the time frame used; the 'size scale' displays the seismic parameter chosen to represent each event. The distribution of seismicity in space and time corresponds very well with the locations of mining activities at the time. Figs. 3.10a,

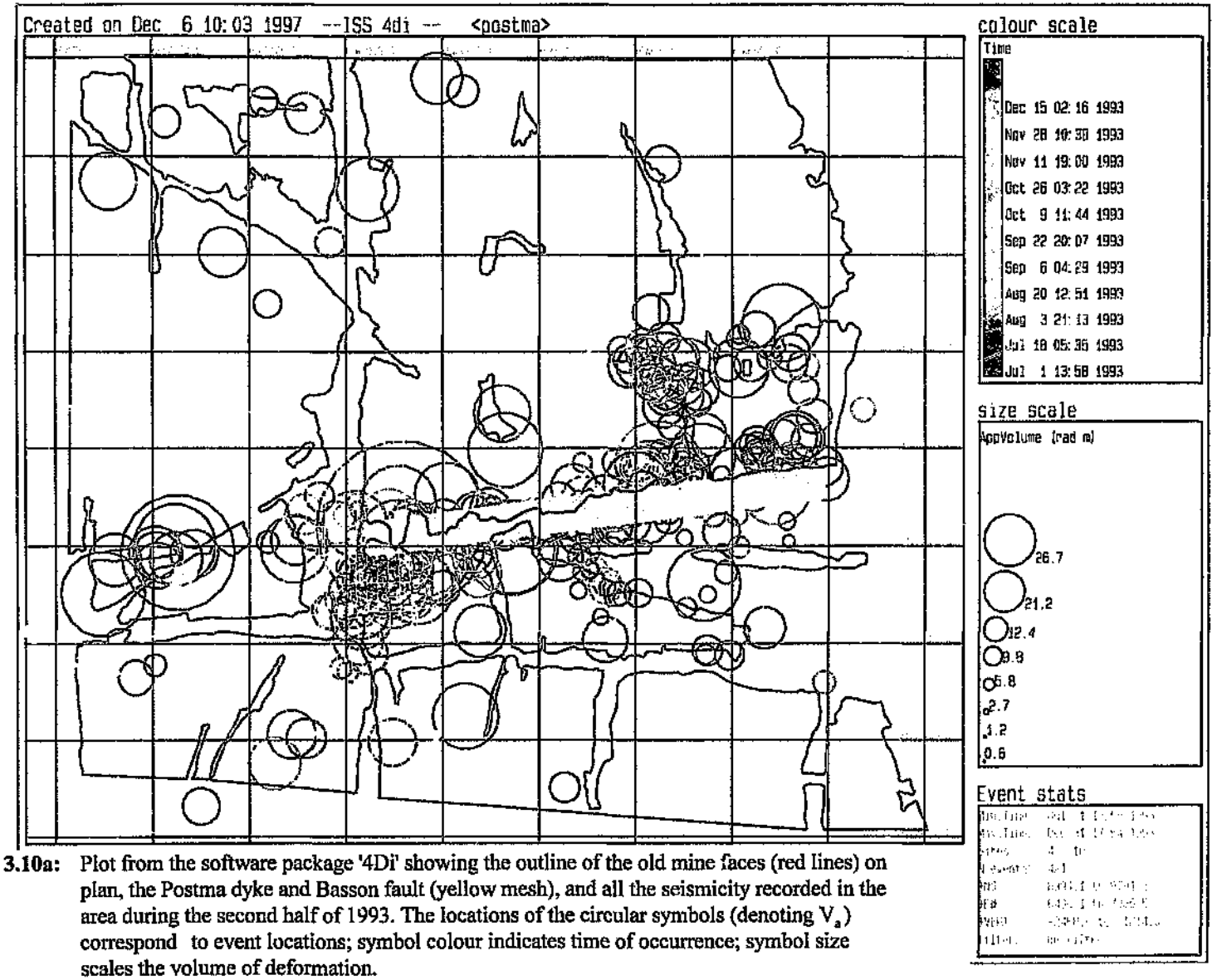


Fig. 3.10a: Plot from the software package '4Di' showing the outline of the old mine faces (red lines) on plan, the Postma dyke and Basson fault (yellow mesh), and all the seismicity recorded in the area during the second half of 1993. The locations of the circular symbols (denoting V_a) correspond to event locations; symbol colour indicates time of occurrence; symbol size scales the volume of deformation.

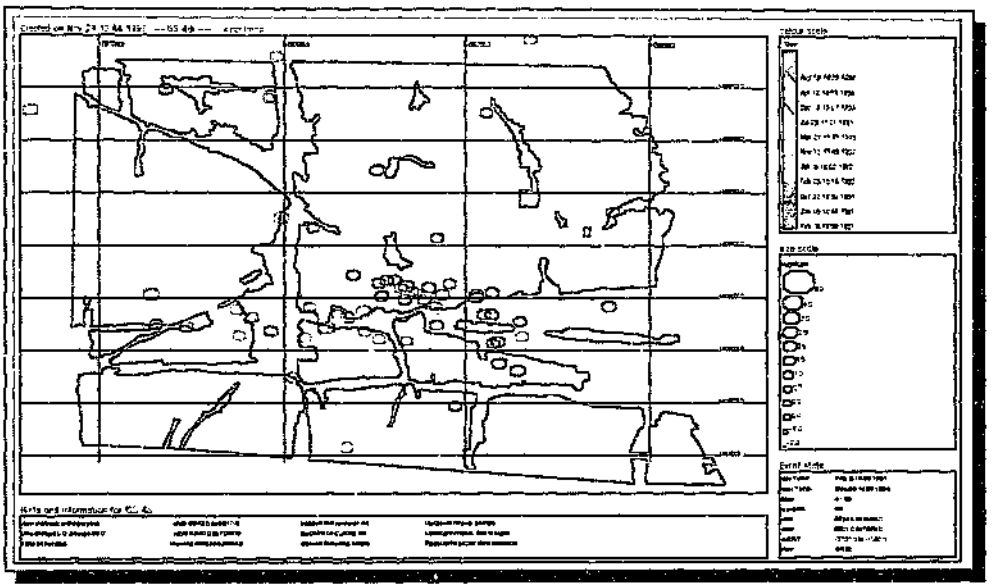


Fig. 3.11a: Selected events with local magnitudes greater than 1.5 in the time period 1/1/91 until 31/12/94. The symbols representing the events, in this case, denote local magnitude.

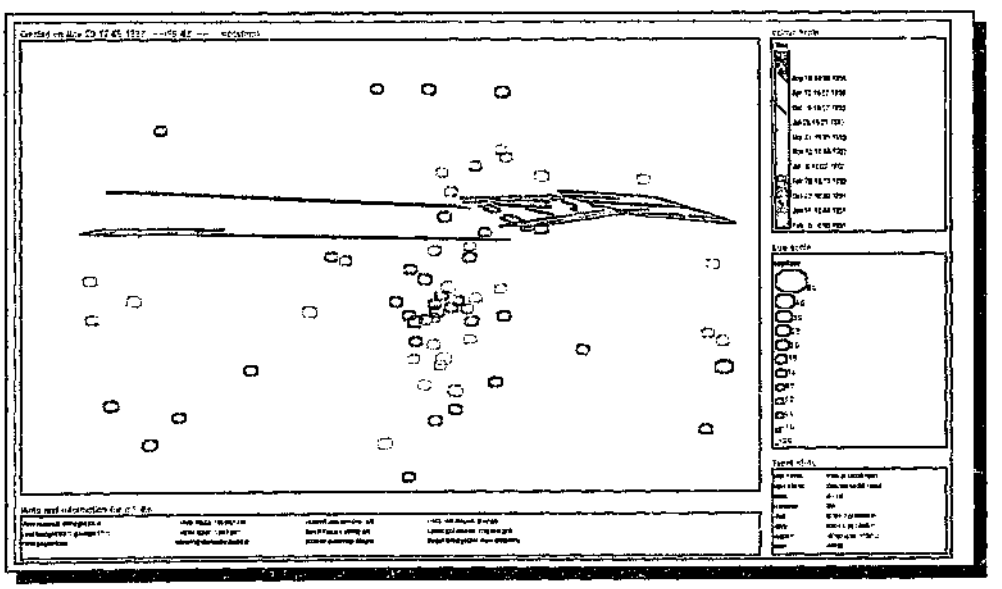


Fig. 3.11b: Same as fig. 3.11a but looking sectionaly eastwards along the reef horizon. For vertical scale consider the vertical extent (dip length) of the Basson fault model (280m).

3.10b (Appendix C) and 3.10c (Appendix C) show all the seismicity recorded during the second half of 1993, and first and second halves of 1994, respectively. Subsequent to the largest event ever recorded in the area, a local magnitude 3.7 at the Postma dyke - Basson fault intersection on 27th June 1994, mining operations were shifted about 250m eastwards, followed by an accompaniment of the mining-induced tremors. (The possibility of stress-loading of the Postma dyke, or stress transfer, is investigated later, in Section 3.4.1)

Events are clustered close to the working faces on plan. The termination of excavations at various sites led to a cessation of the occurrence of events. In section there is a larger variation in depth of hypocentres, with the events distributed in a tabular fashion, vertically, around the Postma dyke.

Fig. 3.11a shows a selection of events greater than local magnitude 1.5; fig. 3.11b shows their spread in depth (the '4Di' plot, in this case, shows a sectional view, looking eastwards along the reef horizon, orthogonal to the grid (mesh) representing the Basson fault). Very few of these events are located close to the sites visited during the first quarter of 1994. With due consideration being given to errors in hypocentre (up to 30m), there is a division of locations, differentiating between small-scale (approx. less than magnitude 1.0) and larger scale seismicity (greater than magnitude 1.5). The 'microseismicity' appears to be more directly associated with the mining activities, while the larger events, forming part of a different population, seem to correlate more with geological structure (although still a result of the mining, but on a macro scale) and, to a lesser degree, actual remnants, rather than active stope faces. The Postma dyke, in this case, is especially prone to the larger events, consistent with

previous statements (e.g.van Aswegen, 1990, p722; Aref, Jager and Spottiswoode, 1994, p2,7-8) that larger events can arise due to slip along planes of weakness or failure of highly stressed parts of the rockmass (e.g. dykes, pillars, remnants and abutments).

(3.4) State of Stress Inferred Seismically

The seismic parameters of energy index (EI), apparent stress and seismic stress are expected to indicate whether or not a particular volume of the rock is more stressed than the norm.

The stressed conditions observed underground are corroborated by the high values of energy index of some events located close to the working places (on plan), as shown in fig. 3.12 with selected events having EI > 1 (i.e. events whose measured seismic energy is greater than the average seismic energy released for the same seismic moment -- refer to Section 2.4, Chapter 2). Fig. 3.13 is a contour plot (see Section 2.5.2, Chapter 2 for a description of the contouring process) of seismic stress for the same time period as fig. 3.12. Comparing with fig. 3.6, there is a strong correlation between the zones with elevated stress, as inferred seismically, and the mapped sites with recent mining activity. As reef became exhausted and mining operations ceased in the southern portion of Site 3 (48-D12) during this time period, the seismic stress regime ebbed into background levels, but remained high at working places, including the other sites visited.

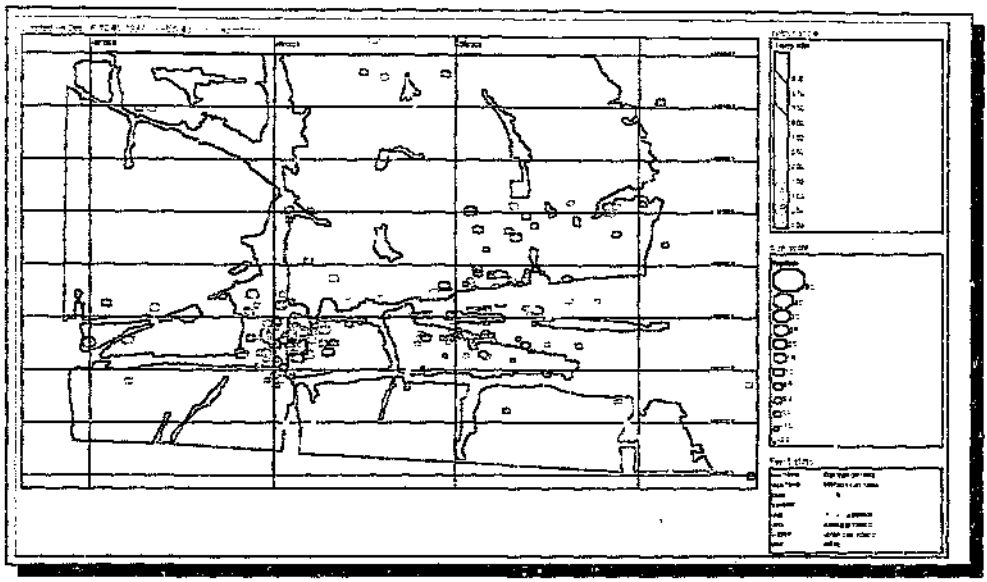


Fig. 3.12: Selected seismic events during the 6 months encompassing the last quarter of 1993 and the first quarter of 1994 with EI > 1.0. Symbol colour portrays the energy index of the tremors; symbol size corresponds to local magnitude.

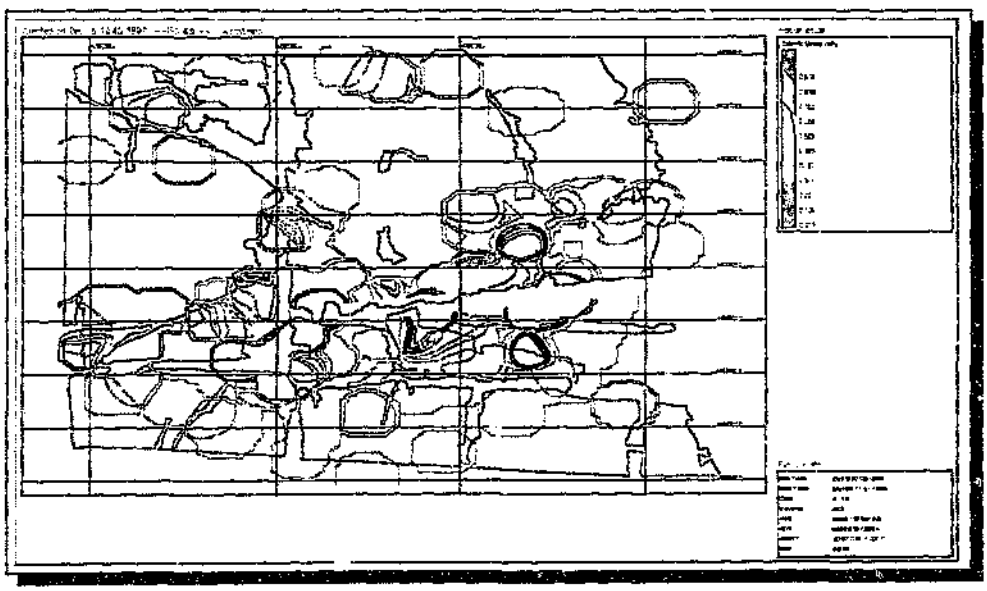


Fig. 3.13: Contour plot of seismic stress. The time range of seismicity is the same as fig. 3.12.

Differences in the seismic character between 'conventional' (open) and undercut mining areas:

Two different stoping methods are likely to lead to the formation of different fracture patterns, and hence character of seismic energy released. In the Postma area, with 'open stoping' and 'undercutting' of the band of Khaki shale being performed in close proximity (for a photographic record see Appendix A, vol. 2), such variations may be subtle and difficult to discern, even with good seismic coverage.

In Site 1 (see fig. 3.6), undercutting of the shale band was performed adjacent to an open mining method in places. It is anticipated that the spatial seismic resolution is insufficient to allow the differences in mining to be captured at this site. Sites 2 and 3, on the other hand, with open stoping in the former and undercutting in the latter, an adequate distance apart and further removed from the influence of the Postma dyke and Basson fault, offer a better prospect of success.

In an attempt to provide information about the stress change which takes place at the source areas, and hence differentiate between open and undercut stope panels, events within the seismic moment range 8.5 to 9.5 (in log[Nm]) (i.e. events of similar inelastic deformation) were selected to produce the plot shown in fig. 3.14:

Observations:

A small but discerning pattern in seismicity differentiates Sites 2 and 3: a few events of higher energy index (EI) coupled with larger apparent stress (σ_a) took place close to the 'open' stopes. A much higher number of events also occurred at Site 2 compared to Site 3, during the time period considered (1/1/93 - 30/3/94). This time period corresponds to the time when Sites 1, 2 and 3 were visited, documented and active stoping was taking place.

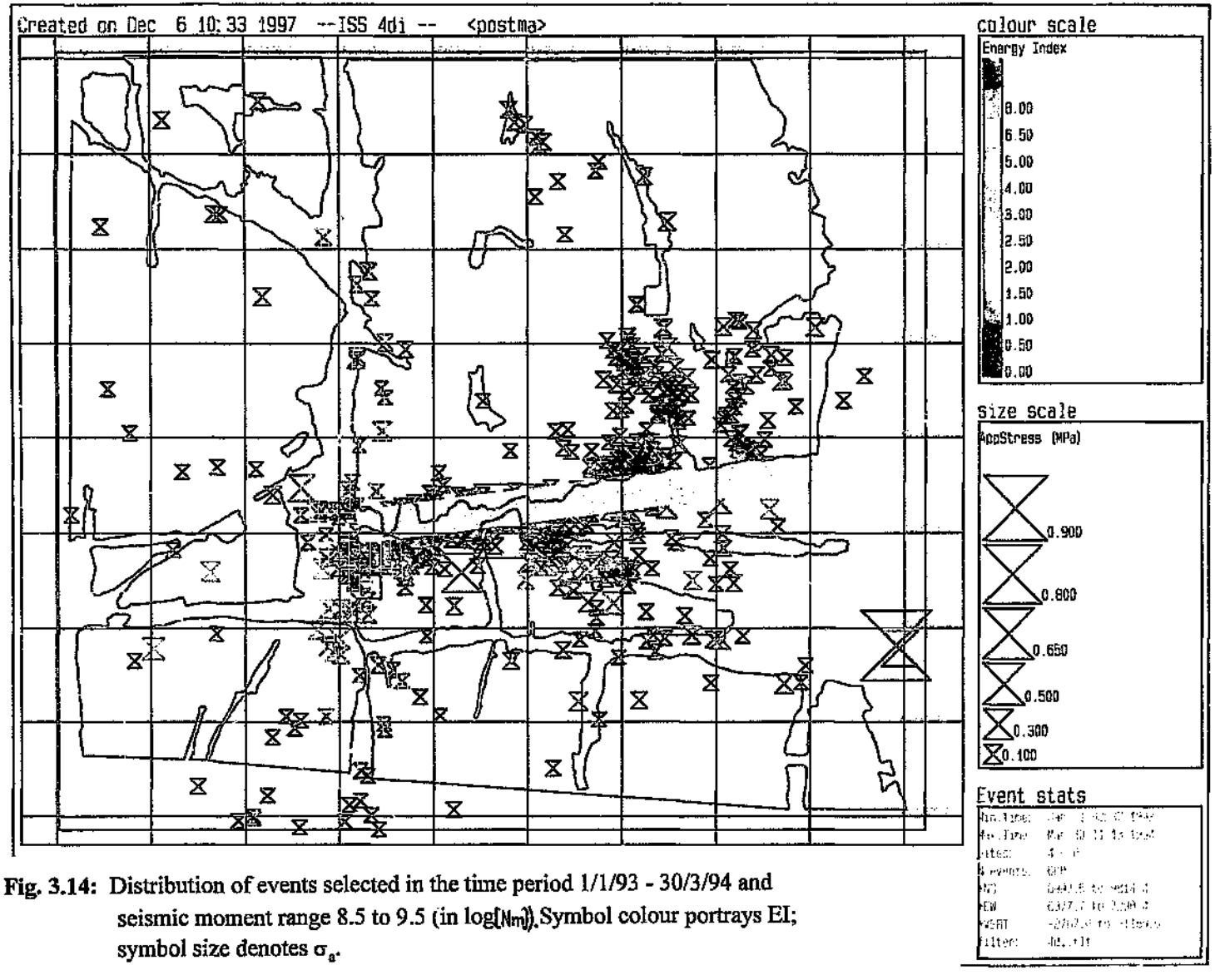


Fig. 3.14: Distribution of events selected in the time period 1/1/93 - 30/3/94 and seismic moment range 8.5 to 9.5 (in log[Nm]).Symbol colour portrays EI; symbol size denotes σ_a.

Similar exercises conducted across other magnitude ranges and time periods support the first observation, where events of comparable M_0 show higher E (and/or EI) and σ_a. A greater number of- and larger events with larger apparent volume (V_a) took place at Site 2 (open stoping) in preference to Site 3 (undercutting of shale).

Discussion:

Site 2 is mostly surrounded by previously mined ground, and as will be shown by numerical elastic modelling in Section 4.1, Chapter 4, is anticipated to be highly stressed. Site 3 strips along the Arrarat fault in the east and the northern contact of the Postma dyke, with blocks of unmined ground situated on the opposite side of the dyke, in the south. Mining spans at both sites also varied considerably (see figs. 3.7 to 3.9). An inhomogeneous stress distribution thus complicates an analysis of seismicity, from which information about stress changes in the source areas could be provided, but where events may not simply just reflect dissimilar mining strategies. For these reasons a proper characterisation of the recorded seismicity, which might capture the different mining methods (viz. 'open' and undercut) is elusive.

The lower magnitude seismicity, with some events having high values of EI, suggest a particular high-energy, low-deformation rockmass response at Site 2, even with wider openings and a weak hangingwall. Rockmass deformation at Site 3 in the direct vicinity of the Arrarat fault may have come through aseismic creep, with dissipation of strain energy, explaining the lack of recorded seismicity. However, it remains inconclusive as to whether this is a response to these particular mining methods or a result of the high variation in local stress conditions.

(3.4.1) Stress transfer along the Postma dyke

The contour plots of seismic stress and filtered apparent stress (figs. 3.13a and 3.13b, respectively) point to an increased potential for a localised dynamic instability at the intersection of the Postma dyke and Basson fault because a large amount of stress change with smaller magnitude (M_L mostly less than 1.5) seismicity has taken place (in a geologically weak volume of rock). As discussed in the next chapter, this zone produced a large magnitude event (M_L 3.7) some three months later.

Although the middle part of the Postma dyke was seismically active before the large event took place due to minor works in the area, the immediate acceleration in the occurrence of seismic events subsequent to the large event suggests a possible loading of the rockmass as a result of stress transfer towards this and other parts of the dyke. Kijko, Funk and v.Z. Brink (1993, p1-5) demonstrated that clusters of seismicity, separated by more than 1000m, within a mine, can and do interact. It is likely, therefore, that stress transfer between areas occurs commonly.

Two ways of testing whether the increased rate of seismicity was, in fact, due to stress transfer over a distance of some 250m both involve an empirical analysis of the E - M_0 relation:

In the first instance consider figs. 3.15a and 3.15b, both showing the relation between E and M_0 using events recorded six months before (3.15a) and after (3.15b) the large event, selected 100m on either side of the Postma dyke and thus likely to be directly associated with it. The latter reveals that for the same seismic moment, more seismic energy was released on average, indicating more stressed conditions than before.

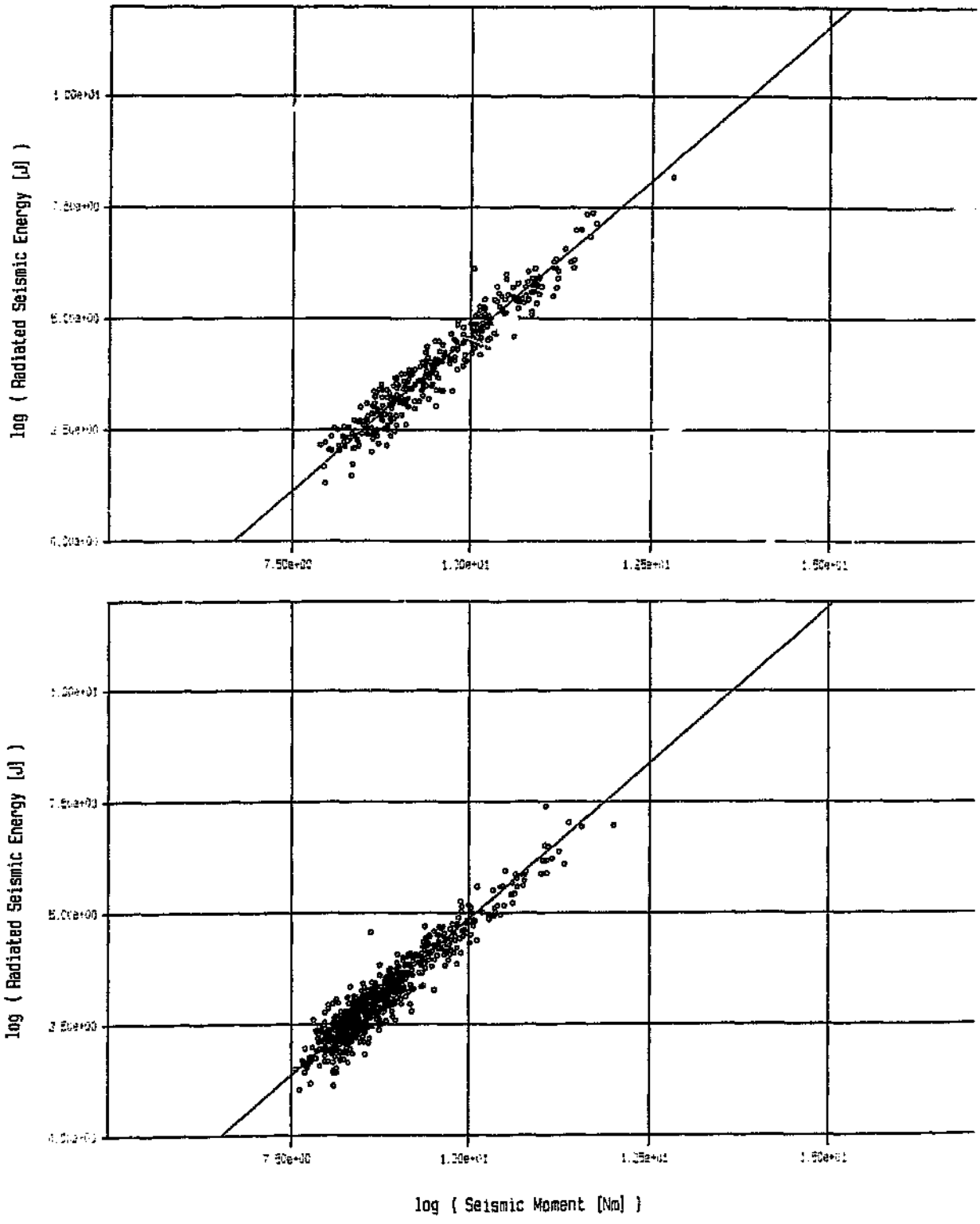


Fig. 3.15a (top): Relation between E and M_0 using events selected 100m either side of the Postma dyke during the first half of 1994.

Fig. 3.15b (above): Same as fig. 3.15a, but using events recorded during the second half of 1994.

(Events selected within a restricted magnitude range (e.g. M_L -0.5 to 0.5) indicate a similar displacement in the best-fit line.)

In the second approach, events were selected about the dyke as before, but filtered to include only those of comparable deformation. in the local magnitude range -0.5 to 0.5. An empirical E - M_0 fit thus obtained shows, in fig. 3.16, that prior to mid-May 1994 (the large event occurred on the 27th June 1994, as indicated by the inverted arrow on the time axis) the dyke was generally less stressed (lower $\log_{10}$EI, time averaged over 15 days to smooth out short term fluctuations) than after. Before the large event the majority of events clustered close to the fault - dyke intersection. Immediately after, most events occurred at the centre region of the dyke, while operations ceased near the fault - dyke intersection. The stress decreased sharply from a 'background' level from mid-March 1994, reached a low towards late-March and thereafter began to increase. This fluctuation reflects nucleation processes leading to an M_L 2.7 tremor which took place on the Postma dyke on 24 April 1994 (evaluated in greater detail in Section 4.2.5 of Chapter 4). Stress conditions on the dyke attained the 'background' level again in late April 1994, continued to build up towards the M_L 3.7 event in late-June and peaked a few days after its occurrence. The increase in stress just before this event may be a result of the loading of some asperity close to the fault-dyke intersection, the ultimate failure of which may have given rise to the M_L 3.7 event (discussed in the next chapter). However, the overall stress condition of the dyke is shown by fig. 3.16 to be higher following the big event over the next 2 -3 weeks, an unlikely result of the transferral of men and equipment from the former working area in such a short period of time, demonstrating a loading effect brought about by the large event. After this transfer of stress the incidence of seismicity may have been further exacerbated by a step-up in the stoping operations at the centre region of the

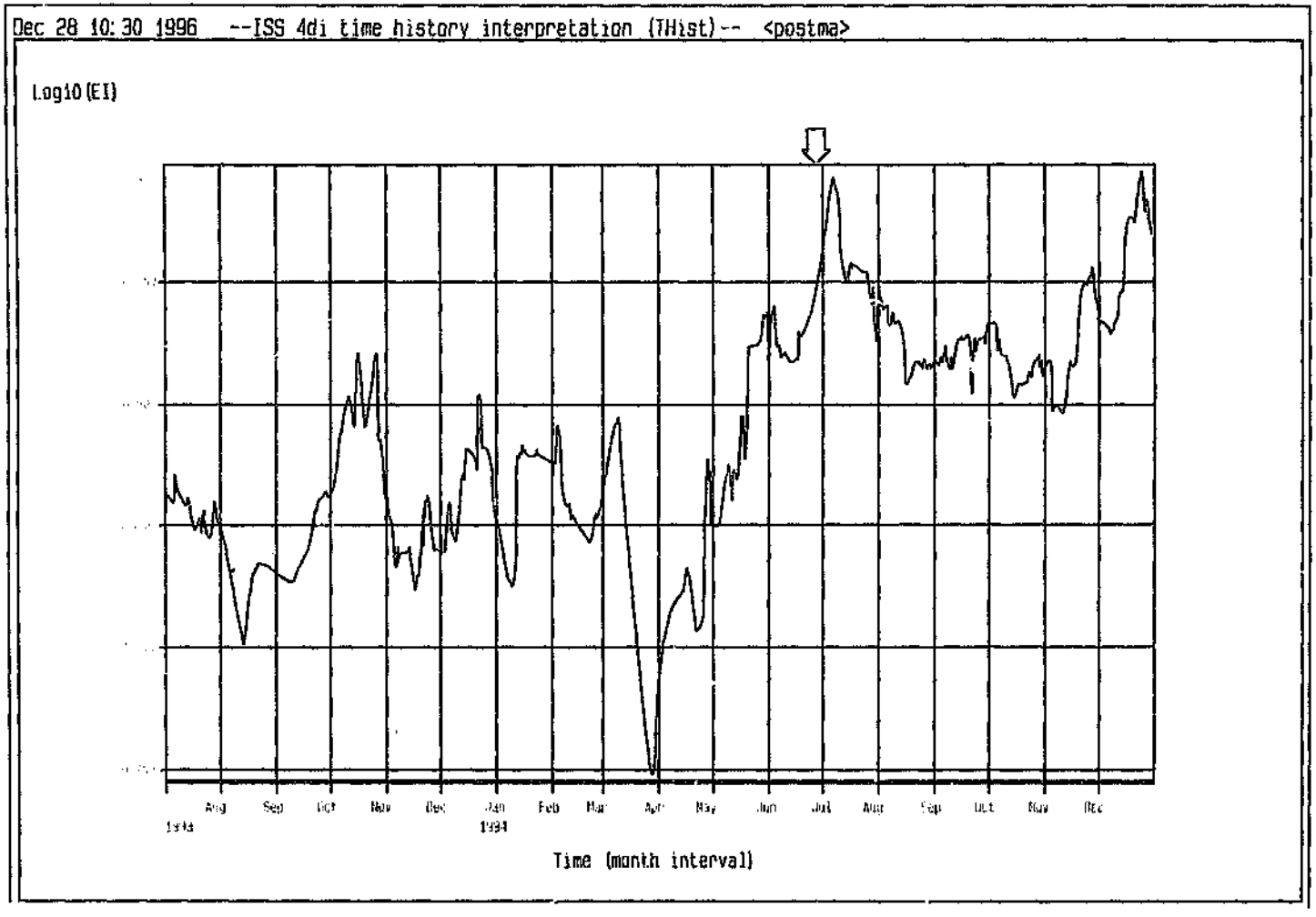


Fig. 3.16: Time-variation of EI during the period between July 1993 and December 1994. The data was averaged over a 15-day time-window to reduce short term fluctuations.

dyke, but the general stress level remained distinctly higher for the duration of 1994, compared to that prior to mid-May 1994.

(3.5) Summary and Discussion

The geophone coverage of the study area was found to be sufficient to allow recording of events of moment magnitude greater than -0.6, enough for a detailed investigation of seismicity. An analysis using the software package 'Errmap' (Sciocatti, 1994) indicated what the extent and limits of detectability were for events of magnitude 0.1 and 0.8, respectively. Vertical resolution is expected to be poorest due to the tabular distribution of seismic stations on reef, but the spatial location accuracy in the areas of interest should be better than 30m.

Mining operations in the Postma area were usually done under adverse conditions, and consequently the mining practices were adapted to extract the reef in an optimal but unconventional manner, according to recommendations issued by the Rock Mechanics Department of the mine. A general eastward dip of a reef dictates that the advance of mining, under normal conditions, should be in a northerly and/or southerly direction(s), accompanying the progress of strike gullies along the plane of the reef. This was seldom the case in the Postma area, with its scattered mining. The shooting of updip and downdip panels was often required, but the direction of face advance was site dependant.

The photographs taken at the various sites brings the state of the rockmass into perspective. Typical of stressed areas there is a high frequency of fractures around the

underground openings, the predominant orientation of which follows the advancing stope face shape. Stress concentrations which occur on sharp edges/corners of a mining layout explain the elevated amounts of failure and deformation observed at these points. It was not possible to correlate any photographic evidence of slip along planes of weakness with specific tremors occurring in the area, mainly because all the seismicity registered during the first quarter of 1994 was mostly of very small magnitude. These small tremors were not capable of inducing large ground motions leading to noticeable relative movement between parting planes.

It was shown by the photographs taken of the hangingwall close to and removed from the advancing face that the condition of the rockmass deteriorates. The rate at which it deteriorates is a function of amounts of closure.

In the period 1/1/91 to 31/12/94, 270 events with local magnitudes greater than 1.0 were recorded; 18 greater than 2.0 and 2 greater than 3.0. There is a distinct separation of larger events in relation to the locations of the smaller magnitude seismicity. The division seems to occur between local magnitudes of 1.0 and 1.5. Events of greater magnitude coincide with geological structure; those of less magnitude are more readily associated with the active stope faces.

The irregular mining configurations, tied in with other factors such as geological disturbances and high levels of stress, no doubt exacerbates the incidence of seismicity in the Postma area. The high state of stress inferred seismically supports the observations underground.

An almost immediate shift in the occurrence of seismic events in a cluster close to the intersection of the Postma dyke and Basson fault to another part of the dyke, some 250m east, after the incidence of a large event, but before the transfer of full-scale stoping operations to this latter region, most probably took place as a result of stress transfer along the dyke (refer to figs. 3.15a, 3.15b and 3.16). This observation concerning the rock surrounding underground excavations, shedding and/or picking up loads as the rockmass adjusts to stress distributions due to mining, supports the notion of some rheological nature of the rock, which the numerical stress modelling programmes in common use, from experience, cannot usually cater for. This is an important consideration, investigated in greater depth in the next chapter.

4

QUANTITATIVE ANALYSIS OF SEISMICITY IN THE POSTMA AREA

(4.1) Stress Levels and Implications of Mining Adjacent to the Postma Dyke and Basson Fault.

A plane of weakness in an otherwise strong rock mass may be subjected to shear stresses induced by mining. Once the cohesive strength of such a plane is exceeded, asperities (i.e. a roughness on a fault surface subject to slip; sometimes also a previous unslipped portion -- as described in section 2.3.1, Chapter 2) loaded beyond their stress carrying capability will fail in shear, rupture occurs along the plane, and a slip-type event is produced. An analysis of stresses on such geological structures models the effects of mining.

(4.1.1) Calculation of stresses using PC-based elastic-continuum modelling:

The stress concentrations induced by mining are largest immediately in front of stope faces. They are especially severe in pillars, remnants or abutments. Shear stress lobes form ahead of the face, occasionally impinging on pre-existing planes of weakness, inducing excess shear stress (ESS), depending on the shear strength of the plane at some point of interest, creating the possibility for a slip/shear

type seismic event. The ESS concept (Ryder, 1988, p153; refer to Section 2.3.3, Chapter 2) allows the modelling of the effects of mining on geological structures, 'measuring' the shearing effect of mining induced stresses on geological structures. Various parameters influence the extent and magnitude of ESS zones (e.g. mining extent, convergence, depth, K-ratio, fault dip and displacement; described in Section 2.3.2, Chapter 2). The amount of ESS can indicate zones with greater potential for deformation and/or slip.

A boundary element computer program routinely used by rock mechanics practitioners in South African mines employs elastic-continuum theory to model multiple tabular excavations, which may be arbitrarily oriented with respect to one another. The program calculates stresses on- and off-reef, anticipated displacements and other parameters useful for the planning of mining layouts.

The depth of mining in the Postma area is around 1500m below surface. A vertical stress gradient of 0.030 MPa/m produces a vertical stress of 45 MPa; the horizontal stress is half of that. Elastic-continuum modelling shows that the virgin stress field may be altered by induced stresses due to the mining in such a way that the direction of the major principal stress in the resulting field stress either promotes or arrests a tendency for slip along a plane of weakness. Such a plane, favourably oriented, intersecting the shear lobe induced by a mining slot of sufficient extent at depth, might experience relative slip. If the plane of weakness is subjected to significant normal stresses, then it undergoes a clamping effect, the influence of induced shear stresses is limited, and the formation of positive ESS zones could be inhibited.

Both the Postma dyke and Basson fault have steep dips on average, and are expected to intersect shear stress lobes, if and where present, over considerable lengths of their surface. Since shear stresses usually increase with steeper fault planes, the extent of zones of positive ESS, along with ESS_{max}, are expected to be substantial.

The results of elastic modelling are illustrated in figs. 4.1 to 4.6. Vertical stresses, principal stresses and ESS's were calculated over the Postma area and part of the lengths of both the Basson fault and Postma dyke.

Observations:

Fig. 4.1 shows a gridded surface superimposed on the mined-out reef of the Postma area; at intersection points of the grid the amount of vertical stress (TZZ in MPa) was calculated. At these points the amount of TZZ is represented by the size of the symbol. As expected, the stress is greatest across the spans of rock where mining has not taken place, irrespective of the strain and coseismic or aseismic deformation that may have already occurred, an important aspect which this numerical modelling does not take into account. In these places TZZ is around 50 MPa, but may be over twice as much in remnant/pillar situations.

Figs 4.2a and 4.2b show orthographic views of the mined-out reef in the Postma area, looking westwards and northwards, respectively, and the curvature of the principal stress vectors about the openings in the rock. The length of the stress vectors indicates the strength of the stress field at that point. Maximum stress is shown ahead of stope faces, where abutments are formed naturally at fault-reef or dyke-reef intersections; a dome of destressed rock is created above and below the mined-out reef.

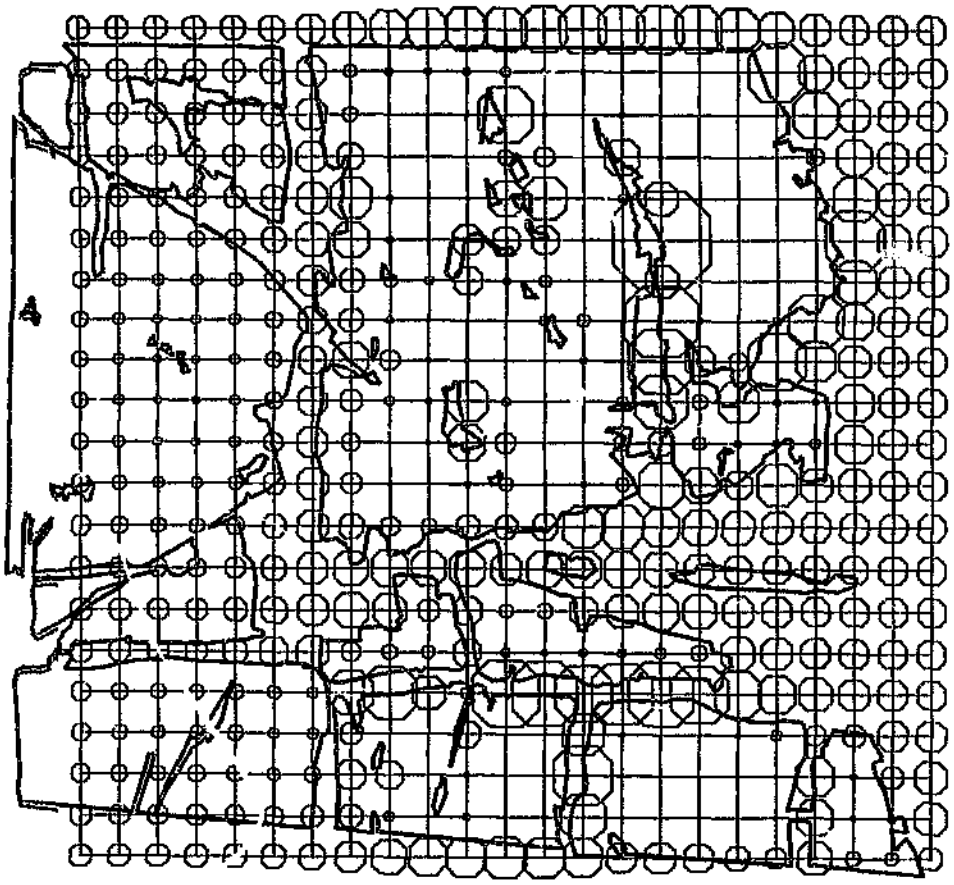
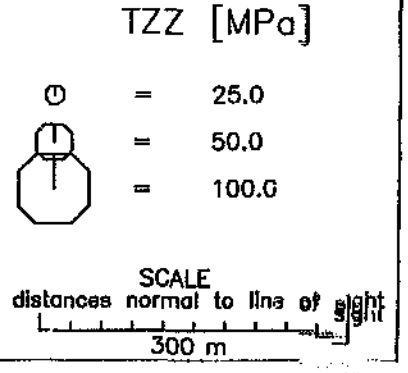


Fig. 4.1:
The Postma area with a gridded surface superimposed on the mined-out reef. At intersection points of the grid the amount of vertical stress (TZZ in MPa) was calculated using elastic-continuum modelling. The amount of TZZ, altered by mining, is represented by the symbol size.



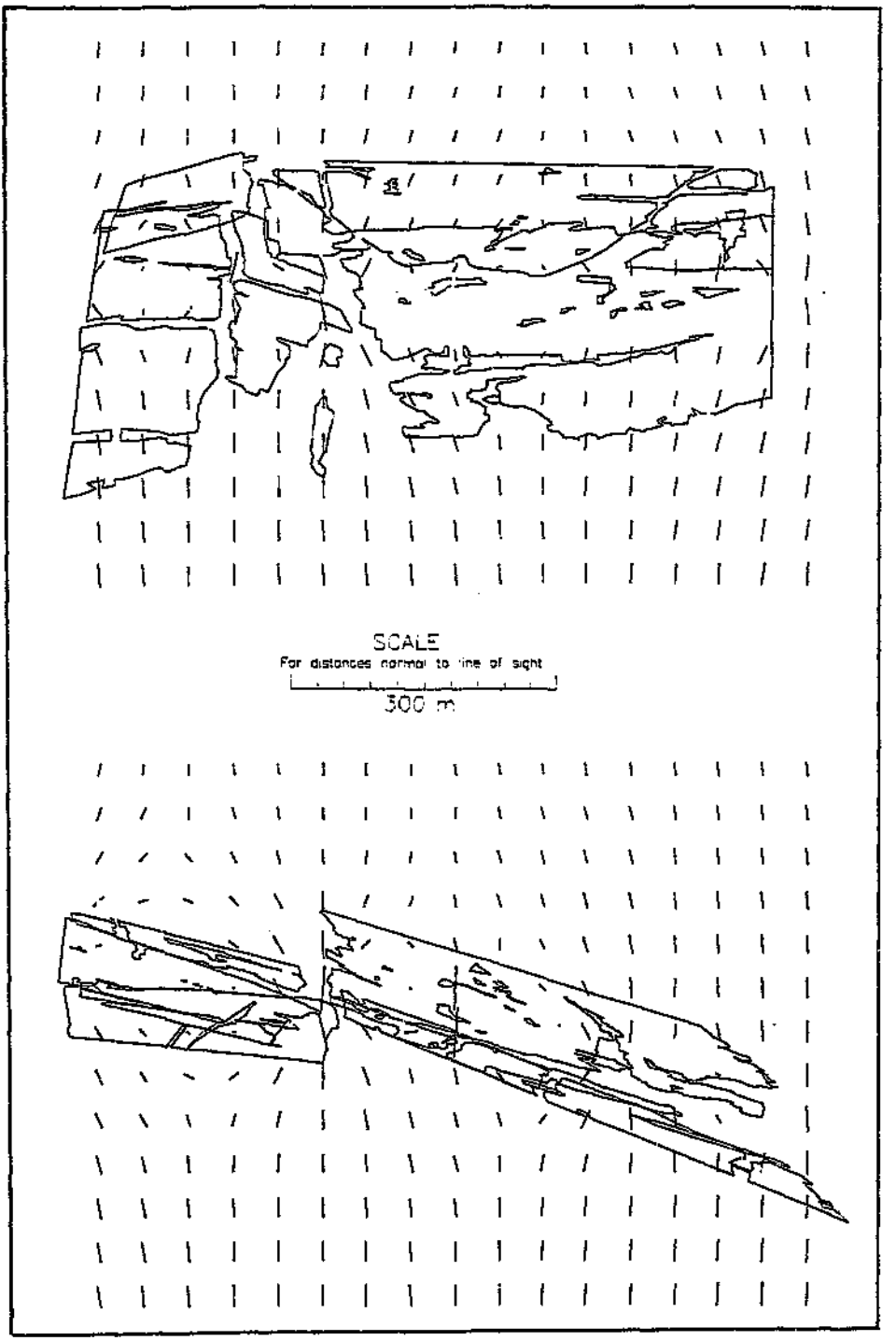


Fig. 4.2a (top): Orthographic view of the mined-out reef of the study area, looking westwards. The 'dashes' represent principal stress vectors on a vertical plane orthogonal to the line of view, the length of which indicates the strength of the stress field at that point.

Fig. 4.2b (above): Same as fig. 4.2a, but looking northwards.

TZZ along part of the Basson fault, as shown in fig. 4.3a, lies mostly in the range 25 - 50 MPa over the length of the fault loss area, but approaches 50 MPa in places, notably where the stoping did not fully extend to the fault surface, resulting in the creation of a bracket pillar / remnant.

The TZZ along the 'surface' of the Postma dyke (fig. 4.3b) is considerably higher at the reef-dyke contact, above 50 MPa at some points. Downdip from the reef the dyke is shown to be more stressed than updip, with a gradual increase in the stress with depth.

Figs. 4.4a. and 4.4b show the extent and magnitude of the major principal stress (σ_1) calculated for the Basson fault and Postma dyke, respectively, at the same points on the grid model. As expected, σ_1 increases ahead of the stope faces, curving around the mining slot slightly, and re-establishing its prior direction some distance into the hanging- and footwall parts of the fault and dyke.

The angle at which σ_1 intersects the fault and dyke is noteworthy, bearing in mind that ESS reaches a maximum when this angle swings to 45^0. In the case of the Basson fault (fig. 4.4a) the angle of incidence of σ_1 appears to be close to ideal over a considerable length of the surface, but more so in places where the mining intersects or approaches close to the plane of weakness.

The disturbance of the stress field by mining in the vicinity of the Postma dyke is greatest around the western blocks of the mined-out reef immediately south of the dyke, and in this zone ESS is expected to be at a maximum (fig. 4.4b)

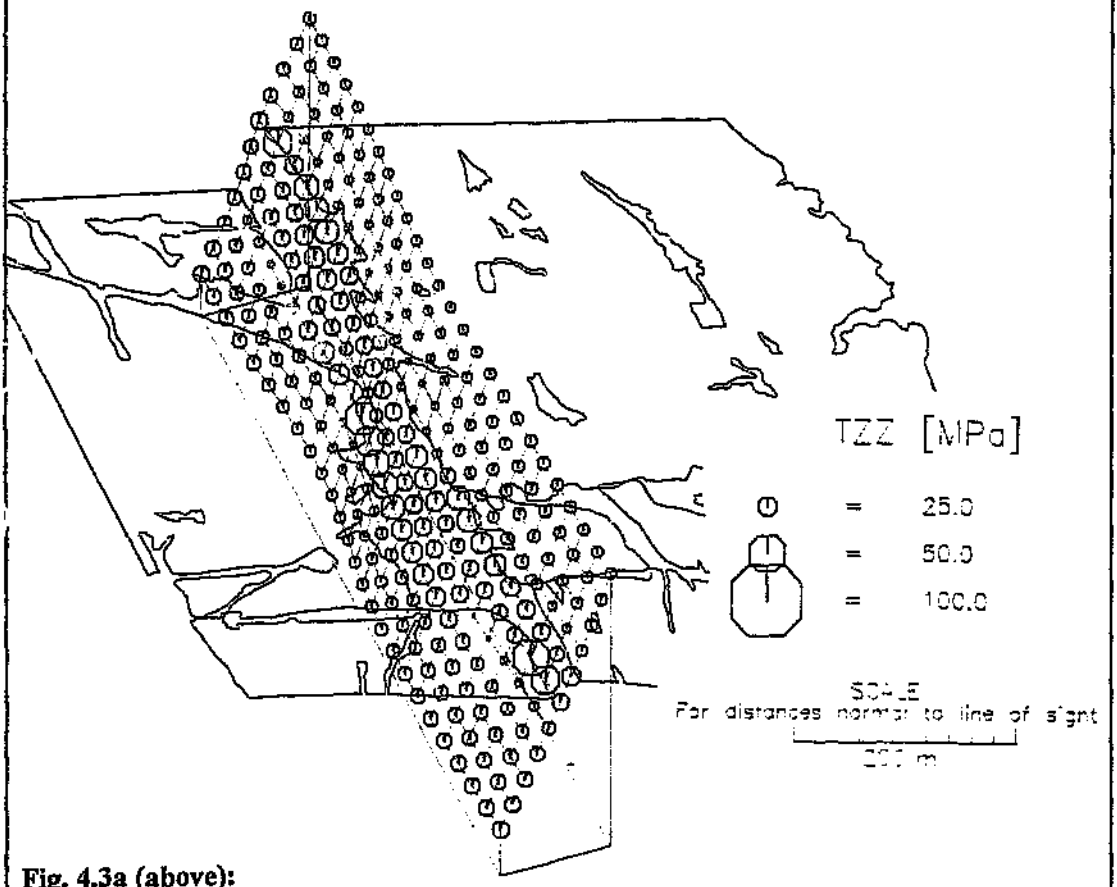
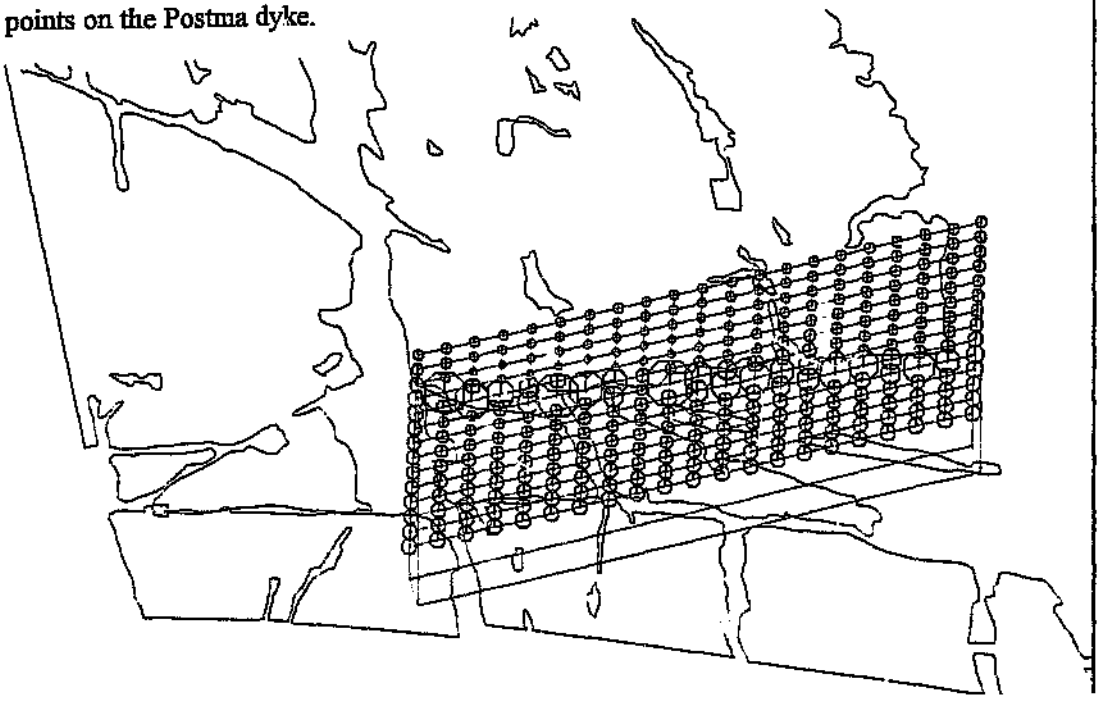


Fig. 4.3a (above):
The Postma area with a gridded model representing the Basson fault, using the same principle demonstrated in fig. 4.1.

Fig. 4.3b (below):
Similar to fig. 4.3a, but showing the calculated (elastic-modelled) vertical stresses at points on the Postma dyke.



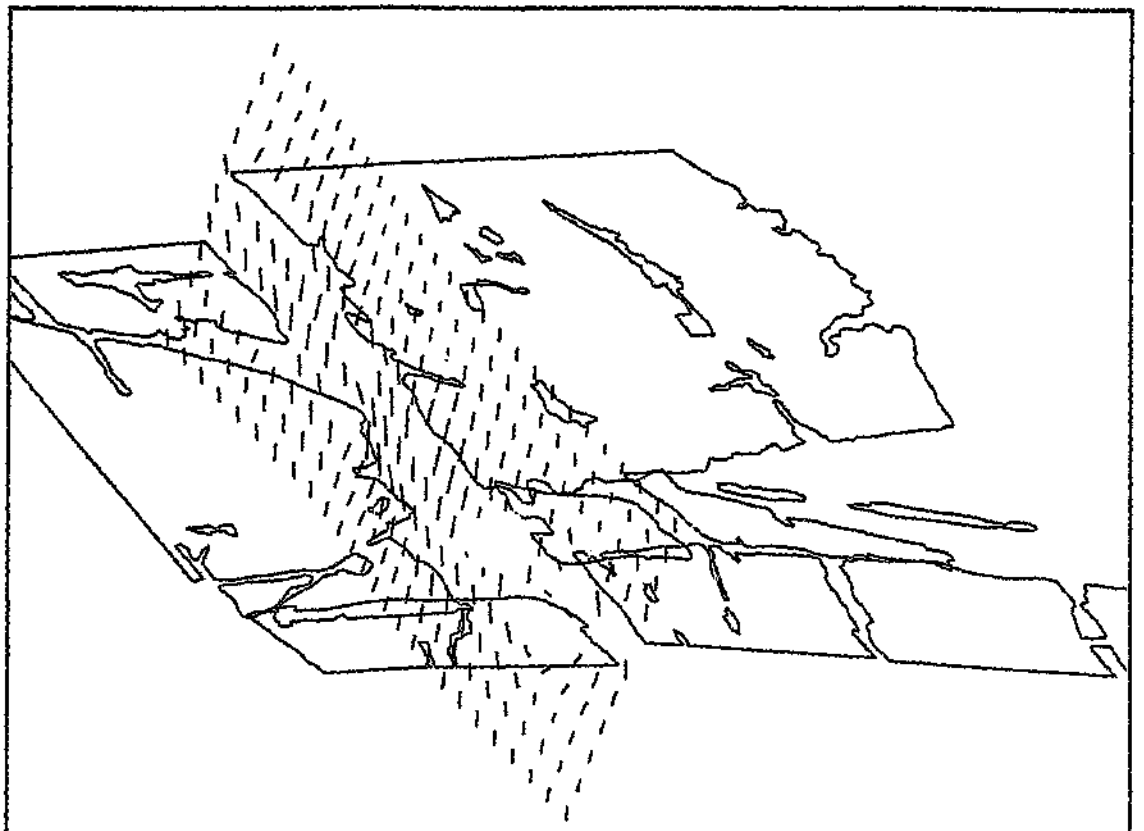
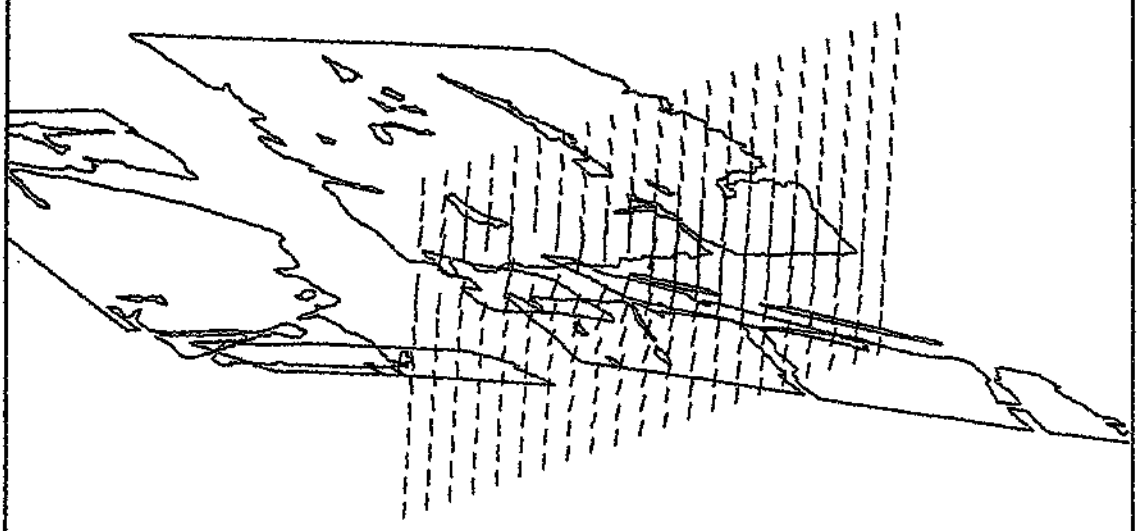


Fig. 4.4a (above): Extent and magnitude of the major principal stress, with orientation of stress vectors about the mined-out reef, at the same points on the grid model.

Fig. 4.4b (below): Similar to fig. 4.4a, but showing the principal stress acting on the Postma dyke.



The stage of mining to which the modelling applies corresponds to that represented by the mined-out reef in figs. 4.1 to 4.5 respectively (the modelling in figs. 4.1 and 4.2 coincides with an earlier mining stage). The ESS results (figs. 4.5a and 4.5b) delineate zones on both surfaces prone to slip, in general agreement with the statements above. One such zone on the Basson fault is indicated by prominent positive ESS vectors where the downthrown side of the mining, on the west side of the fault, impinges onto the fault, bringing the influence of the shear stress lobes onto it. It should be noted that although ESS is still being shown on this part of the fault (stoping terminated in 1971 and 1973 on the west and east sides of the fault, respectively) an investigation of the seismic database revealed that a number of events of large magnitude occurred in the area some two decades later, as discussed in Section 4.1.2.

A more representative ESS analysis should highlight the influence of the new mining, and disregard that of the old. The ESS modelling results represented in figs. 4.6a and 4.6b correspond to the change in stress brought about by the recent (post-1992) mining only (see fig. 3.6, Chapter 3, for the locations of newer mining areas). They were calculated using the difference between the stress situation at the stage of mining shown in fig. 4.5 and that of two years prior (i.e. the mined-out reef of fig. 3.6 minus the hatching).

Comparing fig. 4.6a and 4.5a, positive ESS has now all but disappeared along the fault. In the vicinity of the fault/dyke intersection the creation of significant positive ESS may be imminent if that portion of the lagging reef is mined and extended closer to the fault in the east.

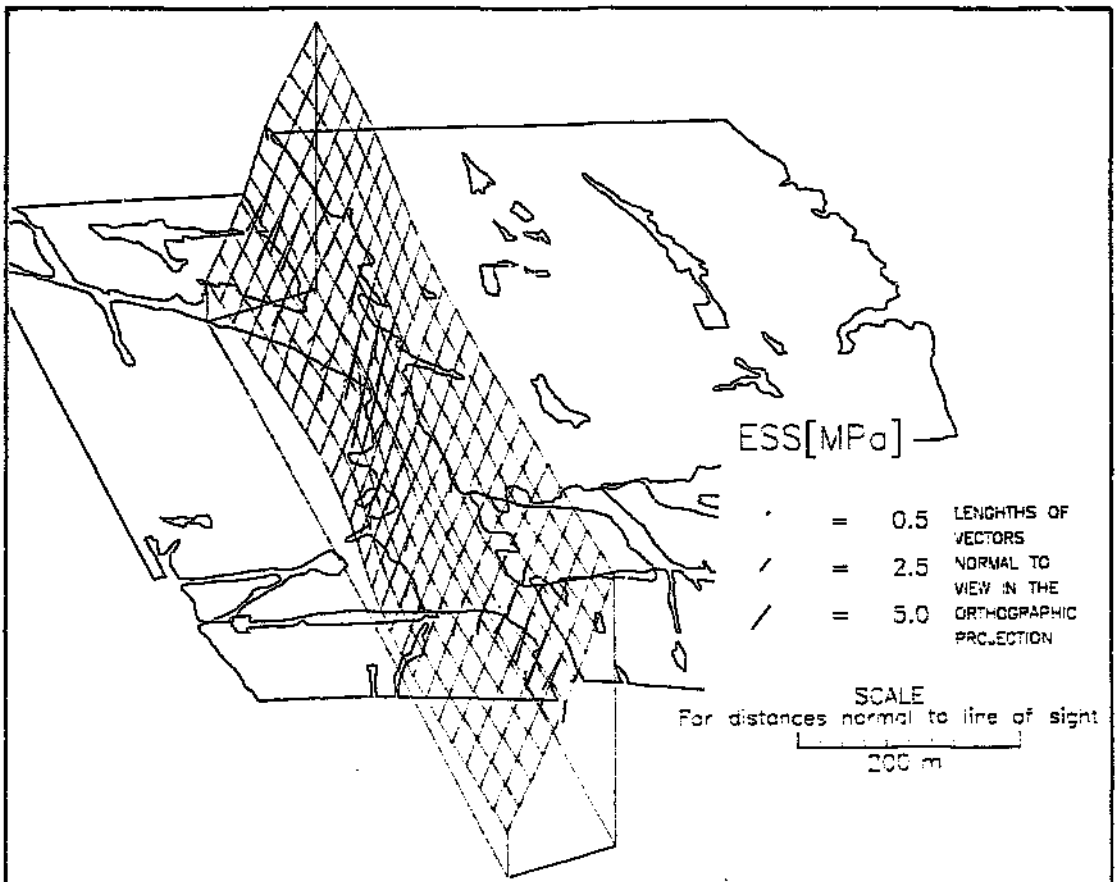
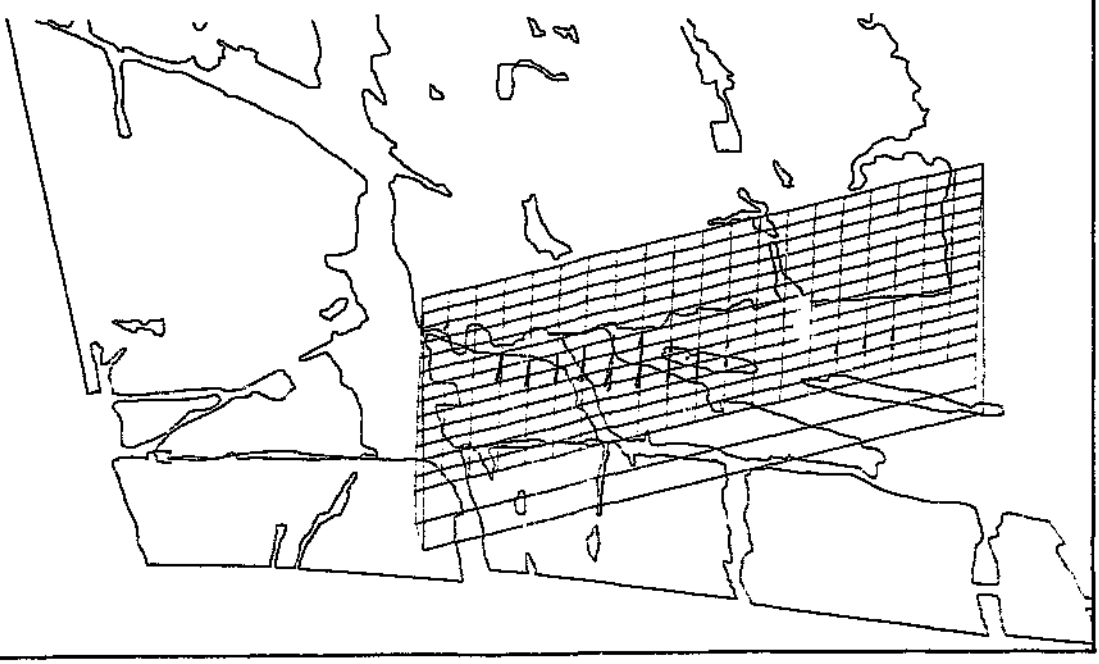
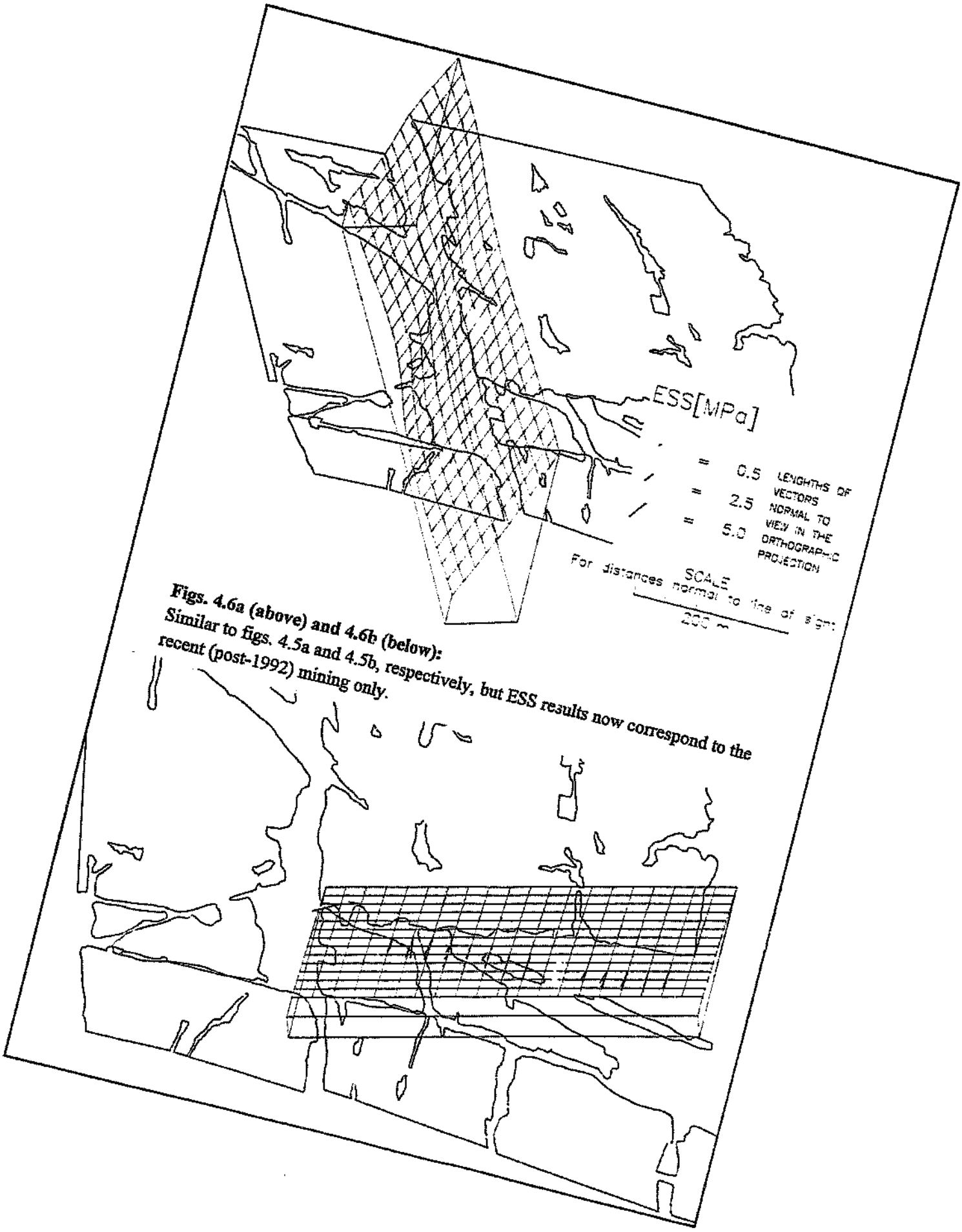


Fig. 4.5a (above): Extent of positive ESS at points along the Basson fault. The stage of mining to which the modelling applies corresponds to that represented by the mined-out reef.

Fig. 4.5b (below): Similar to fig. 4.5a; ESS results at points of the Postma dyke.





Figs. 4.6a (above) and 4.6b (below):
Similar to figs. 4.5a and 4.5b, respectively, but ESS results now correspond to the recent (post-1992) mining only.

A zone of concern, as indicated in fig. 4.5a, where recent re-development is taking place, is located further north at the intersection of the Basson fault with one or more minor NW-SE-trending faults. Positive ESS appears to be present over the remaining length of the fault-loss part to the north, illustrating a combined effect of shear stress lobes due to the extensive -- but old -- mining adjacent to the fault, in the hanging- and footwall. The lack of new mining, as revealed in fig. 4.6a, however, shows that the risk of slip is probably negligible at this stage.

Similar observations pertain to the Postma dyke. An elongated region roughly in the middle-to-left part of the gridded surface (fig.4.5b) appears auspicious, especially as mining operations are focused in this central area, but fig. 4.6b now reveals a surprising decrease in the extent of positive ESS in this zone. However, mining at Site 3 caused the potential for unstable slip to be increased at this point on the dyke, as indicated by the ESS vectors at the right-bottom region of the grid model in fig. 4.6b.

Discussion:

Positive ESS, considering pertinent factors, is likely to be present and greatest when the direction of the principal stress is at 45^0 to a possible plane of slip. Both the Postma dyke and Basson fault have steep dips, and elastic modelling shows that at various points the stress field' reorientation due to mining is conducive to the creation of zones of positive ESS.

The focus of an event is likely to be in the area of highest ESS. Ryder (1988, p155) explained that if ESS > 15 MPa for a fault or joint, or greater than 30 MPa for intact

rock, then a prior event should have occurred. If ESS < 5 MPa, then no burst activity is likely, and if ESS < 0 MPa, no event is possible. For the modelling on the Postma dyke an angle of friction of 25^0 was used (the Basson fault, being weaker than the dyke, was evaluated with an angle of 20^0).

Regions where ESS_{max} is close to 5 MPa are indicated on the Postma dyke. If the release of stress or strain energy has not already occurred through sudden failure or aseismic creep, then these areas could form the source regions of imminent events, particularly if mining continues in the vicinity.

At the intersection of the Postma dyke and Basson fault (fig. 4.6a), in the vicinity of recent mining (at Site 1 -- see fig. 3.6, Chapter 3), a more intensive zone of positive ESS, rather than the short vectors emphasising minor ESS, was anticipated. The modelling, in this instance, failed to indicate the likelihood of a major seismic event which took place in mid-1994. However, the modelling which took all the mining into consideration, present and past, indicates zones of large ESS north and south of Site 1 at the fault loss part of the Basson fault, which might have crept and/or slipped in conjunction with numerous small events, causing that part of the fault in the vicinity of Site 1 to be stress loaded. When the shear strength of this asperity was exceeded by the contribution of further (recent) mining, violent slip took place, shedding strain energy in this part of the fault/dyke and transferring load elsewhere.

Elastic modelling cannot cater for non-elastic strain. Modelled stress, as such, did not take the fractured zone or the rheological nature of the rockmass into account. The inclusion of seismicity analysis is necessary to better evaluate the rockmass response

to mining, and to verify input parameters and results (Dennison and van Aswegen, 1993, p8), as investigated in the next section.

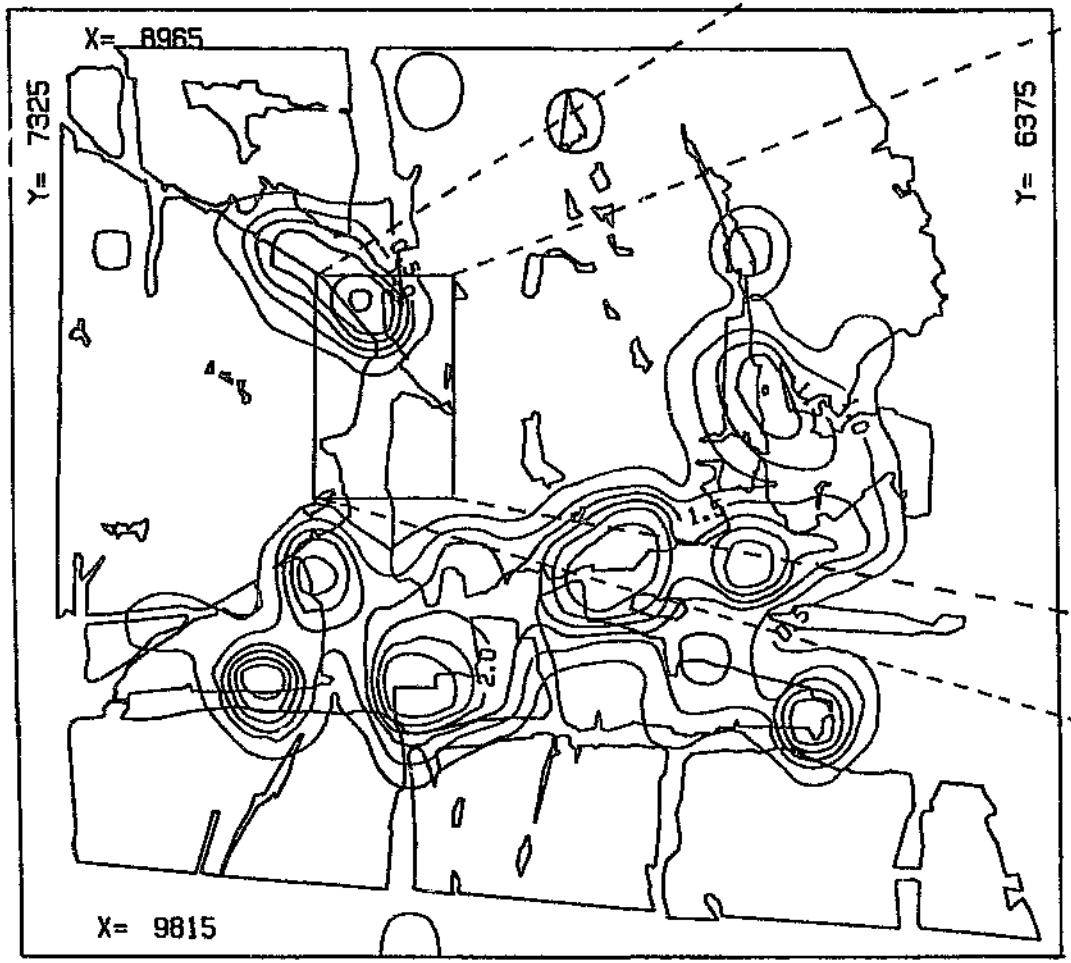
(4.1.2) Seismic stress and deformation rates through recorded seismicity:

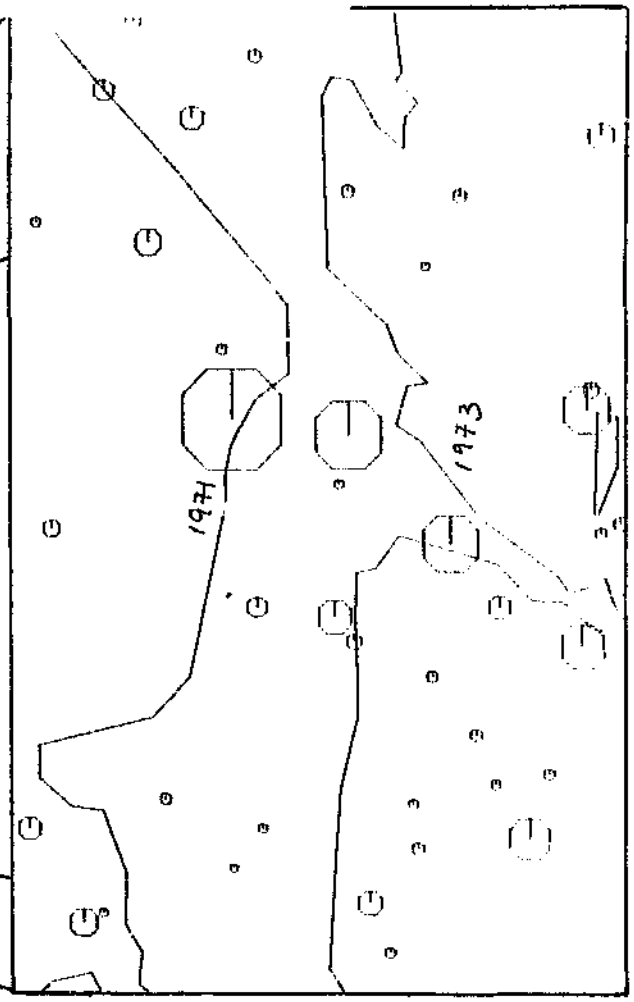
Asperities govern preseismic processes (Gibowicz, 1986, p623); Dennison (1993) used the models to explain spatial variations in seismicity and shear deformation. According to the asperity model, as adopted here, seismic events occur as a result of accumulations of strain energy, induced by adjacent deformation on zones of greater shear strength. Influencing factors (see Section 2.3.2, Chapter 2) include the undulatory character of faults, depth of mining, the presence and constituent character of gouge, dip and K-ratio.

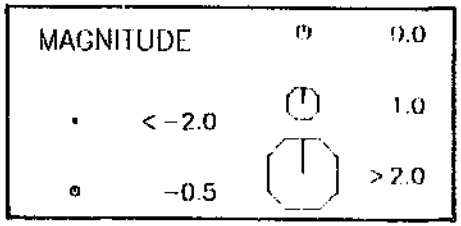
van Aswegen and Butler (1993) discussed how the asperity model was applied successfully to predict the source region of a major fault slip event. The authors found that the spatial distribution of small seismic events of relatively high apparent stress in the environment of the asperity delineated the source region quite accurately.

The results of a similar analysis are demonstrated in fig. 4.7 where potential asperities are delineated by high values of EI (suggesting a higher than average shear stress at the rupture location).

Fig. 4.7: Below: contours of average EI during the second quarter of 1993. Note the seismic gap and absence of higher stress in the middle-to-bottom half of the rectangle. Right: expanded rectangle, showing events located in the area between July 1990 and April 1993, indicating a release of strain energy (or shear stress) in this part of the Basson fault.







Observations:

A contour plot of EI using recorded seismicity in the study area during the second quarter of 1993 is shown in fig. 4.7. The length of the Postma dyke appears to be more stressed than average, because generally over its length EI > 1.0 (see Section 2.4, eqn. [11], Chapter 2), and more highly so in places, notably the intersection of the dyke with the Basson fault. Stretches of the Basson fault show a surprising relative lack of stress (or a lower shear stress situation, on average). When the seismic database is accessed far enough back in time (before the time window for the selection of events used to create the contour plot), it can be seen that various events of large magnitude ($M_L > 1.0$) occurred in the area between July 1990 and April 1993, probably releasing some of the locked-up stress/strain-energy in this portion of the fault. The rectangle to the right of fig. 4.7, which enlarges a portion of the Basson fault on which a seismic gap and lower EI is evident, shows the location of some of these earlier events, scaled by octagons denoting local magnitude, the centre of which represents event foci.

Mining on the west and east sides of the Basson fault terminated in 1971 and 1973, respectively.

Selective analysis of seismicity around geological discontinuities:

A different type of analysis singles out the geological structure of interest and its seismic response to mining-induced stress changes, by selecting those events within some distance of the hangingwall and footwall of the 'plane' of interest. The 'plane' may be adapted to follow the actual plane of weakness more closely, especially if measurements of its dip and strike have been done at exposed points and are available, as is the case with the Postma dyke and Basson fault.

A combination of seismic parameters pertaining to stress (e.g. energy index (EI), eqn. [11]) and strain rate (e.g. seismic viscosity, eqn. [16]) as indicators of nucleation processes (refer to Section 2.4, Chapter 2), should overcome, to some extent, the limitations imposed by the inherent inability of elastic modelling to cater for non-elastic deformation and time-dependent deformation processes within the stressed rock mass.

All seismic events recorded with a minimum of four sites were selected within 100m of the hangingwall and footwall of the grids representing both the Postma dyke and Basson fault, during the first, second, third and fourth quarters of 1994, and then used to produce the contours of $\log_{10}$(seismic viscosity) and $\log_{10}$(EI) corresponding to these surfaces. The energy-moment relation needed to calculate the values of EI is particular to these selected events.

Events related to the plane of the fault and the plane of the dyke are expected to be well-located and distinguishable from seismicity occurring elsewhere in the Postma area (the local network sensitivity was evaluated in Section 3.1, Chapter 3). At the zone of intersection of the two planes of weakness there may be some common use of events in the analysis of the seismic response of the structures, due to their closeness, but it is quite impossible to separate the events associated with one or the other structure.

Contours of seismic viscosity are overlaid on contours of EI for visual effect and ease of evaluation/interpretation of these parameters. The location of the largest event recorded to date in the region (M_L 3.7 on 27th June 1994) is indicated on the contours

of the second quarter of 1994 by an 'hourglass' symbol. The contours of this quarter only take that seismicity leading up to -- but excluding -- the large event into consideration (refer to Section 2.5.2, Chapter 2, for a description of the contouring process).

Observations:

Figs. 4.8a, 4.8b, 4.8c and 4.8d -- the latter three figures are located in Appendix D -- (corresponding to the seismic activity recorded during the first, second, third and last quarters of 1994, respectively, represented as seismic viscosity and EI) are looking northwards, along the Basson fault, onto the grid assimilating the Postma dyke. The spread of greatest seismic fluidity along the dyke, as indicated by the contours of seismic viscosity (refer to Section 2.4, Chapter 2) coincides with the area of active mining at the time as well as extending well into the footwall of the reef.

During the first half of 1994, with the mining of Site 1 (44-13A -- refer to fig. 3.6, Section 3.2, Chapter 3, for the locations of various sites) the extent of part of the seismic viscosity lows are in the direct vicinity of the reef and the fault-dyke intersection, reaching down-dip over a distance of some 300m. As the mining of Site 2 (46-S4) and Site 3 (48-D12) declined over the last months of 1993, with a gradual commencement of stoping on the south side of the dyke, the influence of mining on these blocks on the dyke was reduced, and is disregarded for the time period investigated here. Workings on the south side of the dyke became more pertinent during (and following) the first quarter of 1994, as shown in fig. 4.8a.

During the second half of 1994 mining operations ceased at the fault-dyke intersection and shifted approximately 250m eastwards, in conjunction with a similar spread of the

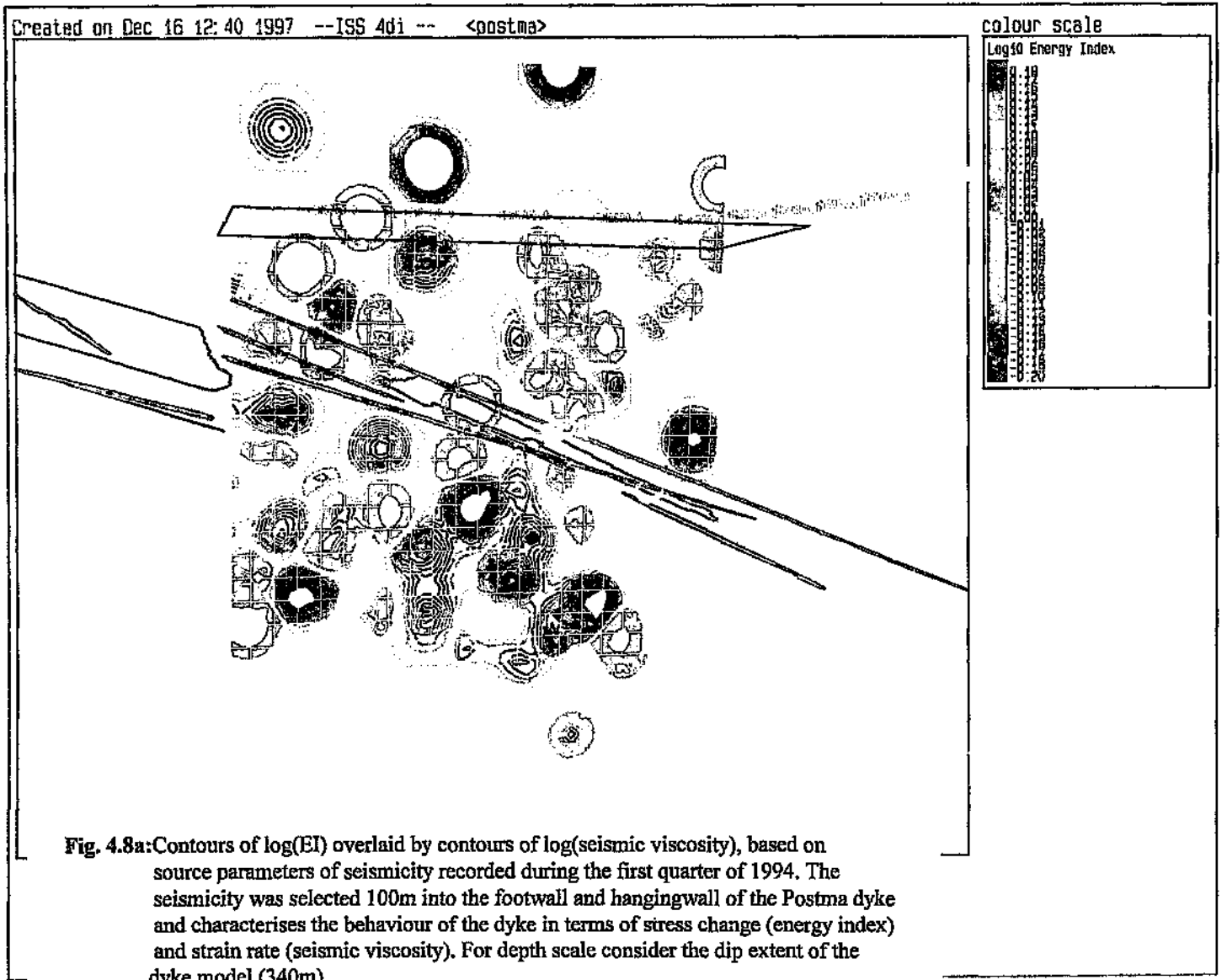


Fig. 4.8a: Contours of log(EI) overlaid by contours of log(seismic viscosity), based on source parameters of seismicity recorded during the first quarter of 1994. The seismicity was selected 100m into the footwall and hangingwall of the Postma dyke and characterises the behaviour of the dyke in terms of stress change (energy index) and strain rate (seismic viscosity). For depth scale consider the dip extent of the dyke model (340m).

greatest seismic fluidity, extending from the reef-dyke intersection preferentially downdip along the dyke.

The peripheral regions surrounding the greatest viscosity lows (or areas of easier coseismic stress transfer -- refer to Section 2.4, Chapter 2), are often accompanied by patches of higher than average EI, as indicated by the overlays, during all four quarters. In some instances high stress zones correlate well with zones of relatively high, or high gradients in, seismic viscosity (i.e. where the seismic fluidity, or seismic flow of rock, is resisted -- see Section 2.4, Chapter 2); in other cases EI highs actually coincide with local minima of seismic viscosity.

A similar analysis conducted along the Basson fault (figs. 4.9a, 4.9b, 4.9c and 4.9d during the same time periods as before, with seismicity represented as before; the latter three figures are located in Appendix D) reveals that the least seismic viscosity was generally experienced very close to the intersection of this fault with the Postma dyke. A zone of higher than average EI is usually observed embracing the intersection of the two planes of weakness, with patches of highs and lows close to the displaced reef horizon along the fault (figs. 4.9 a-d), mostly in the footwall of the reef. The peripheral areas of the lowest seismic viscosity near to the fault-dyke intersection correlate with high EI patches, generally enclosing a more broken (containing a larger number of events and relatively less stressed, with EI < 1.0) interior. Compared to the other quarters of 1994, much more seismic activity took place in the environs of this part of the fault during the second quarter (fig. 4.9b in Appendix D). The zone of low seismic viscosity broadened northwards past the dyke intersection along the fault. An arm extended in the immediate footwall of the lower displaced reef horizon, but its reach was broken by several seismic gaps.

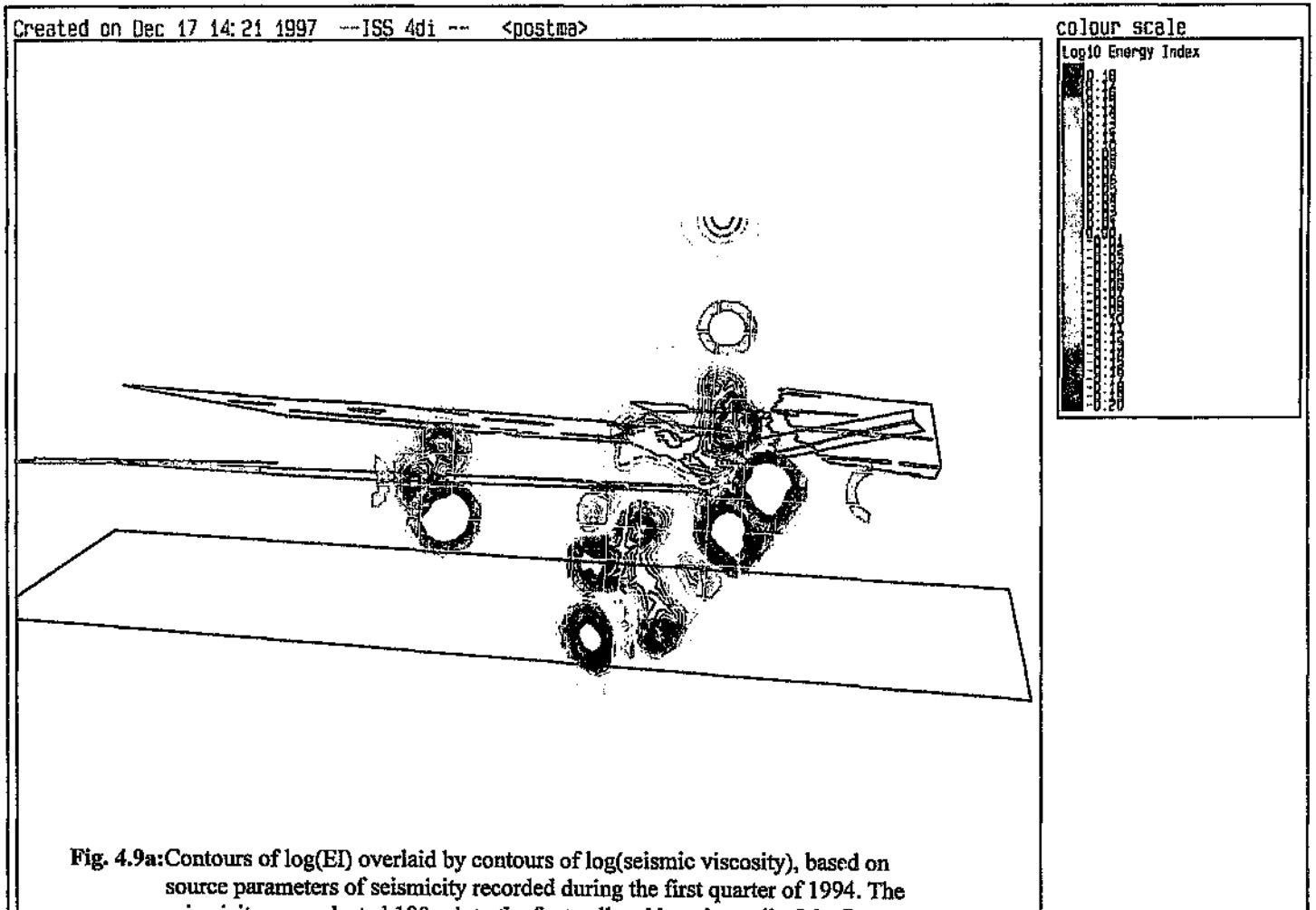


Fig. 4.9a: Contours of log(EI) overlaid by contours of log(seismic viscosity), based on source parameters of seismicity recorded during the first quarter of 1994. The seismicity was selected 100m into the footwall and hangingwall of the Basson fault and characterises the behaviour of the fault in terms of stress change (energy index) and strain rate (seismic viscosity). For depth scale consider the dip extent of the fault model (340m).

Although the mining operations ceased in the vicinity of the fault dyke intersection immediately following an M_L3.7 event in the area at the end of June 1994, and shifted eastwards to another block of unmined reef, some residual seismic flow is evident from fig. 4.9c (Appendix D) in the lower part of the zone of intersection. A reactivation of seismic activity is seen here during the last quarter of 1994 (fig. 4.9d (Appendix D)). Development work close to the fault approximately 350m north of the fault-dyke intersection produced some deformation, manifested through seismic activity and reflected in the seismic viscosity lows in the area, which shifted and consolidated closer to the lower reef horizon, in comparison to the previous semester.

Discussion:

The influence of mining adjacent to geological planes of weakness is demonstrated to good effect in the series of contour plots of seismic parameters pertaining to stress and strain rates (figs. 4.8a - 4.8d and 4.9a - 4.9d -- see also Appendix D). Seismic viscosity delineates areas of accelerated (or decelerated) seismic inelastic deformation (refer to Section 2.4, Chapter 2). Places where high gradients are shown (transition zones from maxima to minima or vice-versa), coinciding with higher than average stress (EI > 1.0), are anticipated zones of instability. In the same context, at asperities or aberrations, where the 'seismic flow' or slip/deformation of rock is resisted (i.e. places showing relatively high seismic viscosity or seismic gaps), there is often an accumulation of stress and strain-energy, with a potential for sudden release. Some gaps or enclaves (delineated by higher values of- or higher gradients in seismic viscosity) are observed to open up from one time period to the next, while others indicate deformation where it was previously resisted. These seismic gaps shift with time, according to the response of the fault planes to mining-induced stress changes,

normally coseismically, demonstrating the rheological nature of the planes of weakness.

A noteworthy observation concerns the extent of the seismic viscosity lows (or higher seismic fluidity), with a tendency to spread downdip, away from the mining, along the geological structures. This spread is not some misguiding effect caused by poor-quality seismic data, as the spatial location accuracy of events in this area was found to be sufficient to justify the observed variation in depth (see Section 3.1, Chapter 3). Consideration of the induced shear stress implies that the fault should slip along dip, substantiated by the numerical modelling (see figs. 4.4 a-b and 4.5 a-b).

Modelled ESS on the Postma dyke and Basson fault has shown that the possibility of slip along either plane of weakness exists at various points, albeit short vectors on the Basson fault emphasise minor likelihood of shear deformation. The Postma dyke, on the other hand, is not only shown to have large shear stress vectors acting on it in the proximity of Site 1 (44-13A), due to the recent mining, and thus be more prone to slip, but it is also a stress concentrator, especially at the reef-dyke contact, as demonstrated by elastic modelling in fig. 4.3b. Seismic and non-seismic slip should initiate at sites of ESS_{max}, then migrate down-dip. This notion is consistent with the patterns of seismicity described above.

The elastic stress modelling which took all mining in the Postma area into consideration, most of which was completed more than a decade and a half ago, correlates poorly with recent seismicity. ESS induced recently by the 'new' mining (e.g. environs of Site 44-13A) on the principal structures complements the recent seismic activity better. The M_L3.7 event took place in an environment of increasing

ESS, in the vicinity of zones having large, established ESS on both the fault and the dyke.

It seems that, contrary to expectation, the large, damaging events do not always occur within areas delineated by high modelled shear stress (or ESS_{max}) (mentioned also by van Aswegen, 1990, p722-723; Dennison and van Aswegen, 1993, p6-8), but are rather adjacent to ESS lobes where shear deformation has been arrested. Interpretation of such modelled results provides an explanation consistent with the asperity model and recognition of potentially hazardous asperities might be regarded as spatial prediction of large tremors.

Concerning the undulatory character of geological discontinuities, there is a greater potential for slip in places where the dip steepens in relation to other regions, since the clamping forces acting normal to the fault are reduced. The dip of the Postma dyke is generally closer to vertical than that of the Basson fault and thus more adept to slip. There is a larger throw of the reef horizon across the fault than the dyke, both in a normal sense. A greater clamping effect and higher shear stresses are expected in that part of the fault between the displaced reef horizon, compared to the dyke. A favourable orientation of the principal stress in relation to the fault and a reduction in the clamping force should promote a tendency for slip on either side of the clamped portion, usually observed to be greater in the footwall of the reef -- in partial agreement with the results of elastic modelling (ESS_{max} is manifested in the fault-loss part of the fault, but shear stress is present in the footwall of the reef also (see figs. 4.5a and 4.5b)), and supported by the contours of deformation (e.g. fig. 4.9b, Appendix D).

The contours of seismic viscosity during the second quarter of 1994 reveal that the greatest rate of strain took place at the fault-dyke intersection (figs. 4.8b and 4.9b in Ap ndix D). Larger events should arise from the breaking/shearing of asperities and/or aberrations on planes of weakness under the influence of a redistribution of stresses due to mining, as the state of stress tries to balance itself into equilibrium. The large amount of strain around the fault-dyke intersection, coupled with this existing geological complexity underscores the likelihood of large magnitude seismicity occurring, and provides an indication of where the likelihood of a strong tremor is increased.

The stress modelling augmented the evaluation of seismicity by directing attention to the zone of intersection of the planes of the dyke and fault, which display greater shear strength than adjacent regions. The incidence of seismicity due to the mining loaded the 'clamped' zone until it slipped suddenly. Both methods of analysis, independent of each other, are mutually beneficial, lending themselves to an enhanced understanding of the processes leading to violent deformations of the rock surrounding underground openings.

The M_L3.7 event (27th June 1994), nevertheless, occurred within the zone of greatest deformation (figs. 4.8b and 4.9b (see Appendix D) represent the seismic activity along the Postma dyke and Basson fault during the second quarter of 1994, before the event), in an area of larger than average EI, in the saddle of a small zone on the dyke exhibiting more resistance to the 'seismic flow' (fig. 4.9b, Appendix D). Such observations compiled on a regular basis could supply feedback information for the verification of design parameters and assumptions while mining (e.g. rock strength and/or angle of friction).

If one looks at the seismicity along the Postma dyke (figs. 4.10a and 4.10b) two weeks preceding the M_L 3.7 event it can be seen that it occurred within a seismic gap (no previous events near its focus in the time period considered) close to where a stress drop took place (since EI is less than average -- fig. 4.10b), characterising a 'softening' process in the source region (refer to Section 2.4, Chapter 2), on the edge of a locality of greater deformation (i.e. near the base of a high in cumulative seismic strain (fig. 4.10a)).

From Section 3.4.1, Chapter 3, it appeared that stress transfer had taken place along the Postma dyke following the M_L 3.7 event, from its focus to approximately 250 m east of the fault-dyke intersection. However, this stress transfer (which is thought to have eased the load at the event focus) appears to have begun to reverse itself by the end of 1994 because seismic activity was beginning to reoccur close to the Basson fault (figs. 4.8d and 4.9d -- see Appendix D), possibly because of a re-loading of the dyke as a result of resumption of mining and stress balance following from the seismicity at the stopes 250m east of the intersection. A similar temporal variation in stress / strain behaviour can be observed along the Basson fault prior to the M_L3.7 event (figs. 4.9a and 4.9b (Appendix D)). A strong interaction in seismicity is thus seen to take place across distances in the order of hundreds of metres along the geological structures.

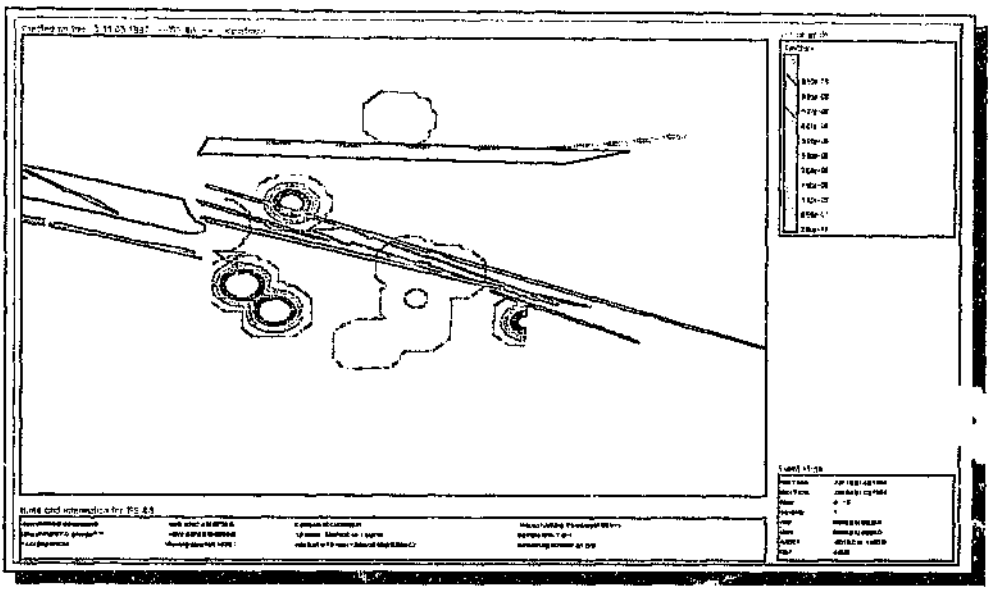


Fig. 4.10a: A sectional perspective view of the Basal Reef horison, looking northwards along the strike of the Basson fault and onto the footwall side of the Postma dyke. Seismicity selected 100m either side of the Postma dyke two weeks preceding the M_L3.7 event (its location is indicated above by the 'hourglass' symbol) is contoured in terms of seismic strain. Contour highs indicate regions of greater rock deformation.

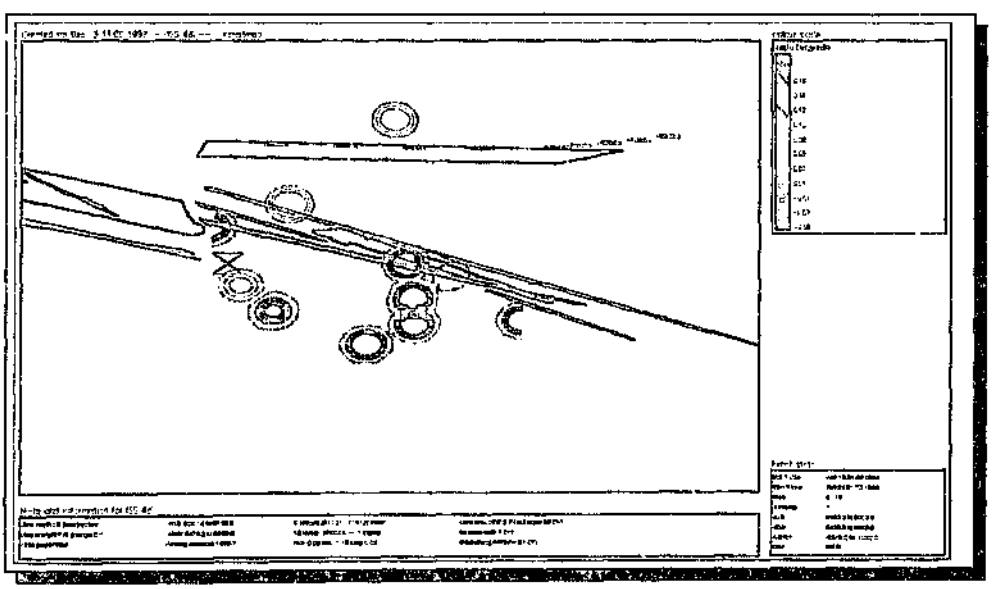


Fig. 4.10b: Same as fig. 4.10a but the contours now show EI, thus contour lows indicate regions where stress drop took place.

(4.1.3) Summary

A major drawback of elastic-continuum modelling is that the fractured zone around underground openings, geological structure, as well as the time-behaviour of aseismic and coseismic deformation processes -- i.e. the rheological nature of the rockmass -- is not taken into account. There is a lack of feed-back information, and, consequently, input parameters and results are difficult to verify and modify. An analysis of seismicity mitigates these circumstances and identifies those parts of the rockmass which have failed coseismically (it is conceivable that a stabilising pillar, for example, might have failed, with associated re-distribution of stress, unbeknown to elastic modelling, leading to a false perspective of spatial stress concentration).

The results of elastic modelling should distinguish the zones on planes of weakness where shear stresses induced by recent mining are conducive to instability. An increase in ESS (along a part of some plane of weakness) is expected to precede a large event (whose focus would not necessarily be in the area of highest ESS), provided the shear stress can accumulate to the point of sudden shear of asperities or aberrations on the plane of dislocation. In the case of the M_L3.7 event, substantial shear stresses are absent from the locality of the event hypocentre, although it occurred close to zones of large, existing ESS on both structures.

A robust quantification of the rockmass response to stress changes combines stress and strain rates, to spatially distinguish 'tight', stressed parts on a plane of weakness from those experiencing an 'easier seismic flow' (refer to Section 2.4, Chapter 2). Generally, where contours of EI show high values, superimposed contours of seismic viscosity show high gradients, implying that the locked parts of a plane of weakness

are usually more stressed than the environs, i.e. a higher stressed boundary surrounds a less stressed (more broken by previous seismicity) inner region corresponding to strain energy dissipation around a stoping area near a geological discontinuity. It appears that continued mining close to such discontinuities diffuses the seismic energy release over distances of hundreds of metres.

Continuous monitoring of seismicity along with regular evaluations of ESS on geological discontinuities becomes indispensable in the optimal planning of mining operations, particularly in the verification -- and modification -- of support requirements. Such analysis, over the longer term, does not characterise the short-term behaviour of the rockmass which realistically, and in practicality, could be used for the prediction in time of large events, with some measure of precision. An evaluation of the rockmass response to stress changes in the days or hours preceding a major event, with due attention being given to the system sensitivity in that volume of rock giving rise to such an event, should address the difficult subject of prediction a whole lot better, as investigated intensively in the subsequent section.

(4.2) Back Analysis of Large Events to Identify Precursors

It has been proposed that quantitative seismology can indicate temporal and spatial variations in the state of stress and strain throughout the rockmass surrounding mining excavations. The timely recognition of high gradients in physical seismic parameters pertaining to strain rate and stress in time and space just prior to major seismic events constitutes an early warning mechanism. It is the aim of this section to test particular methodologies and to identify those seismic parameters, or their combination, which, from a practical point of view, can best be used for early warning, and to show that precursory applications of quantitative seismology are best served by methods employing seismicity recorded in the few days (or few hours) immediately preceding a major event.

This work is an extension of partial investigations already conducted on the Postma area as part of a research programme, and the analysis is done in greater detail.

The 1997 edition of 'Seismic Monitoring in Mines' describes the procedures to be taken into account when doing back analysis of seismic events. The basic system requirement for local sensitivity is a minimum local magnitude M_{min} (with the minimum number of triggered stations equal to, or greater than, 5) at least three orders of magnitude smaller than the magnitude of the event of interest (i.e. $M_{min} \leq M_i - 3$). In the Postma Area the system is capable of resolving moment magnitudes greater than -0.6 (shown previously in section 3.1, Chapter 3). According to the criteria above, these small, non-damaging recordable events should provide information concerning the potential for impending seismicity of magnitude 2.5 and above.

A selection of events in the study area of local magnitude greater than 2.5 produced ten tremors, the location of which are shown in fig. 4.11, corresponding to Table 3. The volume of the rockmass affected by the inelastic deformation due to these tremors is represented by the radii of circles (where the radius of a circle equals the radius of a sphere with volume = apparent volume (V_a)). The centre of each circle coincides with the event focus (fig. 4.11).

Full use of the available seismic database was made, taking all recorded seismicity into consideration to give maximum historical information for the delineation of the 'preparation zone' of the large tremors (refer to Section 2.5.1, Chapter 2).

For each of these ten events, analysed individually and in sequence, contoured parameters delineate and describe the seismic activity prior to but excluding the seismic event. The location of each event is superimposed on the contours by apparent stress (σ_a). Areas selected for the time-history analysis are confined to the location of greatest seismic activity (i.e. the preparation zone), initially identified by contours of seismic Deborah number (De_s) and seismic fluidity (η_s^{-1}), two seismic parameters distinguishing the volume of rock deformed (softened) by seismic activity (refer to Section 2.4, Chapter 2), just prior to the occurrence of the tremor.

Case study description:

(4.2.1) Event 910825 of local magnitude 2.5:

Event 910825 refers to event number 1 of Table 3. Figs. 4.12, 4.13 and 4.14 (figures are located in Appendix E) show all the recorded seismicity in the

Table 3: Some source parameters attributed to the seismic events of local magnitude ≥ 2.5 located within the Postma Area in the time period 1 January 1991 to 31 December 1994.

Event number	Date and time	Local magnitude	Seismic moment (logJ)	Seismic energy (logJ)
1	25/08/91; 03:29	2.5	12.8	7.5
2	26/08/92; 07:17	2.8	12.8	8.5
3	26/08/92; 23:16	2.6	12.4	8.3
4	14/03/93; 10:15	2.6	12.8	8.2
5	08/11/93; 14:59	2.6	12.7	8.1
6	24/04/94; 11:26	2.7	12.8	8.2
7	13/05/94; 17:39	2.8	12.9	8.4
8	27/06/94; 06:10	3.7	14	9.9
9	27/06/94; 06:11	3.2	13.4	9.2
10	27/06/94; 06:13	2.7	12.9	8.2

Event number	Apparent stress (bar)	Energy Index	Apparent volume (radius in m)
1	1.27	0.1	173.3
2	14.45	1.5	76.6
3	22.69	3.3	49
4	7.38	0.8	90.9
5	7.38	0.8	88.8
6	7.26	0.8	93.4
7	9.28	0.9	92.4
8	24.52	1	158.9
9	20.92	1.4	104.6
10	5.83	0.6	107.4

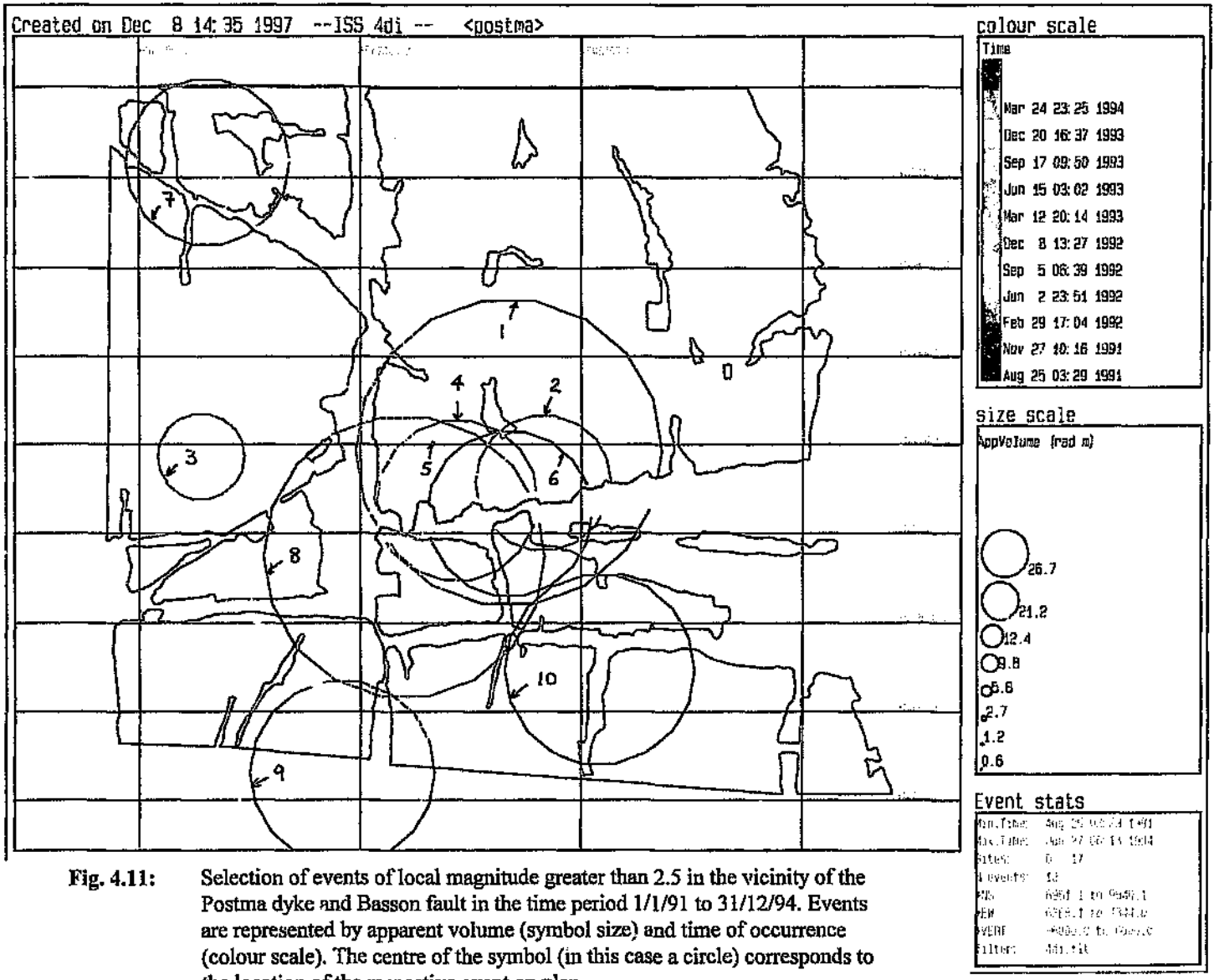


Fig. 4.11: Selection of events of local magnitude greater than 2.5 in the vicinity of the Postma dyke and Basson fault in the time period 1/1/91 to 31/12/94. Events are represented by apparent volume (symbol size) and time of occurrence (colour scale). The centre of the symbol (in this case a circle) corresponds to the location of the respective event on plan.

Postma Area from 1 January 1991 to 25 August 1991, in terms of EI, σ_a and V_a, respectively (36 seismic events in total -- see observations / interpretation later). Symbol colour indicates time and symbol size scales its magnitude. The figures include event 910825; its location corresponds to the centre of the circle of event number 1 shown in fig. 4.11. Bearing in mind that the sensitivity of the seismic system was somewhat reduced in relation to that obtained in the second half of 1993 and during 1994, the analysis and interpretation of recorded events must likewise be adapted. Only the larger magnitude seismicity was detected, with 36 events recorded. The distribution of these (in plan) is mostly limited to the centre of the study area, particularly close to the intersection of the Postma dyke and Basson fault, and to an area about 80 - 100m north of the middle of the dyke. The latter is most probably associated with the extraction of one of the pillars in the immediate vicinity (the digitising shown in the figures corresponds to the mining prior to the second quarter of 1994). Fig. 4.15 (Appendix E) shows a section looking westwards onto the Basson fault, along the reef horizon. Here it becomes clear that there exists a large variation in the depth of hypocentres, but the reduced sensitivity existing at the time would accompany a reduced accuracy of location, specifically in terms of errors in the z-component (depth).

Considering the volume of rockmass affected by these tremors, fig. 4.14 (Appendix E) shows that the zone of intersection of the Postma dyke and Basson fault had already experienced a large amount of interactive seismicity by August 1991 -- the outline of the circles scaling the volume of deformation intersect quite extensively.

Delineation of the 'preparation zone':

A 'preparation zone' refers to a volume of rock containing the greatest stress and strain changes, in preparation for a future large event -- see Section 2.5.1, Chapter 2. The

spherical radius of apparent volume for event 910825 is calculated to be 173m (refer to Table 5). The area for events' selection (as shown in the figs. 4.12 and 4.14 (Appendix E)) is approximately 1300m x 1300m, somewhat less than 10 times the source volume mentioned previously (see Section 2.5.1, Chapter 2), but the seismicity is clustered within a smaller area. Contours of seismic Deborah number (fig. 4.16) and seismic fluidity (fig. 4.17, Appendix E) delineate this clustering, and the area chosen as the preparation zone is decreased further, as shown in fig. 4.18 (Appendix E) with the new selection of events used for the time-history plots that follow.

The analysis of event 910825 is difficult because a limited data base containing only 30 events recorded in the area prior to event 910825 (fig. 4.12, Appendix E) is available. This limitation was due to the insensitivity (i.e. a lower number of stations in the region) of the seismic network at the time.

Observations / interpretation:

Two events of high EI, southeast of event 910825 and in the footwall of the Postma dyke (figs. 4.12 and 4.15, Appendix E), support the stress modelling (see Section 4.1.1), and indicate higher conditions of stress at this site than the norm. The apparent stress of these events, a model independent measure of stress drop, show high values (fig. 4.13, Appendix E). The events caused some release of stress, but owing to the mining layout and the harder dyke material with a tendency to accumulate energy, the possibility of sudden and violent release of this energy should continue, particularly if the mining operations encroach the dyke from the south, as planned.

Figs. 4.19, 4.20 to 4.23 (Appendix F1) show a time (history) variation of log(EI), seismic diffusion (d_s) seismic softening (S_s), seismic viscosity (η_s) and log(Sc_s). (All parameters used, describing the seismic source, are explained in Section 2.4, Chapter

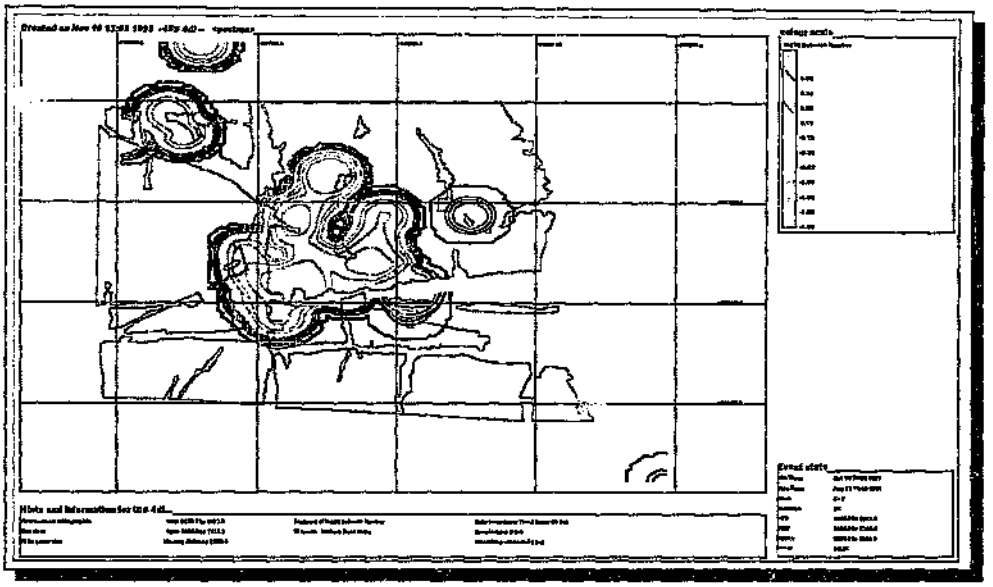


Fig. 4.16: Contours of seismic Deborah number based on source parameters of seismicity recorded in the time period 1/1/91 to 25/8/91 (up to, but excluding, event 910825) to delineate the clustering of seismicity in the Postma area and enable the 'preparation zone' for event 910825 to be identified.

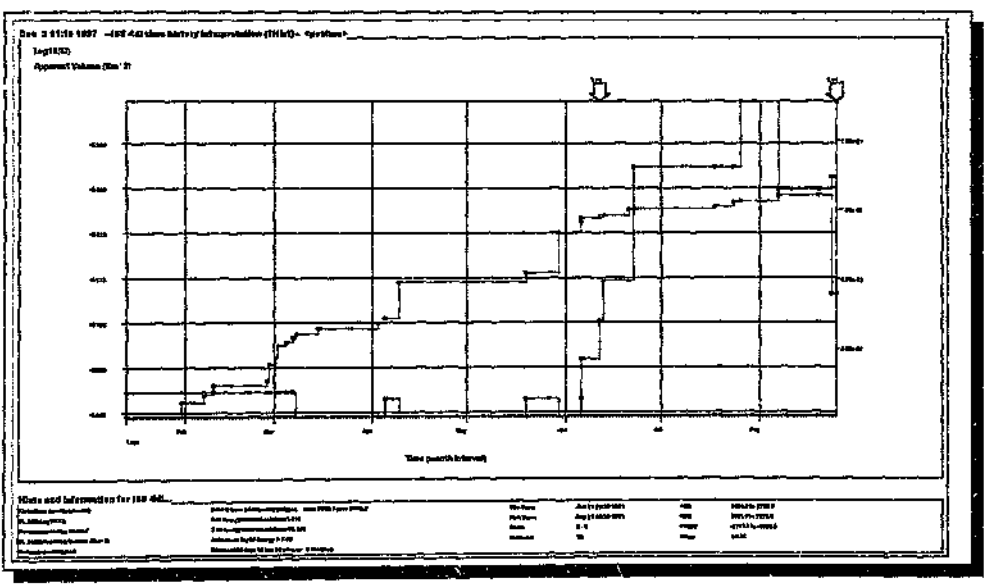


Fig. 4.19: Time-history of ΣV_s and moving median EI (window length: 8 samples and/or 5 days) for the seismicity associated with the 'preparation zone' of event 910825. The arrows depict the large events (denoted by logE > 7.0) in time -- the second arrow (latest in time) refers to event 910825.

2). In addition, $\Sigma(V_a)$ was used as reference for each of the series of plots. Even with a limited data base consisting of relatively few (31) seismic events, some of these parameters display a marked change prior to event 910825.

A window length of ***8 samples and/or 5 days*** was used -- for this and subsequent events -- in their time-history evaluation (see Section 2.5.2, Chapter 2).

The seismic parameter of cumulative apparent volume (ΣV_a) had been increasing steadily since mid-July (fig. 4.19). Energy index (EI) had been decreasing steadily since the beginning of August and was at its lowest within the area for the selection of events just prior to event 910825 (fig. 4.19). The curve for seismic diffusion (d_s) (fig. 4.20, Appendix F1) was expected to show an increase, corresponding with a local increase of seismic fluidity (fig. 4.22, Appendix F1). Instead it shows a slow decrease from late June. Variation in seismic softening (S_s), on the other hand, is more dramatic, with a sharper rate of change from a maximum in mid- to late June (fig. 4.21, Appendix F1). Seismic viscosity (η_s) shows a steady decrease from late July (fig. 4.22, Appendix F1), and seismic Schmidt number (Sc_s) a very similar pattern (fig. 4.23, Appendix F1). In effect there is an easier transfer of stress with seismicity (strain softening, as explained previously -- refer to Section 2.4 and Section 2.6, Chapter 2), a drop in stress and an increase in the strain rate in the weeks leading up to the event.

The collection of proceeding figures (4.24, 4.25 to 4.30 (Appendix F1), 4.31, 4.32 to 4.37 (Appendix F1)) display contours over the long term (from the beginning of 1991) as well as over a shorter term (all seismicity three months before the event). Event 910825 is excluded; its position is merely indicated.

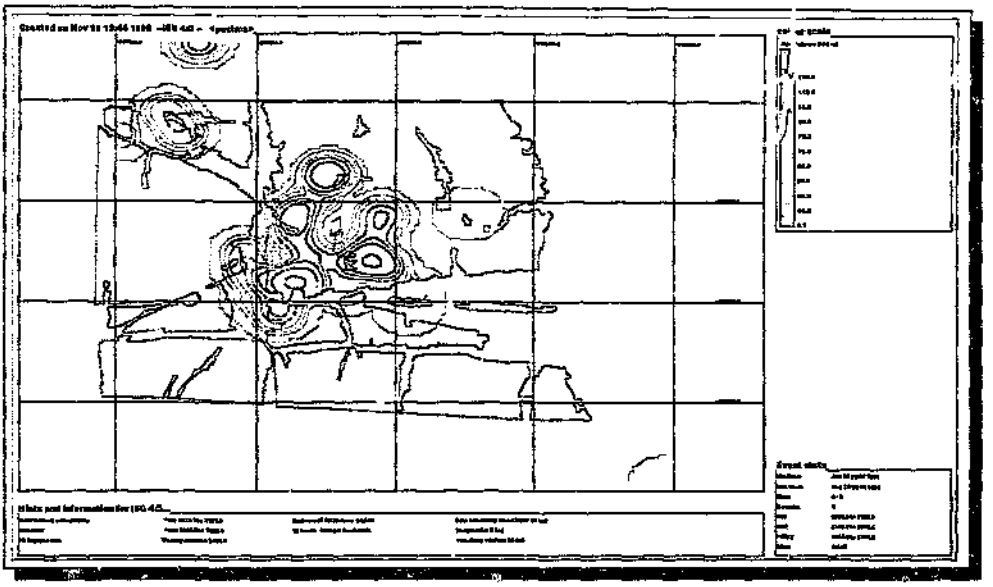


Fig. 4.24: Contours of apparent volume using seismicity recorded in the time period 1/1/91 to 25/8/91 (up to, but excluding, event 910825 – its position is merely indicated by the 'hourglass' symbol).

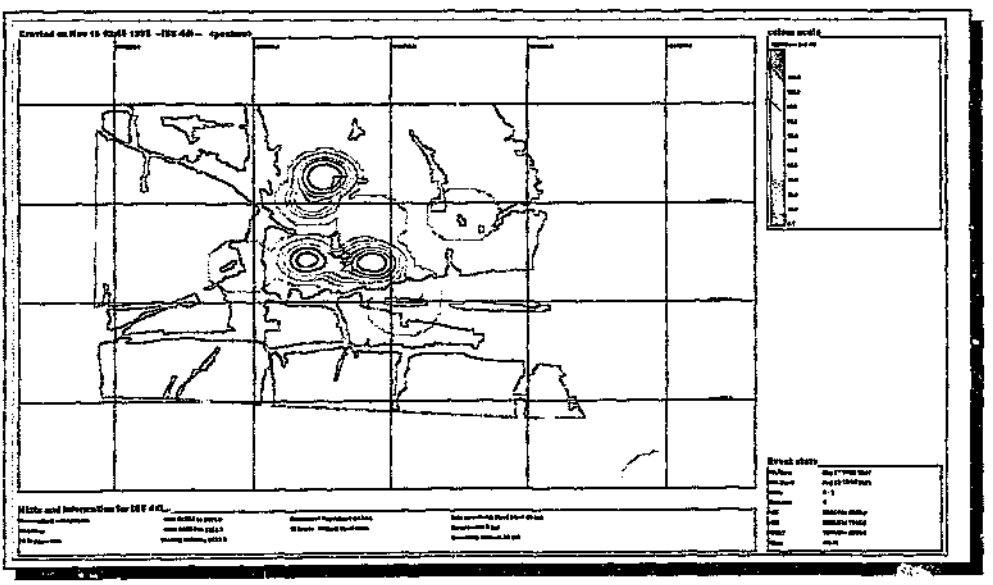


Fig. 4.31: Similar to fig. 4.24; time period of seismicity ranges over the three months before event 910825.

Table 4 lists a summary of results for the evaluation of the contoured seismic parameters.

All subsequent figures of time-history and contour plots are located in Appendices F2 to F7.

(4.2.2) Events 920826a and 920826b of local magnitudes 2.8 and 2.6 respectively:

Figs. 4.38, 4.39 to 4.40 (Appendix F2) show the increased number of events from 1 January 1991 to 26 August 1992, almost a year to the day since event 910825. The low sensitivity of the seismic system remains as before. Fig. 4.41 (Appendix F2) shows a section looking east onto the Basson fault, depicting the distribution of events in depth.

Observations / interpretation:

For the same reasons as previously, there is a large scatter of hypocentres in depth (fig. 4.41, Appendix F2), with most of the seismicity in the footwall of the reef, clustered close to the dyke and the intersection of the dyke and the fault.

The inner 'rectangle' enclosing the digitised area (Basal Reef) forms a polygon for the selection of events used in the time-history analysis that follows. The same polygon will be used for the subsequent cases also, as it encloses the seismicity of direct relevance to the study. The first event is in the plane of the Postma dyke, about 200m

Table 4: Summary of results for contoured seismic parameters for event 91082[5]

Time range from 910101 to just before event	
Seismic parameter	Observations
apparent volume	Event is located in a high gradient region, about 80m north of the middle of the Postma dyke.
log(energy index)	The previous highs coincide with lows for log(EI), and the event is located in a zone of higher log(EI).
log(inverse Deborah number)	The event plots at the base of a local high; a more prominent high correlates loosely with the intersection of the Postma dyke and the Basson fault.
log(relaxation time)	Within zone of lowest log(relaxation time).
log(fluidity)	The event is located on the slope of a local high on its right. The contours are very similar to those delineating log(inverse Deborah number).
seismic stress	There is minimal correlation between the event and the indicated high, located about 200m south-east of and in the footwall of the dyke.
seismic strain	Similar to apparent volume, log(EI) and log(inverse Deborah number).

Time range from 910528 to just before event	
Seismic parameter	Observations
apparent volume	Event is located within a saddle between two highs, but closer to the base of a higher gradient region, the result of recent seismic deformation.
log(energy index)	The lows are more prominent in comparison to the longer time range.
log(inverse Deborah number)	The picture has changed considerably -- the regional high is no longer located close to the fault/dyke intersection, but further north. The contours surrounding the event are similar to those of apparent volume and log(EI).
log(relaxation time)	The zone is now smaller but the focus of the event is still within lowest values.
log(fluidity)	The event is located between local highs, east and west.
seismic stress	Similar to the case with the longer time range.
seismic strain	Event sits in a seismic gap between two zones, east and west, of higher strain.

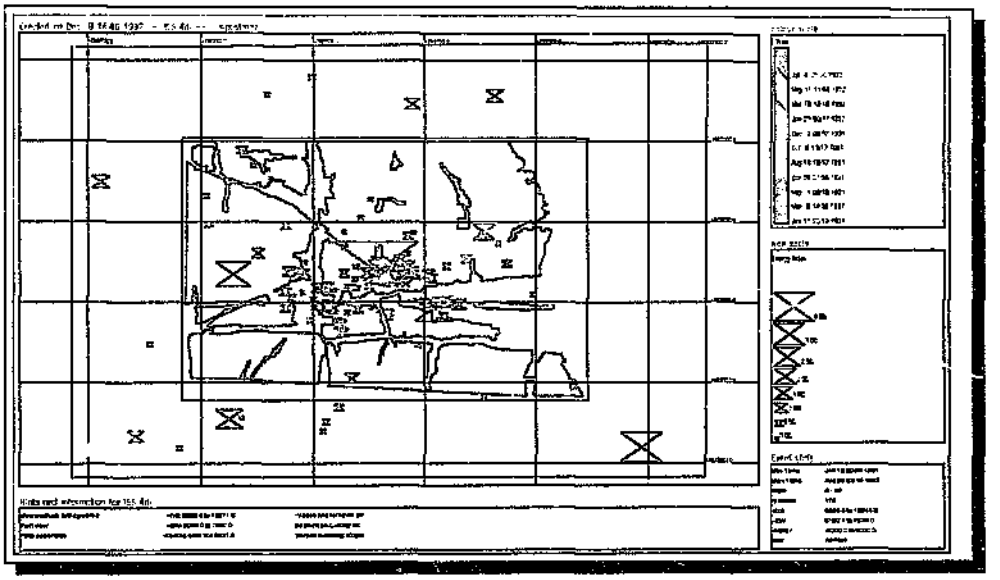


Fig. 4.38: Distribution of recorded events in the time period 1/1/91 to 26/8/92 in terms of energy index (symbol size) and time of occurrence (colour scale). Events 920826a and 920826b are included. The inner 'rectangle' enclosing the red lines (old mine faces) forms a polygon for the selection of events used in subsequent time-history analysis.

into the footwall of the reef. The second event, possibly caused by the first, is located west of the fault-dyke intersection in the plane of the fault, over 300m in the footwall of the reef.

Figures 4.42 to 4.46 (Appendix F2) show the variation of log(EI), d_s, S_s, η_s and $\log(Sc_s)$ with time. For events 920826a and 920826b ΣV_a is a very strong indicator, while log(EI) behaves opposite to that which is expected, increasing sharply, with a stiffening of the rockmass, a few days before the events. It seems that the softening associated with the nucleation zone (i.e. low EI values) was surrounded by a harder (stronger), more loaded zone producing higher EI events, the union of which (inside the polygon area) would create a rise in EI a short time before the main event. Seismic diffusion increases by an order of magnitude during the last few days; the seismic softening curve began an upward trend in early July (indicating an hardening process) and began to increase rapidly by the beginning of August, reaching a maximum a few days before the events. Seismic viscosity was following a downward trend, akin to the curve pertaining to $\log(Sc_s)$, although the latter was more pronounced.

In comparison to the graphs corresponding to the first case (event 910825), ΣV_a shows an increased rate of deformation just prior to the event. Seismic diffusion is indeterminate at this stage, along with seismic softening. Seismic viscosity and $\log(Sc_s)$ in both cases indicate downward trends. Log(EI) does not correlate, but will be tested later (at the end of Section 4.2), along with Schmidt number and seismic softening, for their sensitivity to varying lengths of time windows.

Contours were done for 12 months and 3 months, ending just before event 920826a and event 920826b (see figs. 4.42 to 4.58 -- Appendix F2). The results are tabulated in Table 5.

Table 5: Summary of results for contoured seismic parameters for events 920826a and 920826b

Time range from 910826 to just before event 920826a	
Seismic parameter	Observations
apparent volume	Event 920826a is located on the slope of a very prominent high, stretched generally east-west, close to the plane of the dyke. The second event, possibly caused by the first, is located west of the fault-dyke intersection in the plane of the fault, over 300m in the footwall of the reef.
log(energy index)	The first event is within a region of lower EI (contrasting with the trends followed by the time-history analysis, as discussed in the text); second event lies in an area of intermediate values.
log(inverse Deborah number)	Similar situation to apparent volume
log(viscosity)	First event plots within an area of lowest seismic viscosity; second event lies outside the boundaries of the contours in a less fluid environment.
seismic stress	First event lies in a region experiencing greater stress change surrounding the Postma dyke, south-east of a prominent high; second event lies on the edge of this region.
seismic strain	Similar to contours of apparent volume and log(inverse Deborah number).

Time range from 920526 to just before event 920826a	
Seismic parameter	Observations
apparent volume	Over the short term the first event coincides very well with a local high.The second event, as before, lies outside the seismogenic region.
log(energy index)	More pronounced, localized lows make their appearance and event 920826a falls within such a zone.
log(inverse Deborah number)	The situation here is again analogous to the case with apparent volume.
log(viscosity)	Event 920826a plots within a lobe of low viscosity (or high fluidity), as expected.
seismic stress	With 3 months of data, the very prominent high appears closer, in the vicinity of the first event.
seismic strain	Although not coinciding with the two sectors of greatest strain the first event nevertheless is associated with a local (lesser) high.

(4.2.3) Event 930314 of local magnitude 2.6:

Observations:

The fast rate of change in the curve of ΣV_a has consistently been acclaimed as a good indicator of imminent larger magnitude instabilities. In this case it is insufficient to bring attention to event 930314 (see fig. 4.59 -- Appendix F3). The event is coincidental with the plane of the dyke. The remaining parameters display a behaviour very similar to the previous case (events 920826a and 920826b) -- as shown in figures 4.59 to 4.63 (Appendix F3).

The results of the contours are summarised in Table 6. See figs. 4.64 to 4.75 in Appendix F3.

(4.2.4)Event 931108 of local magnitude 2.6:

During the second half of 1993 the seismic coverage in the Postma Area was greatly enhanced by the addition of two new stations to the existing network in the area, and by November 1993 over 1200 seismic tremors had been recorded. An enhanced sensitivity to ground motions means that when no seismicity is recorded the rockmass is, in fact, 'quiet' and not because of a lack of coverage. Event 931108 registered a local magnitude of 2.6.

Observations:

The hypocentre was about 250m into the reef footwall, coinciding with the plane of the dyke and approximately 180m from the plane of the Basson fault, in its footwall.

Table 6: Summary of results for contoured seismic parameters for event 930314

Time range from 920314 to just before event	
Seismic parameter	Observations
apparent volume	Event is within the zone of greatest inelastic deformation.
log(energy index)	Contours encompass a time frame that is large, blurring the later detail, but stressed areas (with a release of high energy values) and softer areas are still delineated.
log(inverse Deborah number)	Similar to the contours of apparent volume.
log(viscosity)	Event lies within the area of lowest viscosity.
seismic stress	The event plots at the edge of a prominent maximum.
seismic strain	Similar to seismic stress (and apparent volume and log(inverse Deborah number). With this length of time window most contours display an analogous behaviour, dominated by the regional high some 80m east of event 930314.

Time range from 921214 to just before event.	
Seismic parameter	Observations
apparent volume	Over the short term the areal extent of the contours is reduced; the event falls on the slope of and closer to a local maximum which now becomes evident.
log(energy index)	Event lies in a zone of lower EI.
log(inverse Deborah number)	Similar to the contours of apparent volume.
log(viscosity)	The inner boundaries showing the deflated values of viscosity correlate well with the (outer) boundaries of greatest apparent volume, but no indication is given of the actual location of the event to come.
seismic stress	Along with seismic strain (below), these contours point to a developing high at the intersection of the Postma dyke and Basson fault, adjacent to which the event is located.
seismic strain	The contours here are dominated by the deformation further north along the Basson fault (refer to seismic stress above). Nevertheless, event 930314 lies in an enclave between three local highs, in a region of lower EI, experiencing a lower rate of deformation than the surroundings.

The curves of ΣV_a and log(EI) shown in fig. 4.76 (Appendix F4) display the 'classical' features a few days before the expected event -- a sharp drop in EI and an increased rate of change in V_a. Seismic diffusion climbs, viscosity falls, and, consequentially, Schmidt number also decreases, all within hours before event 931108 (figs. 4.77 to 4.80 -- Appendix F4). (It is interesting to note that an event of magnitude 1.3 and high seismic energy preceded event 931108 by 52 hours, as indicated by the second-last inverted arrow on the top frame of the graph. It too was well predicted and underscored the potential for large tremors.)

The results of the contour analyses are given in Table 7 (see figs. 4.81 to 4.92 -- Appendix F4).

(4.2.5) Event 940424 of local magnitude 2.7:

The improved seismic coverage is again evident in the time-history analysis (see figs. 4.93 to 4.97 -- Appendix F5). The event is located about 200m into the reef footwall, in the plane of the dyke. van Aswegen (1994) had previously analysed this event, giving an interpretation of the preceding seismicity in a slightly different way, as a case study in the 1997 edition of 'Seismic Monitoring in Mines', Chapter 11. In addition to looking at the time-history behaviour, he also used iso-surface three-dimensional contours.

Observations:

In agreement with van Aswegen's findings, the curves of ΣV_a and log(EI) indicate the potential for a large event well in advance. Seismic diffusion rises over the last three days. From the second week of April there is a considerable variation in seismic

Table 7: Summary of results for contoured seismic parameters for event 931108.

Time range from 921108 to just before event	
Seismic parameter	Observations
apparent volume	The event is located on a high gradient, close to the regional maximum. It coincides with the plane of the dyke.
log(energy index)	The contours are difficult to interpret for this time range mainly due to the influence of seismicity dissociated from event 931108. It, nevertheless, occurs at the edge of a region of lower EI.
log(inverse Deborah number)	Similar to the contours of apparent volume.
log(viscosity)	The large area of lowest viscosity (highest seismic fluidity) embraces the focus of the event but without indication of a more specific location.
seismic stress	In comparison with the previous event stress highs have developed and intensified closer to the intersection of the Postma dyke and the Basson fault. Event 931108 plots in a trough between two local highs; the one on the right of this event is associated with event 930314.
seismic strain	Seismic strain intensifies in the vicinity of the fault-dyke intersection. The maximum from the previous event shifts westwards along the dyke and event 931108 plots on its slope.

Time range from 930808 to just before event	
Seismic parameter	Observations
apparent volume	The event is situated at the foot of a very prominent high less than 50m south of the focus.
log(energy index)	The event occurs in a high gradient region between a high and a low.
log(inverse Deborah number)	Three prominent highs correlate with the plane of the dyke; event 931108 plots northwest of a close local maximum.
log(viscosity)	Similar to the contours of log(inverse Deborah number).
seismic stress	The intensities of stress as indicated by the contours over 12 months have converged at the fault-dyke intersection and event 931108 is now situated at the very edge of this strong anomaly. The high to the north of the fault-dyke intersection was associated with an event of magnitude 2.4 on 15th February and has dessipated.
seismic strain	The local maximum close to the event corresponds to the zone of deformation also delineated by the contours of apparent volume.

softening, from a high to a low four days before event 940424, followed immediately by a sharp increase over the last four days. The curves of seismic viscosity and log(Schmidt no.) are again very similar; both decrease sharply over the last three days.

Observations about the contoured parameters (figs. 4.98 - 4.109 -- Appendix F5) are summarised in Table 8.

(4.2.6) Event 940513 of local magnitude 2.8:

The focus of this event is removed from the clustering of seismicity around the Postma dyke, and it plots west of the Basson fault, about 20m in the reef footwall, in the north-western part of the digitised section (see fig 4.11). It is included in this study to illustrate an important point: even though it plots within the polygon used for the normal selection of events it is spatially removed from the more seismically active area around the dyke. Fig. 4.110 shows the curves of ΣV_a and log(EI) for event 940513. There is no clear indication of the coming event. A systematic approach of covering an entire area of interest by using smaller, overlapping (rectangular) polygons for the selection of tremors, as displayed in fig. 4.111, with a moving window averaging 5 samples and/or 10 days, provides a simple, workable method of analysis, and, from polygon to polygon, the indicators begin to emerge. The size of the polygons is approximately 2.5 times the diameter of event 940513.

Table 8: Summary of results for contoured seismic parameters for event 940424.

Time range from 930424 to just before event	
Seismic parameter	Observations
apparent volume	Also coincidental with the plane of the dyke and of about the same size as events 931108 and 930314, this event plots next to a lobe that extends eastwards from the regional high.
log(energy index)	Does not provide good information which might be useful in delineating trends.
log(inverse Deborah number)	Again, very similar to the contours of apparent volume.
log(viscosity)	Event falls inside region of lowest seismic viscosity, as expected.
seismic stress	A stress high is developing about 120m south of the fault-dyke intersection. Event 940424 lies on a trough between two zones of higher than average stress along the dyke
seismic strain	The contours are dominated by the regional high and the event is situated about 120m eastwards from its apex.

Time range from 940124 to just before event	
Seismic parameter	Observations
apparent volume	The deformation being experienced by the fault-dyke intersection still overshadows the regional strains, but the rockmass surrounding the middle of the dyke is also being affected and the event plots closer to this recent development.
log(energy index)	A sharp drop in energy index from south-east to north-east of event 940424 is noticed.
log(inverse Deborah number)	The situation here is analogous to that shown by apparent volume.
log(viscosity)	In a departure from previous tendencies, the event is located on an edge of a region of lowest viscosity, in a seismic gap.
seismic stress	A zone immediately south-east of the location of the event is undergoing a stress buildup. Another 'regional' high is situated on the eastern arm of the dyke close to the intersection with the Arrarat fault.
seismic strain	According to these contours there is virtually no indication of the coming event. A sharp hike in strain has occurred over the short term on the middle northern edge of the digitized section.

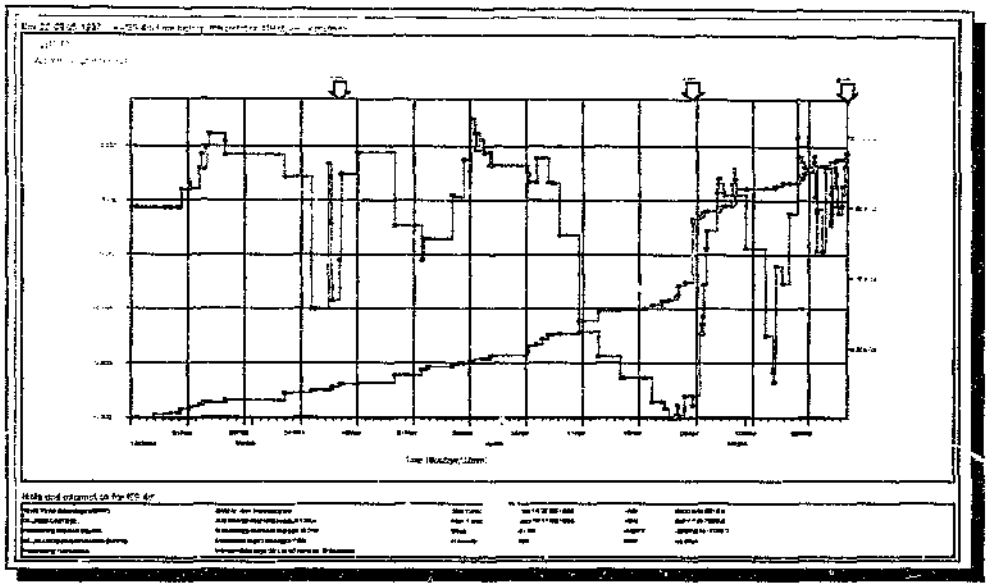


Fig. 4.110: Time-history of ΣV_s and log(EI) for event 940513 using the same polygon for events' selection as for previous cases (with a moving median window of 8 samples and/or 5 days). Since event 940513 is spatially removed from the clustering of seismicity around the Postma dyke, the polygon used for the previous selection of events must be modified in order to obtain better precursory trends/results.

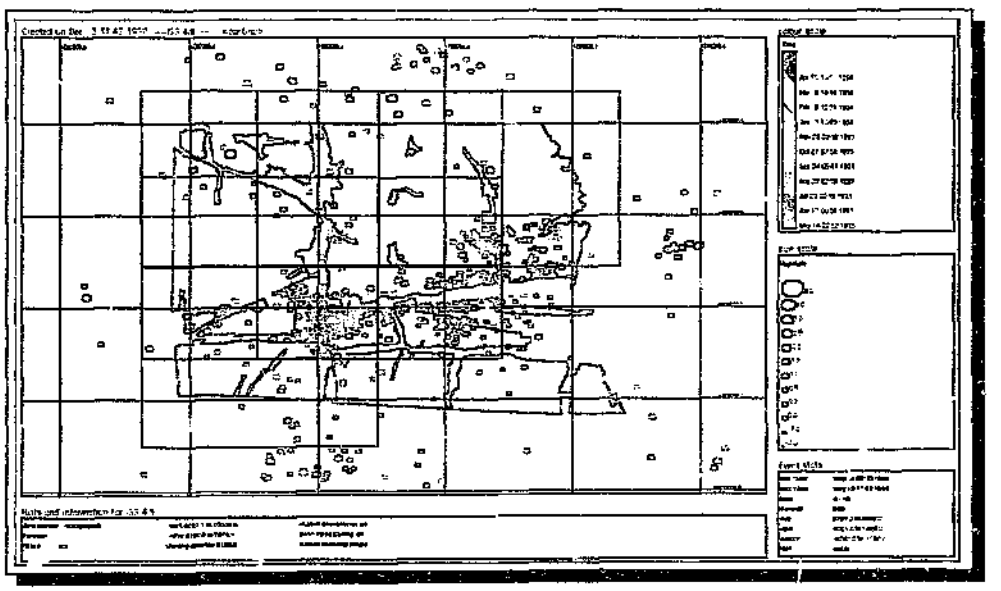


Fig. 4.111: The use of smaller, overlapping polygons creates a systematic means of covering an entire area of interest. As delineated above the polygons overlap by 50% from left to right and from the top down. The analysis of seismicity then entails looking at those events located within each of the individual polygons and identifying precursory trends. The distribution of recorded events in the time period 14/5/93 to 13/5/94 is also shown.

Observations:

The polygon which produces the best time variations is shown in figs. 4.112a and 4.112b (Appendix F6); ΣV_a, EI, seismic softening and seismic viscosity display the expected changes quite well. The curves of EI (log(EI)) and seismic softening both change significantly over the last few days before the event -- see figs. 4.113 to 4.117, Appendix F6.

Results of the contours are given in Table 9. See figs. 4.118 to 4.130, in Appendix F6.

(4.2.7) Events 940627a, 940627b and 940627c of local magnitudes 3.7, 3.2 and 2.7 respectively:

Observations / interpretation:

Slip along the Basson fault, close to the intersection with the Postma dyke, caused the first of a number of large seismic events to occur on 27th June shortly after 6 a.m. Event 940627a (see Table 5 and figs. 4.131, 4.132 to 4.133 (Appendix F7)) was the largest to have been recorded in this area since the monitoring of seismicity began. If there was some doubt as to whether the previous events might have caused relative movement between the Postma dyke and Basson fault, that uncertainty is dispelled with event 940627a. A spherical volume of deformation with a radius of about 160m embraces the fault-dyke intersection, as seen in fig. 4.132 (a section looking northwards along the plane of the Basson fault -- Appendix F7) and fig. 4.133 (a section looking eastwards along the plane of the Postma dyke, in the reef horizon -- Appendix F7). van Aswegen (1994; personal communication) observed fresh shearing soon after the event as part of the underground damage distribution,

Table 9: Summary of results for contoured seismic parameters for event 940513.

Time range from 930513 to just before event	
Seismic parameter	Observations
apparent volume	A low number of recorded tremors on the northwestern corner of the digitized section over the past year compared to the central area translates into poorly defined contours here. The greatest deformation correlates with the zone of greatest seismic activity.
log(energy index)	The zone around event 940513 shows higher than average energy index, pointing to stiff, moderately stressed conditions.
log(inverse Deborah number)	Similar to apparent volume
log(viscosity)	Low local values of seismic viscosity were present.
seismic stress	The energy index observed is supported by these contours.
seismic strain	Very little strain has taken place over the past year.

Time range from 940213 to just before event	
Seismic parameter	Observations
apparent volume	Over the short term the overall picture does not change.
log(energy index)	These values are higher than the norm in the vicinity of the event.
log(inverse Deborah number)	Virtually the same as the case for apparent volume.
log(viscosity)	The regional contours are less congested but there is no marked change.
seismic stress	The central area still dominates. The area of event 940513 appears more stressed over the last three months.
seismic strain (a)	Obscure in a regional sense, but ...
seismic strain (b)	...a focus on the area of interest reveals a prominent high on the slope of which the event is located. In association with the time-history analysis these are the best results obtained.

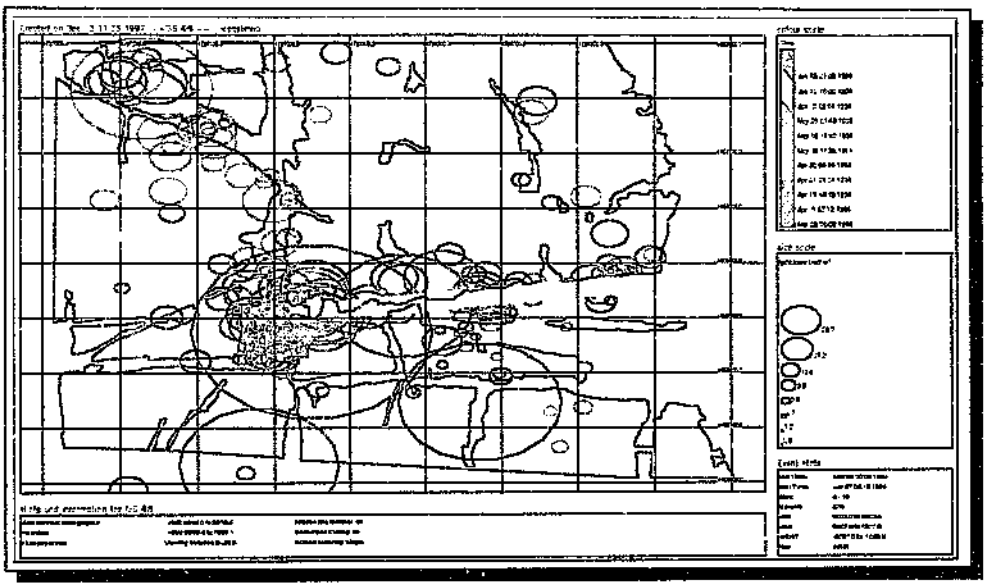


Fig. 4.131: Distribution of seismicity recorded in the time period 28/3/94 to 27/6/94 (three months before and including events 940627a, 940627b and 940627c). Note the greater concentration of events near the fault-dyke intersection, close to the hypocentre of event 940627a.

which indicated that slip had taken place both along the Basson fault and the northern contact zone of the Postma dyke.

Three of the closest geophone sites to the Postma area (16, 41 and 42 -- see fig. 3.3a, Chapter 3) were inoperative some time before and during the weekend prior to the events, effectively reducing local sensitivity considerably. As a result, warning of the approaching tremors was impaired and could have been much clearer, as indicated by figs. 4.134 to 4.138 (Appendix F7). In fact, better indicators were presented for earlier events of smaller magnitude. If the polygon is modified, as in the previous case, to select only the seismicity mostly associated with the Postma dyke (fig. 4.139, Appendix F7) the curves remain almost unchanged over the short term (figs. 4.140 to 4.144, Appendix F7). This reveals that the seismicity of importance, analysed in the few days and weeks before the major tremor, is localised, close to the focus of event 940627a. As will be shown later, such a clustering of recent tremors may 'pinpoint' with greater accuracy the location of the future event, within a larger polygon area, in association with indicators obtained through contouring and time-history analysis.

Observations concerning the contours are listed in Table 10. See figs. 4.145 to 4.168 (Appendix F7).

Sensitivity of source parameter calculations to the length of time windows used:
The sensitivity of source parameters to the length of time windows used during time-history analysis is expected to vary. The responses of EI, Sc_s and S_s were tested for two events. For event 940513 (see figs. 4.169 -- 4.177 in Appendix G) the curve of log(EI) maintains its downward trend as the number of samples is increased (for a

Table 10: Summary of results for contoured seismic parameters for events 940627a, 940627b and 940627c.

Time range from 930627 to just before events	
Seismic parameter	Observations
apparent volume	Event 940627a sits on the gradient, close to the apex, of the greatest volume of deformation. The subsequent events offer little correlation with this and other contoured parameters, and are thought to arise as a consequence of the ground motions induced by event 940627a.
log(energy index)	Minimal correlation at this stage.
log(inverse Deborah number)	Similar to that observed with apparent volume.
log(viscosity)	As expected for event 940627a. Events 940627b and 940627c are located on 'hard' patches of rock devoid of seismic activity.
seismic stress	Over the last year a seismic stress concentration has developed on the intersection of the Basson fault and another dyke, some 120m south of and roughly parallel to the Postma dyke.
seismic strain	The regions of strain highs show up very prominently. The two later events are shown lying on relatively undeformed areas.

Time range from 931227 to just before events	
Seismic parameter	Observations
apparent volume	Over the last 6 months the western lobe of this parameter (at the fault-dyke intersection) diminishes in size and intensity relative to the eastern lobe. The high observed on the north-western corner was produced by event 940513.
log(energy index)	The overall picture does not change significantly.
log(inverse Deborah number)	The contours are analogous to those of apparent volume.
log(viscosity)	Greatest fluidity is still observed at the Basson fault - Postma dyke intersection and dyke middle area.
seismic stress	Previous stress high has diminished and shifted about 50m north-westwards; sharp highs continue to cover the eastern arm of the Postma dyke.
seismic strain	This parameter has become focused just off-centre of the Postma dyke due to event 940424. The previous strain high (associated with event 931108) at the fault-dyke intersection has now all but disappeared.

Table 10 cont: Summary of results for contoured seismic parameters for events 940627a, 940627b and 940627c.

Time range from 940327 to just before events	
Seismic parameter	Observations
seismic stress	This is the only parameter which has varied considerably when wheighted against the previous time range. Of interest is the increase in stress over the central portion of the Postma dyke and the further development of the highs along the Basson fault.
others	Very little change has occurred over the last three months to the last 6 months as shown.

Time range from 940527 to just before events	
Seismic parameter	Observations
apparent volume	The high on the north-western portion of the plot is due to an event of magnitude 2.2 which occurred two weeks before event 940627a. Over the last month the remaining coseismic deformation took place mostly at the fault-dyke intersection.
log(energy index)	Event 940627a located on the eastern edge of a high in EI at the fault-dyke intersection.
log(inverse Deborah number)	Similar to apparent volume.
log(viscosity)	The central part of the Postma dyke is now more viscous than before.
seismic stress	A portion of the Postma dyke, off-centre and to the east, continues to show a stress high after the dessipation of the previous concentration in its centre. There are no distinct anomalies in the immediate vicinity of the event hypocentres.
seismic strain	The disappearance of the previous bull's-eyes leaves a picture with a raised level of cumulative strain at the intersection of the Basson fault and Postma dyke.

fixed number of 5 days) but loses its sharpness. Sc_s maintains its integrity quite well. The graphs of seismic softening, on the other hand, appear to be very sensitive, going from one extreme to the other.

For event 940424 a larger area with a greater number of recorded events was analysed. Two window tests were performed. In the first instance (figs. 4.178 to 4.189 -- Appendix G) the number of days was held constant (5) but the number of samples was varied. In the second instance (figs. 4.190 to 4.198 -- Appendix G) the number of samples was held constant (8) and the number of days was varied. Both cases show the greater sensitivity of seismic softening with respect to the other parameters, in agreement with the findings for event 940513.

(4.3) Summary:

Elastic stress modelling, without further rheological characterisation of the rockmass response to mining-induced stress changes, may be misleading. As an example, consider a stabilising or bracket pillar, designed with the aid of numerical modelling, which might have failed coseismically. Or, a seismic event may have occurred elsewhere as a result of relative slip along some plane of weakness other than where anticipated by modelled ESS. An investigation of recorded seismicity should reveal recent spatial and temporal transfer of stresses which might be used as feed-back information for the verification and/or modification of original design parameters and assumptions. In effect, the design of the next stage or sequence of mining becomes proactive with the mining itself.

The results of ESS modelling on both the Postma dyke and Basson fault were correlated with the behaviour of the structures in terms of stress (EI) and strain rate (seismic viscosity). A poor agreement with the recent deformations was observed in older places, but the youngest regions of induced ESS complement the locality and extent of seismic activity.

Concerning the dissipation of strain energy along the Postma dyke and Basson faults in reaction to the stoping nearby, it appears that the seismic energy release diffuses downdip initially and then broadens with time, over considerable distances which are, in likelihood, greater than the actual linear extent of the stoping.

Such analysis is essentially performed over a longer period of time to that useful for predictive purposes. The seismic activity occurring in the days or hours immediately

before a major event should characterise rockmass instability, and the seismicity in the Postma area leading to 10 events with calculated magnitudes greater than 2.5 was analysed in terms of time and spatial variations. Polygons for the division and selection of seismicity were adapted according to the distribution of events.

A limited data base was available for event 910825 but all the time-history curves for this event (with the exception of seismic diffusion) displayed the expected trends (i.e. a drop in stress and an increase in strain rate) leading to the tremor. For events 920826a and 920826b, however, the time analysis showed a pattern opposite, in most cases, to that which was prescribed. Cumulative apparent volume predicted the event remarkably, with an accelerated seismic deformation in the days prior to it. The rockmass appears to have stiffened very rapidly, over the last days, with fast increases in energy index, seismic diffusion and seismic softening. In a true time-history fashion, the energy indicators (the inverted arrows on top of the graph axis for log(E) $\geq$7.0) coincided well with large increases in these parameters over the preceding months. Although there is a decrease in viscosity (i.e. an increased strain rate over stress) around the Postma dyke and its intersection with the Basson fault (this is where most seismicity occurs -- see the contours described above), there is a general pick-up of stress and, consequently, the occurrence of precursory events of higher energy index. The sharp increases over the short term point to the developing instability.

The next event, 930314, displayed a similar behaviour, but with disappointing results shown by V_a, which was anticipated to be a good precursor (as before).

The installation of additional stations close to the Postma dyke (less than 300 m away) contributed to a marked improvement in sensitivity and accuracy of location of events during the latter part of 1993.

Events 931108 and 940424 were clearly predicted. It is possible, but unlikely, for the former to have broken some asperity linked to the intersection of the Postma dyke and Basson fault. In the case of event 940513 the focus of rupture was distant and independent from the area experiencing greatest activity and deformation. A polygon embracing all the seismicity associated with the digitised plan will include irrelevant information, clouding the prediction of the event. A novel, simple yet robust method for the selection and interpretation of seismicity is introduced, where an area of interest is divided into overlapping polygons. In a top-to-bottom and left-to-right approach, each polygon overlaps the one above and the one preceding by 50% of its area (or more, depending on circumstances and/or requirements). A systematic analysis of the seismicity is then accomplished by looking at the events within the polygons, individually and in sequence, until the entire area has been covered. Such a procedure may be automated, allowing for quick identification of hazardous regions which might have been missed by the conventional method. With event 940513 a taylor-made application is demonstrated.

With event 940513 the window length used in the time-history back-analysis had to be modified to 5 samples and/or 10 days, as opposed to the usual 8 samples and/or 5 days, for the sought precursory indicators to emerge (refer to Section 2.5.1, Chapter 2 and Section 4.2). This is due to the smaller number of events in the smaller area as well as a decreased rate of occurrence of tremors in time. There is no optimum window length that allows the best graphical trends (precursors) to appear. It remains a function of a particular seismically active area with its own signature, and, as such, must be determined empirically, whenever possible, using past patterns of seismicity.

Some source parameters are also more sensitive to the length of the moving median windows used during time-history analysis than others. From graphical trends, it appears that seismic softening is especially sensitive to the length of time window used. However, since the best length format ' letermined empirically) is likely to produce acceptable results for all the source parameters, there seems to be no need to create different time windows for different source parameters. From a practical point of view this is very advantageous.

The spatial variation of the seismicity was investigated over the long term (12 months when possible) and over the short term (the last three months before the event). For event(s) 940627 the contouring was performed for 12, 6, 3 and 1 month(s) respectively. It is clear that over the long term a lot of redundant information comes into play, with the smaller seismicity becoming overshadowed by the contribution of the larger events. Analysis over the short term is more indicative of more recent, more pertinent changes in the state of stress and strain of the rockmass, particularly seismic gaps. Depending on the amount of deformation of the rock and the rate of closure taking place, it will take many years for the rockmass to 'heal'. Any contoured representation of cumulative deformation, over a long period of time, should delineate relatively intact patches of rock, which depending on the mining rates and strategies in the vicinity should tend to accumulate strain energy, with a possible sudden release in the future.

Observations regarding the contoured seismic parameters were tabulated (Tables 4 to 10); a summary of these and other parameters pertaining to time-histories, regarding their usefulness as a predictive tool, is given in Table 11. The rating of 'good', 'fair' or poor' was done through a visual inspection of the plots; these were then graded as

Table 11: Summary of the precursory performance of the seismic parameters investigated for two methods of analysis. Regarding the contours, the long term analysis refers to the period of 'months in advance'; the short term analysis refers to 'weeks in advance'.

Method of analysis	Seismic parameter	Indication of large event in advance	
		In long term (months or weeks)	In short term (weeks or days)
Time-histories	Energy index	Fair	Good
	Apparent vol	Fair	Good
	Seismic diffusion	Fair	Good
	Seismic softening	Fair	Fair
	Seismic viscosity	Fair	Fair
	Seismic Schmidt no.	Fair	Fair
Contours	Energy index	Poor	Poor-Fair
	Apparent vol	Fair-Good	Fair-Good
	Inv. Deborah no.	Fair	Fair
	Seismic viscosity	Poor	Fair
	Seismic stress	Poor	Fair
	Seismic strain	Fair	Fair

either 1 (no clear indication of the future event), 2 (some indication of the future event) or 3 (distinct indication of the future event). An average value for all ten events was then calculated; a rating < 1.4 was labelled 'poor', a rating from 1.5 to 2.4 was labelled 'fair' and a rating > 2.5 was termed 'good'.

The time variation of seismicity, as a method of short term prediction, is best served by the parameters of energy index, cumulative apparent volume and seismic diffusion, a few days before the event (see Table 11). On a scale of weeks, the parameters of seismic softening, viscosity and Schmidt number will bring attention to an unstable area.

As a method of longer term 'prediction', the spatial variation of seismicity should be scrutinised. The largest events were found to plot at - or on the gradients of - or adjacent to - local maxima/minima which developed recently, as indicated through the contouring of various seismic parameters -- see Table 11. These can be used to verify the unstable rockmass conditions pointed out by the time-histories, and to locate the most likely area for the event to come. Contours of apparent volume, inverse Deborah number and seismic strain -- over the short term -- produced the best results.

It is often the small seismic events causing minimal damage to a working face or other areas of development on the mine, clustering close together, that act best as spatial precursors. Larger magnitude seismic events have been known to occur far away from active mining without any prior indication. When the stresses acting on a volume of rock surpass the strength of the rockmass and its ability to support these stresses, it fails. In the cases cited, the back-area events were all a consequence of the ground

motions and propagation of wave energies induced by the first (larger) events. These ground motions created sufficient additional stress (or a change in stress) for failure. From a practical point of view it is advantageous to locate the point of rupture of a future event at least to within the scale of the faces being stoped. Figs. 4.199 to 4.205 in Appendix H show the seismicity in the last days before an event. Such clusters of seismicity, when used in conjunction with the contours over the short term, will 'pin-point' with some measure of accuracy the probable focus of the event.

The frequency of occurrence of larger seismic events is very often quite regular. As such, the energy indicators on time-history plots may even be used as 'likelihood indicators' of the failure processes. Although other areas of the Welkom goldfield have shown better results, figs. 4.206 to 4.211 (in Appendix I) exemplify this application, where the larger events (as indicated by the inverted arrows along the time axis of the graph) occur with predictable frequency.

As a concluding remark to this section, it should be strongly noted that the response of the rock mass to mining-induced stress changes is particular to the study area. It is known that rock mass conditions (a function of the depths of mining, geometries and densities of geological discontinuities, their frictional properties, constituent material and strength of the country rock, rate and extent of mining) vary from area to area; some seismic parameters recorded by a seismic network in a mining region might be significantly higher (or lower) than those recorded in another (e.g. van Aswegen, 1990, p722). Those parameters, or combinations of parameters, exposing nucleation processes leading to instability in the Post~a area are likely not to be as successful when applied to another mining area or district. However, the basic approach to the characterisation of the rock mass response should not differ significantly.

5

CONCLUSIONS

Recent advances in the throughput of seismic monitoring systems and seismic data analysis and interpretation methods have made it possible to describe earth tremors quantitatively, in terms of time, location, radiated energy and seismic moment. From this, a range of seismic parameters can be derived, describing the physics of seismic flow of rock.

This research has tested different methods for the evaluation of the response of geological discontinuities to mining-induced stress changes, in a small section of an intermediate depth gold mine in the Welkom district.

The sensitivity of the local network to ground motions in the Postma Area was found to be sufficient to record events with moment magnitudes greater than -0.6. The spatial location accuracy was expected to be better than 40m for smaller events, improving with increasing magnitudes as more stations recorded the events, at the workplaces visited and along the lengths of the Postma dyke and most of the Basson fault. The seismic coverage was, thus, deemed adequate for a detailed investigation of recorded seismicity.

Locations of 'small' magnitude ($M_L < 1.0$) events were found to correlate well with active stoping faces; larger magnitudes ($M_L > 1.5$) were observed to coincide more

readily with geological planes of weakness, particularly the Postma dyke and/or its intersection with the Basson fault.

The highly fractured state of the rockmass observed *in situ* was corroborated by the results of numerical elastic modelling and reflected in the high state of stress inferred seismically, lending enhanced confidence to seismicity analysis. The spatial and temporal distribution of the great majority of recorded events lay close to the active mining areas at the time.

Elastic modelling revealed that ESS was created on both the Postma dyke and Basson fault in the vicinity and as a result of the recent mining, indicating the possibility of slip along either plane of weakness. The largest event ever recorded in the area (M_L 3.7 on the 27th June 1994) occurred close to the fault-dyke intersection, in a region shown by the stress modelling to be of greater shear strength than adjacent parts on both planar surfaces.

Events selected within 100m of the hangingwall and footwall of both the Postma dyke and Basson fault differentiate between the seismic response of these structures to stress transfer, found to occur even along the same structure -- from one part of the dyke to another after a large event -- and characterise the behaviour of the discontinuities in terms of EI (a measure of stress change) and seismic viscosity (a measure of strain rate). Insight was given into the rheological character of the rockmass, which cannot be obtained through elastic numerical modelling alone. Both procedures -- seismic analysis and stress modelling -- are, however, complementary, and provide feed-back information for the modification of input parameters and/or

strategies while mining (e.g. variations of angle of friction and/or rock strength in accordance with seismic softening along a geological discontinuity, or using the distribution of seismic diffusion to aid the design (type and density) of support).

A whole range of seismic parameters (apparent stress, energy index, apparent volume, seismic strain (and/or strain rate), seismic stress, seismic viscosity, seismic relaxation time, seismic Deborah number, seismic diffusion, seismic Schmidt number and seismic softening) describe the seismic source and each contribute, of their own accord, to an understanding of the state of stress and strain surrounding underground excavations. The occurrence of potentially damaging seismic tremors may be preceded by observable changes in some seismological parameters. It was shown that high temporal and spatial gradients in seismic parameters pertaining to **stress** (energy index and seismic stress), **strain softening** (energy index, seismic viscosity, seismic diffusion, seismic Schmidt number and seismic softening) and **strain rates** (apparent volume, seismic strain, seismic viscosity, seismic Deborah number, seismic diffusion, seismic Schmidt number and seismic softening) just before imminent major seismic events may be recognisable timeously, with practical applications towards rockburst prevention and control measures and, consequently, greater safety in the underground working environment.

Some seismic parameters (energy index, apparent volume, seismic diffusion, inverse Deborah number and seismic strain -- refer to Table 11, Chapter 4, Section 4.3), viewed over a short period of time, in the form of time-history graphs, in conjunction with contour plots were found to be the best indicators or precursors of $M_L > 2.5$ in this particular mining area on the Basal Reef.

The rockmass response is. however, expected to be strongly site-sensitive and site-specific. Those parameters, or combinations of parameters (summarised in Table 11), which clearly exposed nucleation processes leading to instability and, hence, large scale deformation, might not be as successful when applied to another mining area or district.

Such analysis was shown to be practical and implementa' the rock mechanics department of mines already using such capable seismic systems.

Recommendations:

The choice of seismic system for the evaluation of recorded seismic activity is an important point to consider for those mines without adequate seismic coverage. A system which provides continuous, reliable source parameter calculations for the quantification of the rock mass behaviour is essential. It is recommended that such a system have the density of sensors and, hence, sufficient sensitivity to record the small events necessary for meaningful analysis of the recorded data, giving insight into developing instabilities which might climax into large scale deformation.

In terms of the successful assessment of the seismic hazard, the processing of seismic data needs to be automated to a greater degree. Stochastic methodologies need to be developed and implemented, to quantify instability of the rockmass and make seismicity analysis and interpretation less subjective, in order to improve on the success rate of prediction, and to mine proactively, guided by the rockmass response.

Future improvements should concentrate primarily on objectivity, rendering investigations less site-dependent, since no two mining areas nor geological situations are the same and the rockmass response varies from area to area. Software needs to be developed enabling such evaluations to become routine in the normal functioning of a rock mechanics department.

The most important changes in seismic information usually takes place in the short term (days or hours up to the present; what happened before becomes irrelevant) and is contained in the relaxation time of the seismic source. This could be taken into account as a model incorporating space-time deformations into numerical calculations of changes in stress, which are generally not considered in rock mechanics practice.

In conclusion, this dissertation contributes to the establishment of routine, practical seismic evaluations in mines. It is hoped that this work will provide stimulus for further research into objective quantification of the seismic response to mining-induced stress changes, which is likely to yield scientific, safety and economic benefits.

REFERENCES:

[1] Adams, D.J., Hemp, D.A. and Gurtunca, R.G.; A seismic system as a tool in rock engineering; CSIR, Division of Mining Technology; Jhb, S.A., 1993.

[2] Aref, K., Jager, A.L. and Spottiswoode, S.M.; The nature and possible source mechanisms of seismic events from a shallow pillar supported platinum mine in South Africa; CSIR, Division of Mining Technology; Jhb, S.A., 1993.

[3] Aki, K.; Scaling law of seismic spectrum; Journal of Geophysical Research, Vol. 72, pp1217 - 1231, 1967.

[4] Aki, K. and Richards, P.G.; Quantitative Seismology. Theory and methods, Freeman, San Francisco, 1980.

[5] Anagnos, T. and Kiremidjian, A.S.; Stochastic time-predictable model for earthquake occurrences; Bulletin of the Seismological Society of America, Vol. 74, no. 6, pp2593-2611, 1984.

[6] Asada, T; Earthquake prediction in Japan; Earthquake Prediction - Present Status; pp13-19, 1986.

[7] Berry, J.A.L.; The structure and seismic potential of the Dagbreek fault zone in the OFS Goldfield; unpublished MSc thesis, Imperial College, London, 1988.

[8] Biswas, N.N.; Earthquake precursors: Fairbanks seismic zone in central Alaska; Earthquake Prediction - Present Status; pp217-222, 1986.

[9] Booth, D.C.; Temporal variations in shear-wave splitting as an earthquake precursor; Scientific-Technical Contributions, International Conference on Earthquake Prediction: State-of-the-Art, Strasbourg, France, pp298-304, 1991.

[10] Brune, J.N.; Tectonic stress and the spectra of seismic shear waves from earthquakes; Journal of Geophysical Research, Vol. 75, no. 26, pp4997 - 5009,

1970; Correction; Journal of Geophysical Research, Vol. 76, pp5002, 1971.

[11] Carlson, J.M., Langer, J.S. and Shaw, B.E.; Dynamics of earthquake faults; Review of Modern Physics, Vol. 66, no.2, pp657-670, 1992.

[12] Churcher, J.M.; The effect of propagation path on the measurement of seismic parameters; Rockbursts and Seismicity in Mines, Fairhurst (ed.), Balkema, Rotterdam, pp198-205, 1990.

[13] Cichowicz, A.; The time variation of microevents parameters occurring before and after large seismic events; Scientific-Technical Contributions, International Conference on Earthquake Prediction: State-of-the-Art, Strasbourg, France, pp16-22, 1991.

[14] Console, R., Murru, M. and Alessandrini, B.; Statistical analysis of foreshocks in Italy; Scientific-Technical Contributions, International Conference on Earthquake Prediction: State-of-the-Art, Strasbourg, France, pp22-26, 1991.

[15] Crampin, S.; Monitoring changes of stress before earthquakes: possibilities for deterministic prediction; Scientific-Technical Contributions, International Conference on Earthquake Prediction: State-of-the-Art, Strasbourg, France, pp305-308, 1991.

[16] Dennison, P.J.G.; An investigation into the effects of adjacent mining and fault character upon the stability of a fault and its related seismic behaviour; submitted thesis, University of the Witwatersrand, Johannesburg, RSA, 1993.

[17] Dennison, P. and van Aswegen, G.; Stress modelling and seismicity on the Tanton Fault: a case study in a South African gold mine; Rockbursts and Seismicity in Mines, Proceedings of the 3rd International Symposium on Rockbursts and Seismicity in Mines, Kingston, Ontario, Canada, 16-18 August, pp327-336, 1993.

[18] Dieterich, J.H.; Preseismic fault slip and earthquake prediction, Journal of Geophysical Research, Vol. 83, no. B8, pp3940-3948, 1978.

[19] Gay, N.C. and Ortlepp, W.D.; Anatomy of a mining-induced fault zone; Geological Society of America Bulletin, Part 1, v.90, pp47-58, 1978.

[20] Gibowicz, S.; Magnitude and energy of subterranean shocks in Upper Silesia, Studia Geophys. Geod, 7, 1-19, 1963.

[21] Gibowicz, S.J.; Physics of fracturing and seismic energy release: A review; Pageoph.; vol. 124; Nos. 4/5; pp611-658, 1986.

[22] Gibowicz, S.J., Mechanics of seismic events induced by mining: a review; Keynote address: Second International Symposium on Rockbursts and Seismicity in Mines, University of Minnesota, Minneapolis, USA, June 8-10, 1988.

[23] Gibowicz, S.J.; Seismicity induced by mining; Advances in Geophysics; Vol. 32, pp1-74, 1990.

[24] Gibowicz, S.J.; Seismic source parameters; Internal report: ISS International Ltd., PO Box 2083, Welkom, 9460, RSA, 1993.

[25] Gibowicz, S.J. and Kijko, A.; An introduction to mining seismology, Vol. 55 in the International Geophysics Series, Academic Press, 1994.

[26] Guha, S.K.; Studies on earthquake precursors; Earthquake Prediction - Present Status; pp31-37, 1986.

[27] Hanks, T.C. and Kanamori, H.; A moment magnitude scale; Journal of Geophysical Research, Vol. [illegible], pp2348 - 2350, 1979.

[28] Hemp, D.A.; The effect of backfill on seismicity and ground motion in a stope. MINEFILL 93. Johannesburg, SAIMM, pp137-146, 1993.

[29] Herrmann, R.B.; A student's guide to the use of P and S wave data for focal mechanism determination; vol. 46, no. 4, Earthquake Notes, October-December

pp29-39, 1975.

[30] Imoto, M.; Changes in the magnitude-frequency b-value prior to large (M greater than 6.0) earthquakes in Japan; Tectonophysics, 193, pp311-325, 1991.

[31] Iyer, H.M.; Earthquake prediction: how close is it to reality?; Earthquake Prediction - Present Status; pp1-11, 1986.

[32] Jones, L.M. and Molnar, P.; Some characteristics of foreshocks and their possible relationship to earthquake prediction and premonitory slip on faults; Journal of Geophysical Research, Vol. 84, no. B7, pp3596-3608, 1979.

[33] Jost, M.L. and Herrmann, R.B.; A student's guide to and review of moment tensors; Seismological research letters, vol. 60, no. 2, April-June, pp37-57, 1989.

[34] Keilis-Borok, V.I. and Rotwain, I.M.; Diagnosis of time of increased probability of strong earthquakes in different regions of the world: algorithm CN; Physics of the Earth and Planetary Interiors, 61, pp57-72, 1990.

[35] Keilis-Borok, V.I. and Kossobokov, V.G.; Premonitory activation of earthquake flow: algorithm M8; Physics of the Earth and Planetary Interiors, pp73-83. 1990.

[36] Keilis-Borok, V.I. and Kossobokov, V.G.; Times of increased probability of strong earthquakes (M greater than 7.5) diagnosed by algorithm M8 in Japan and adjacent territories; Journal of Geophysical Research, Vol. 95, no. B8, pp12413-12422, 1990.

[37] Kijko, A., Funk, C.W. and Brink, A.v.Z.; Identification of anomalous patterns in time-dependent mine seismicity; 3rd International Symposium on Rockbursts and Seismicity in Mines, Kingston, Ontario, Canada, 16-18 Aug 1993; Proceedings A.A. Balkema, Rotterdam, Brookfield, 1993.

[38] Kijko, A. and Funk, C.W.; Space-time interaction amongst clusters of mining

induced seismicity; Internal report, ISS International Ltd, PO Box 2083, Welkom 9460, Republic of South Africa, p1-28, 1994.

[39] Kisslinger, C; Seismic quiescence from local data as a precursor in the central Aleutian Islands; Earthquake Prediction - Present Status, pp23-28, 1986.

[40] Kossobokov, V.G. and Keilis-Borok, V.I.; Reduction of territorial uncertainty of earthquake forecasting; Physics of the Earth and Planetary Interiors, 61, ppR1-R4, 1990.

[41] Kostrov, B.V.; Seismic moment and energy of earthquakes and seismic flow of rock; Phys. Solid Earth, 13, pp13-21, 1974.

[42] Kostrov, B.V. and Das, S.; Principles of Earthquake Source Mechanisms; Cambridge Univ. Press; 1988.

[43] Latoussakis, J., Stavrakakis, G., Drakopoulos, J., Papanastassiou, D., and Drakatos, G.; Temporal characteristics of some earthquake sequences in Greece; Tectonophysics, 193, pp299-310, 1991.

[44] Lindh, A.G.; Estimates of long-term probabilities for large earthquakes along selected fault segments of the San Andeas fault system in California; Earthquake Prediction - Present Status, pp189-200, 1986.

[45] Maxwell, S.C. and Young, R.P.; Seismic imaging of rock mass responses to excavation; Int. I. Rock Mech. Min. Sc.; in press, 1996.

[46] McGarr, A.; Estimating ground motions for small nearby earthquakes; Seismic Design of Embankments and Caverns; Proceedings of a symposium sponsored by the ASCE Geotechnical Division in conjunction with the ASCE National Convention, Philadelphia, Pennsylvania, May 16-20, pp113-127, 1983.

[47] McGarr, A., Spottiswoode, S.M. and Gay, N.C.; Observations relevant to seismic driving stress, stress drop, and efficiency; Journal of geophysical research, vol. 84, no. B5, May 10, 1979.

[48] Meijer, O.; A comparison of the induced fault slip behaviour and related seismicity of the Tanton and Wesselia faults in the Welkom Goldfield; Internal report: ISS International Ltd., PO Box 2083, Welkom, 9460, RSA. November 1993.

[49] Mendecki, A.J. (Ed); Seismic Monitoring in Mines, Chapman & Hall, London, 1997.

[50] Mendecki, A.J., van Aswegen. G., Brown, J.N.R. and Hewlett, P. ; The Welkom Seismological Network; Rockbursts and Seismicity in Mines, Fairhurst (ed.), Balkema, Rotterdam, 1990.

[51] Mendecki, A.J., van Aswegen, G., Brown, J.N.R. and Hewlett, P.; Real time quantitative seismology in mines; Keynote lecture: 3rd International Symposium on Rockbursts and Seismicity in Mines, Kingston, Ontario, Canada, 16-18 Aug 1993.

[52] Minney, D.S. and Naismith, W.A.; Quantitative analysis of seismic activity associated with the extraction of a remnant pillar in a moderately deep level gold mine; Internal report: President Steyn Gold Mine, Jan 1993.

[53] Minter, W.E.L., Hill, W.C.N., Kidger, R.J., Kingsley, C.S. and Snowden, P.A.; The Welkom Goldfield; Mineral Deposits of Southern Africa, 1986, pp497-539.

[54] Mogi, K.; Earthquake prediction program in Japan; Earthquake Research Institute, Tokyo University, p635-666, 1980.

[55] Molchan, G.M.; Strategies in strong earthquake prediction; Physics of the Earth and Planetary Interiors, 61, pp84-98, 1990.

[56] Molchan, G.M.; Structure of optimal strategies in earthquake prediction; Tectonophysics, 193, pp267-276, 1991.

[57] Molchan, G.M. and Dmitrieva, O.E.; Dynamics of the magnitude-frequency

relation for foreshocks; Physics of the Earth and Planetary Interiors, 61, pp99-112, 1990.

[58] Molchan, G.M. and Kagan, Y.Y.; Earthquake prediction and its optimization; Journal of Geophysical Research, Vol. 97, no. B4, pp4823-4838, 1992.

[59] Niazi, M.; Variation of b-value and regional seismicity in southern California; Earthquake Prediction - Present Status; pp87-101, 1986.

[60] Ogata, Y.; Detection of precursory relative quiescence before great earthquakes through a statistical model; Journal of Geophysical Research, Vol. 97, no. B13, pp19845-19871, 1992.

[61] Peacock, S., Crampin, S., Booth, D.C. and Fletcher, J.B.; Shear-wave splitting in the Anza seismic gap, southern California: temporal variations as possible precursors; British Geological Survey, 1987.

[62] Rastogi, B.K.; Patterns of earthquake precursor parameters for some earthquake sequences in India; Earthquake Prediction - Present Status; pp79-85, 1986.

[63] Reiner, M.; Deformation, Strain and Flow; H.K. Lewis, London, 1969.

[64] Ryder, J.A.; Excess shear stress in the assessment of geologically hazardous situations; Journal of the SA Institute of Mining and Metallurgy, vol 88, no. 1, pp27-39, 1988.

[65] Saha, S.N.; Microearthquakes and earthquake prediction oriented studies in northeastern India: present status; Earthquake Prediction - Present Status, pp247-254, 1986.

[66] Sato, H.; Temporal change in attenuation intensity before and after the eastern Yamanashi earthquake of 1983 in central Japan; Journal of Geophysical Research, Vol.91, no. B2, pp2049-2061, 1986.

[67] Sato, H.; A precursorlike change in coda excitation before the western Nagano earthquake (M_s = 6.8) of 1984 in central Japan; Journal of Geophysical

Research, Vol. 92, no. B2, pp 1356-1360, 1987.

[68] Schreider, S.Y.; Formal definition of premonitory seismic quiescence; Physics of the Earth and Planetary Interiors, 61, pp113-127, 1990.

[69] Sciocatti, M.J. and Kijko, A.: Stochastic model for seismic flow using a fractal approach; Internal report, ISS International Ltd, PO Box 2083, Welkom, 9460, Republic of South Africa, p1-22, 1994.

[70] Semadeni, T. and Rochon, P.; Waveform analysis of mine induced seismic events recorded at Rio Algom's Quirke Mine; Rockbursts and Seismicity in Mines, Fairhurst (ed.), Balkema, Rotterdam, pp195-198, 1990.

[71] Scholz, C.H.; The Mechanics of Earthquakes and Faulting, Cambridge University Press, 1988.

[72] Shaw, B.E., Carlson, J.M. and Langer, J.S.; Patterns of seismic activity preceding large earthquakes; Journal of Geophysical Research, Vol. , pp479-488, 1992.

[73] Sobolev, G.A., Chelidze, T.L., Zavyalov, A.D., Slavina, L.B. and Nikoladze, V.E.; Tectonophysics, 193, pp255-265, 1991.

[74] Stevenson, D.A. and Talwani, P.; Anomalous changes in t_s/t_p ratios and two successful predictions at Lake Jocassee, South Carolina, USA, Earthquake prediction in Japan; Earthquake Prediction - Present Status; pp117-134, 1986.

[75] Talebi, S. and Young, R.P.; Characterizing microseismicity associated with stope development; Rockbursts and Seismicity in Mines, Fairhurst (ed.), Balkema, Rotterdam, pp184-194, 1990.

[76] Taylor, D.W.A., Snoke, J.A., Sacks, I.S. and Takanami, T.; Seismic quiescence before the Urakawa-Oki earthquake; Bulletin of the Seismological Society of America, Vol. 81, 4, pp1255-1271, 1991.

[77] van Aswegen, G.; Fault stability in SA gold mines; Mechanics of Jointed and

Faulted Rock, Rossmanith (ed.), Balkema, Rotterdam, pp717-725, 1990.

[78] van Aswegen, G. and Butler, A.; Applications of quantitative seismology in SA gold mines; 3rd International Symposium on Rockbursts and Seismicity in Mines, Kingston, Ontario, Canada, 16-18 Aug 1993; Proceedings, A.A. Balkema, Rotterdam, Brookfield, 1993.

[79] van Aswegen, G. and Meijer, O.; The mechanics of seismic events around faults in mines; Eurock '94, Delft, The Netherlands, Proceedings A.A. Balkema, Rotterdam, 1994.

[80] Wyss, M.; On the status of seismic quiescence as a precursor; Earthquake Prediction - Present Status, pp201-215, 1986.

[81] Yoshida, A.; Change of seismicity patterns as precursors of large earthquakes; Scientific-Technical Contributions, International Conference on Earthquake Prediction: State-of-the-Art, Strasbourg, France, pp167-174, 1991.

QUANTITATIVE ASPECTS OF MINING-INDUCED SEISMICITY IN A PART OF THE WELKOM GOLDFIELD

VOLUME 2

QUANTITATIVE ASPECTS OF MINING-INDUCED SEISMICITY IN A PART OF THE WELKOM GOLDFIELD

Contents **Page no.**

VOLUME 1:

Declaration i

Abstract ii

Dedication iii

Acknowledgements iv

Contents v

List of Figures x

List of Tables xxiii

List of Symbols xxiv

[1] INTRODUCTION 1

(1.1) Organisation of the Dissertation 1

(1.2) Objectives 2

(1.3) The Welkom Goldfield 4

(1.4) The Welkom Seismological Network 8

(1.5) Regional Seismicity 9

(1.6) The Study Area 12

[2] **THEORETICAL BACKGROUND** 18

(2.1) Review of Earthquake Precursory Phenomena 18

(2.1.1) General 18

(2.1.2) Seismic patterns 20

(2.1.3) Seismic wave propagation 30

(2.1.4) Stochastic methodologies in hazard assessment 34

(2.2) Seismic Source Parameters 45

(2.3) Fault / Dyke Stability in the Mining Environment 50

(2.3.1) Asperities 50

(2.3.2) Undulations, depth, fault gauge, dip and K-ratio 52

(2.3.3) Stress variations and excess shear stress 54

(2.4) Recent Hypotheses in Rockmass Stability 59

(2.5) Numerical Aspects in Seismicity Analysis 66

(2.5.1) Time and space windows in the selection of seismic events for analysis 66

(2.5.2) Contouring of seismic parameters 69

(2.5.3) Time-history variations of seismic parameters 70

(2.6) Summary 71

[3] **SEISMIC COVERAGE AND CORRELATION OF SEISMICITY WITH MINING IN THE POSTMA AREA** 74

(3.1) Sensitivity of Local Network 74

(3.2) Location, Methods of Mining and In-situ Observations 78

(3.3) Spatial and Temporal Distribution of Seismicity 88

(3.4) State of Stress Inferred Seismically 92

(3.4.') Stress transfer along the Postma dyke 97

(3.5) Summary and Discussion 101

[4] **QUANTITATIVE ANALYSIS OF SEISMICITY IN THE POSTMA AREA** 104

(4.1) Stress Levels and Implications of Mining Adjacent to the Postma Dyke and Basson Fault 104

(4.1.1) Calculation of stresses using elastic-continuum modelling 104

(4.1.2) Seismic stress and deformation rates through recorded seismicity 117

(4.1.3) Summary 131

(4.2) Back Analysis of Large Events to Identify Precursors 133

(4.2.1) Event 910825 of local magnitude 2.5 134

(4.2.2) Events 920826a and 920826b of local magnitudes 2.8 and 2.6 respectively 142

(4.2.3) Event 930314 of local magnitude 2.6 147

(4.2.4) Event 931108 of local magnitude 2.6 147

(4.2.5) Event 940424 of local magnitude 2.7 149

(4.2.6) Event 940513 of local magnitude 2.8 151

(4.2.7) Events 940627a, 940627b and 940627c of local magnitudes 3.7, 3.2 and 2.7 respectively 154

(4.3) Summary 161

[5] **CONCLUSION** 168

REFERENCES 173

VOLUME 2:

Contents xxvi

APPENDIX A: Sections through the Basal Reef, showing the extent of discontinuities and local structure (figs. 1.7 a-f; refer to fig. 1.6, Sec 1.6, Chap 1) 182

APPENDIX B: Sketches and photographic record of stoping areas visited (figs. 3.8 and 3.9; refer to fig. 3.6, Sec 3.2, Chap 2) 186

APPENDIX C: Concentrations of recorded seismic events in the Postma area during the first and second semesters of 1994, respectively (figs. 3.10b and 3.10c; Sec 3.3, Chap 3) 199

APPENDIX D: Selective analysis of seismicity around the Postma dyke (figs. 4.8 b-d) and the Basson fault (figs. 4.9 b-d) for the contouring of seismic viscosity and energy index. The contours of seismic viscosity are overlaid on contours of energy index for visual effect and ease of combined evaluation/interpretation of the source

	parameters (Sec 4.1.2, Chap 4)	201
APPENDIX E:	(a) All recorded seismicity in the Postma area from 1/1/91 to 25/8/91 in terms of energy ... lex (figs. 4.12 and 4.15), seismic apparent stress (fig. 4.13) and apparent volume (fig. 4.14); (Sec 4.2.1, Chap 4)	209
	(b) Contours of seismic fluidity (fig. 4.17) for the delineation of the clustering of seismicity during the time period considered	211
	(c) Reduced areal extent used for time-history analysis with the new selection of events for seismic evaluation (fig. 4.18)	211
APPENDICES F1 to F7:	Time-history and contour plots used in the analysis of large events ($M_L > 2.5$) to identify precursors; (Section 4.2, Chapter 4)	212 - 308
APPENDIX G:	Sensitivity of source parameter calculations to length of time windows used (figs. 4.169-4.198) (Sec 4.2.7, Chap 4)	309
APPENDIX H:	Clustering of seismicity immediately before the occurrence of a large event (figs. 4.199-4.205) (Sec 4.3, Chap 4)	325
APPENDIX I:	Energy indicators used as 'likelihood' indicators of imminent instability (figs. 4.206-4.211) (Sec 4.3, Chap 4)	330

APPENDIX A

Sections through the Basal Reef, showing the extent of discontinuities and local structure (figs. 1.7 a-f); refer to fig. 1.6, Section 1.6, Chapter 1.

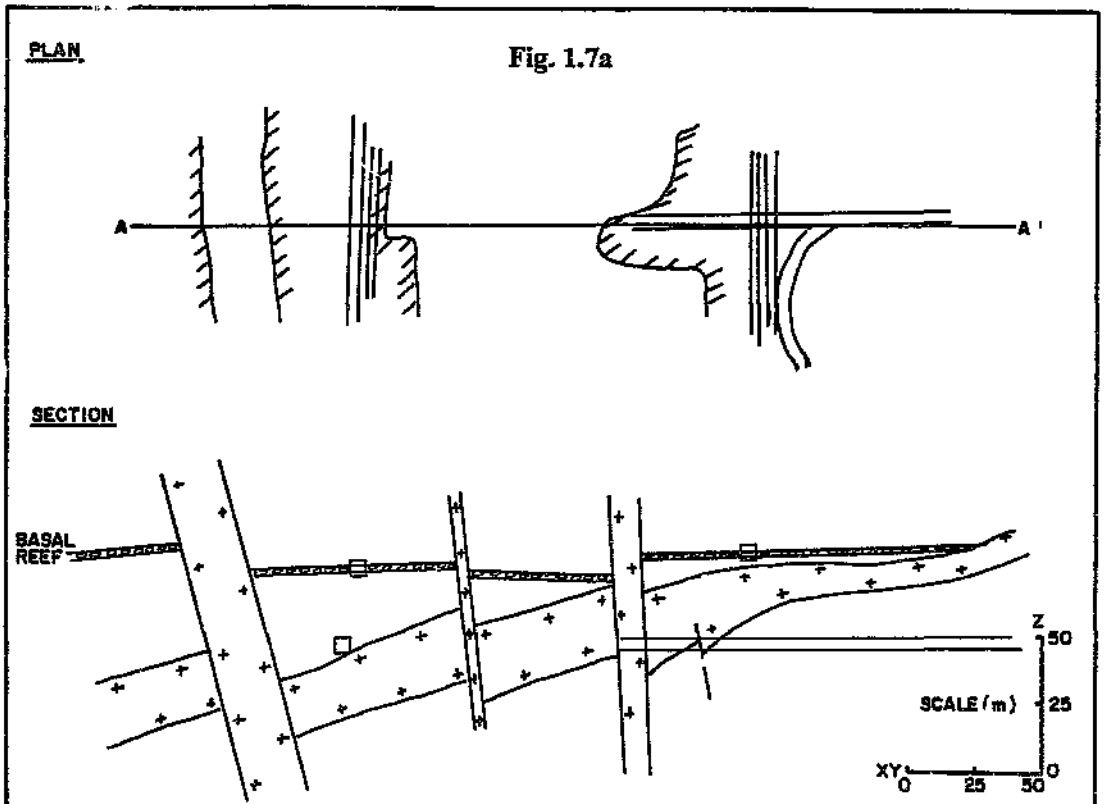


Fig. 1.7a-f: Sections through the Basal Reef, showing the extent of discontinuities and the local structure at depth. The location of each section is delineated in Fig. 1.6.

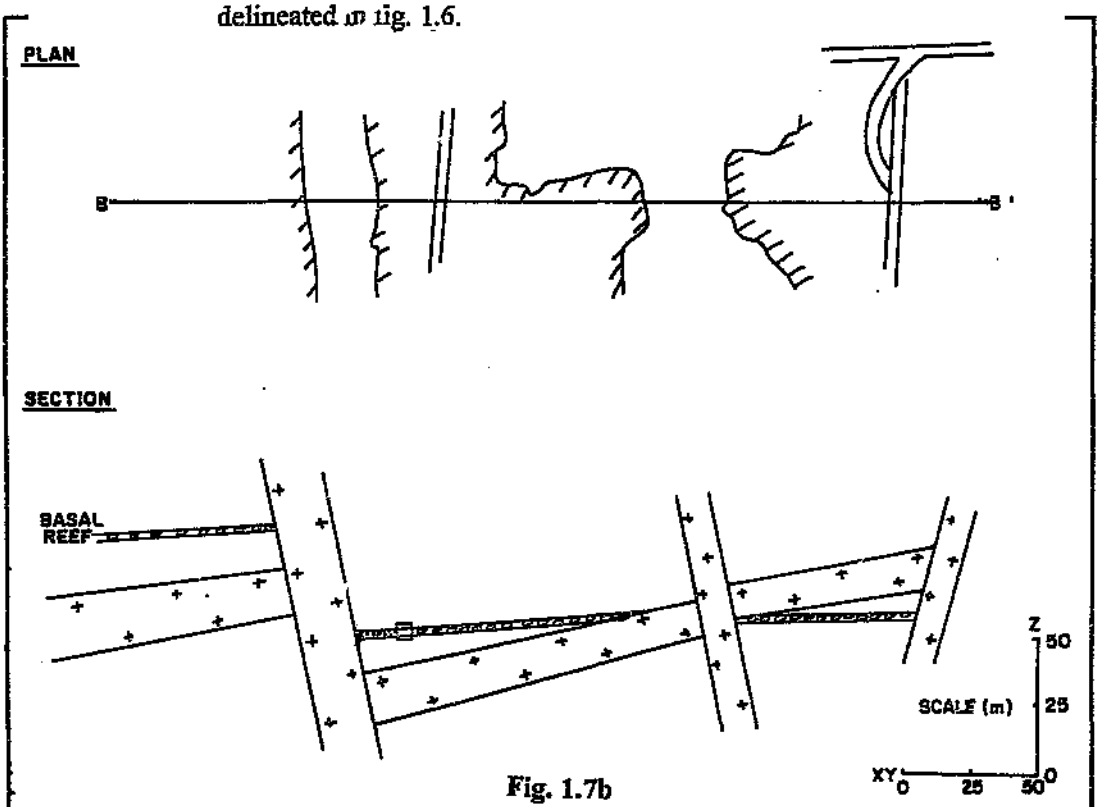


Fig. 1.7b

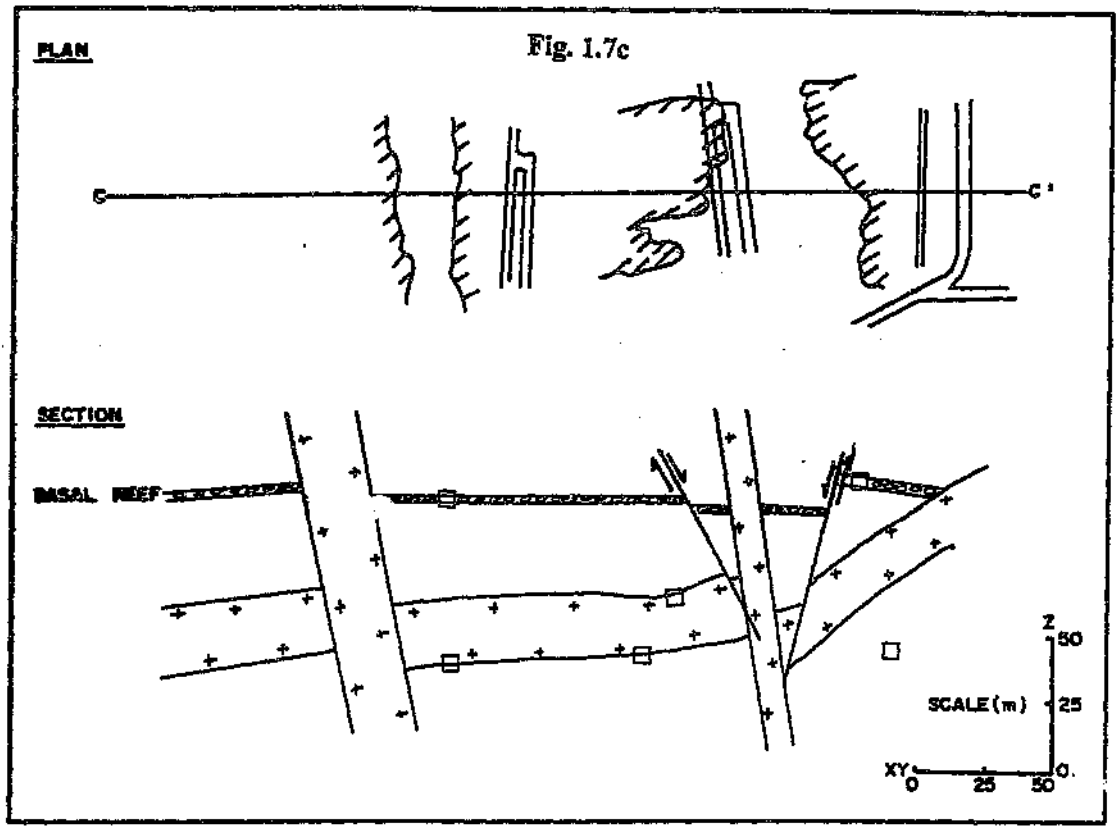


Fig. 1.7c

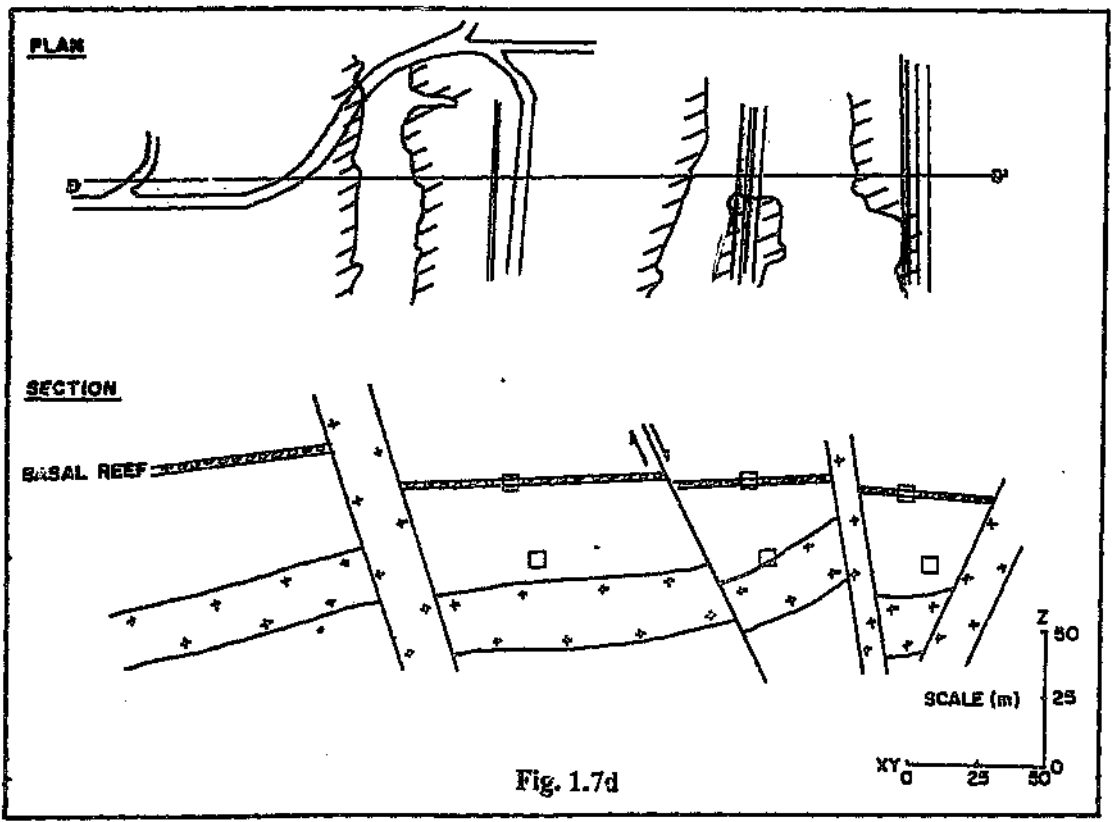


Fig. 1.7d

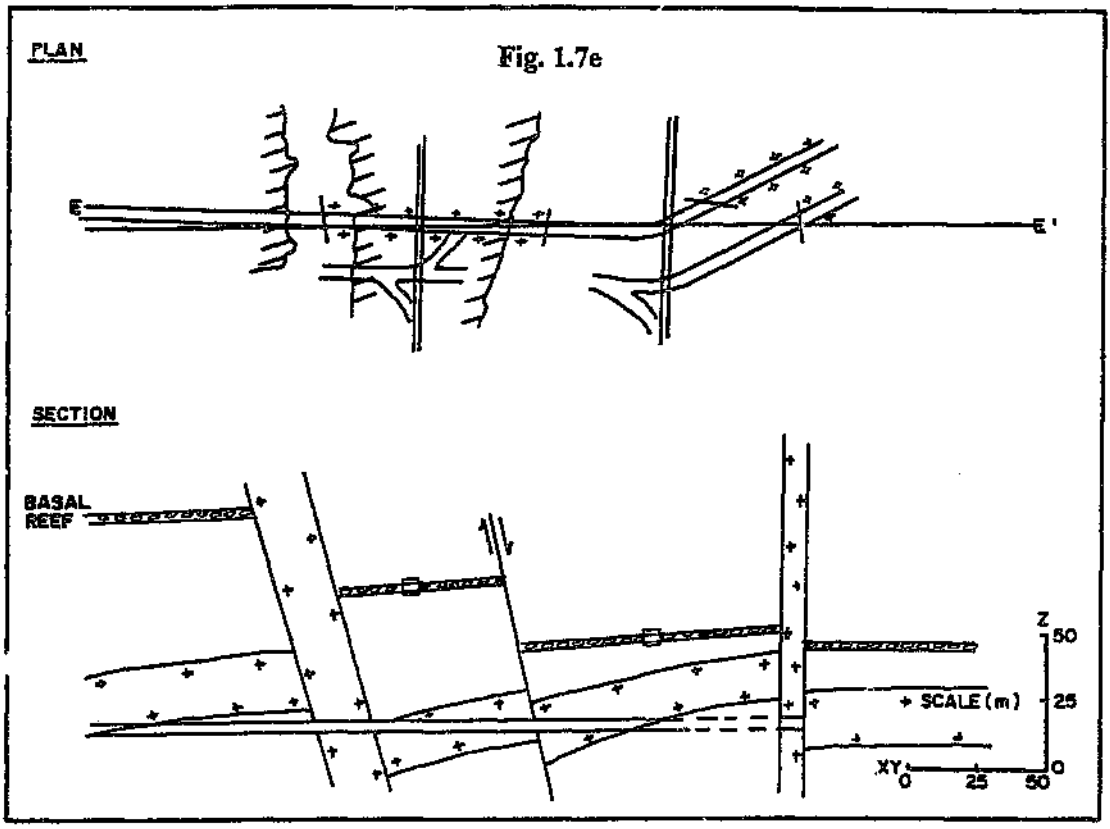


Fig. 1.7e

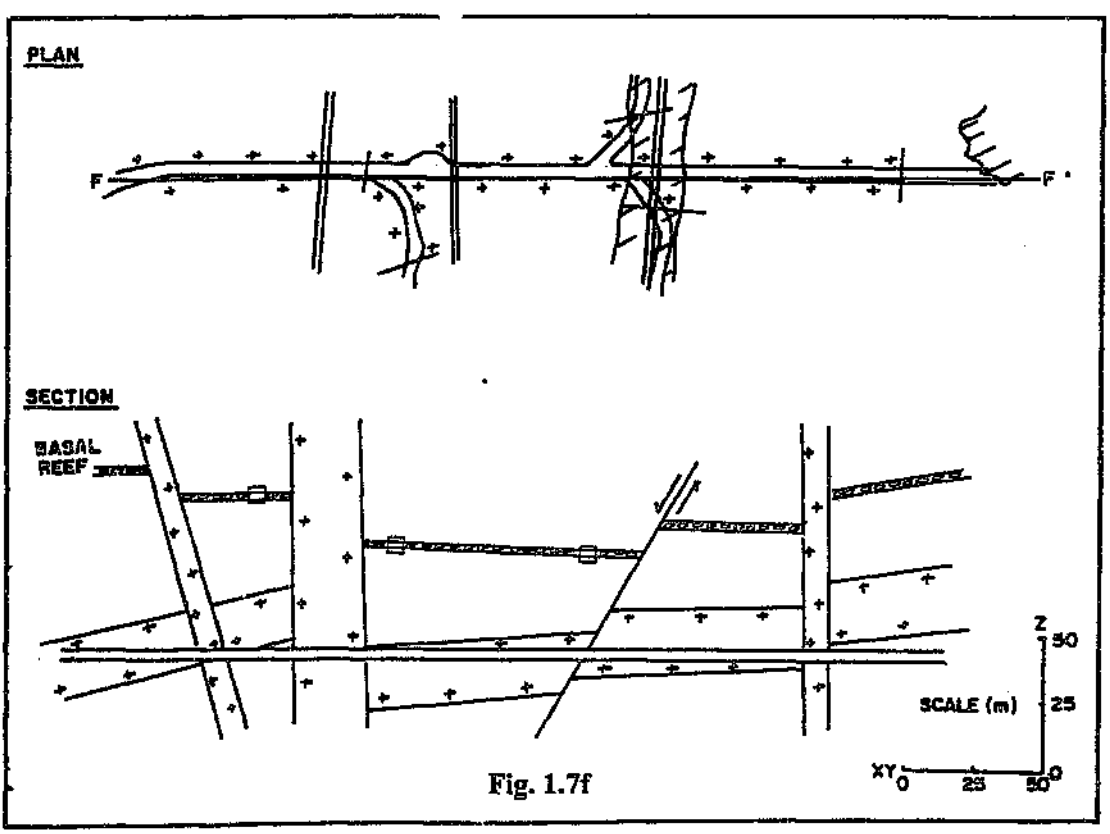
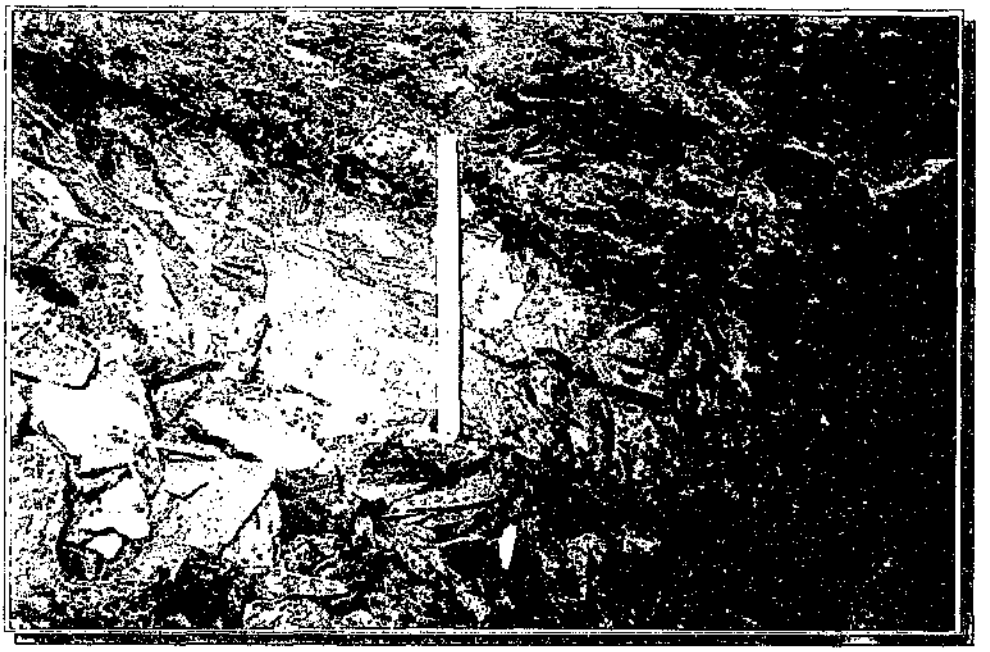


Fig. 1.7f

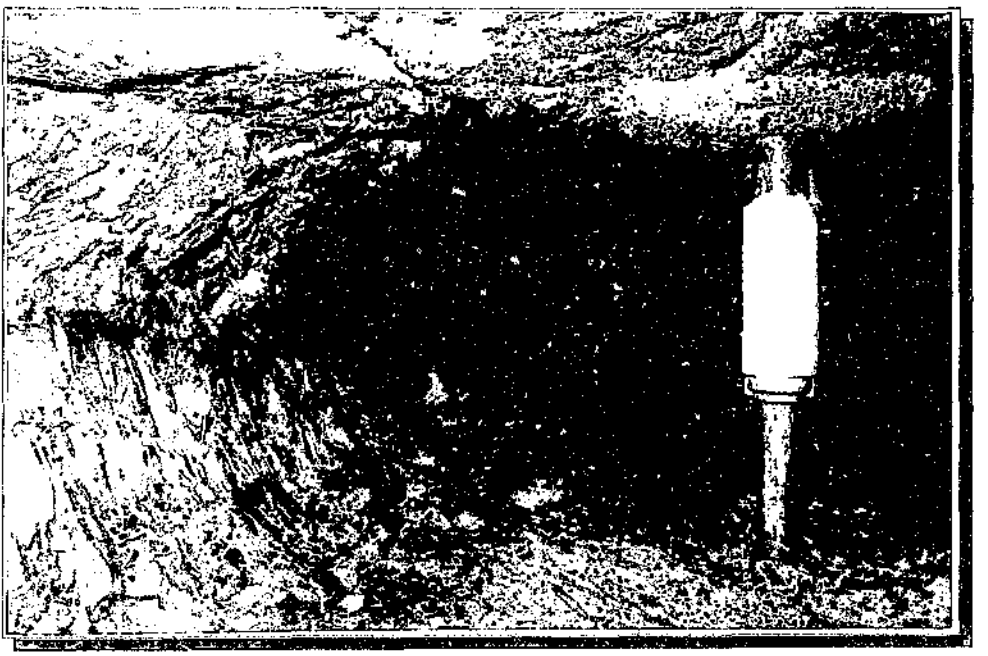
APPENDIX B

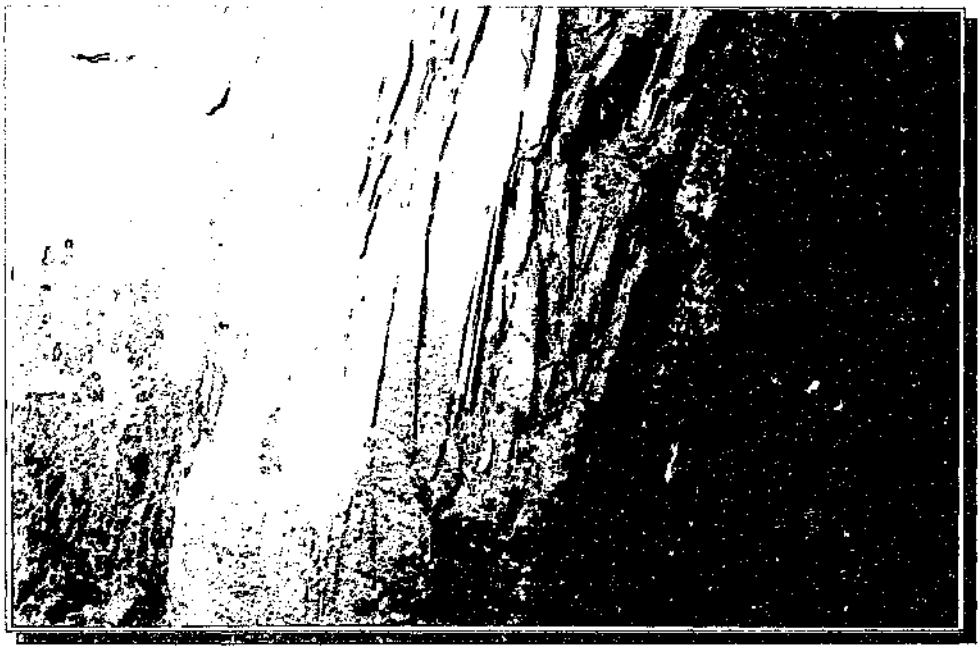
Sketches and photographic record of stoping areas visited (figs. 3.8 and 3.9); refer to figs. 3.6 and 3.7, Section 3.2, Chapter 2.



Above: Site 44-13A-10B: Photo No 1

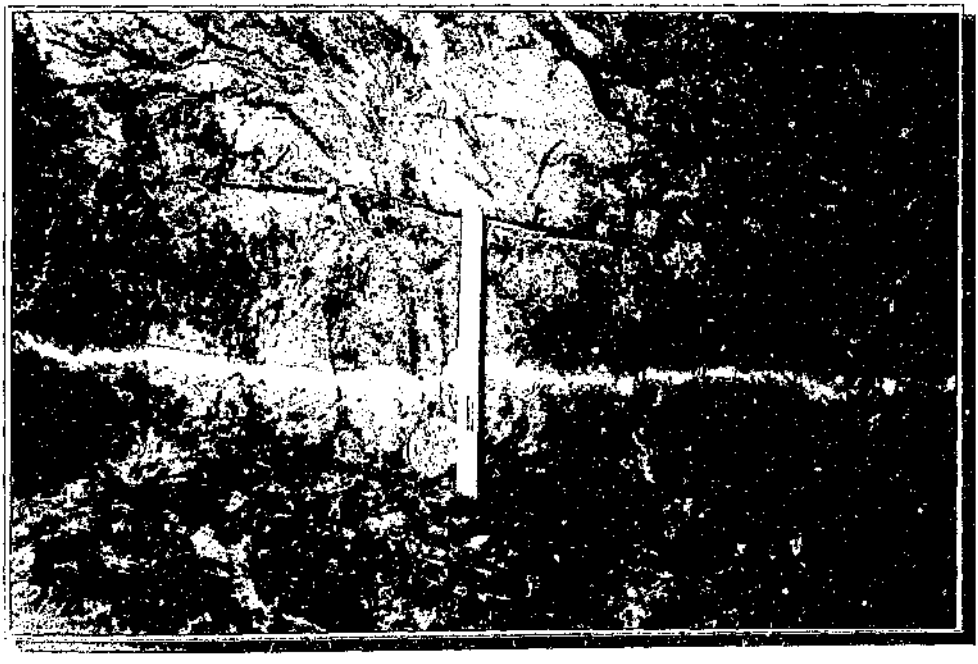
Below: Site 44-13A-10B. Photo No 2

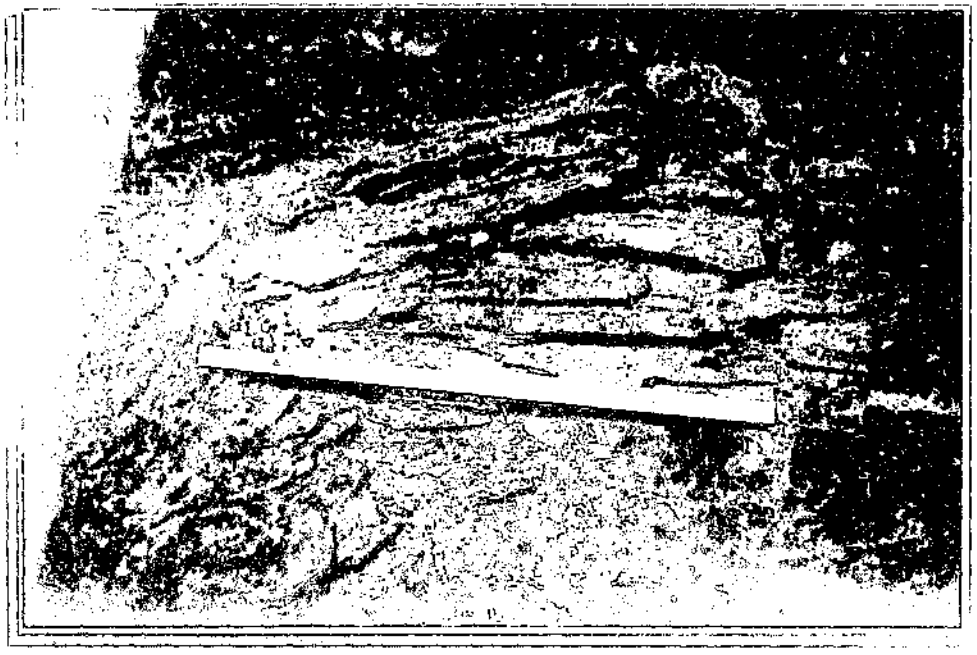




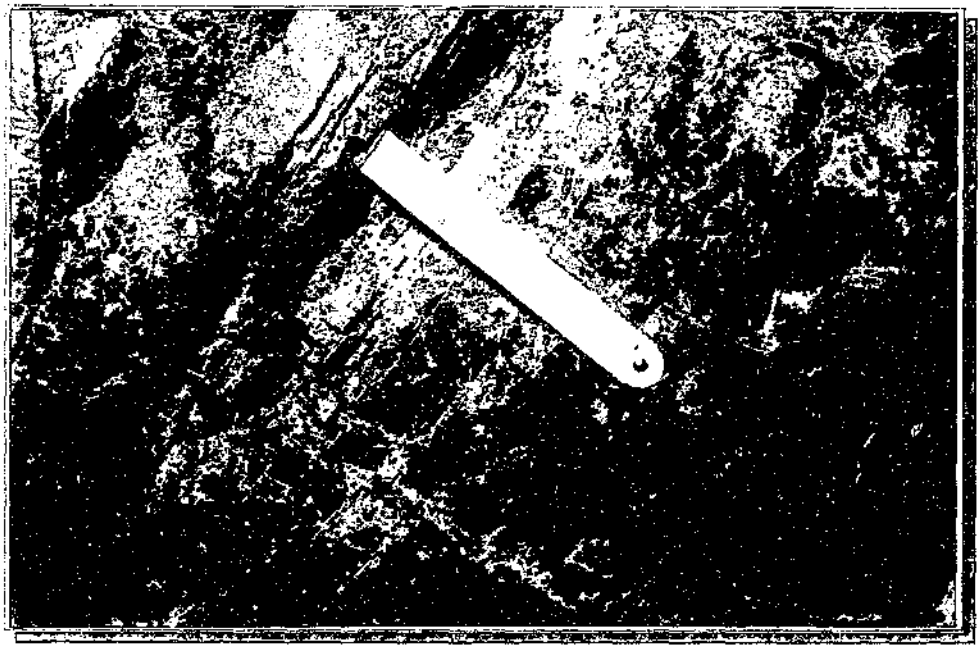
Above: Site 44-13A-10A, Photo No 5

Below: Site 44-13A-10A; Photo No 6



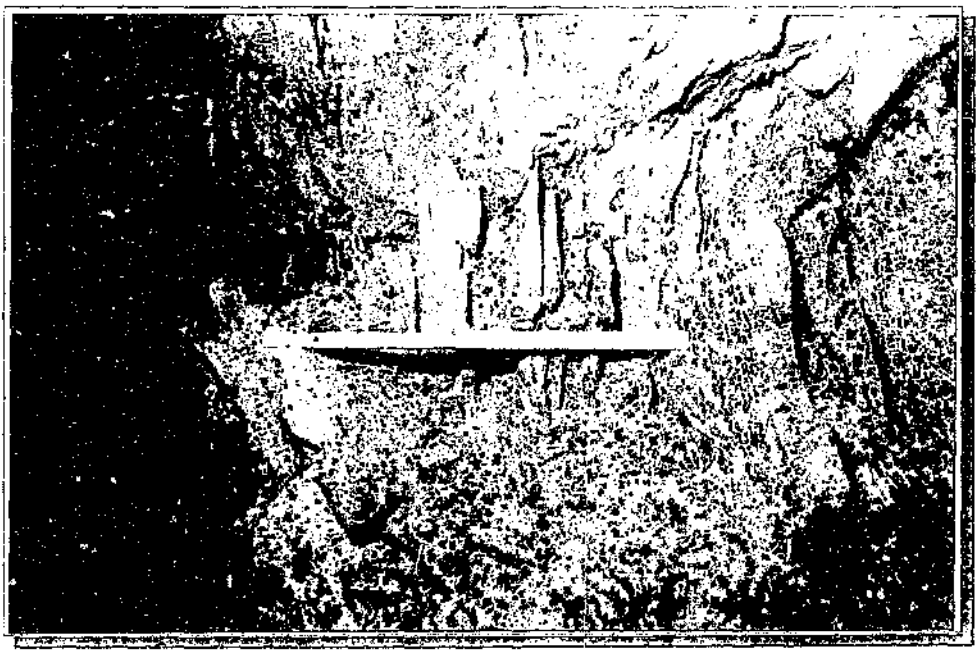


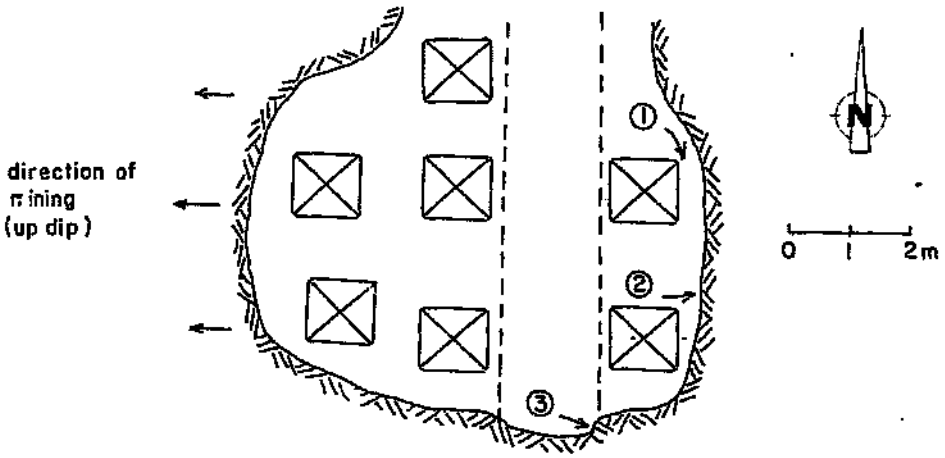




Above: Site 44-13A-10A;. Photo No 11

Below: Site 44-13A-10A. Photo No 12

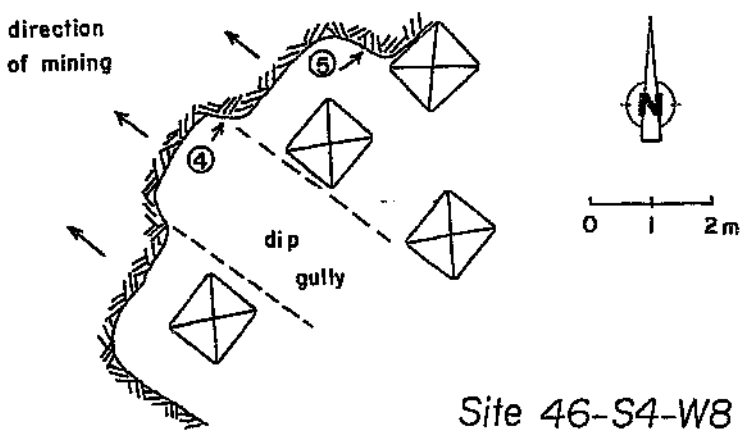




Site 46-S4-S1

Photographs:

[1] opening created by the collapse of hangingwall, the stability of which is adversely affected by the presence of a local sill.
[2] sill contact with reef-bearing quartzites
[3] gully head sidewall
[4] gully sidewall
[5] panel sidewall with khaki shale visible



Site 46-S4-W8

Fig. 3.8:
Panels of site 2, with indication of where photographs were take



Bellevue Site 46-53-41
Photo No 2





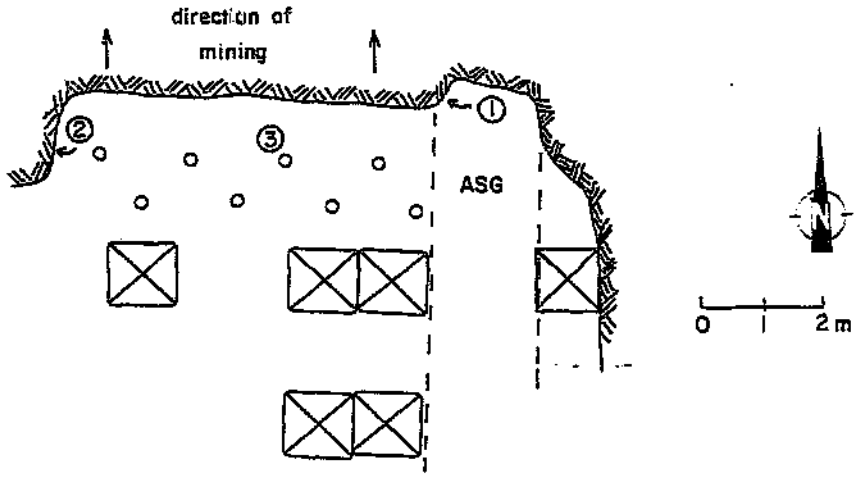
Above: Site 46-S4-S1, Photo No 3

Below: Site 46-S4-W8, Photo No 4





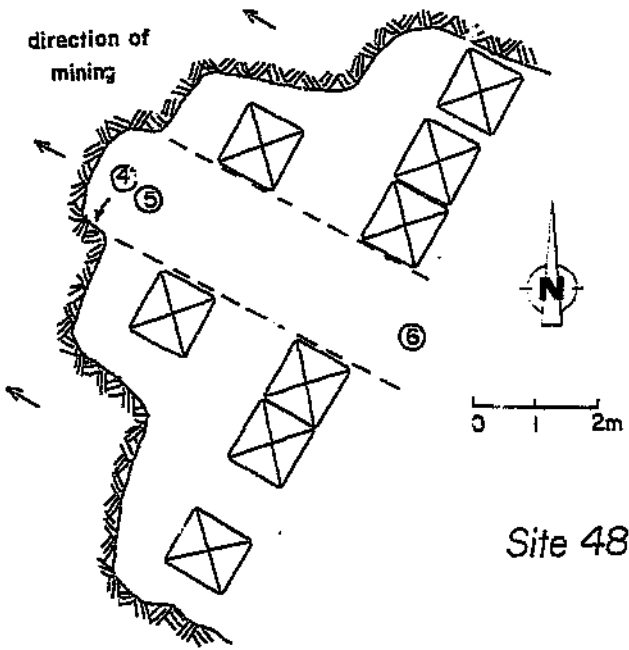
Above: Site 46-S4-W8; Photo No 5



Site 48-DI2- N2

Photographs:

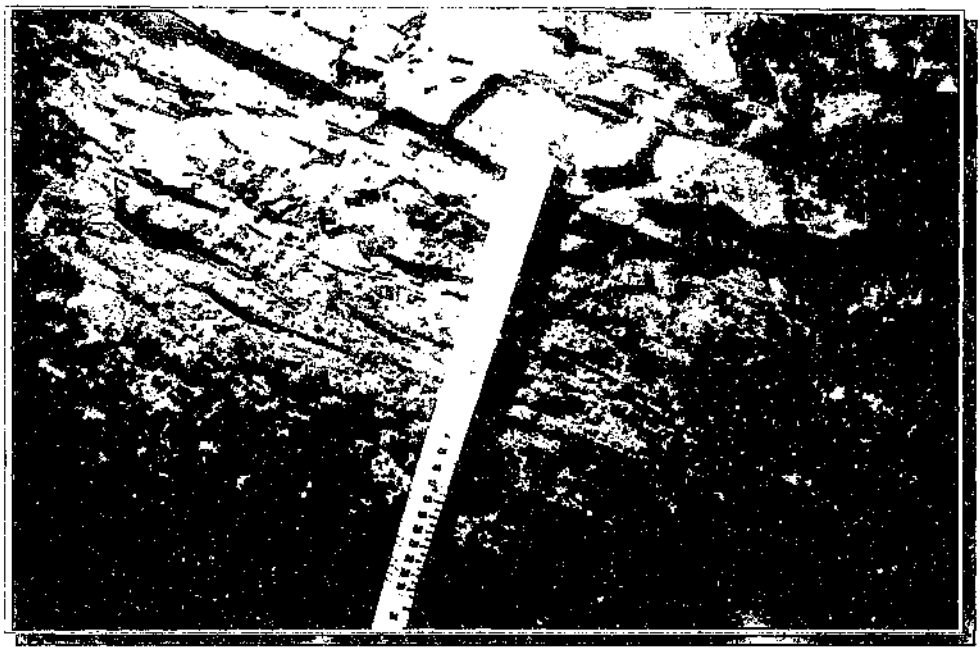
[1] ASG sidewall
[2] north panel sidewall
[3] hangingwall ~ 1.5m behind face (fractures parallel to face shape
[4] dip gully sidewall
[5] dig gully hangingwall close to the face
[6] dip gully hangingwall ~ 20m from face (fractures parallel to advancing face



Site 48-DI2-N6

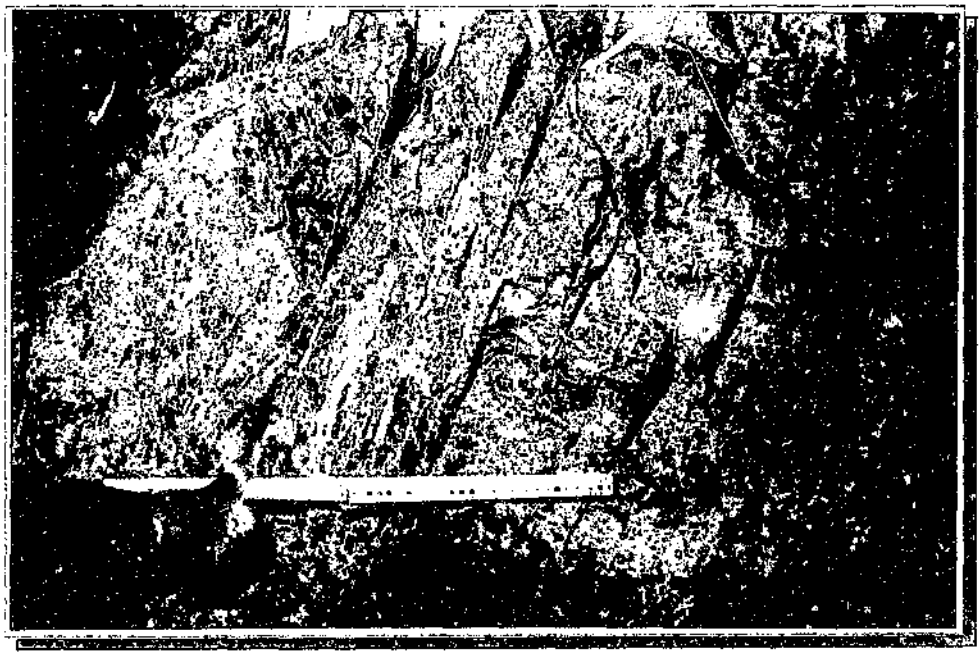
Fig. 3.9:
Sketch of site 3, with areas of mining and locations of photographs.

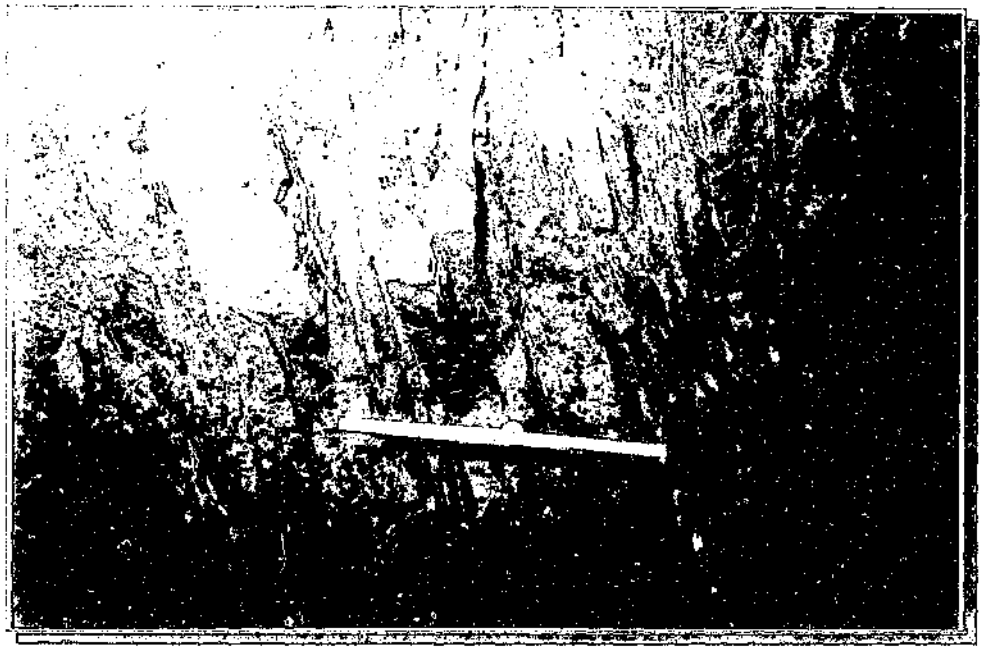
Photo No. 2



Above: Site 48-D12-N2; Photo No 3

Below: Site 48-D12-N6; Photo No 4





Above: Site 48-D12-N6, Photo No 5

Below: Site 48-D12-N6, Photo No 6



APPENDIX C

Concentrations of recorded seismic events in the Postma area during the first and second semesters of 1994, respectively (figs. 3.10b and 3.10c); see Section 3.3, Chapter 3.

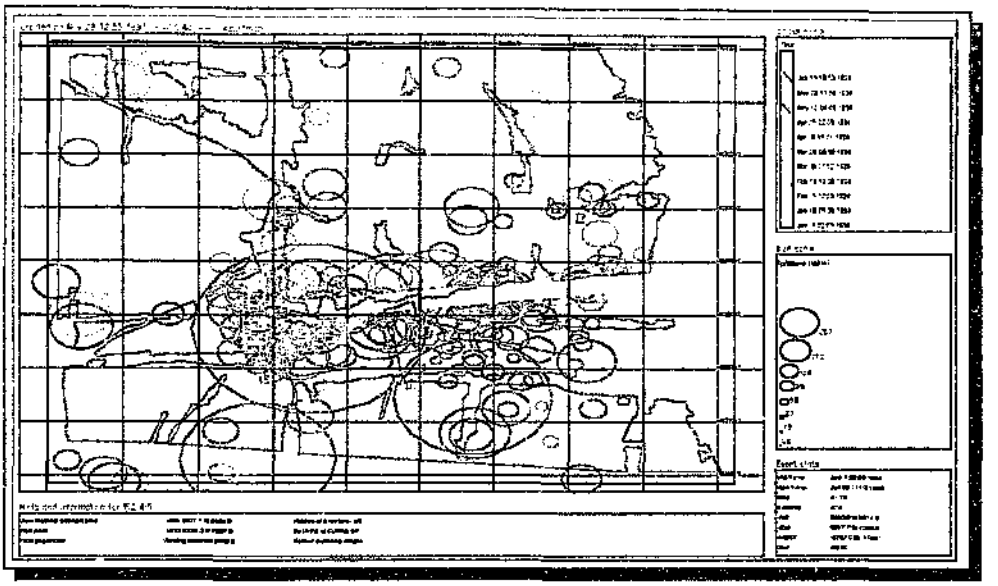


Fig. 3.10b: Same as fig. 3.10a, but showing all seismic events recorded in the Postma area during the first half of 1994.

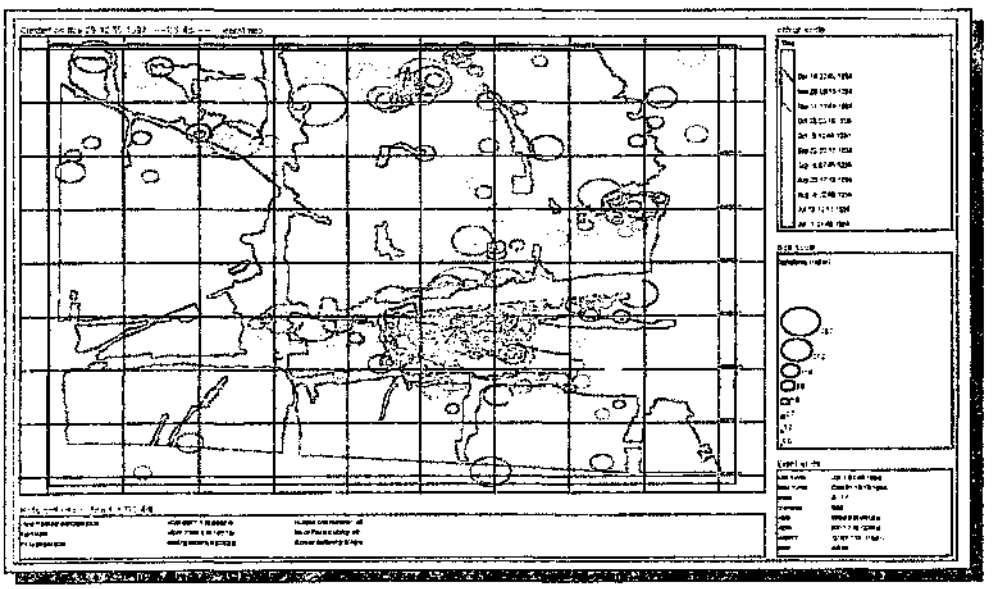


Fig. 3.10c: Same as fig. 3.10a, but showing all the seismic events recorded in the Postma area during the second half of 1994.

APPENDIX D

Selective analysis of seismicity around the Postma dyke (figs. 4.8 b-d) and the Basson fault (figs. 4.9 b-d) for the contouring of seismic viscosity and energy index. The contours of seismic viscosity are overlaid on contours of energy index for visual effect and ease of combined evaluation / interpretation of these source parameters (Section 4.1.2, Chapter 4).

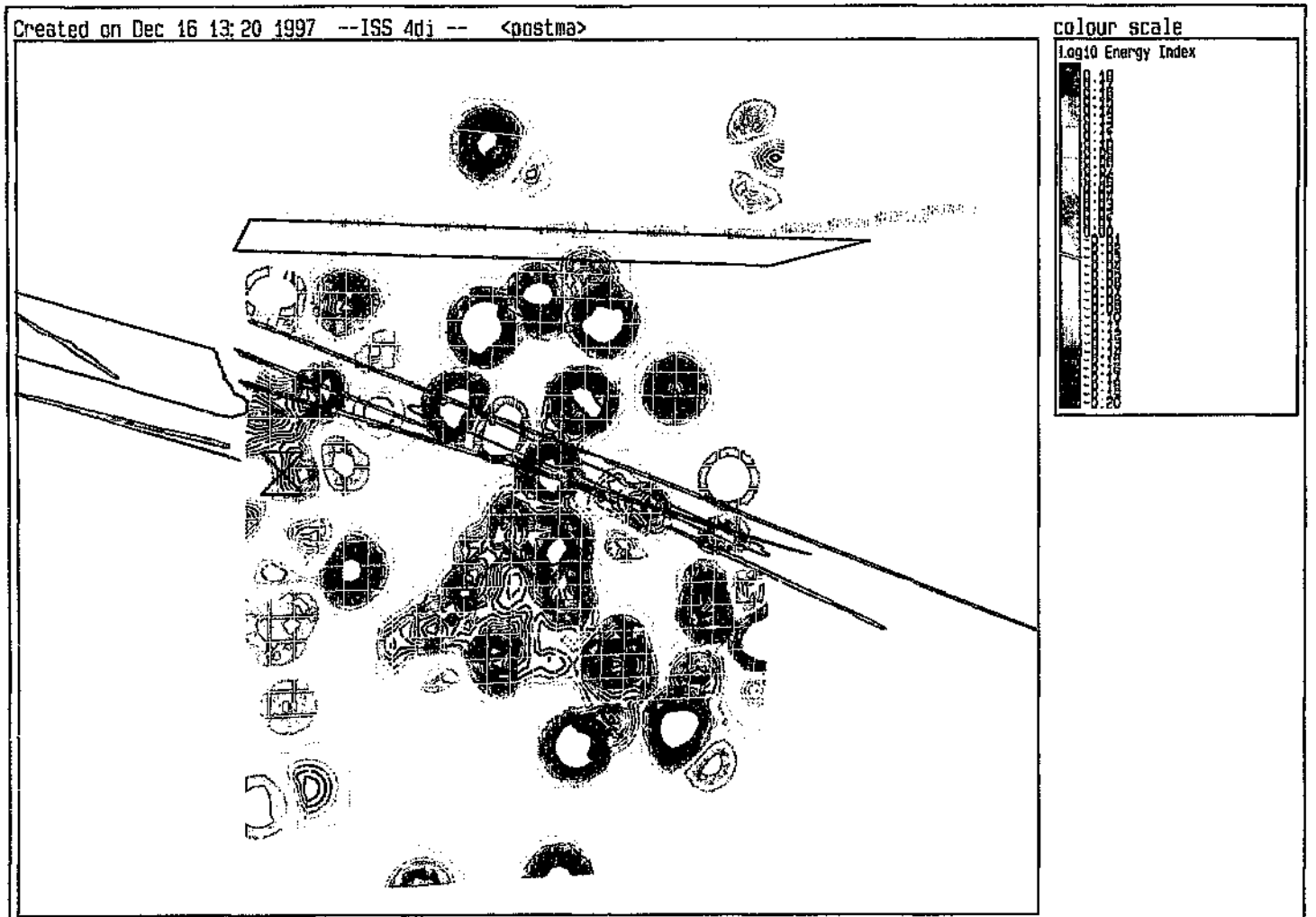


Fig. 4.8b: Same as fig. 4.8a, but the time period of seismicity associated with the Postma dyke is the second quarter of 1994, up to but excluding event 940627a (its position is indicated by the 'hourglass' symbol.

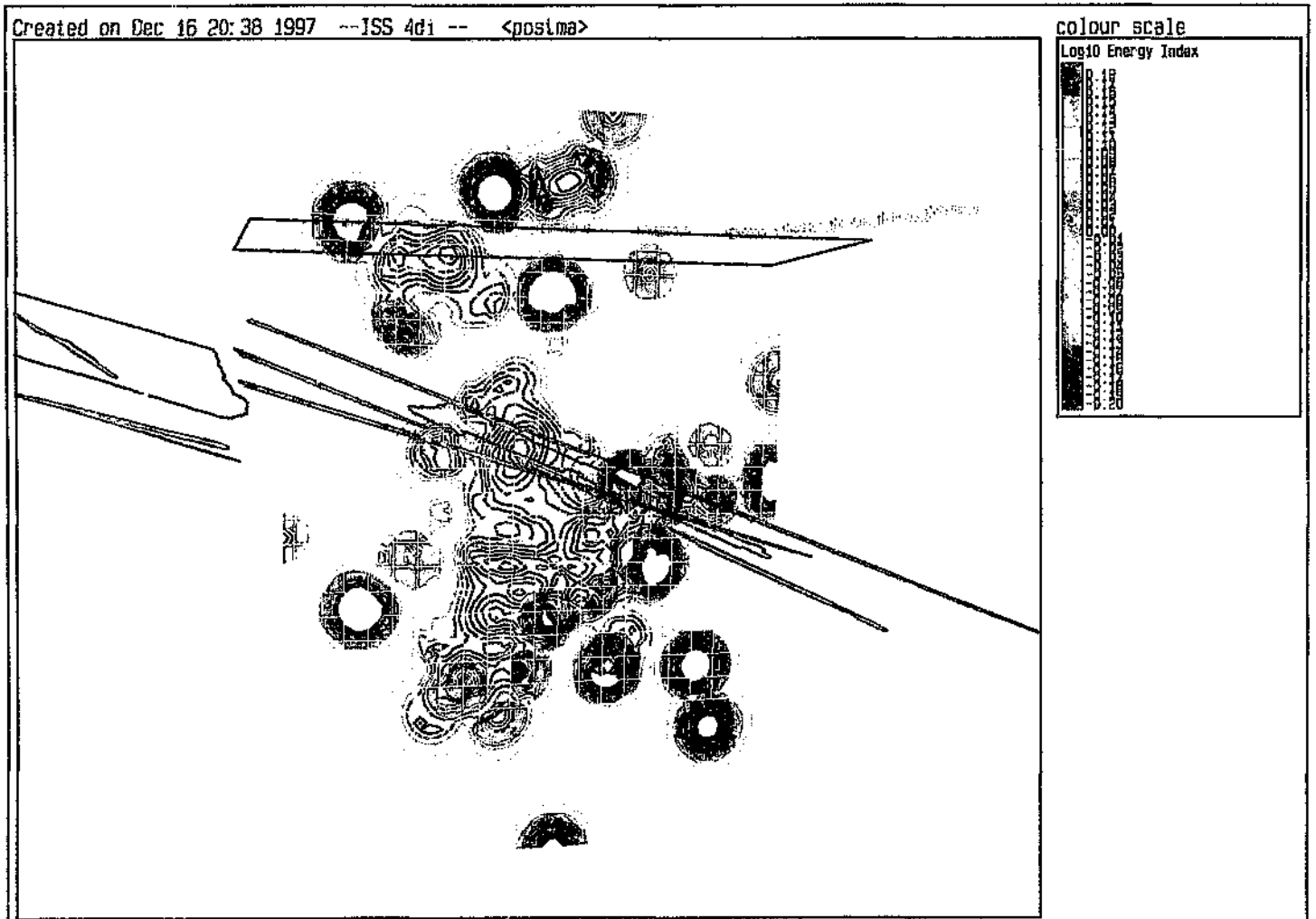


Fig. 4.8c: Same as fig. 4.8a, but the time period of seismicity associated with the Postma dyke is the third quarter of 1994.

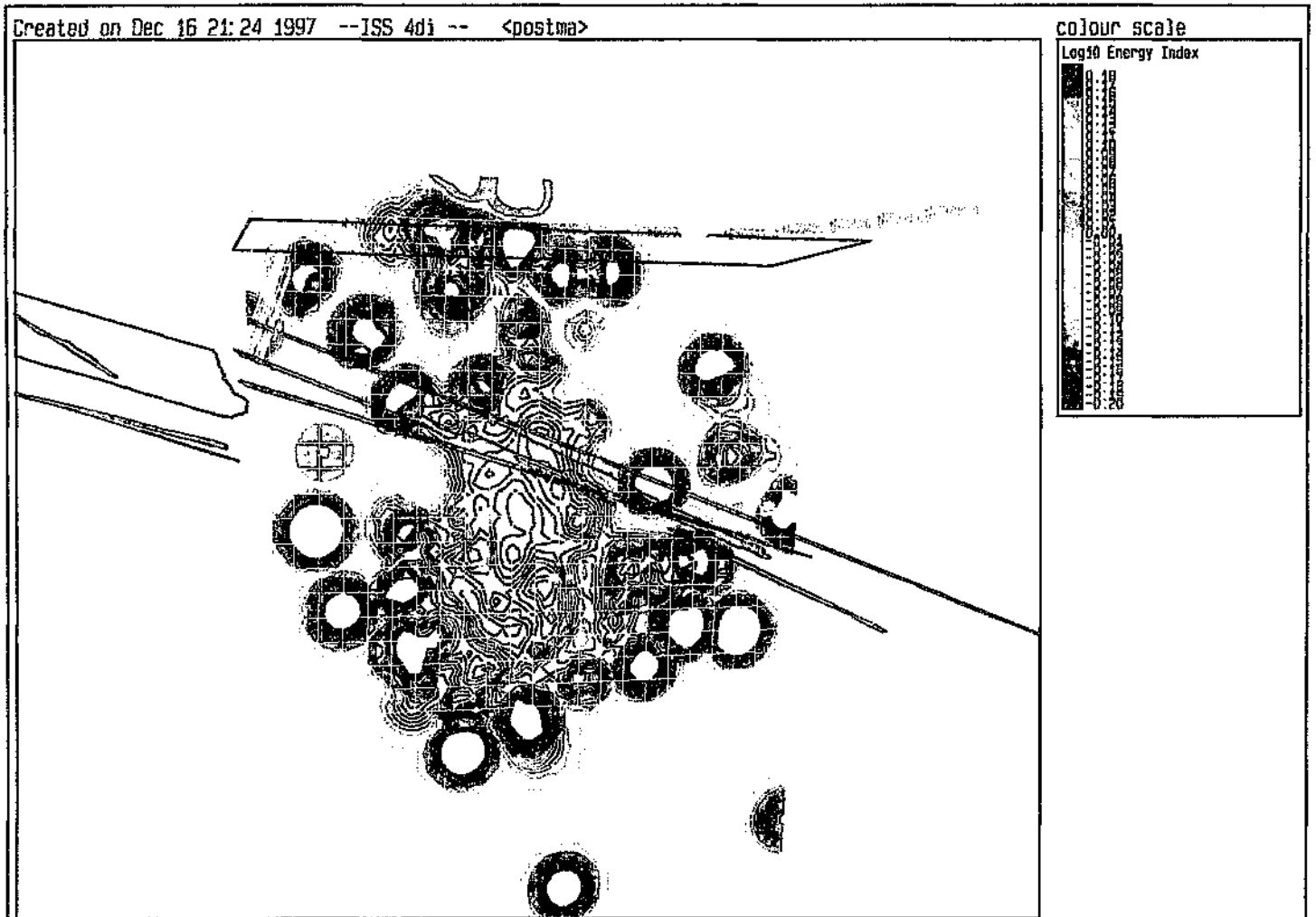


Fig. 4.8d: Same as fig. 4.8a, but the time period of seismicity associated with the Postma dyke is the last quarter of 1994.

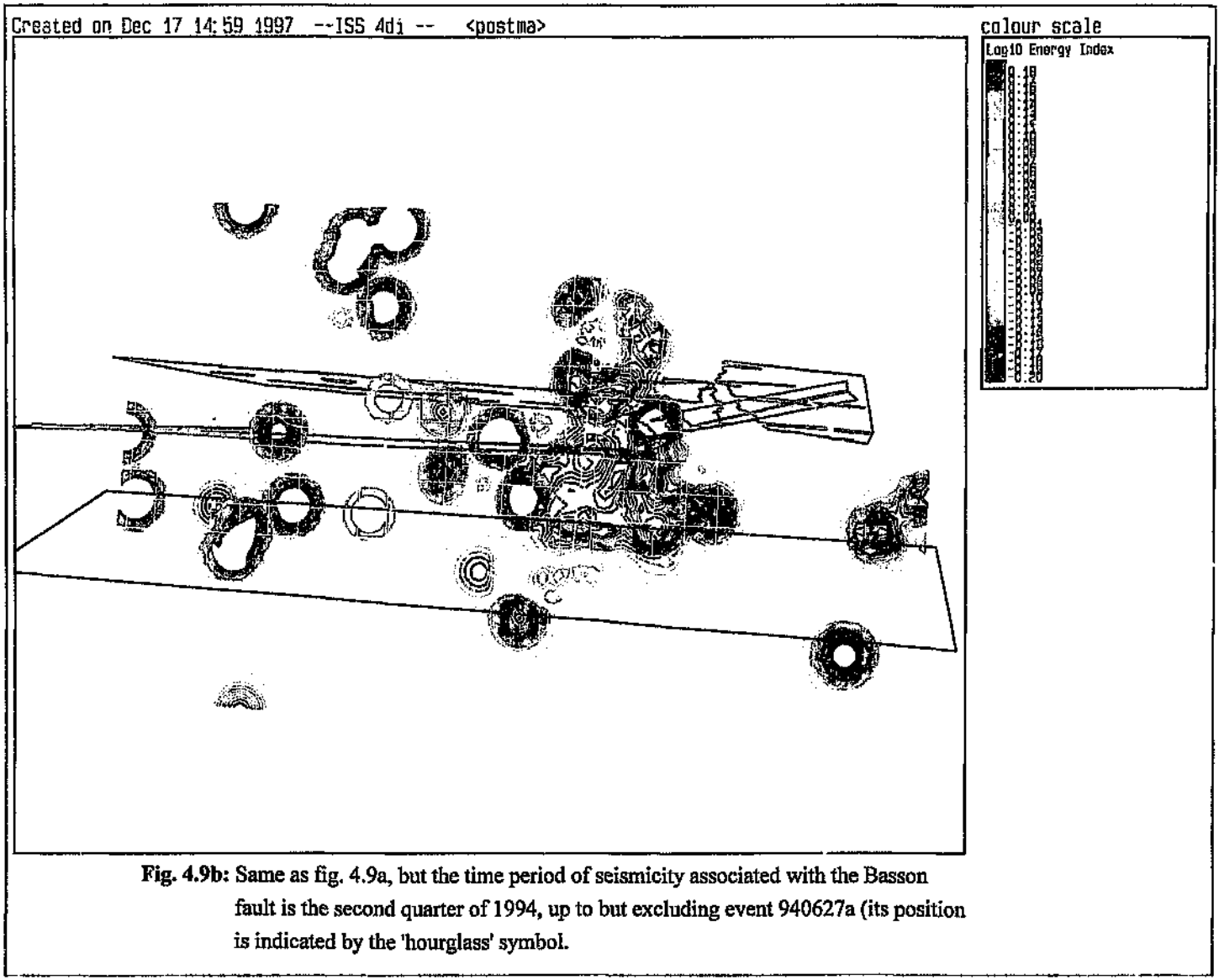


Fig. 4.9b: Same as fig. 4.9a, but the time period of seismicity associated with the Basson fault is the second quarter of 1994, up to but excluding event 940627a (its position is indicated by the 'hourglass' symbol.

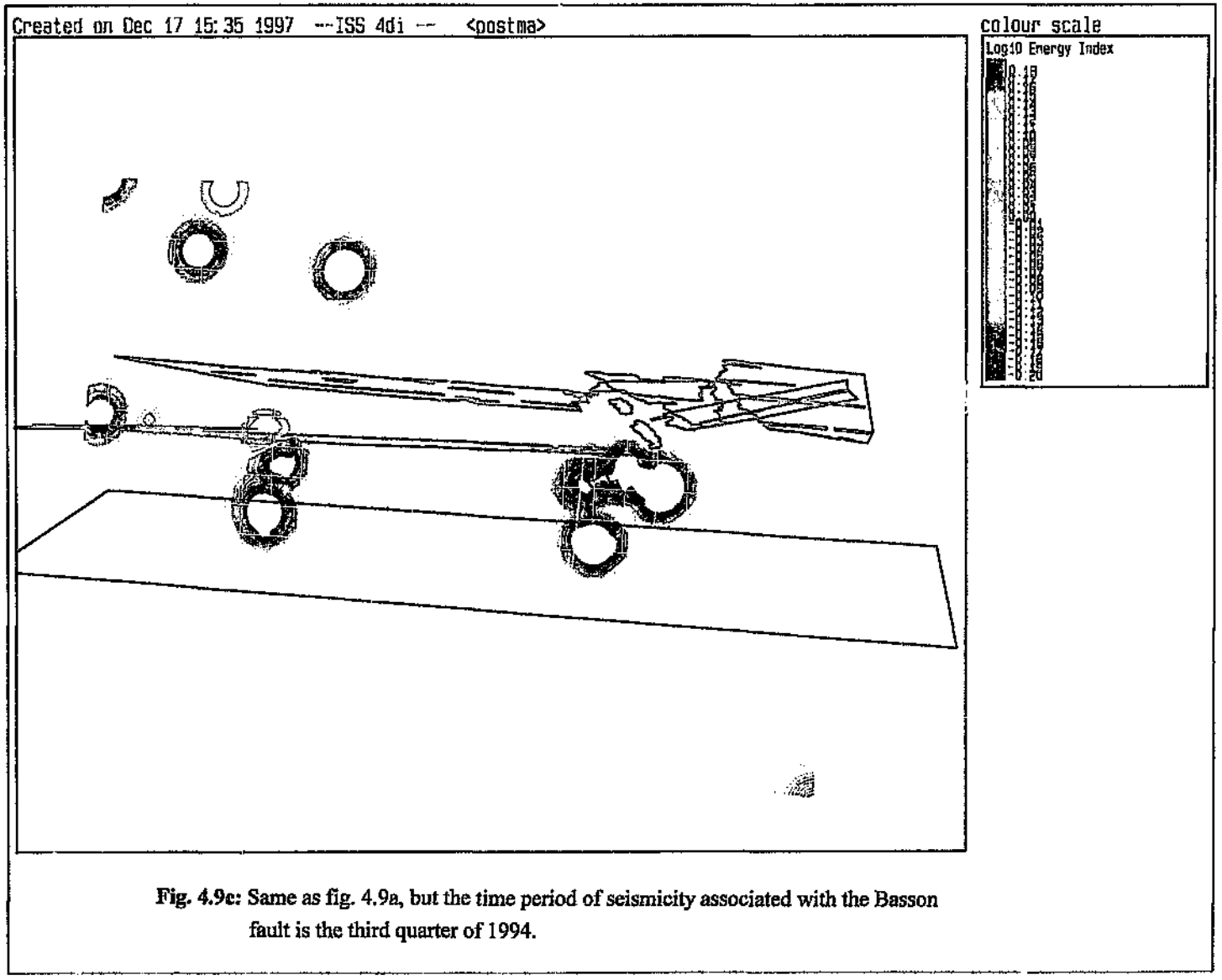


Fig. 4.9c: Same as fig. 4.9a, but the time period of seismicity associated with the Basson fault is the third quarter of 1994.

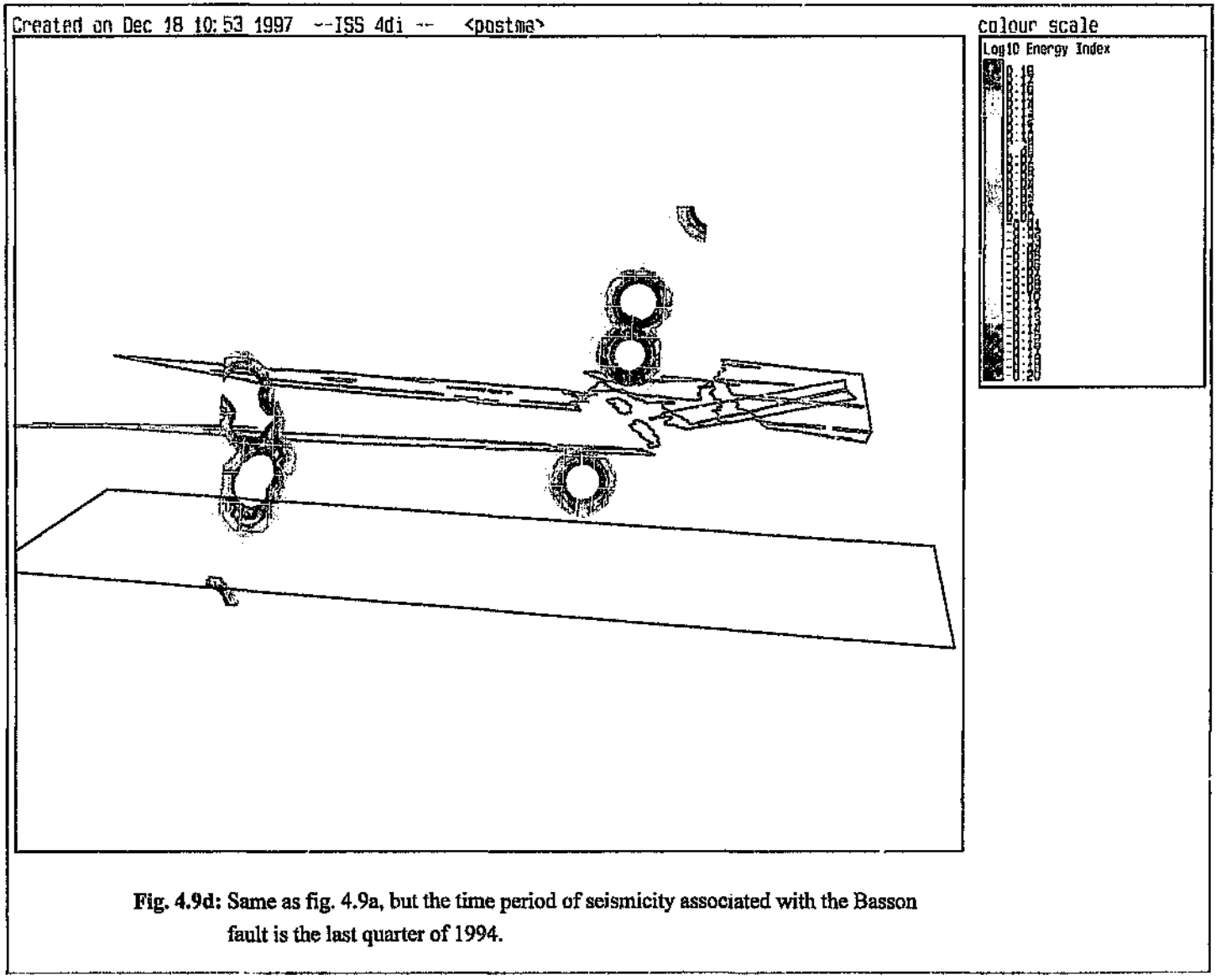


Fig. 4.9d: Same as fig. 4.9a, but the time period of seismicity associated with the Basson fault is the last quarter of 1994.

APPENDIX E

(a) All recorded seismicity in the Postma area from 01/01/91 to 25/08/91 in terms of energy index (fig. 4.12) seismic apparent stress (fig. 4.13), apparent volume (fig. 4.14) and energy index (westward-looking section, fig. 4.15); Section 4.2.1, Chapter 4.

(b) Contours of seismic fluidity (fig. 4.17) delineate the clustering of seismicity during the time period considered.

(c) Reduced areal extent used for time-history analysis with the new selection of events for seismic evaluation (fig. 4.18).

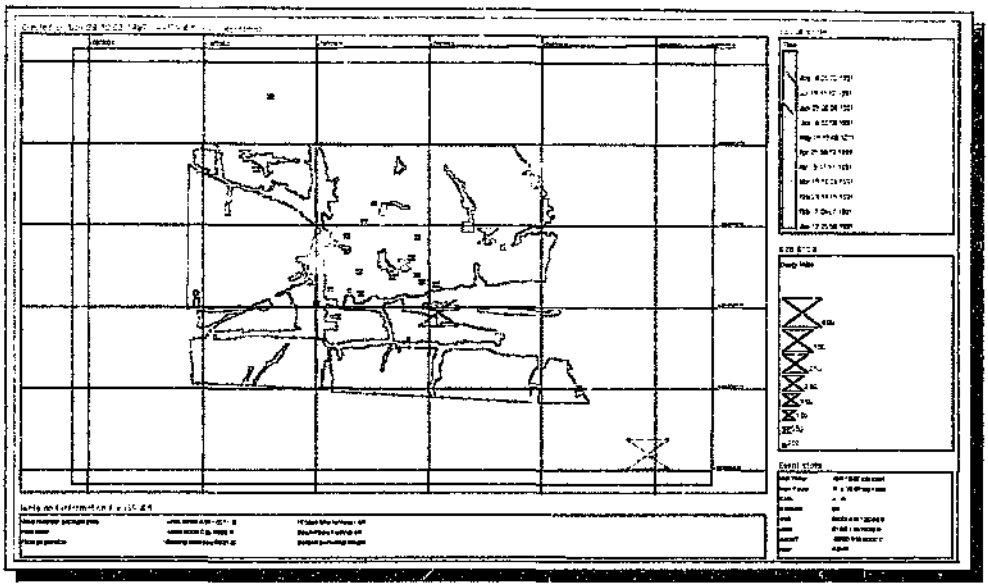


Fig. 4.12: Distribution of events up to and including event 910825 in the vicinity of the Postma area since January 1991. The red lines outline old mine faces (on plan). The mesh represents the Basson fault (north-south) and Postma dyke (roughly east-west). Symbol colour represents event time; symbol size denotes energy index.

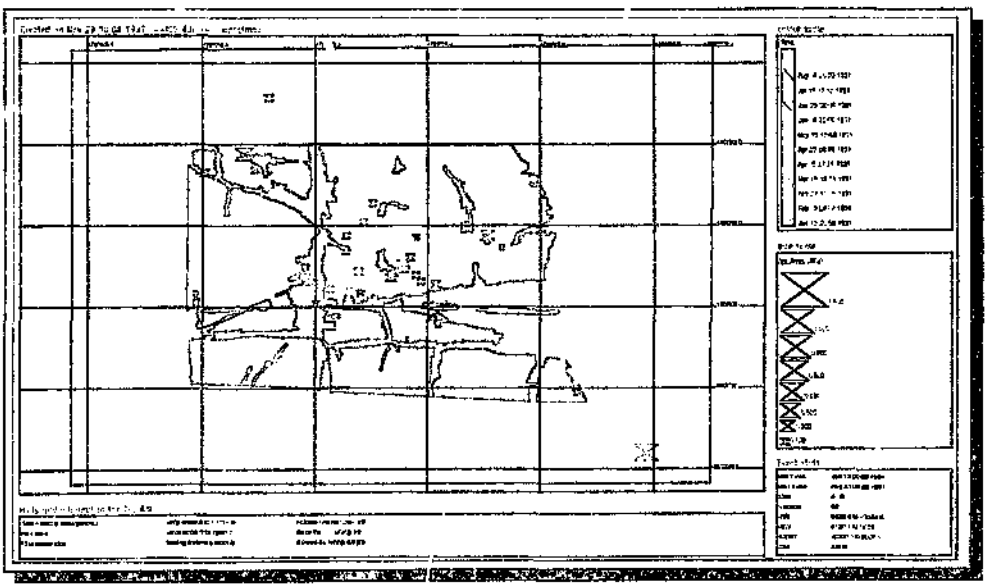


Fig. 4.13: Same as fig. 4.12 but symbol size now portrays apparent stress.

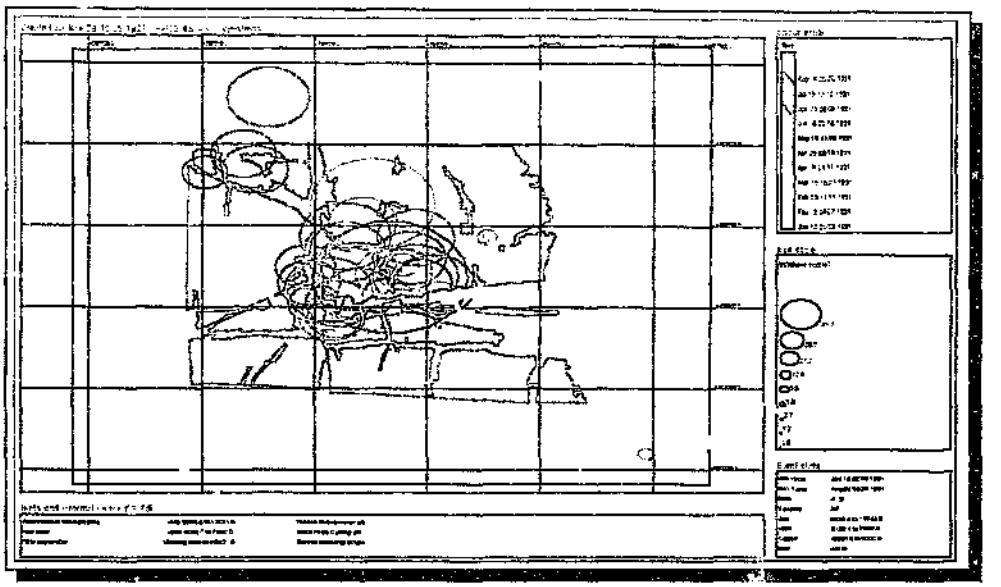


Fig. 4.14: Same as fig. 4.12; symbol size portrays apparent volume.

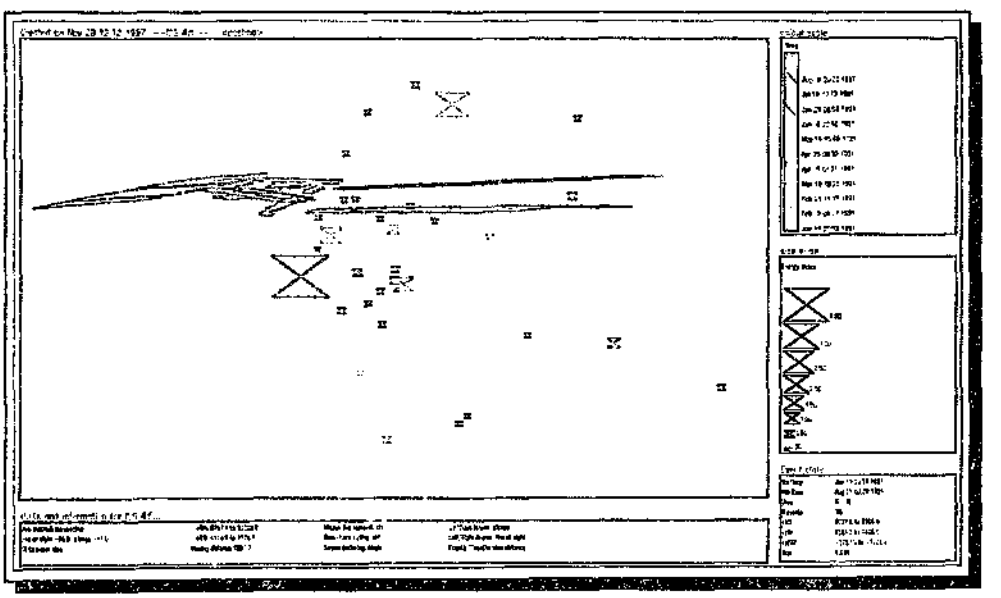


Fig. 4.15: Same as fig. 4.12 but looking perspectively on section, westwards, along the strike of the Postma dyke, onto the mesh representing the Basson fault (for depth scale consider the dip extent of the fault model (280 m).

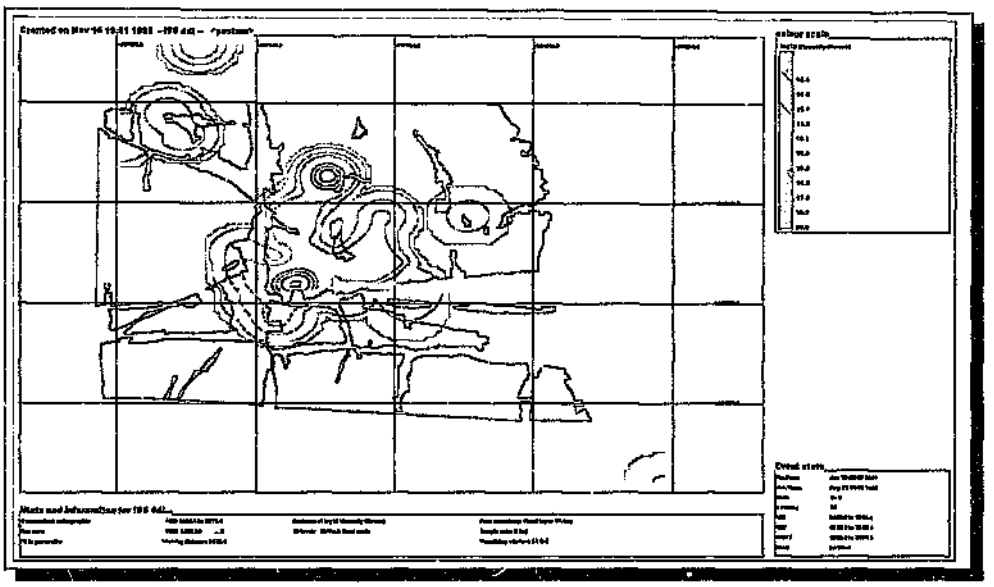


Fig. 4.17: Same as fig. 4.16 (events up to and excluding event 910825), but the contours are of seismic fluidity, for the identification of the 'preparation zone' for event 910825.

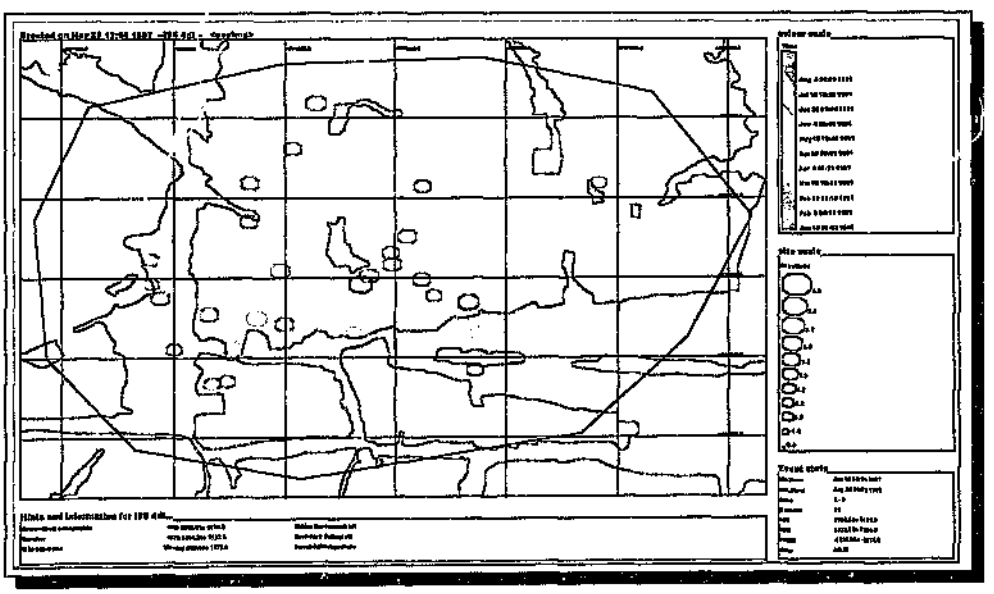


Fig. 4.18: The polygon above denotes the boundary of the smaller area selected for time-history analysis according to contours of seismic Deborah number and seismic fluidity (window length: 8 samples and/or 5 days).

APPENDIX F1

Time-history and contour plots used in the analysis of event 910825 to identify precursors (figs. 4.20 - 4.23, 4.25 - 4.30, 4.32- 4.37); Section 4.2.1, Chapter 4.

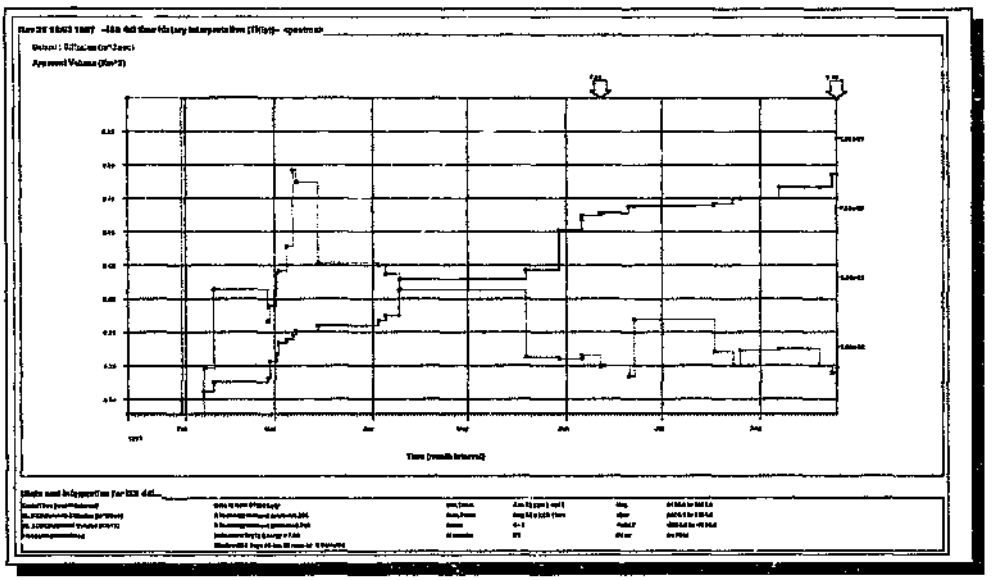


Fig. 4.20: Same data as fig. 4.19 (see main text, Vol I), showing the variation of seismic diffusion with time.

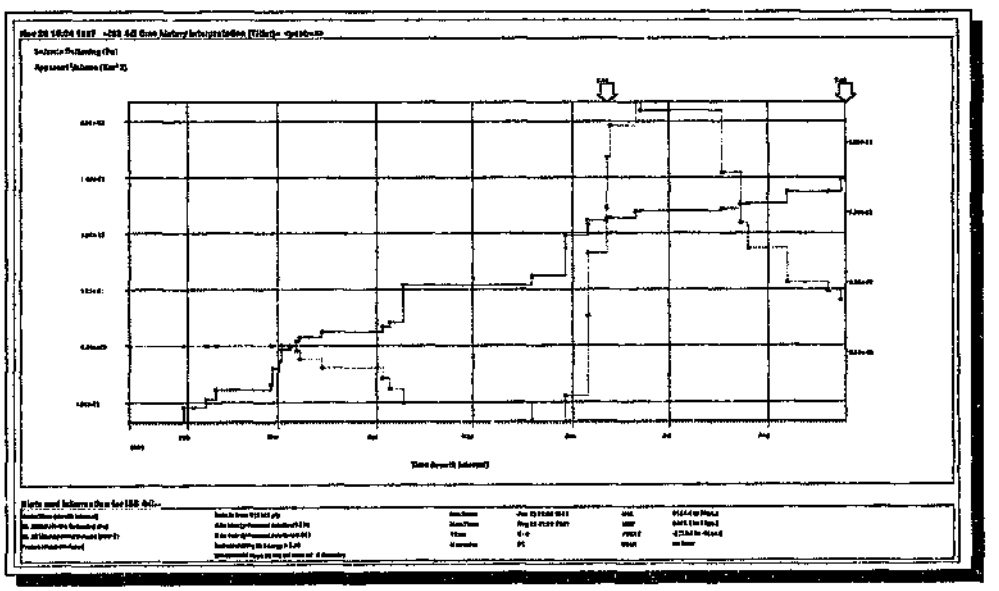


Fig. 4.21: Same as fig. 4.19, showing the variation of seismic softening.

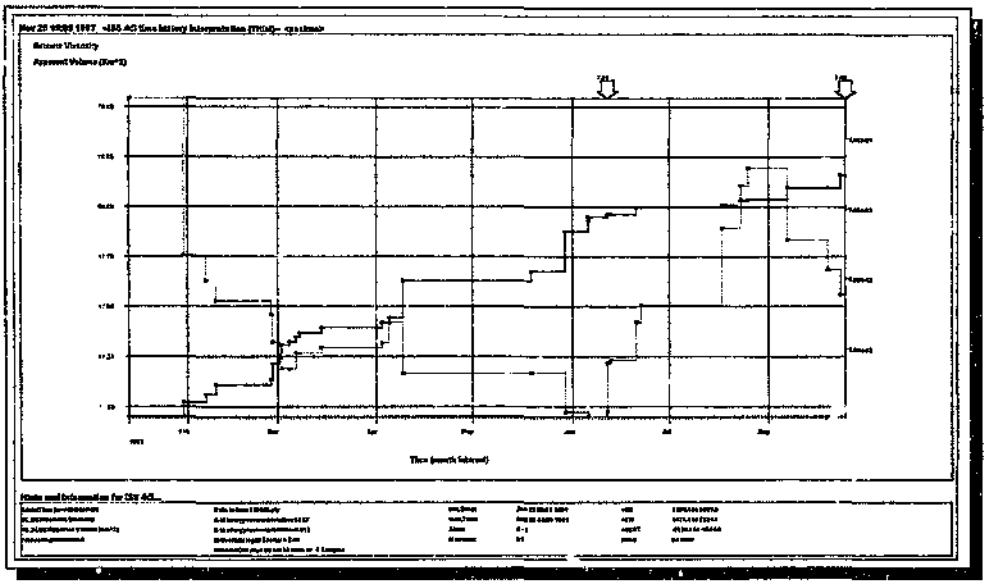


Fig. 4.22: Same data as fig. 4.19, showing the variation of seismic viscosity.

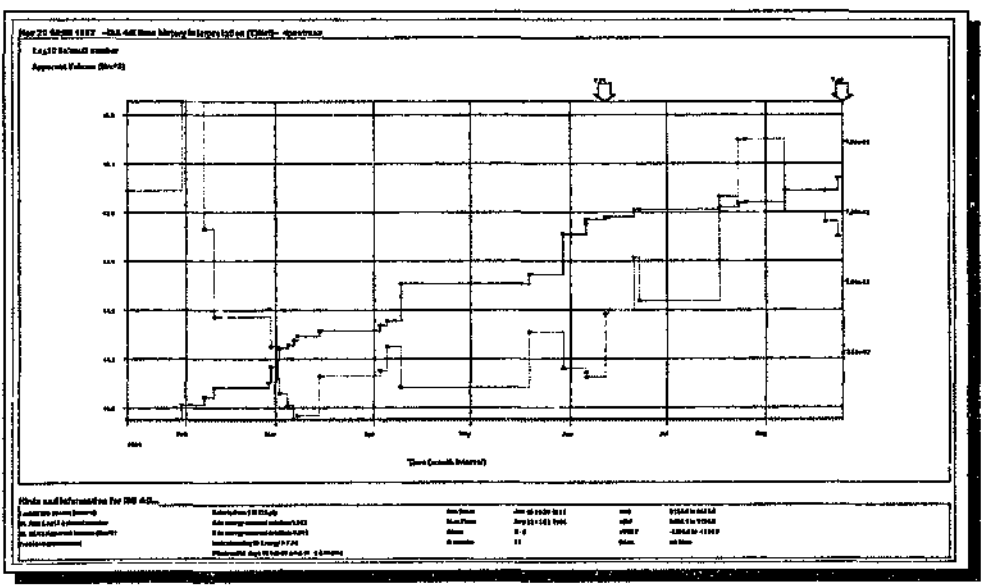


Fig. 4.23: Same data as fig. 4.19, showing the variation of log(seismic Schmidt no.).

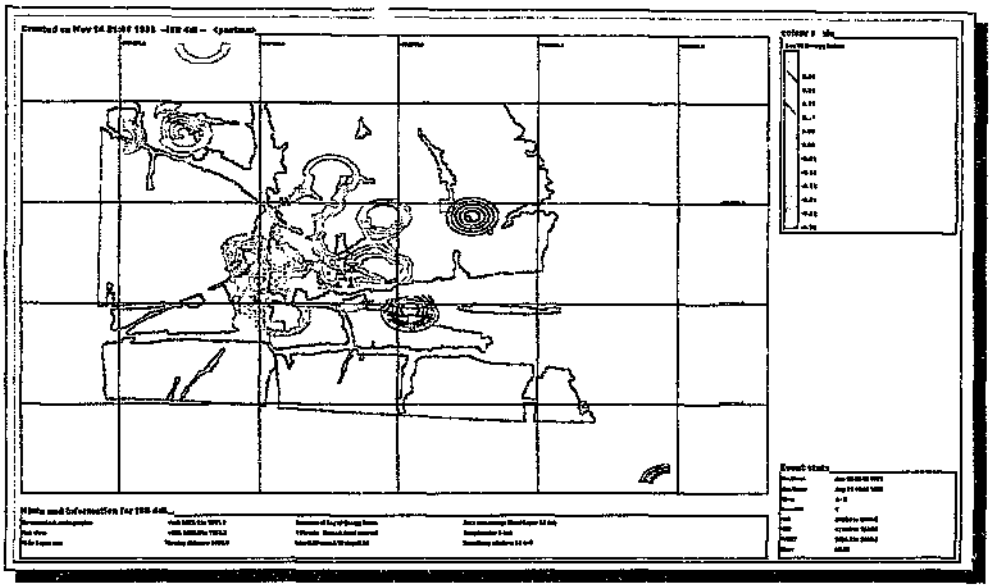


Fig. 4.25: Same as fig. 4.24 (seismicity recorded in the time period 1/1/91 to 25/8/91, but excluding event 910825 -- its position is indicated by the 'hourglass' symbol; contours are of log(EI). Contour highs indicate areas of relatively higher stress.

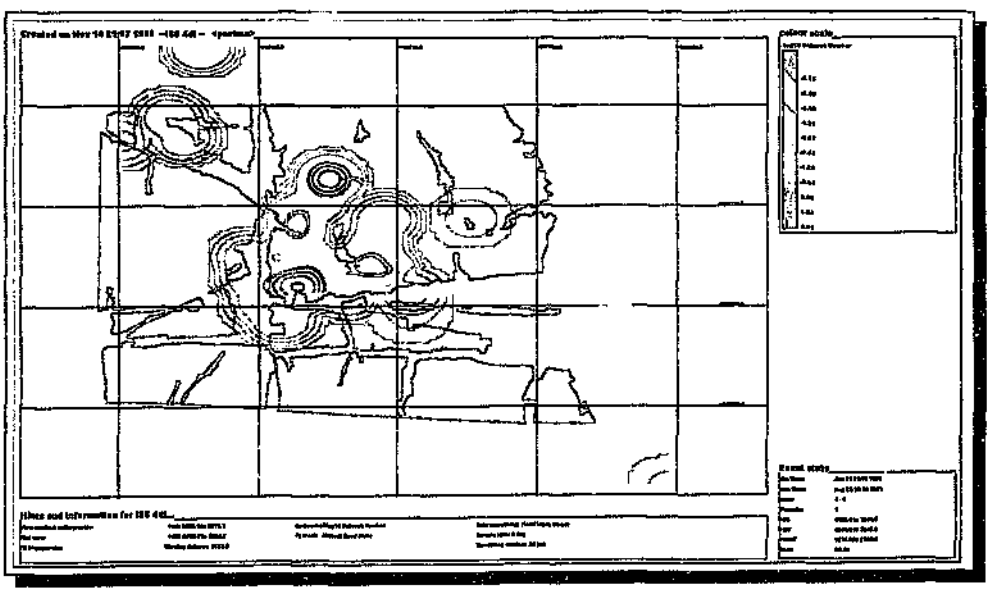


Fig. 4.26: Same as fig. 4.24 but the contours are of log(inverse Deborah no.); contour lows therefore indicate high seismic flow.

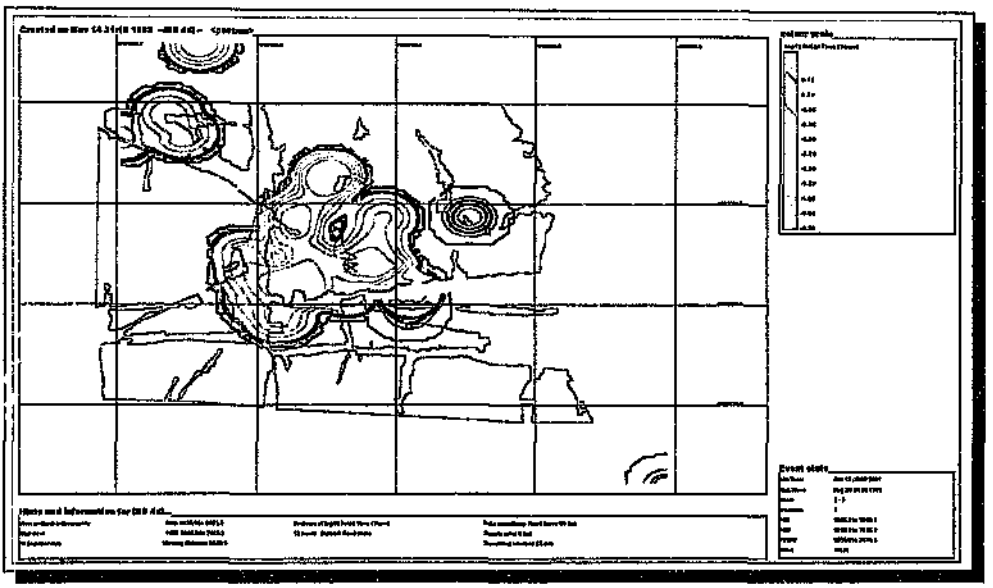


Fig. 4.27: Same as fig. 4.24 but the contours are of seismic relaxation time. Contour lows relate to the time span of useful past data, which in this case (at the locality of event 910825) is relatively short.

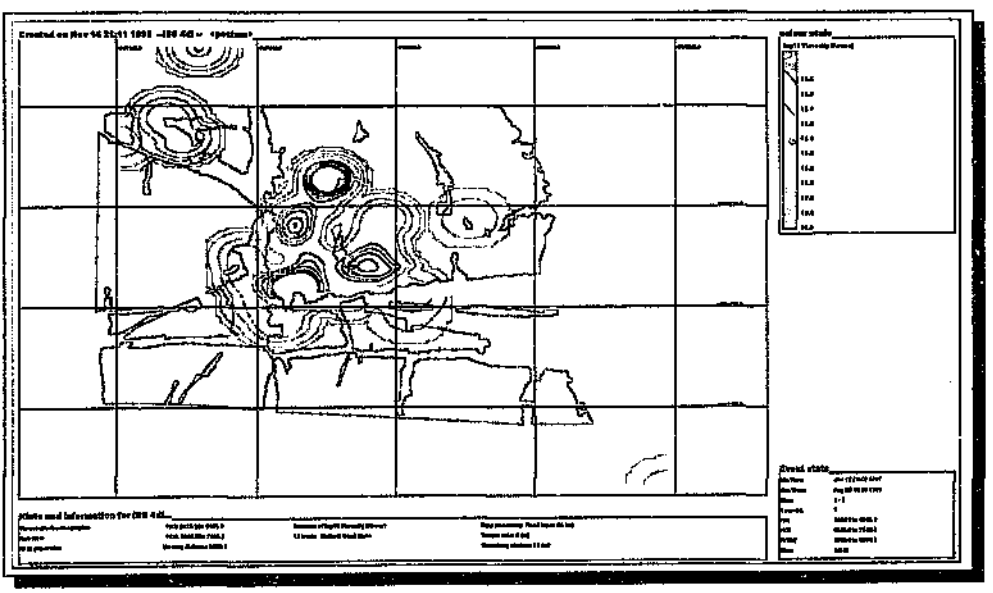


Fig. 4.28: Same as fig. 4.24 but the contours are of log(seismic fluidity), thus contour lows characterise zones of easier stress transfer due to seismicity. Note the similarity to fig. 4.26 (inverse seismic Deborah number).

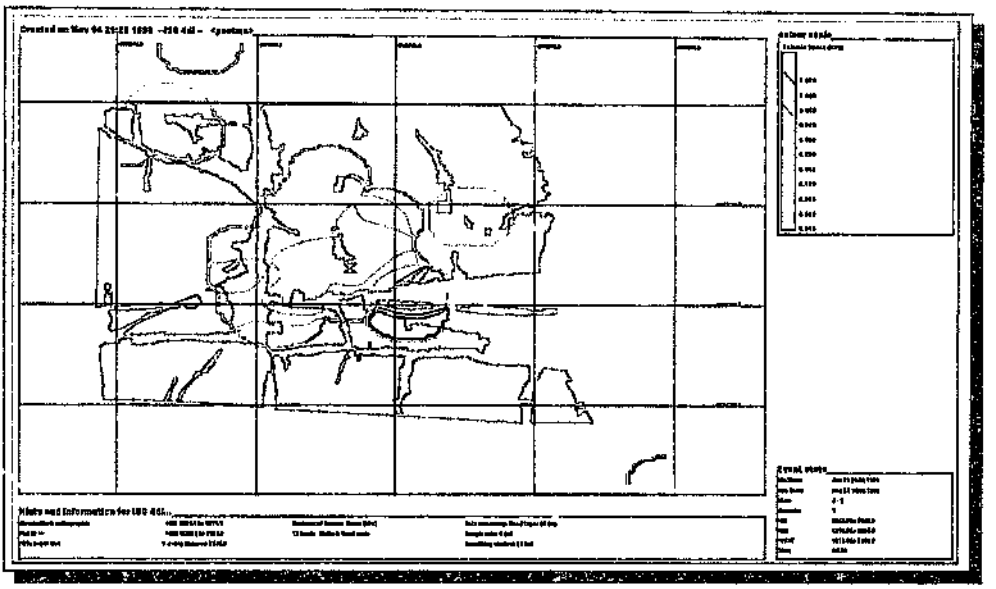


Fig. 4.29: Same as fig. 4.24, but contours are of seismic stress; contour highs highlight zones of high stress change due to seismicity.

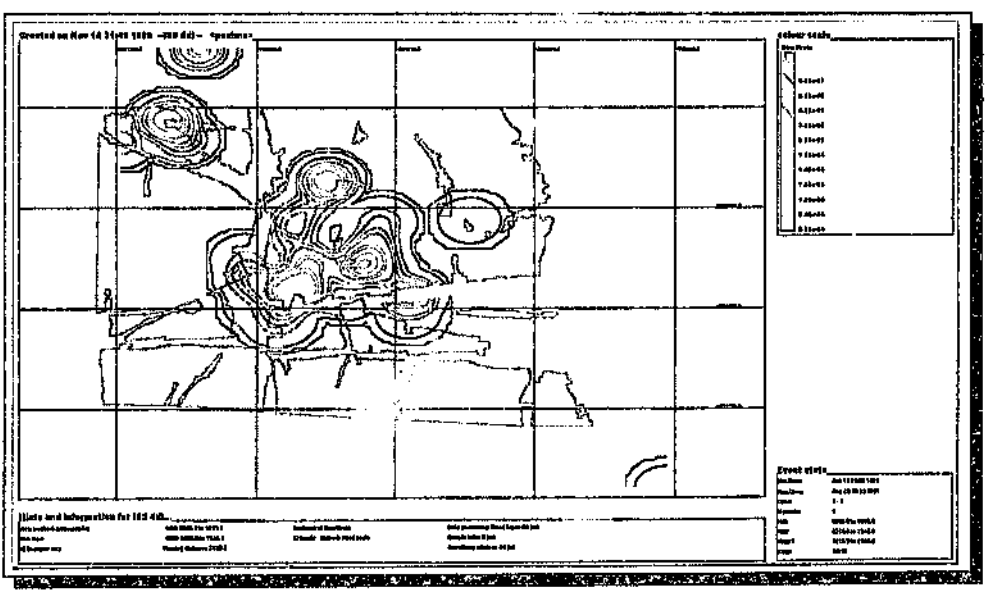


Fig. 4.30: Same as fig. 4.24, but the contours are of cumulative seismic strain; contour highs thus relate to greater rock mass deformation due to seismicity.

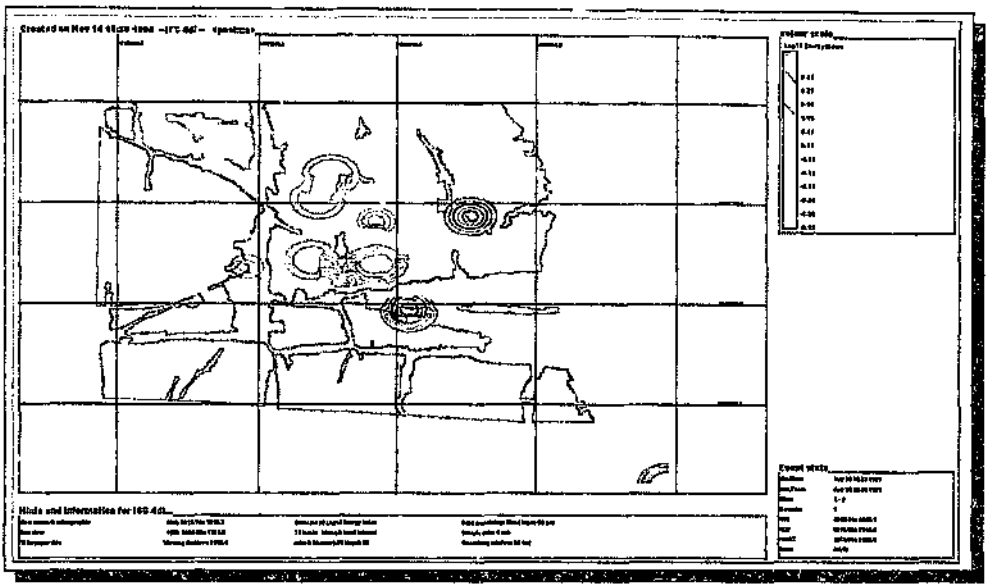


Fig. 4.32: Same as fig. 4.31 (time period of seismicity ranges over the three months before event 910825); contours are of energy index.

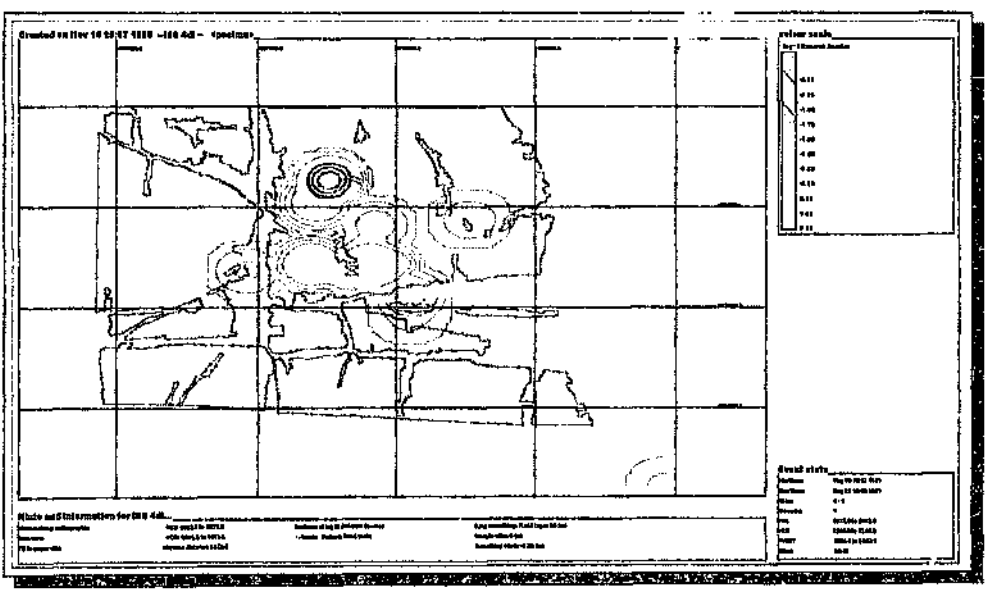


Fig. 4.33: Same as fig. 4.31; contours are of log(inv. seismic Deborah no.).

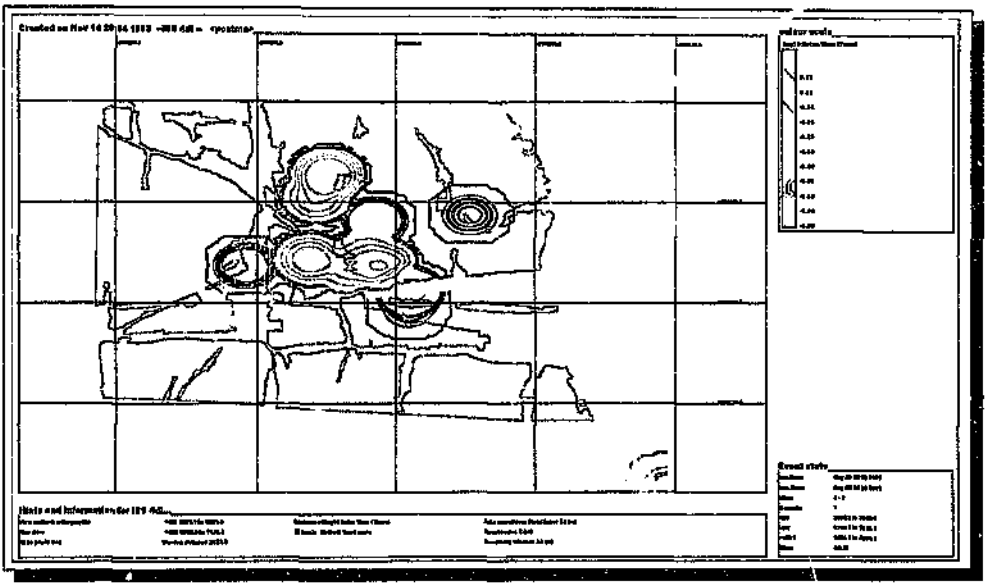


Fig. 4.34: Same as fig. 4.31; contours are of seismic relaxation time three months before event 910825.

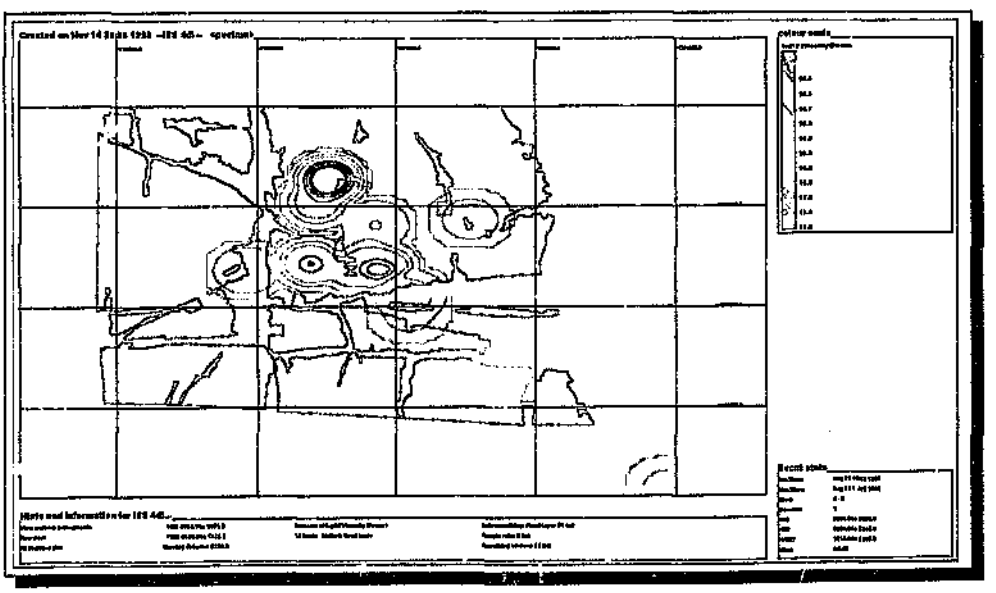


Fig. 4.35: Same as fig. 4.31; contours are of log(seismic fluidity); note similarity to fig. 4.33.

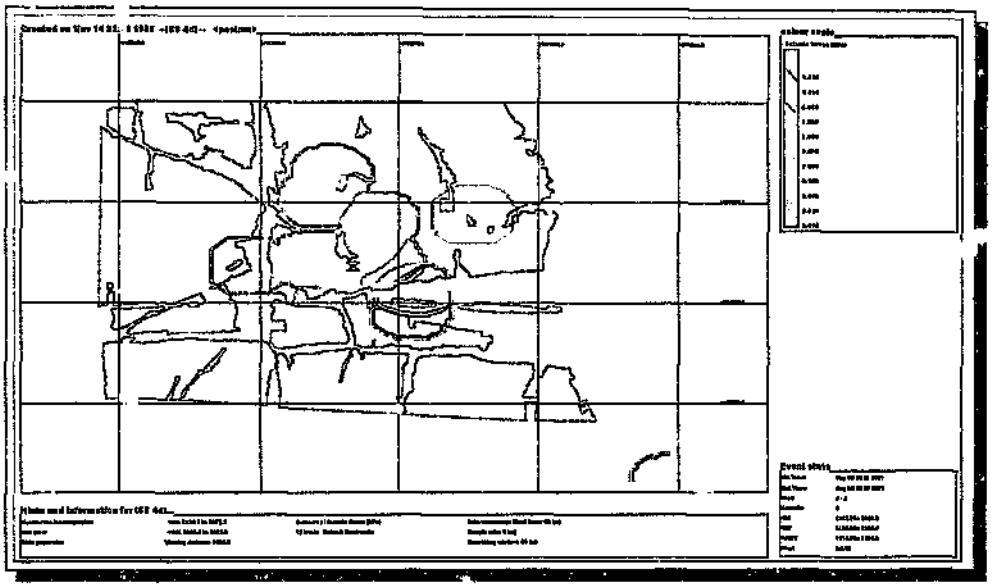


Fig. 4.36: Same as fig. 4.31; contours are of seismic stress.

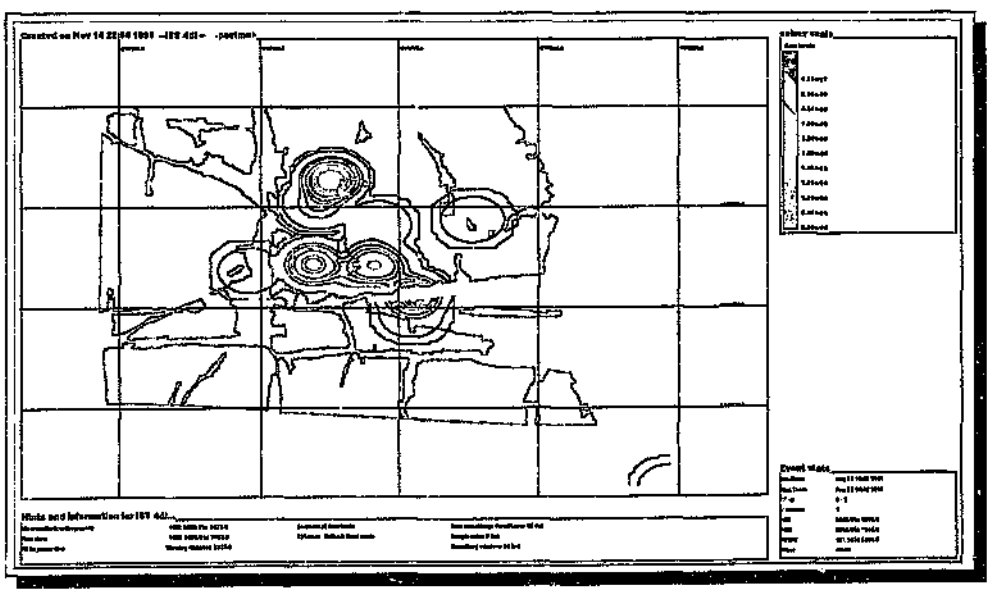


Fig. 4.37: Same as fig. 4.31; contours are of cumulative seismic strain.

APPENDIX F2

(a) Recorded seismic activity in the time period 01/01/91 to 26/08/92 in terms of apparent stress (fig. 4.39) and apparent volume (fig. 4.40). A section looking east onto the Basson fault depicts the distribution of events in depth in terms of event time and apparent stress (fig. 4.41).

(b) Time-history and contour plots used in the analysis of events 920826a and 920826b to identify precursors (fig. 4.42 - 4.58); Section 4.2.2, Chapter 4.

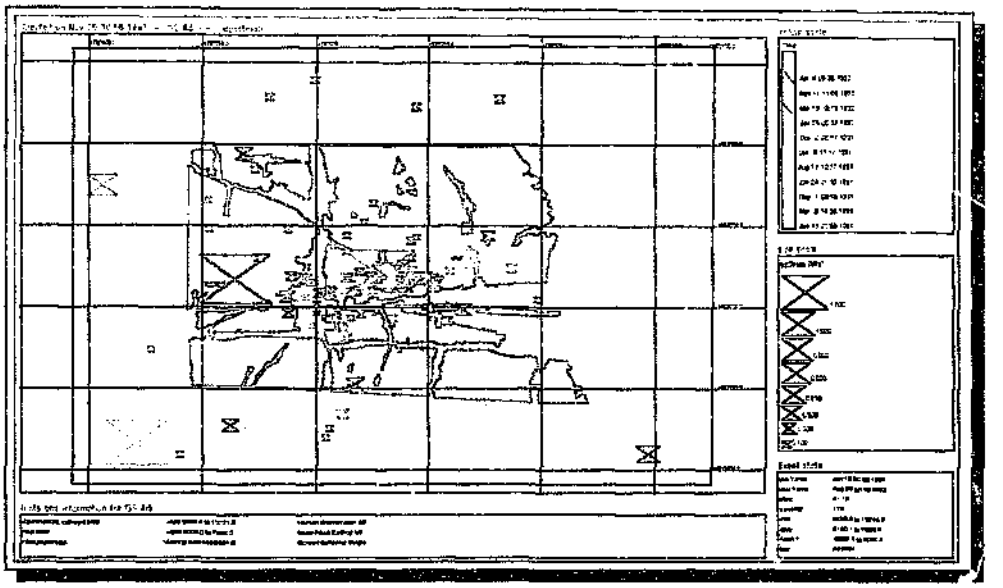


Fig. 4.39: Same as fig. 4.38 but symbol size denotes apparent stress.

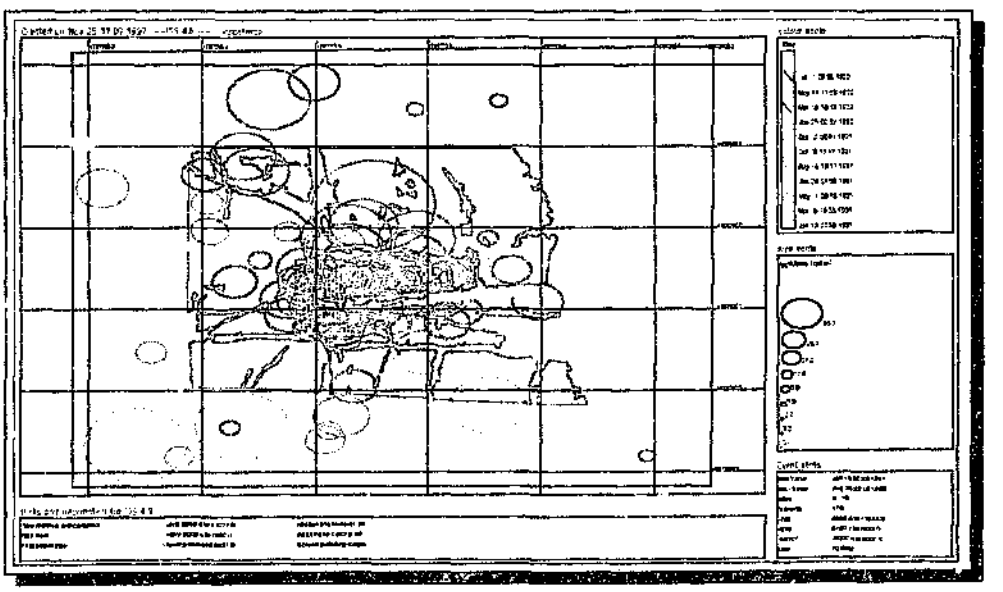


Fig. 4.40: Same as fig. 4.38 but symbol size denotes apparent volume.

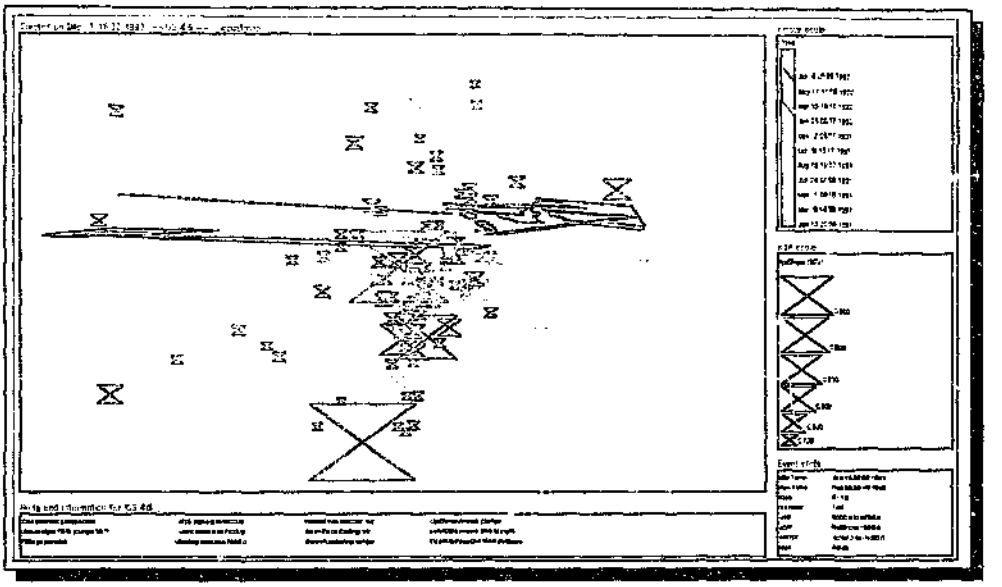


Fig. 4.31: Section looking eastward onto the Basson fault, along the dip of the reef, showing the distribution of recorded events in depth around the Postma dyke (for depth scale consider the dip extent of the Basson fault model (280 m)) in terms of event time and apparent stress.

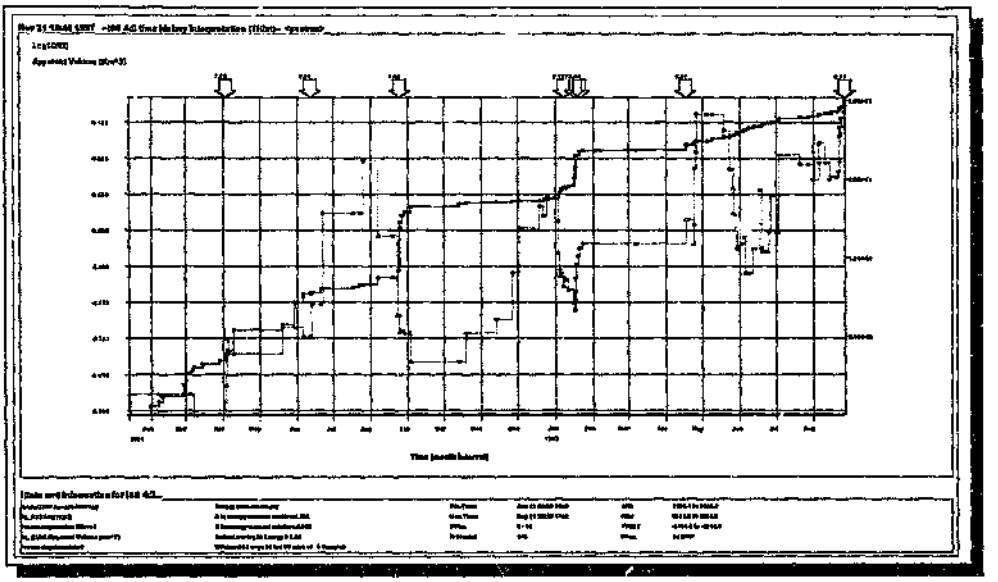


Fig. 4.42: Time-history of cumulative apparent volume and moving median log(EI) for seismicity in the time period 1/1/91 to 26/8/92 (arrows point to large events (log(E) > 7.0) in time; the last arrow refers to event 920826b).

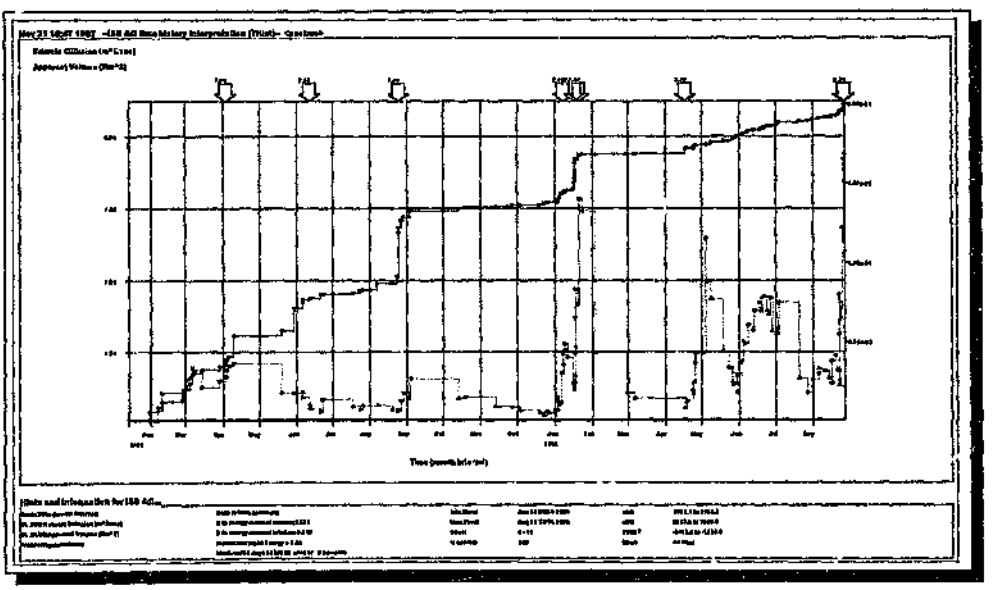


Fig. 4.43: Same as fig. 4.42, showing the variation in seismic diffusion.

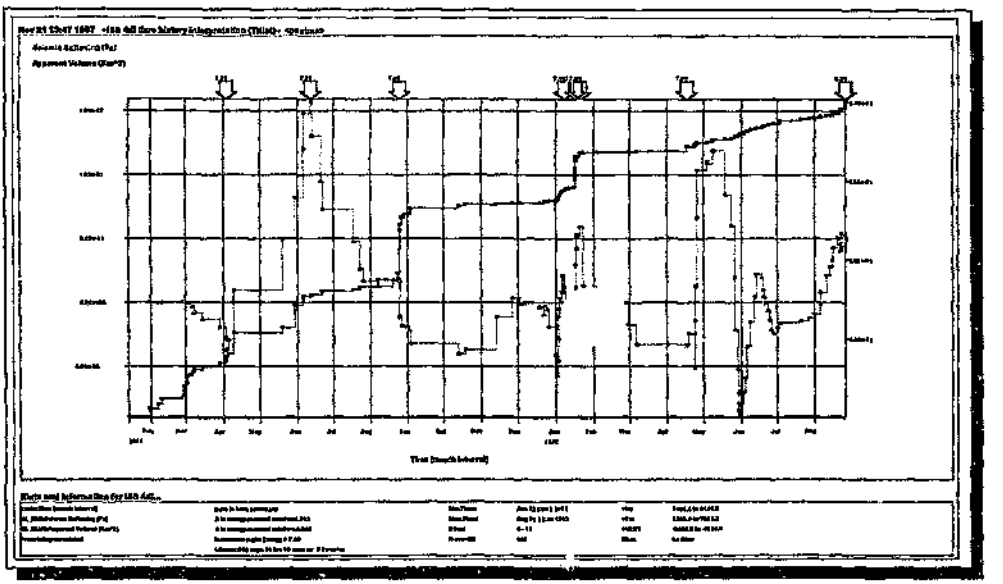


Fig. 4.44: Same as fig. 4.42, showing variation in seismic softening.

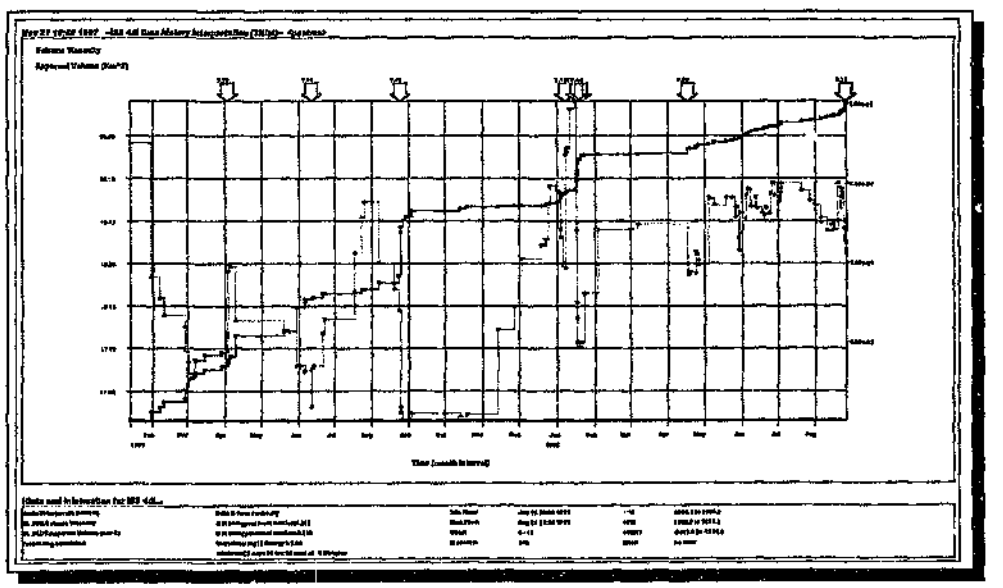


Fig. 4.45: Same as fig. 4.42, showing variation in seismic viscosity.

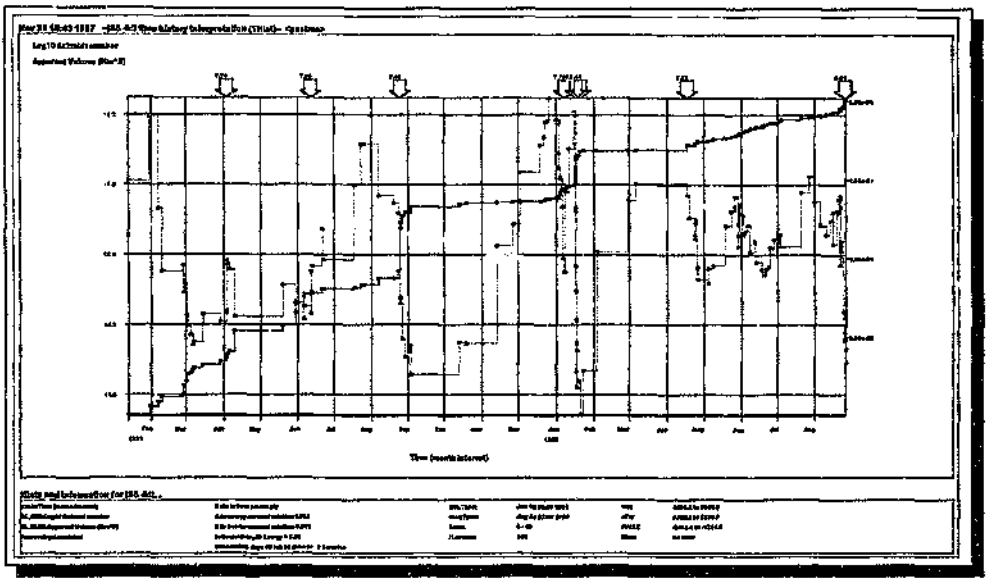


Fig. 4.46: Same as fig. 4.42, showing variation in log(seismic Schmidt no.).

Contour plots of those seismic parameters under investigation relating to the seismicity recorded 12 months before (but excluding) events 920826a and 920826b (figs. 4.47 - 4.52).

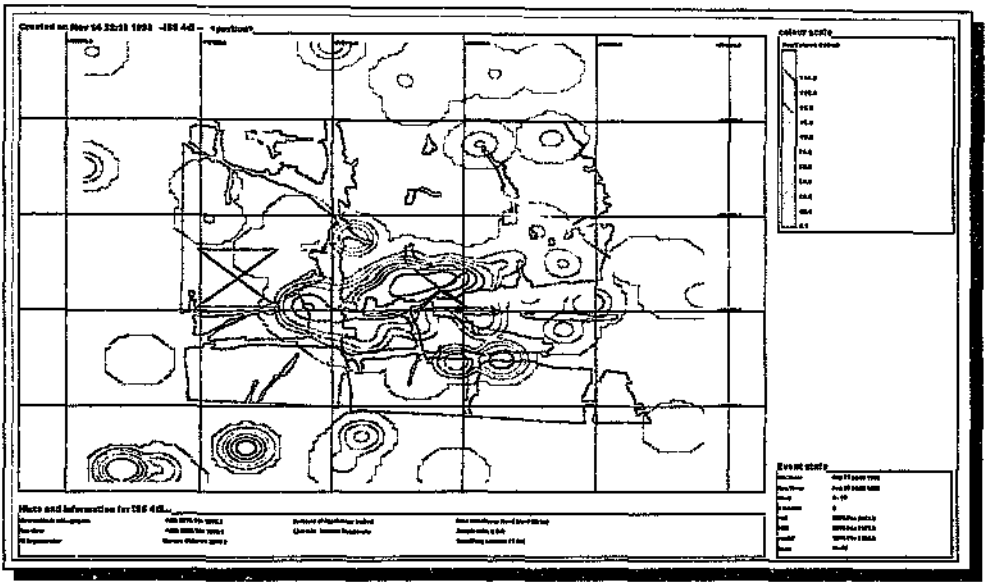


Fig. 4.47: Contours of apparent volume using seismicity recorded in the time period 27/8/91 to 26/8/92 (12 months leading up to, but excluding, events 920826a and 920826b, the locations of which are indicated by the 'hourglass' symbols).

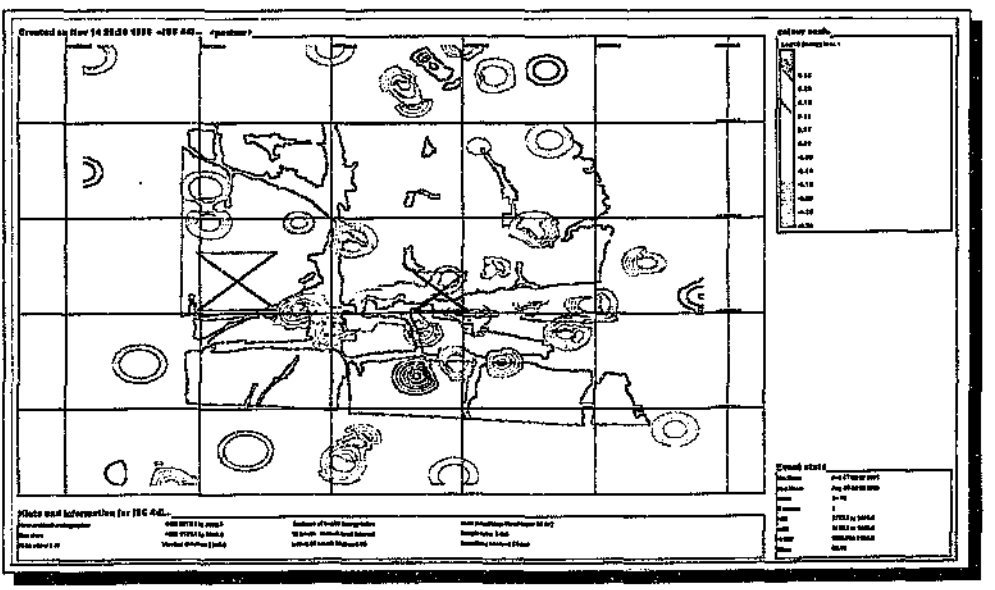


Fig. 4.48: Same as fig. 4.47, but contours are of log(EI).

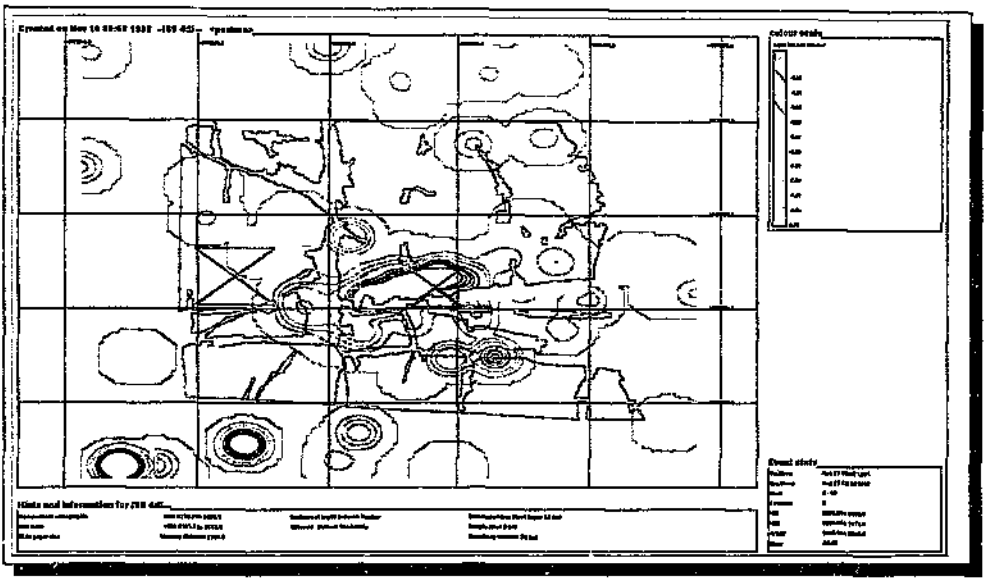


Fig. 4.49: Same as fig. 4.47; contours are of log(inv. Deborah no.).

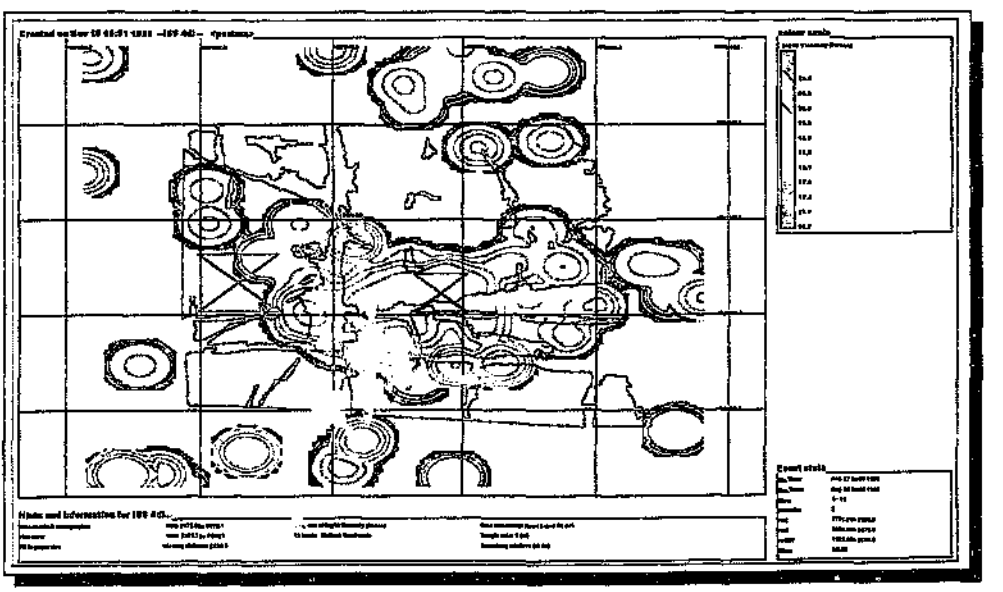


Fig. 4.50: Same as fig. 4.47; contours are of log(seismic viscosity).

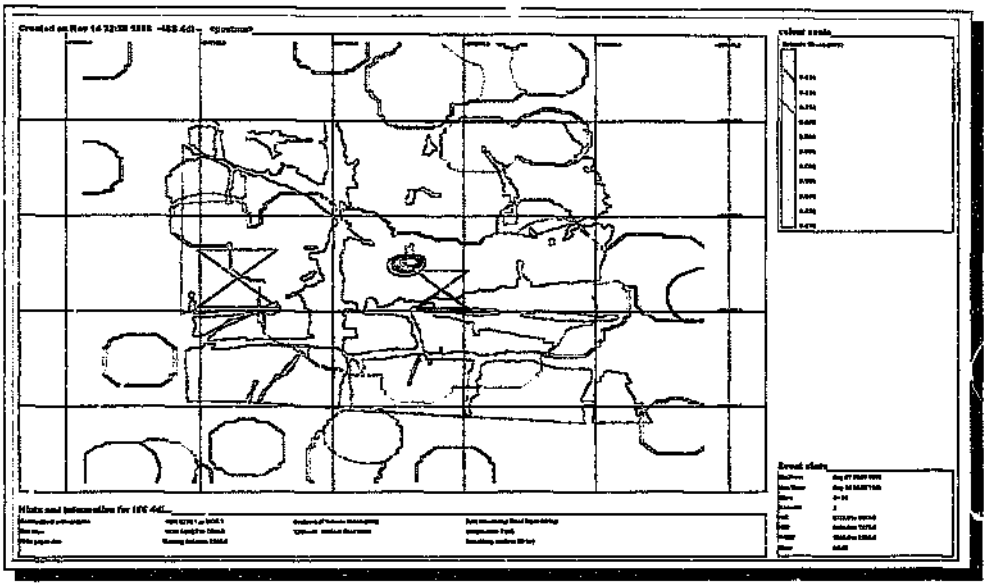


Fig. 4.51: Same as fig. 4.47; contours are of seismic stress.

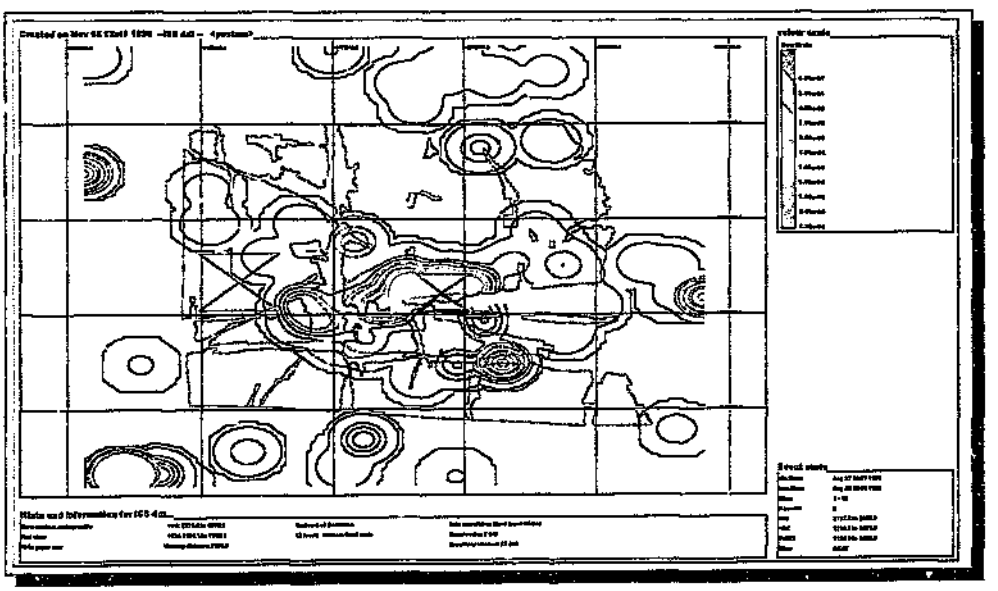


Fig. 4.52: Same as fig. 4.47; contours are of cumulative seismic strain.

Contour plots of those seismic parameters under investigation relating to the seismicity recorded 3 months before (but excluding) events 920826a and 920826b (figs. 4.53 - 4.58).

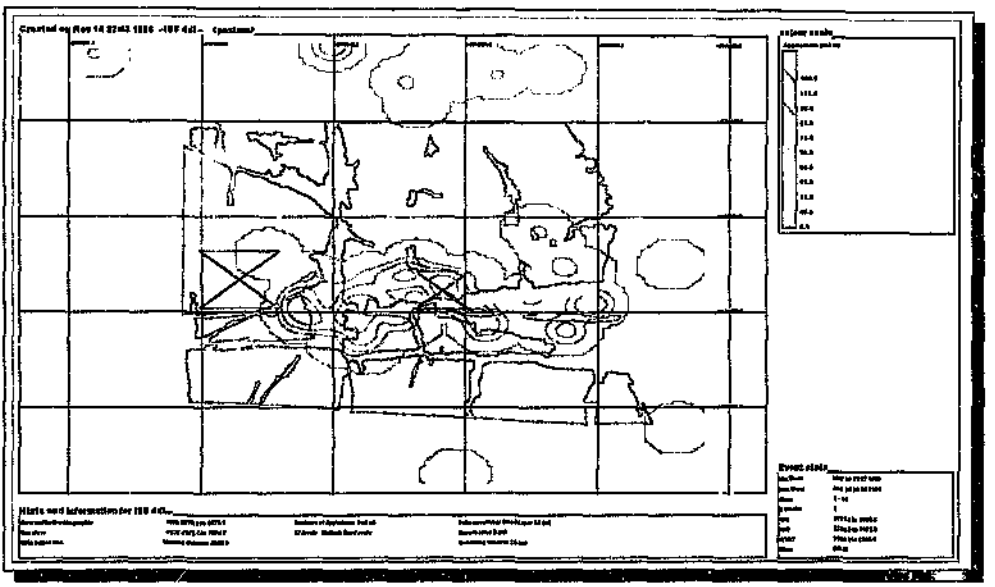


Fig. 4.53: Contours of apparent volume based on seismicity recorded in the time period 26/5/92 to 26/8/92 (three months leading up to events 920826a and 920826b, the locations of which are indicated by the 'hourglass' symbols).

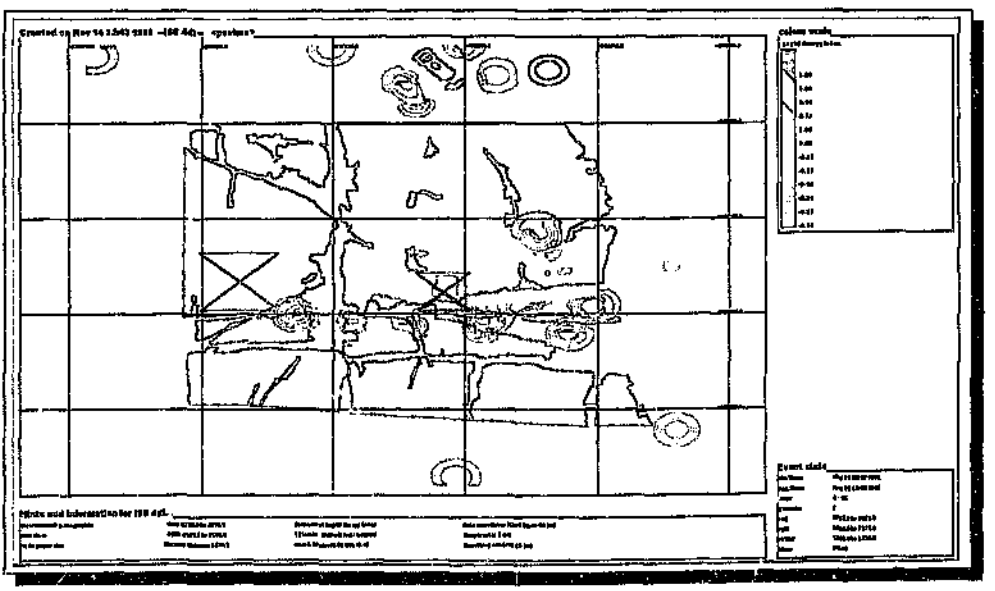


Fig. 4.54: Same as fig. 4.53; contours are of log(E).

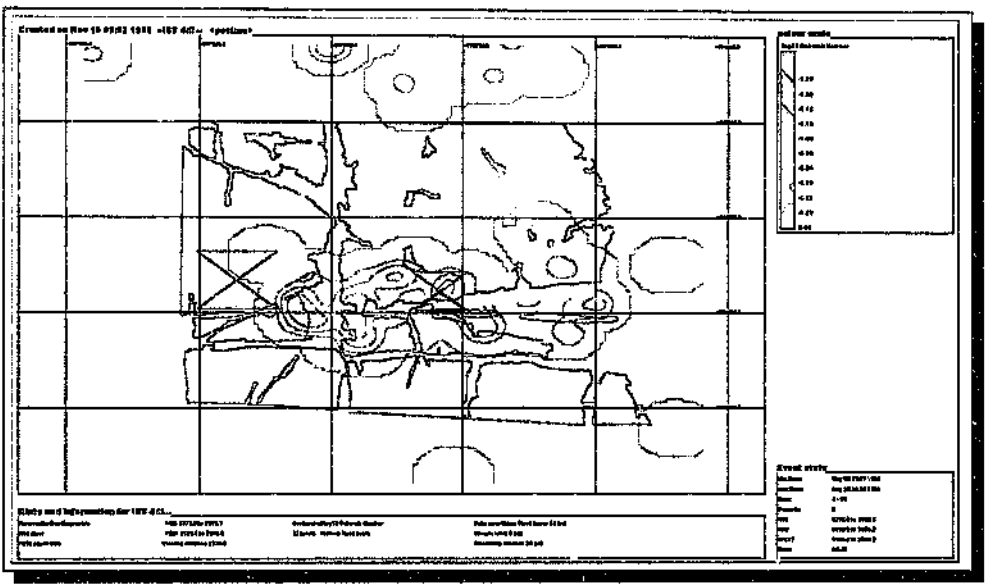


Fig. 4.55: Same as fig. 4.53; contours are of log(inv. Deborah no.).

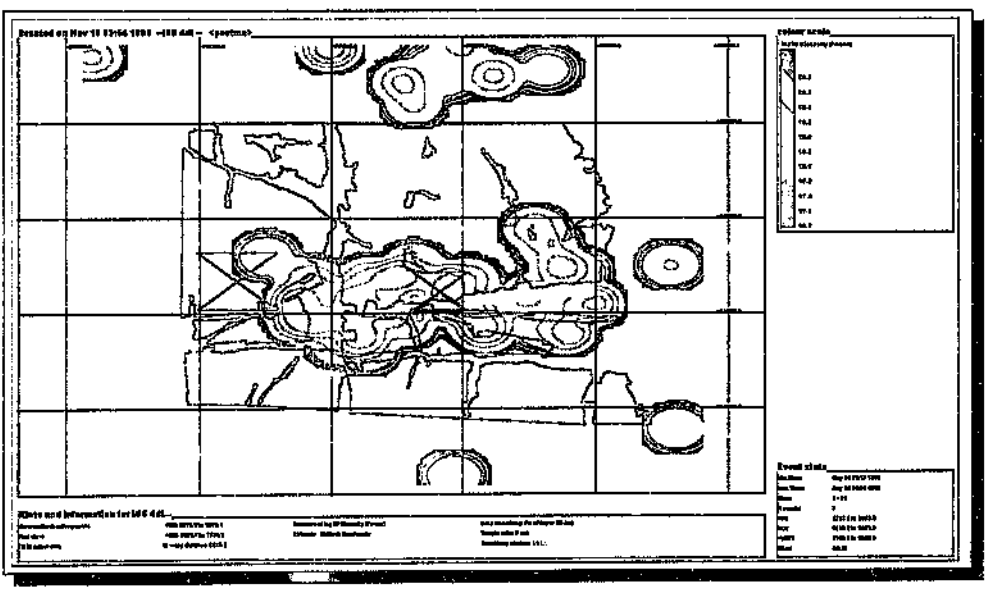


Fig. 4.56: Same as fig. 4.53; contours are of log(viscosity).

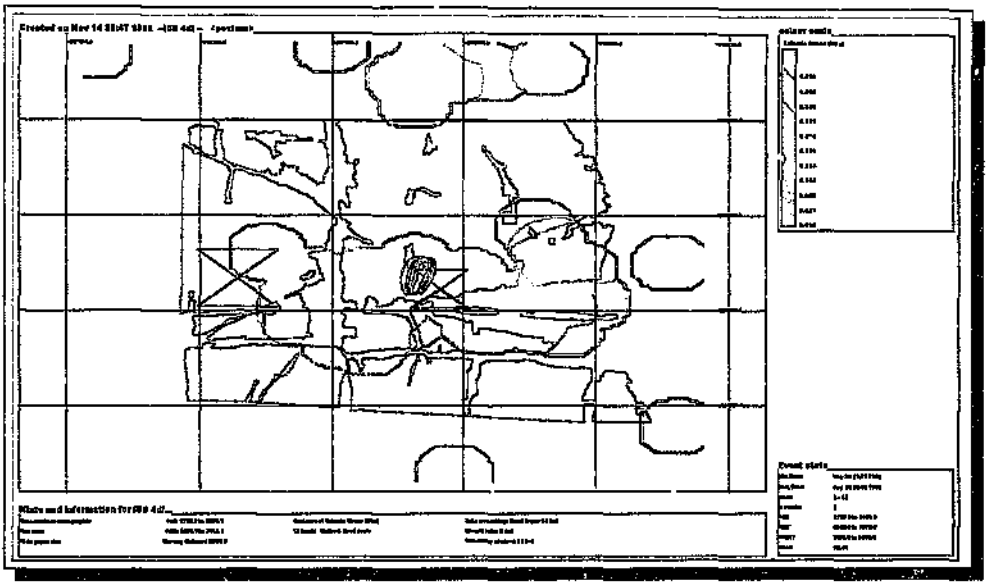


Fig. 4.57: Same as fig. 4.53; contours are of seismic stress.

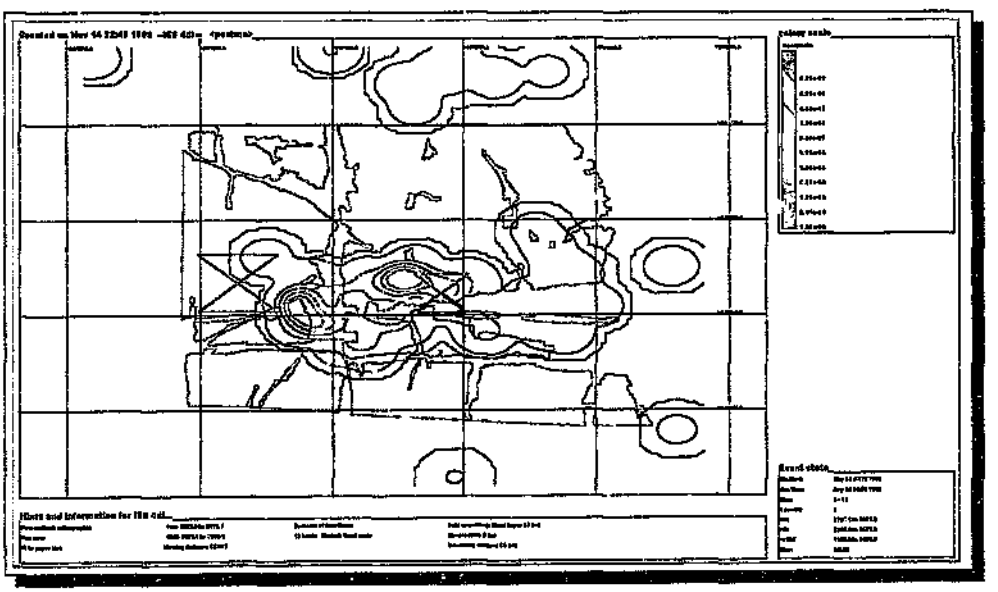


Fig. 4.58: Same as fig. 4.53; contours are of cumulative seismic strain.

APPENDIX F3

Time-history and contour plots used in the analysis of event 930314 to identify precursors (figs. 4.59 - 4.75); Section 4.2.3, Chapter 4.

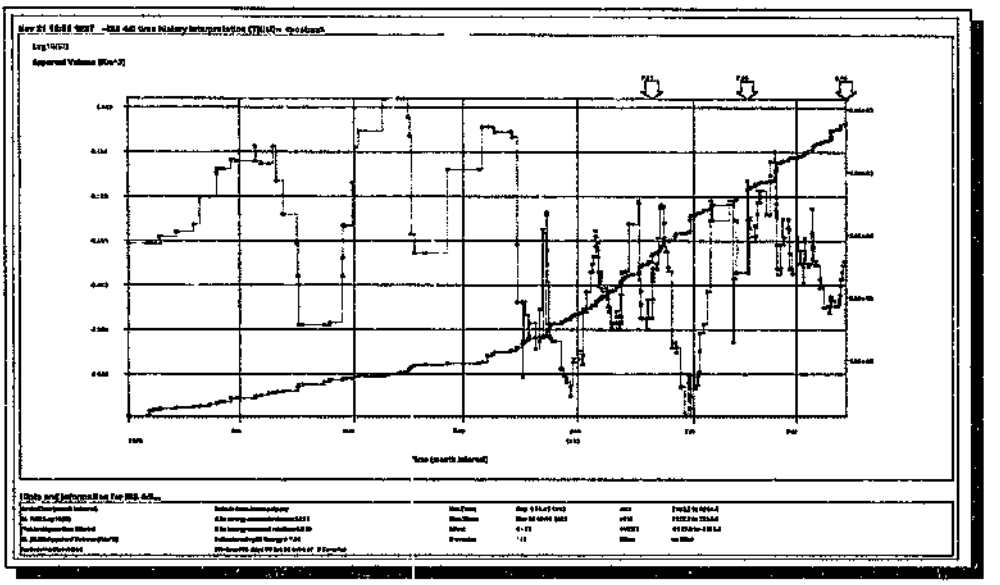


Fig. 4.59: Time-history of cumulative apparent volume and moving median log(EI) for seismicity recorded in the time period 1/9/92 to 14/3/93. The last arrow refers to event 930314.

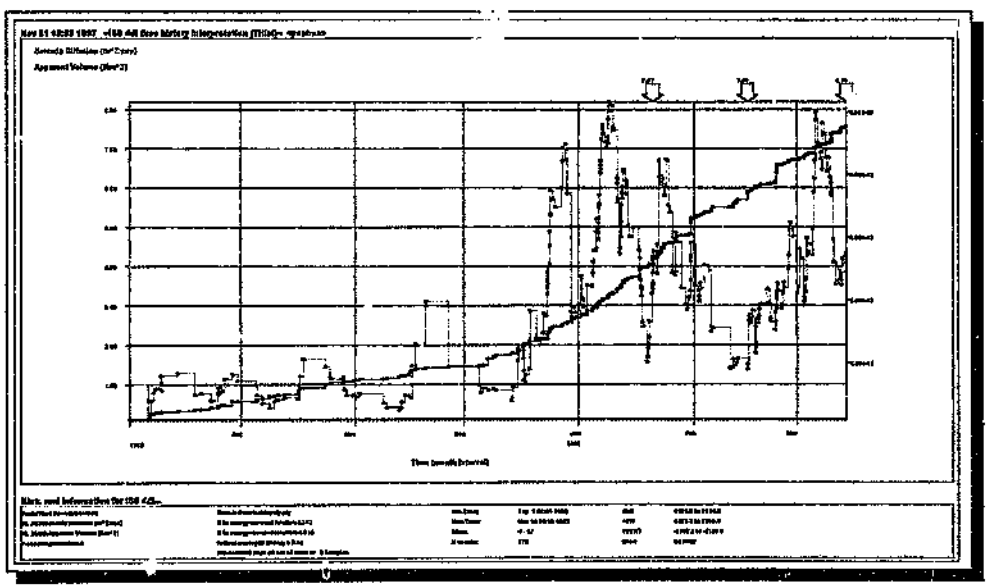


Fig. 4.60: Same as fig. 4.59, showing variation in seismic diffusion.

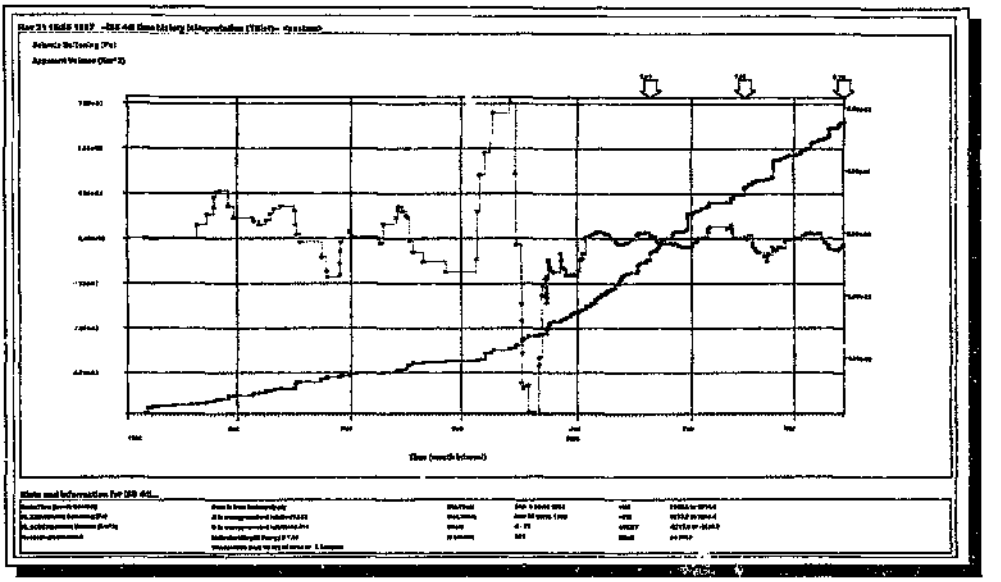


Fig. 4.61: Same as fig. 4.59, showing variation in seismic softening.

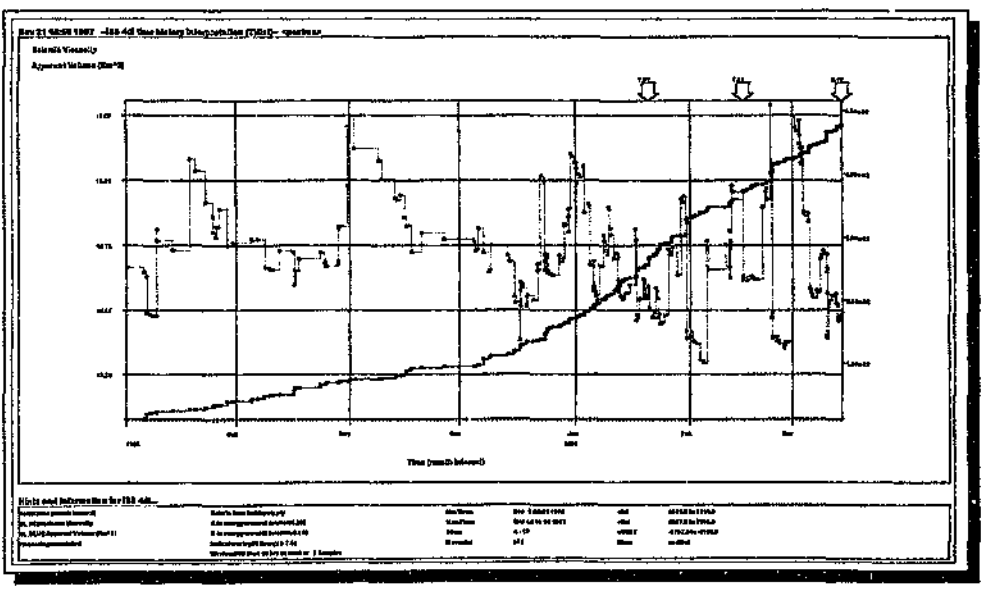


Fig. 4.62: Same as fig. 4.59, showing variation in seismic viscosity.

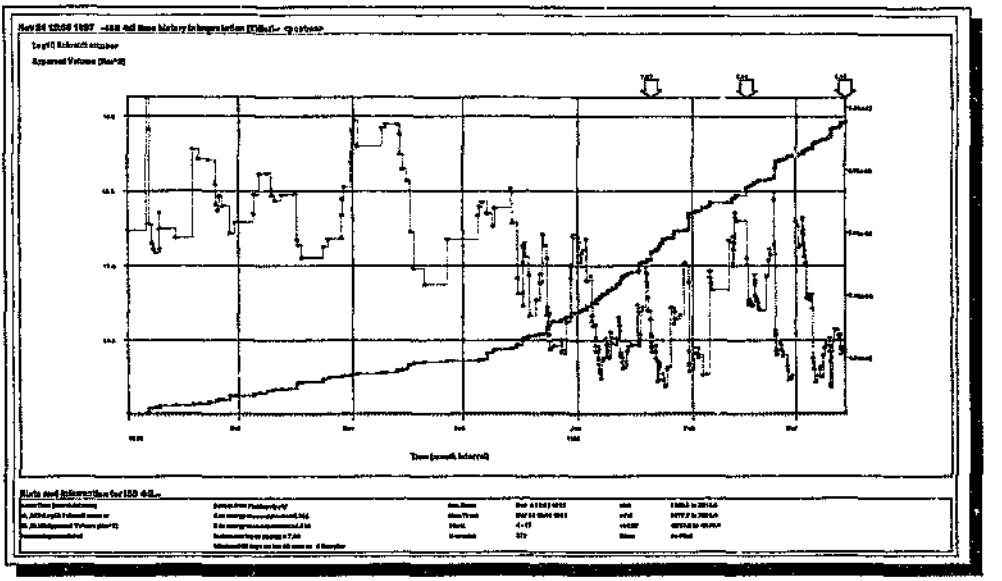


Fig. 4.63: Same as fig. 4.59, showing variation in log(seismic Schmidt no.).

Contour plots of those seismic parameters under investigation relating to the seismicity recorded 12 months before (but excluding) event 930314 (figs. 4.64 - 4.69).

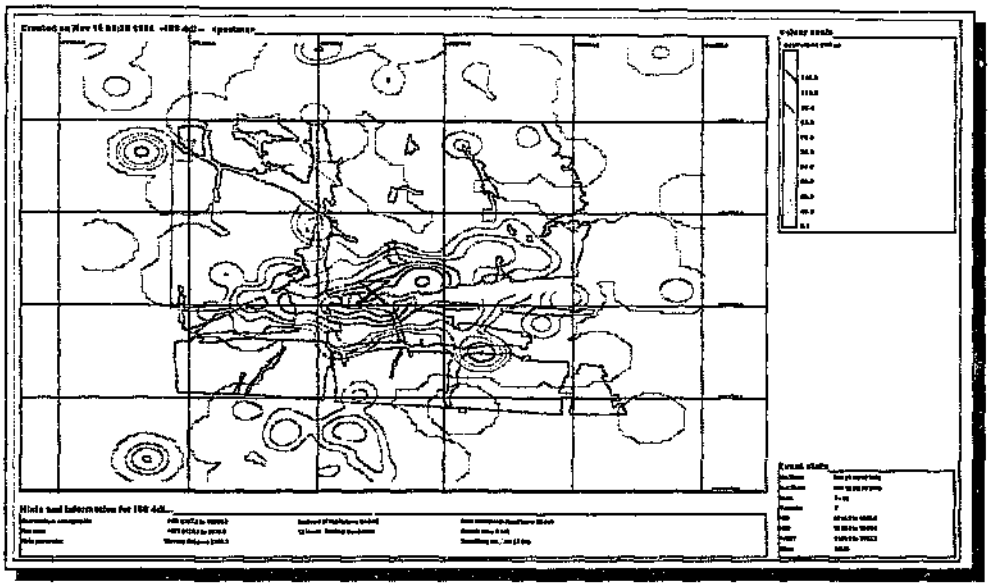


Fig. 4.64: Contours of apparent volume using seismicity recorded in the time period 26/3/92 to 14/3/93 (12 months leading up to, but excluding, event 930314, the location of which is indicated by the 'hourglass' symbol.

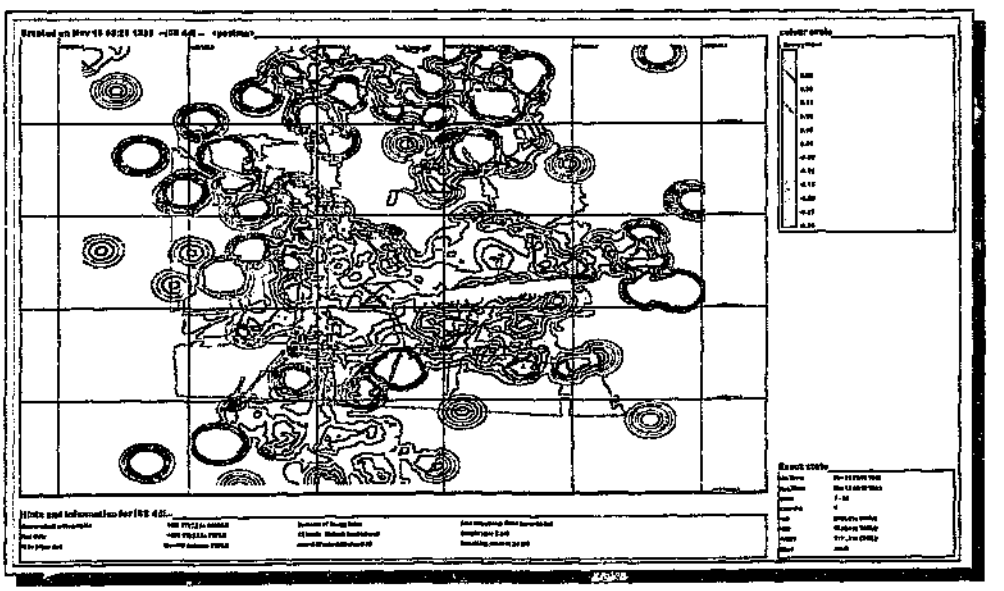


Fig. 4.65: Same as fig. 4.64, but contours are of log(EI).

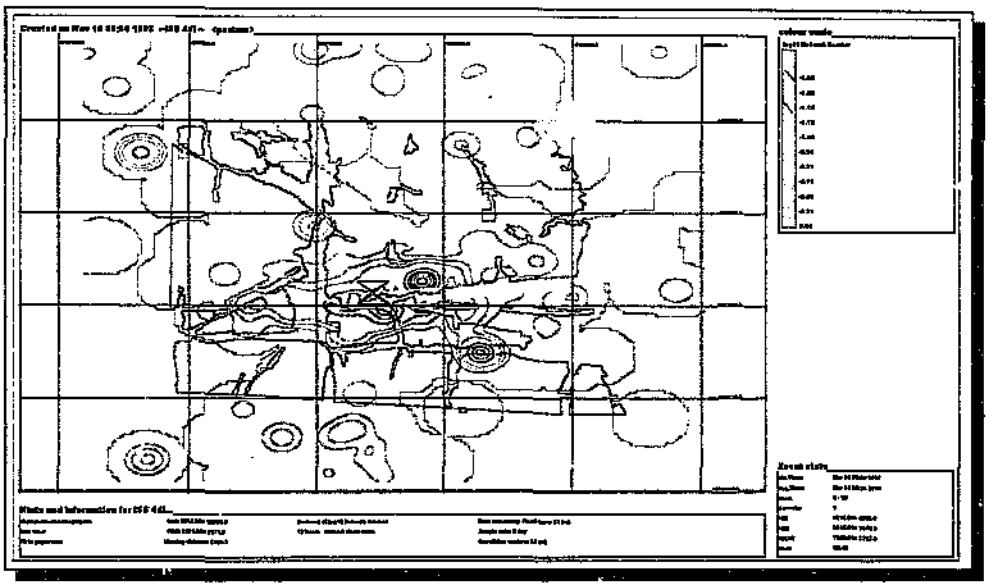


Fig. 4.66: Same as fig. 4.64; contours are of log(inv. Deborah no.).

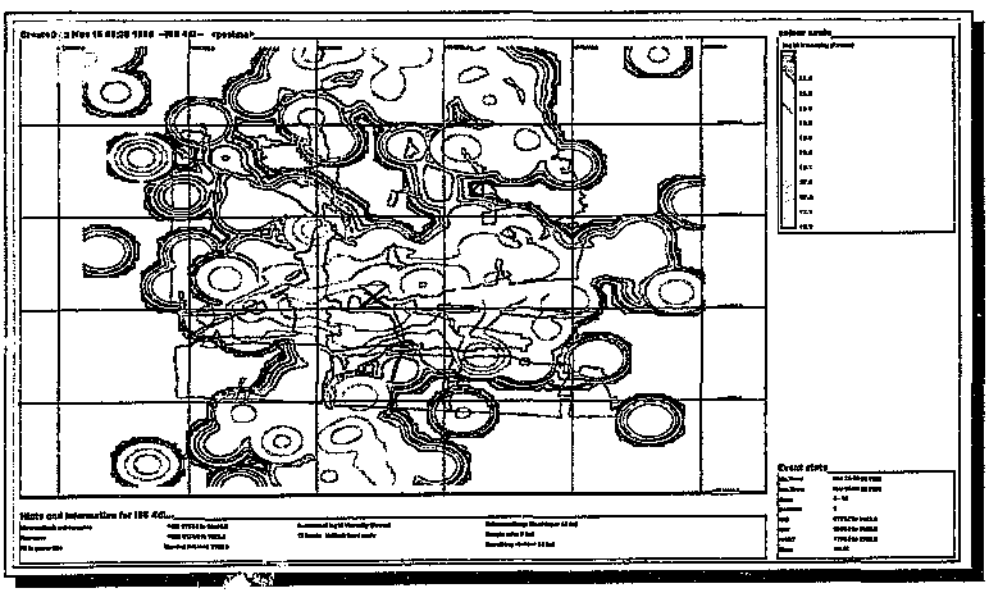


Fig. 4.67: Same as fig. 4.64; contours are of log(viscosity).

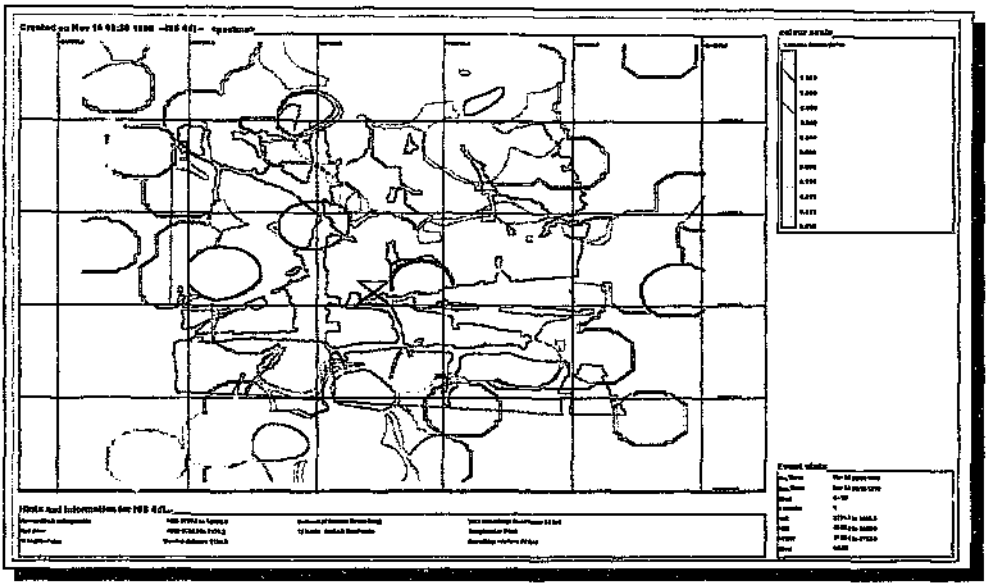


Fig. 4.68: Same as fig. 4.64; contours are of seismic stress.

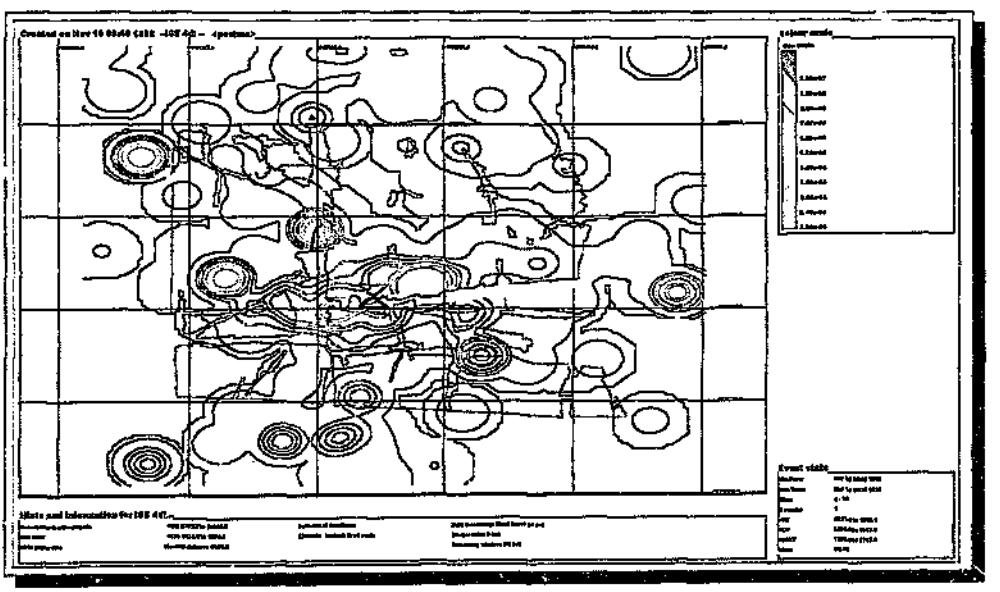


Fig. 4.69: Same as fig. 4.64; contours are of cumulative seismic strain.

Contour plots of those seismic parameters under investigation relating to the seismicity recorded 3 months before (but excluding) event 930314 (figs. 4.70 - 4.75).

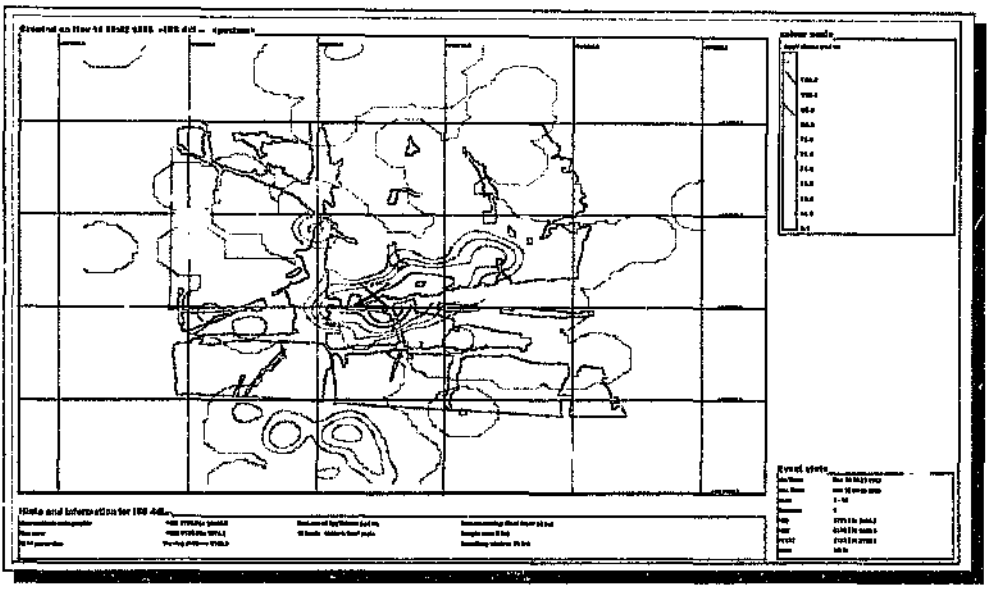


Fig. 4.70: Contours of apparent volume based on seismicity recorded in the time period 14/12/92 to 14/3/93 (three months leading up to event 930314, the location of which is indicated by the 'hourglass' symbol).

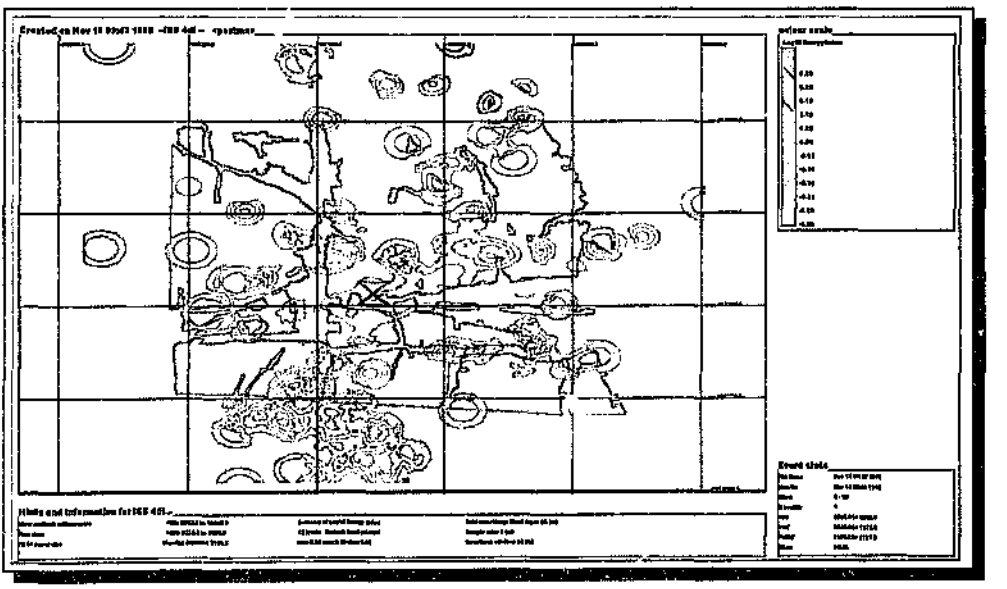


Fig. 4.71: Same as fig. 4.70; contours are of log(EI).

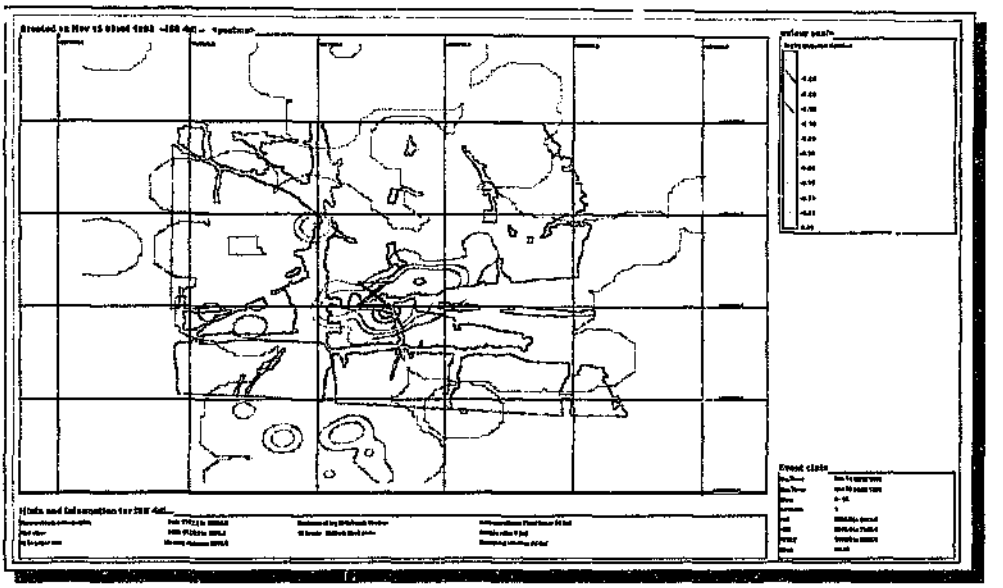


Fig. 4.72: Same as fig. 4.70; contours are of log(inv. Deborah no.).

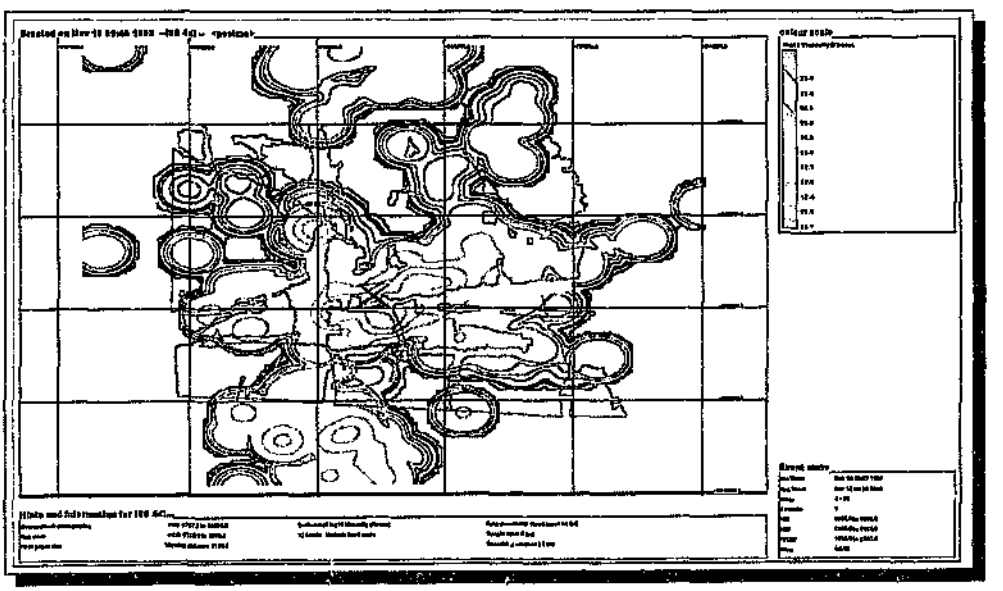


Fig. 4.73: Same as fig. 4.70; contours are of log(viscosity).

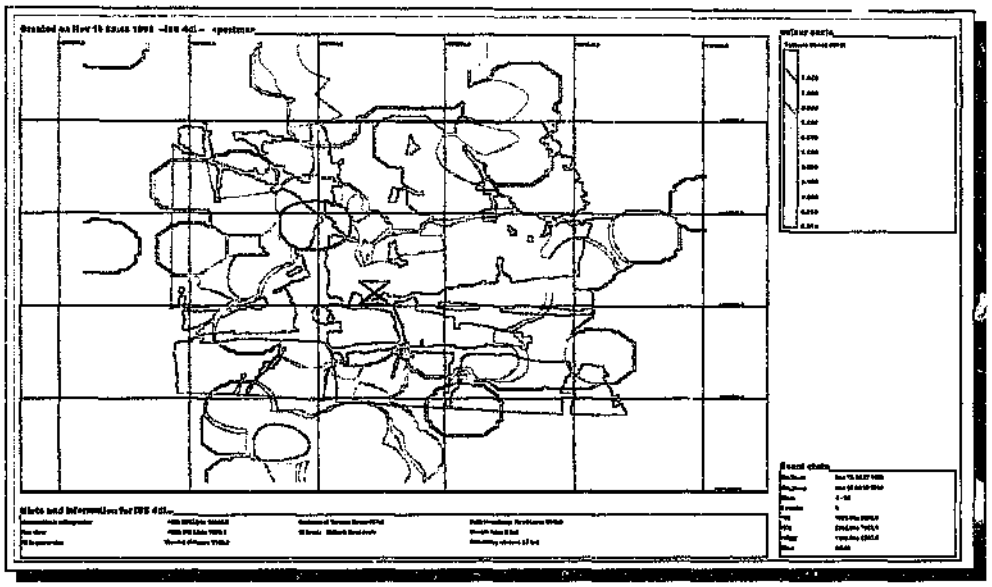


Fig. 4.74: Same as fig. 4.70; contours are of seismic stress.

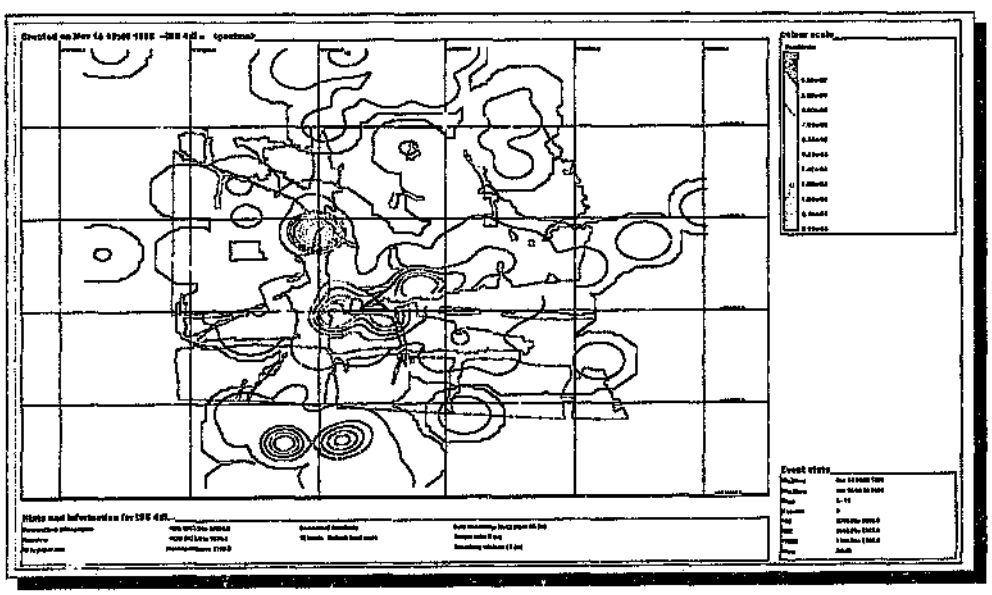


Fig. 4.75: Same as fig. 4.70; contours are of cumulative seismic strain.

APPENDIX F4

Time-history and contour plots used in the analysis of event 931108 to identify precursors (figs. 4.76 - 4.92); Section 4.2.4, Chapter 4.

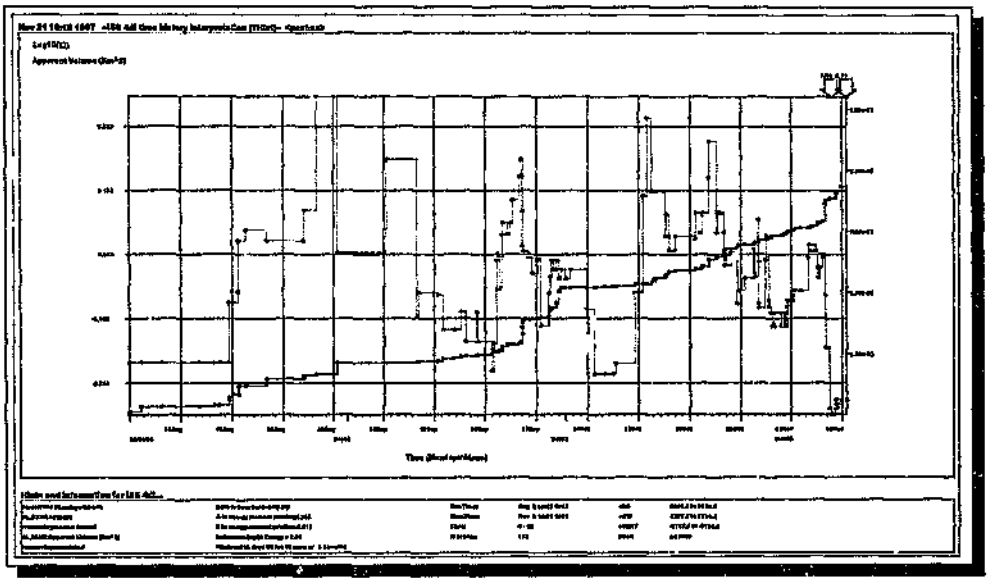


Fig. 4.76: Time-history of cumulative apparent volume and moving median log(EI) for seismicity recorded in the time period 2/8/93 to 8/11/93. The last arrow refers to event 931108.

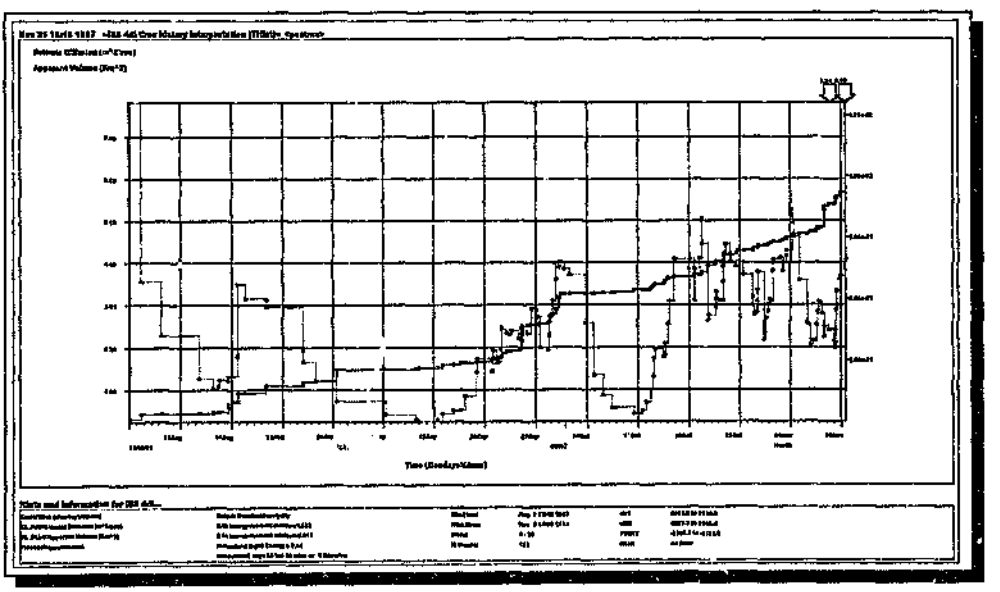


Fig. 4.77: Same as fig. 4.76, showing variation in seismic diffusion.

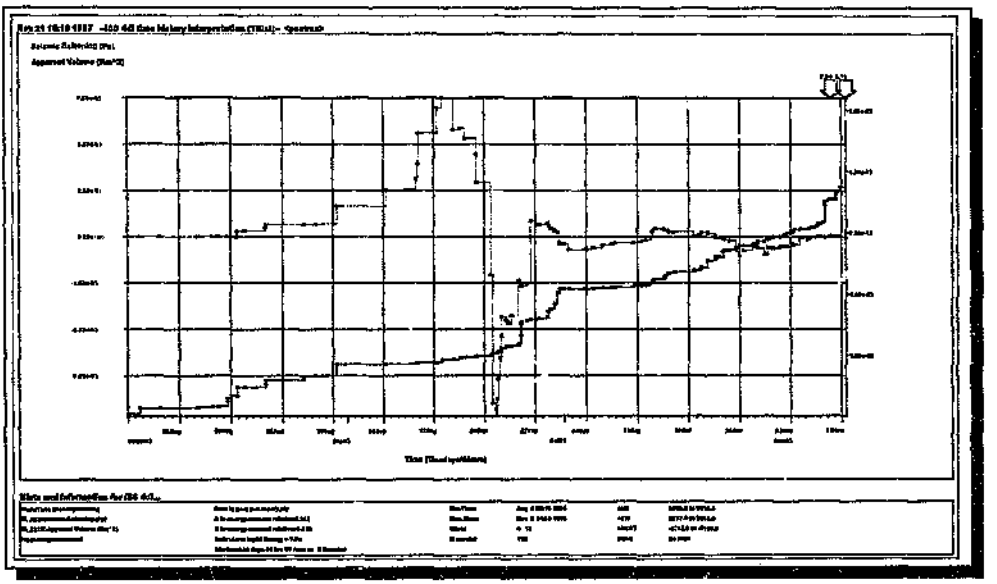


Fig. 4.78: Sama as fig. 4.76, showing variation in seismic softening.

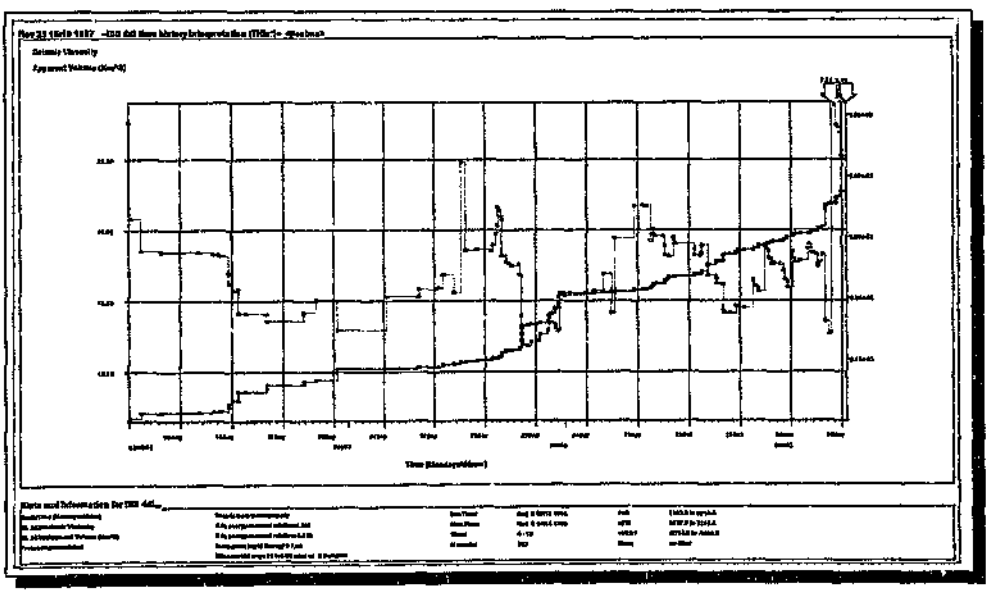


Fig. 4.79: Same as fig. 4.76, showing variation in seismic viscosity.

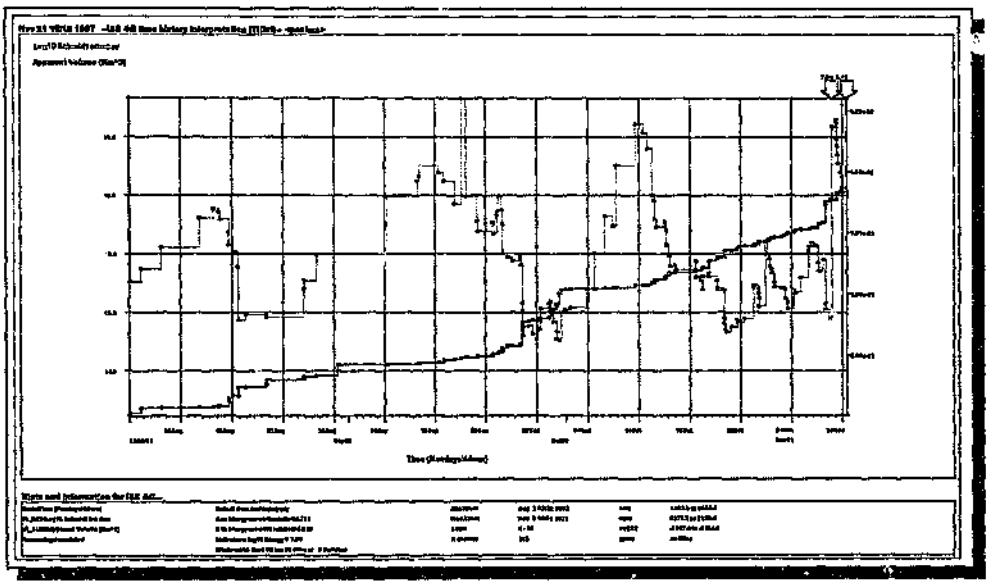


Fig. 4.80: Same as fig. 4.76, showing variation in log(seismic Schmidt no.).

Contour plots of those seismic parameters under investigation relating to the seismicity recorded 12 months before (but excluding) event 931108 (figs. 4.81 - 4.86).

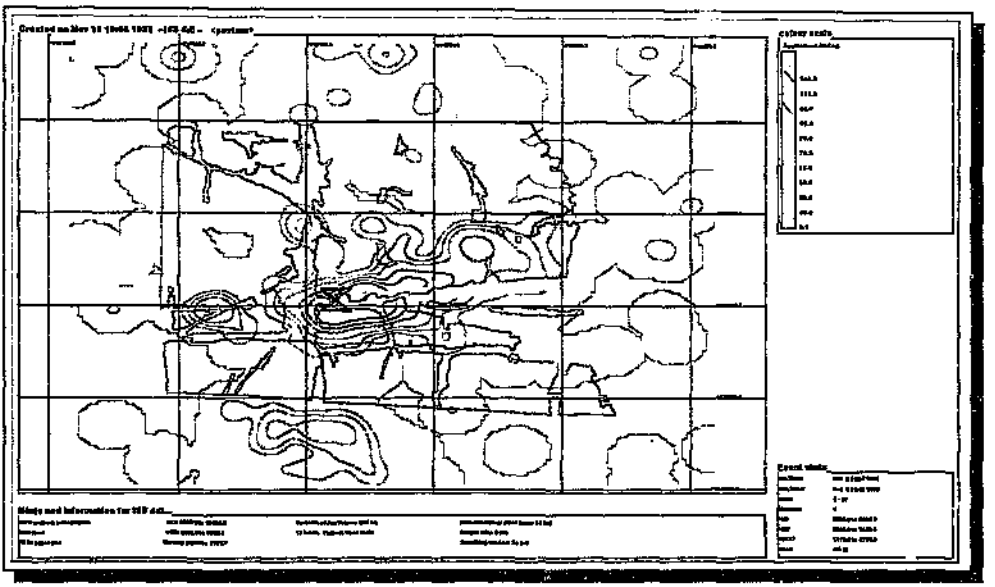


Fig. 4.81: Contours of apparent volume using seismicity recorded in the time period 8/11/92 to 7/11/93 (12 months leading up to, but excluding, event 931108, the location of which is indicated by the 'hourglass' symbol).

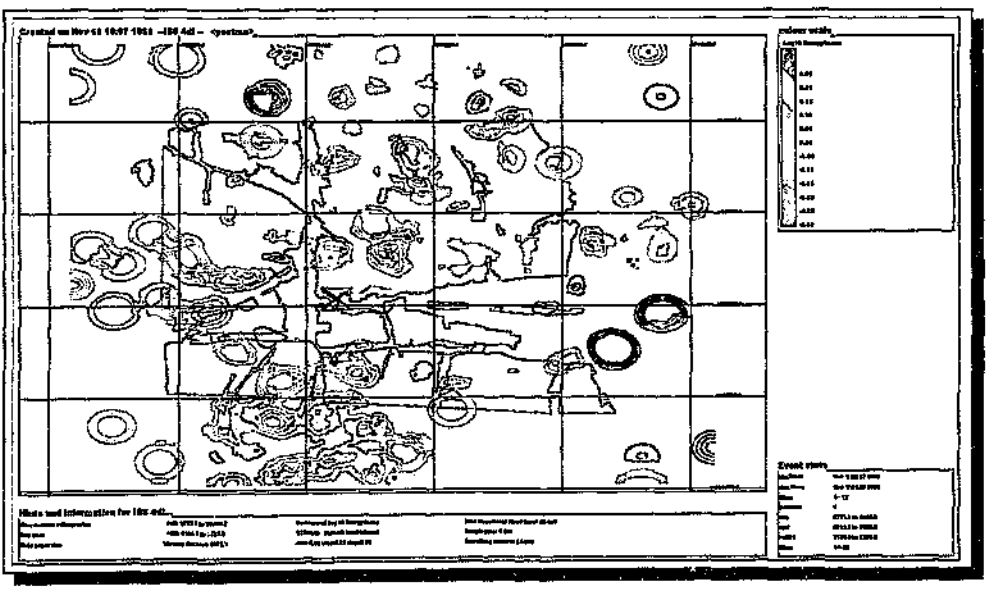


Fig. 4.82: Same as fig. 4.81, but contours are of log(EI).

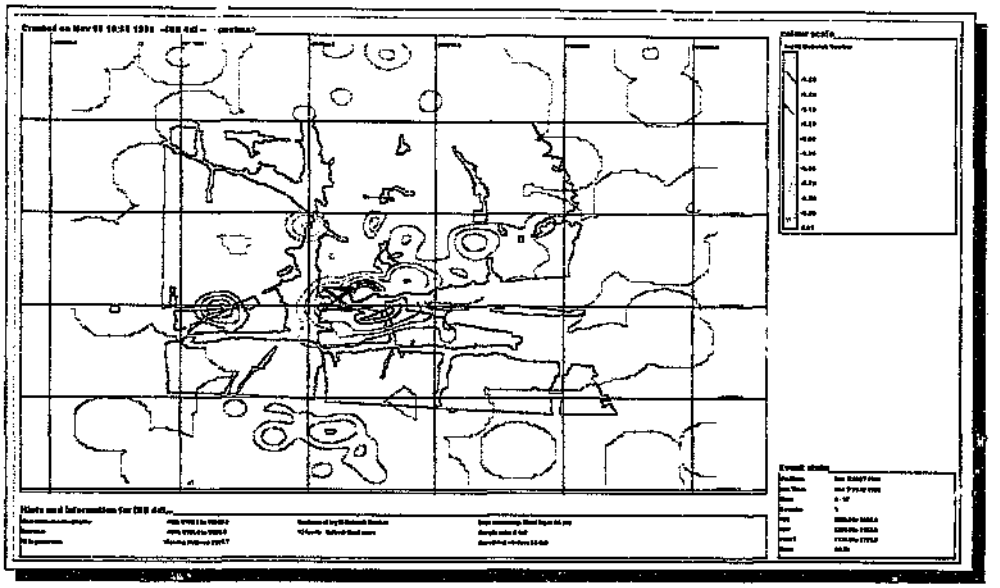


Fig. 4.83: Same as fig. 4.81; contours are of log(inv. Deborah no.).

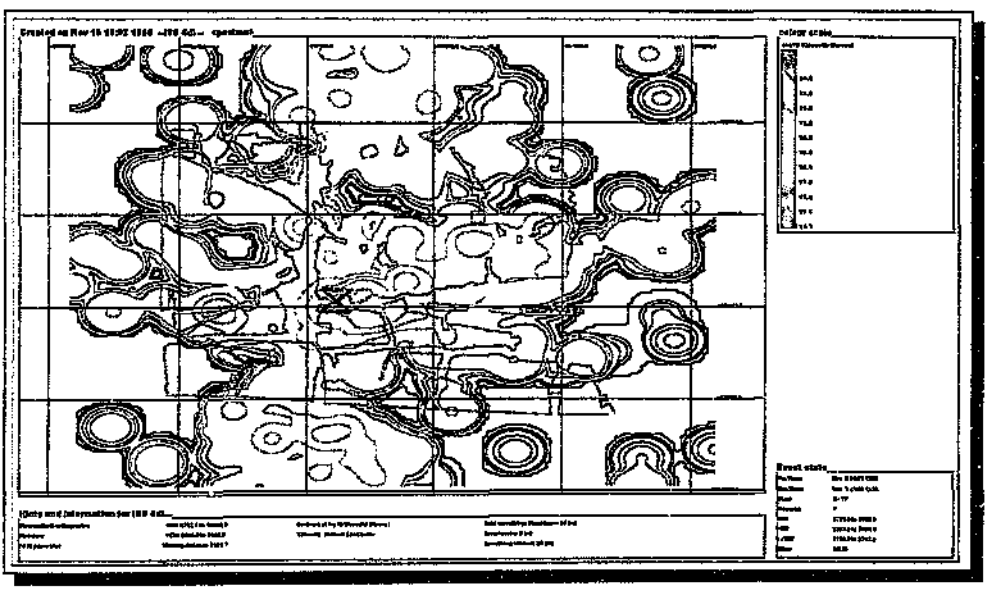


Fig. 4.84: Same as fig. 4.81; contours are of log(viscosity).

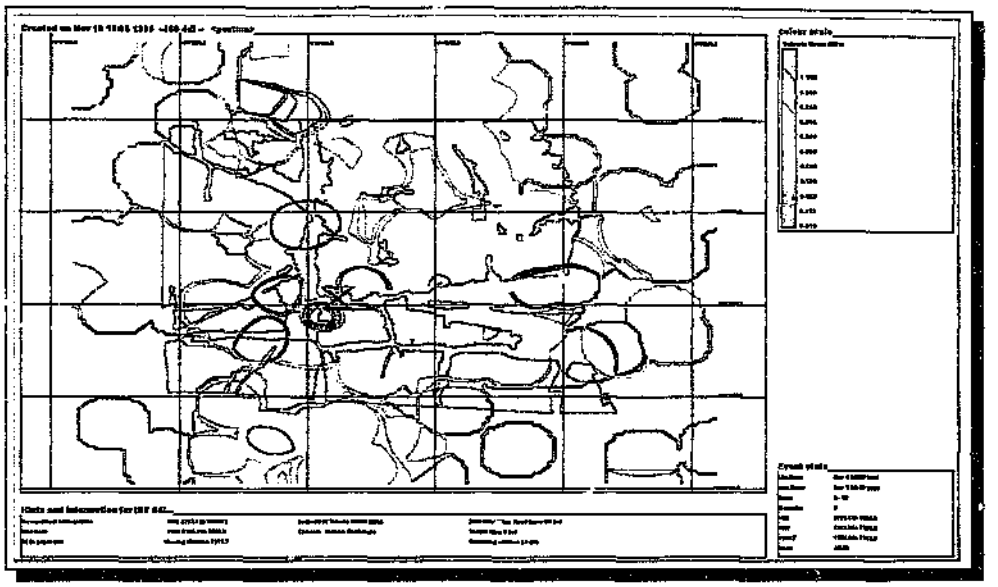


Fig. 4.85: Same as fig. 4.81; contours are of seismic stress.

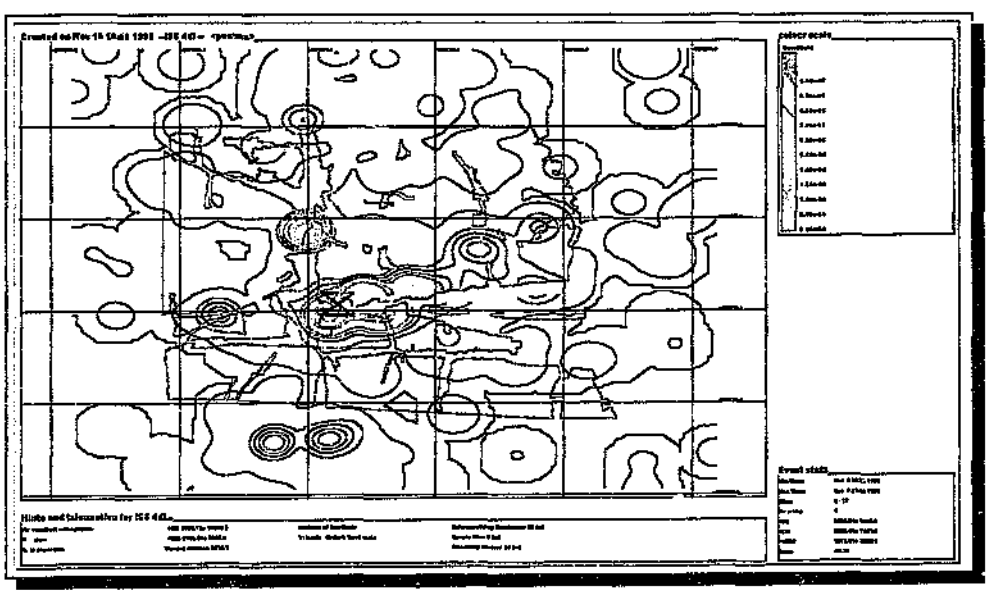


Fig. 4.86: Same as fig. 4.81; contours are of cumulative seismic strain.

Contour plots of those seismic parameters under investigation relating to the seismicity recorded 3 months before (but excluding) event 931108 (figs. 4.87 - 4.92).

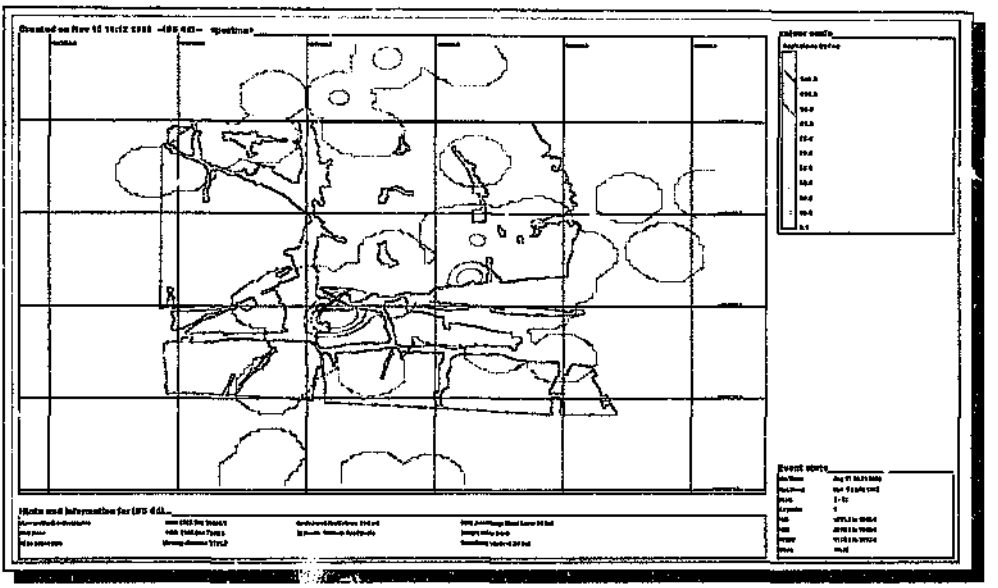


Fig. 4.87: Contours of apparent volume based on seismicity recorded in the time period 10/8/93 to 7/11/93 (three months leading up to event 931108, the location of which is indicated by the 'hourglass' symbol).

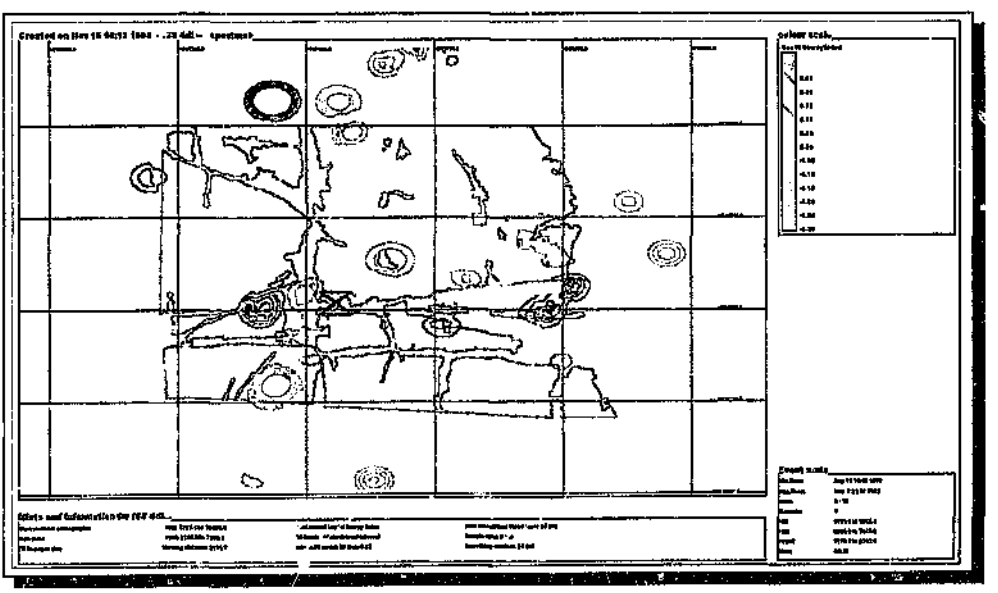


Fig. 4.88: Same as fig. 4.87; contours are of log(EI).

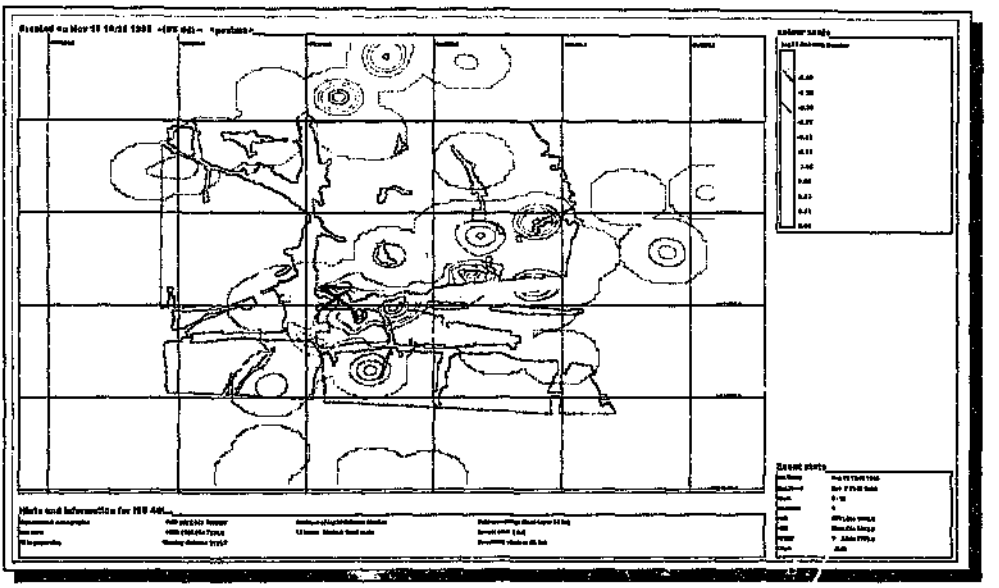


Fig. 4.89: Same as fig. 4.87; contours are of log(inv. Deborah number).

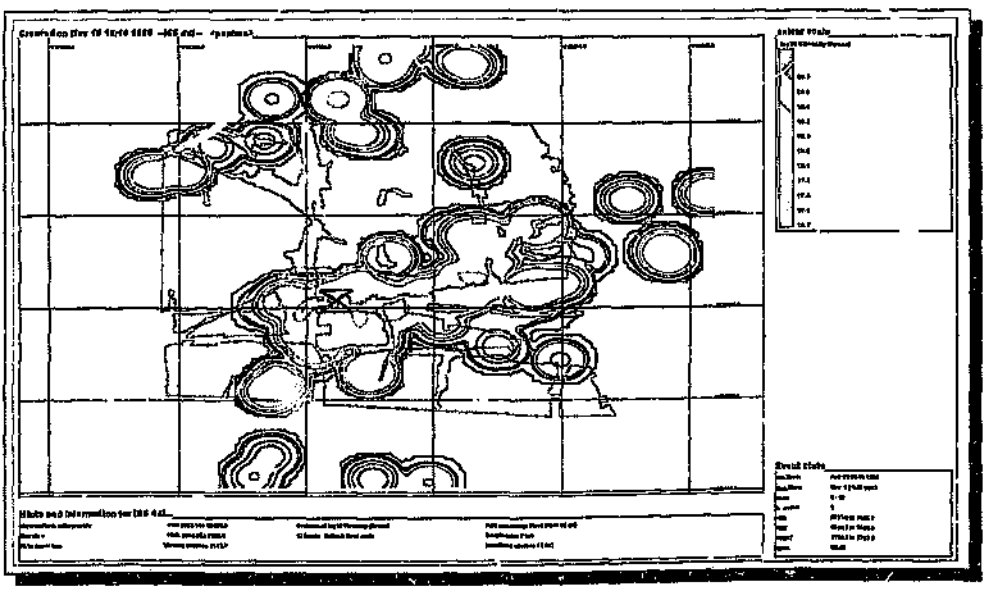


Fig. 4.90: Same as fig. 4.87; contours are of log(viscosity).

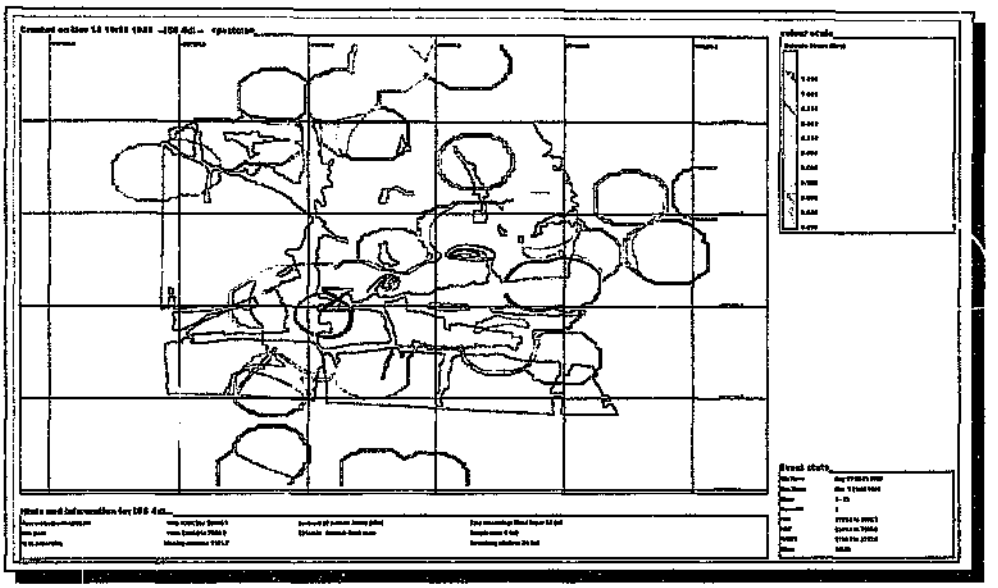


Fig. 4.91: Same as fig. 4.87; contours are of seismic stress.

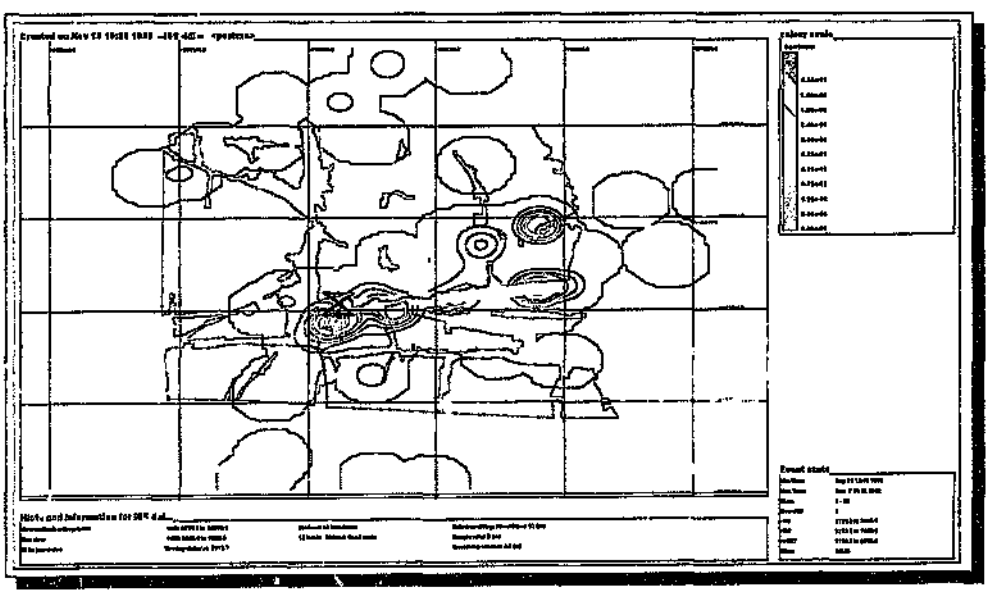


Fig. 4.92: Same as fig. 4.87; contours are of cumulative seismic strain.

APPENDIX F5

Time-history and contour plots used in the analysis of event 940424 to identify precursors (figs. 4.93 - 4.109); Section 4.2.5, Chapter 4.

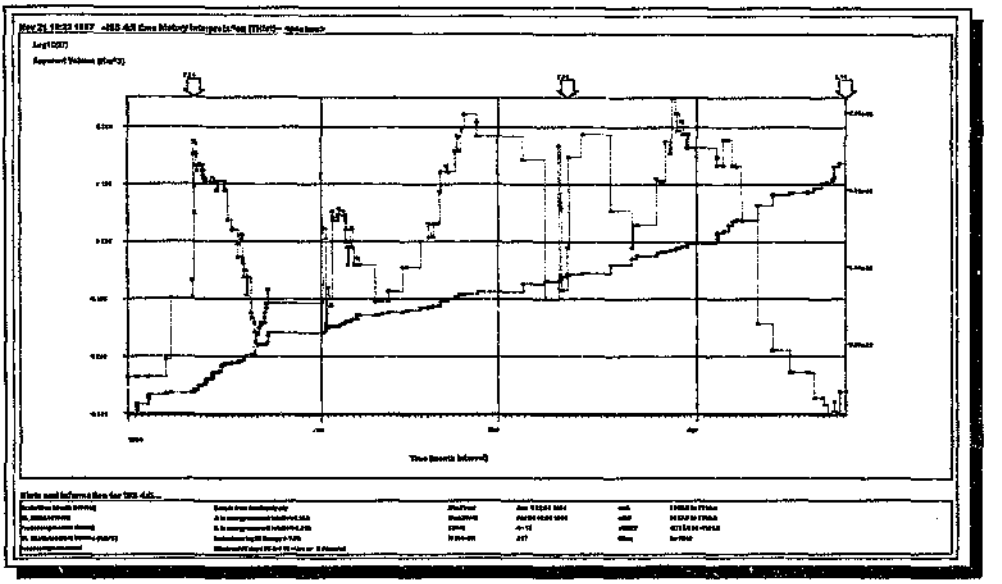


Fig. 4.93: Time-history of cumulative apparent volume and moving median log(EI) for seismicity recorded in the time period 1/1/94 to 24/4/94. The last arrow refers to event 940424.

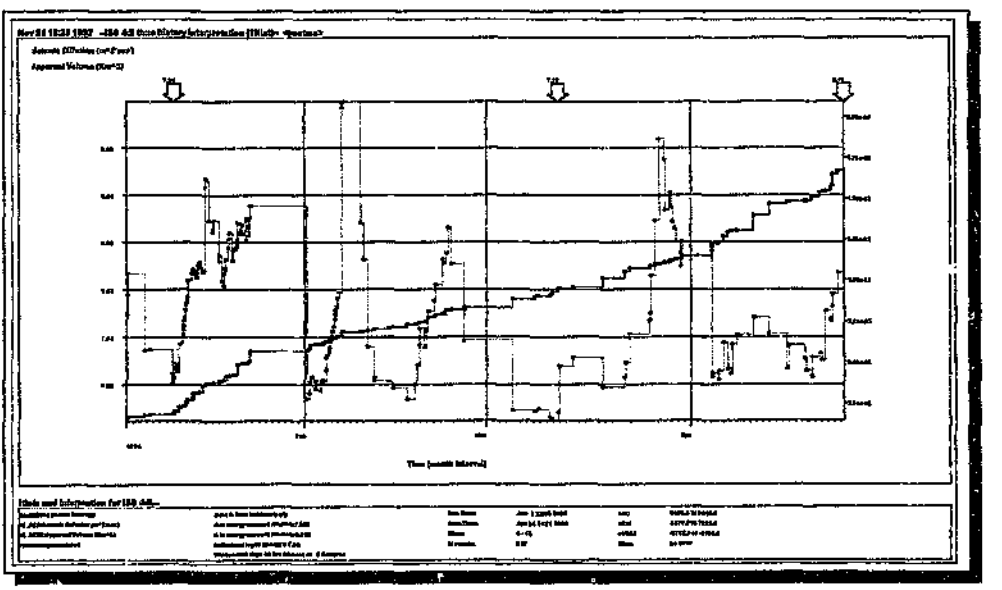


Fig. 4.94: Same as fig. 4.93, showing variation in seismic diffusion.

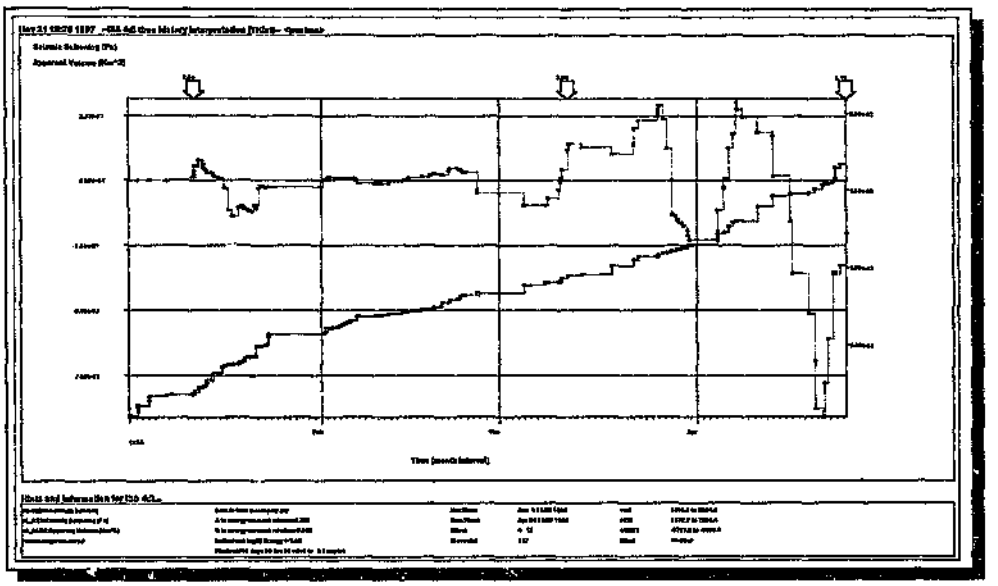


Fig. 4.95: Same as fig. 4.93, showing variation in seismic softening.

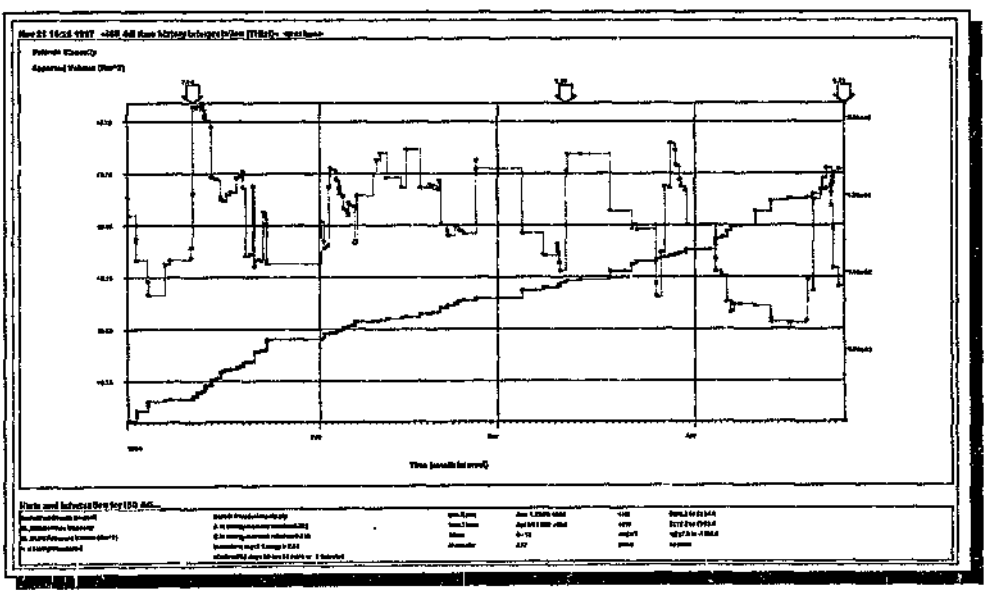


Fig. 4.96: Same as fig. 4.93, showing variation in seismic viscosity.

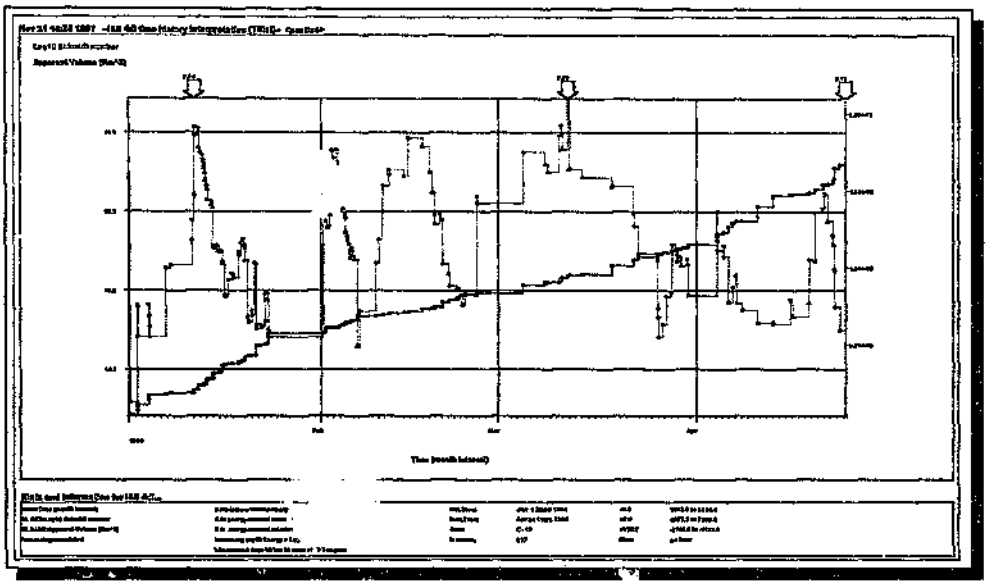


Fig. 4.97: Same as fig. 4.93, showing variation in log(seismic Schmidt no.).

Contour plots of those seismic parameters under investigation relating to the seismicity recorded 12 months before (but excluding) event 940424 (figs. 4.98 - 4.103).

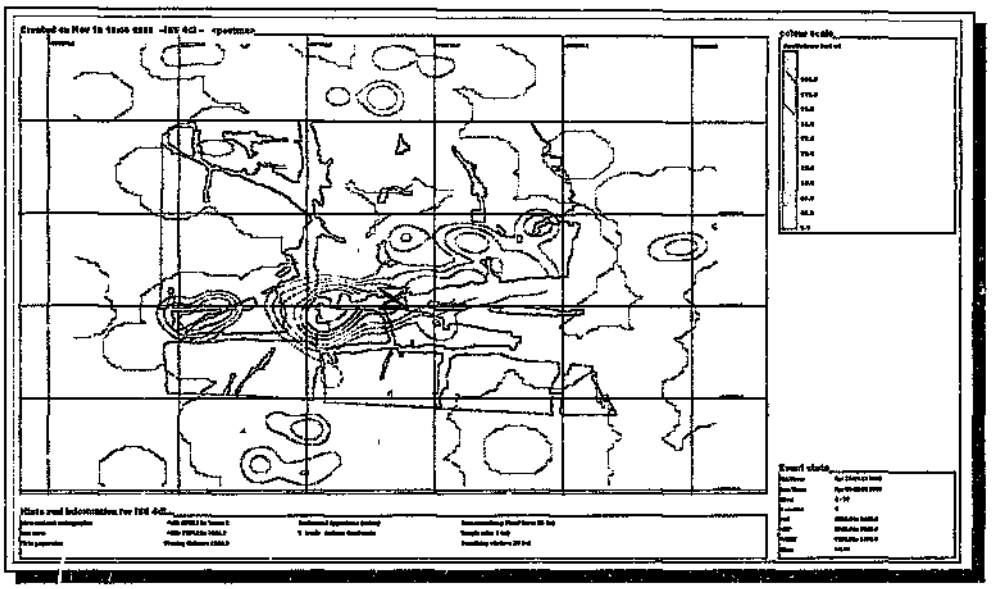


Fig. 4.98: Contours of apparent volume using seismicity recorded in the time period 24/4/93 to 24/4/94 (12 months leading up to, but excluding, event 940424, the location of which is indicated by the 'hourglass' symbol).

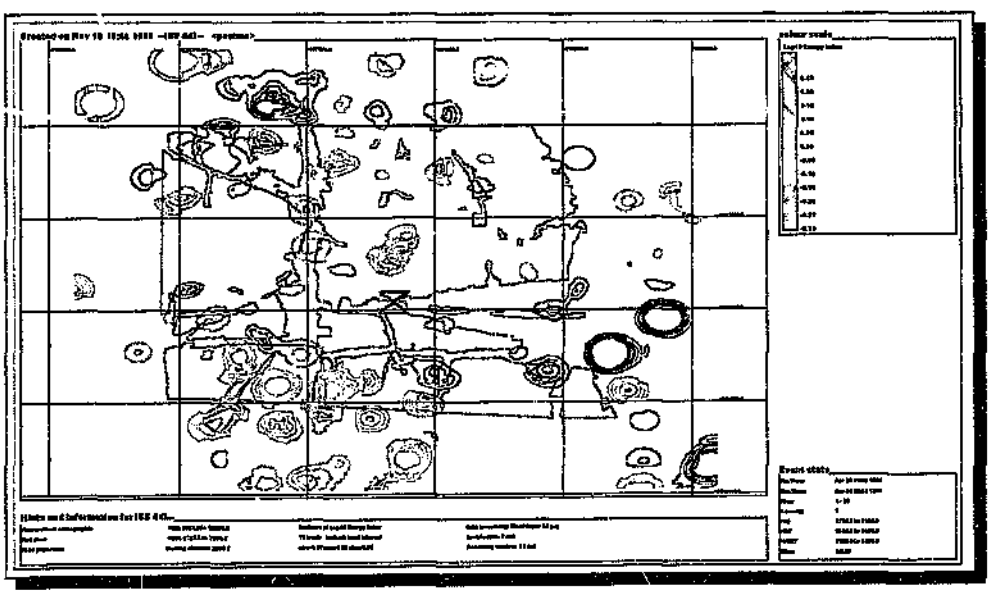


Fig. 4.99: Same as fig. 4.98, but contours are of log(EI).

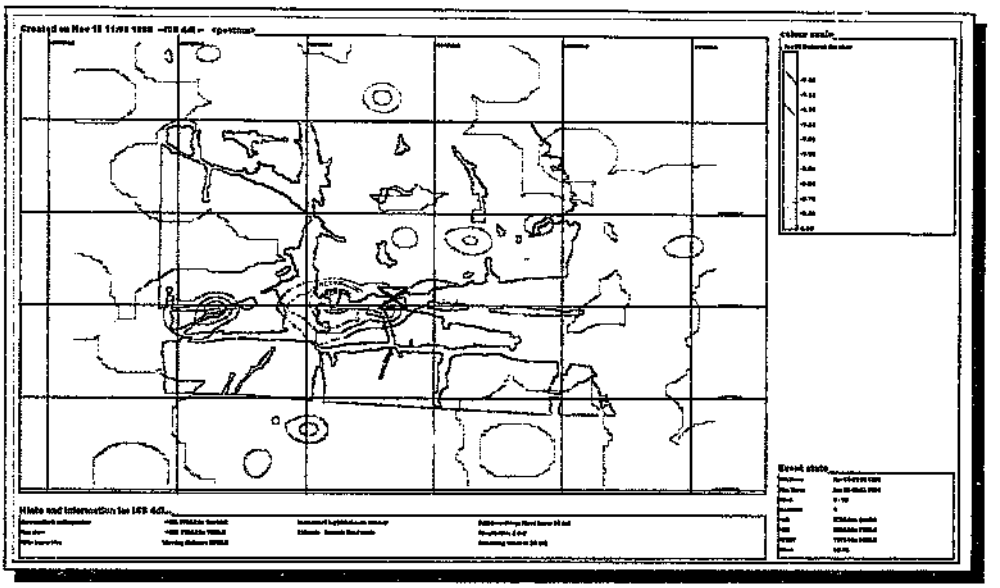


Fig. 4.100: Same as fig. 4.98; contours are of log(inv. Deborah no.).

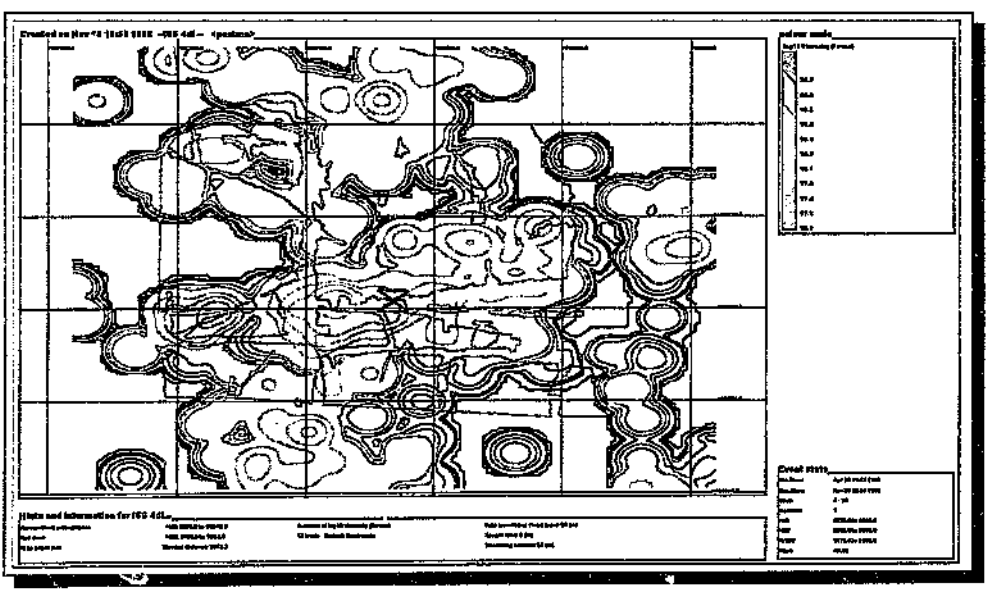


Fig. 4.101: Same as fig. 4.98; contours are of log(viscosity).

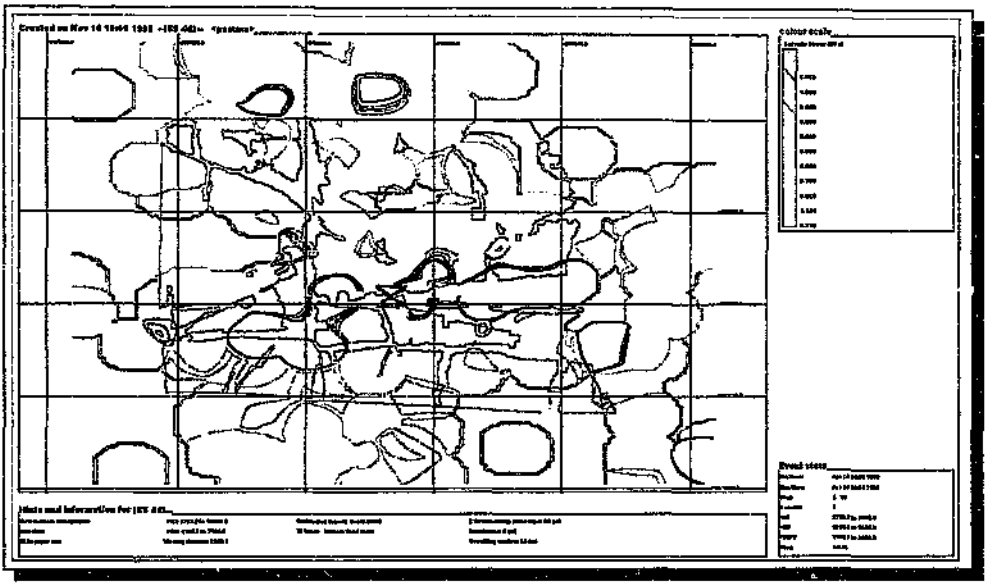


Fig. 4.102: Same as fig. 4.98; contours are of seismic stress.

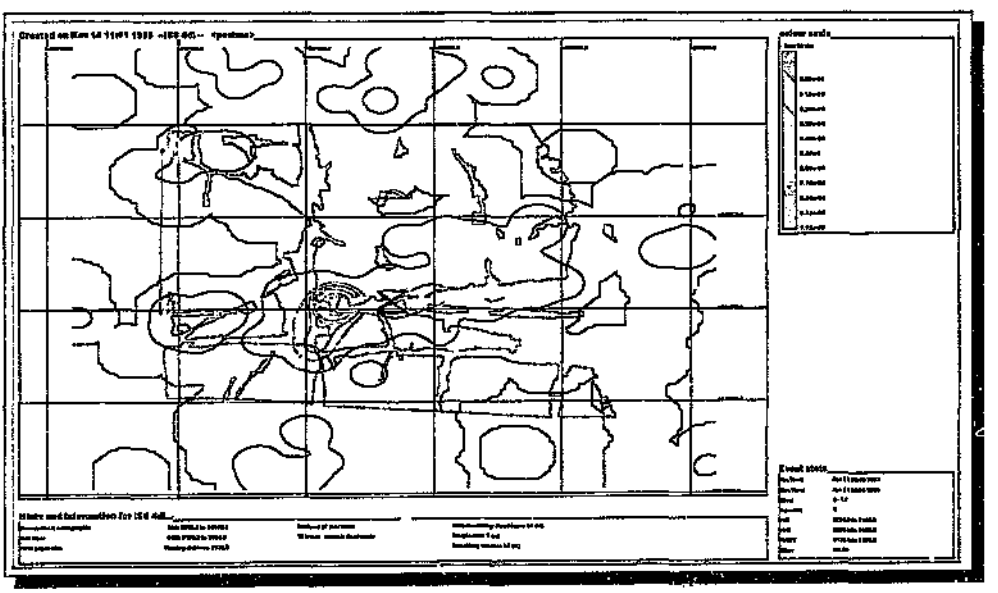


Fig. 4.103: Same as fig. 4.98; contours are of cumulative seismic strain.

Contour plots of those seismic parameters under investigation relating to the seismicity recorded 3 months before (but excluding) event 940424 (figs. 4.104 - 4.109).